Synthesis of waterborne degradable polyester nanoparticles by free radical emulsion polymerization

Fabian Wenzel

Supervised by: Prof. Jose Ramon Leiza

and Dr. Miren Aguirre

Chemical Engineering Group

University of the Basque Country (UPV/EHU)

Donostia-San Sebastián

(2022)

Acknowledgements

I would like to express my sincere gratitude to my supervisors Miren Aguirre and Jose R. Leiza for their patience and guidance. This work could never have been achieved without their support. Working under their supervision gave me the opportunity to grow as a chemist and person. I would like to extend my gratitude to Julie Movellan and Leticia Pardo for supporting me in the lab in the early stages of this work, Shaghayegh Hamzehlou for her support with the modelling and teaching me Predici, Amaia for the GPC and AF4 measurements and JI for the NMR measurements and the extensive support on analysing the spectra. I would like to thank Sara Rubio for contributing to this work in the frame of her Bachelor thesis.

I would like to acknowledge the professors of the Chemical Engineering Group Professors Maria Paulis, Radmila Tomovska and José M. Asua for their supports and kind remarks. A special thanks goes to Inés Plaza for her endless help and kindness.

I would like to gratefully thank Dr. Eugen Fomenko and Dr. Daniel Schmitz-Stapela who provided me the opportunity to join their team as intern and for their support during these three and a half months at tesa. I would like to thank other members of tesa especially Franziska Eberhardt, Kane Stapelfeldt, Janika Stolze and Marc Haenle for their support in the waterborne

laboratory and Dr. Tobias Sokolowski for carrying out the NMR measurements and his support with the evaluation of the spectra.

Sebastian, thank you for making arriving to San Sebastian easy for me and for showing me all the nice restaurants and bars. Ehsan, for showing me how the GC works and help on my work. Aitor, for all the discussions and your helpfulness. Adrian B, for your help on pressure-sensitive adhesives. Noushin and Pankaj, I will not forget our trip to Paris. Elodie, Justine, Alex and Boris for all the fun we had and the unforgettable nights in Bordeaux. Ernesto, I miss the breakfasts of tortilla that we had. Nerea, Maialen, Ana, Sayrung, Hesham, Elvis and Sheraz, all the time we spent in and outside of the laboratory and office it passed by so quickly in the end.

A huge thanks belongs as well to my flatmates, Angela for all the activities we did together and being there during the confinamiento. Robin, I have enjoyed the board games, long walks and the cheese you brought from France. Karla and Lorenz, for the fun we had together.

Contents

Chapter 1. Introduction

1.1. Main motivation and objectives

The idea to live a sustainable life has its roots dating back thousands of years. However contemporary thoughts on sustainability are often dated back to the 1880s and seen as the response to environmental damage caused by the emergence of the industrial revolution.[1] Sustainability has the goal that as many as soon 10 billion people are decently fed and housed without damaging the environment, on which all of us depend.[2]

With increasing industrialization, polymers have radically changed our economy and society within a few decades; they combine excellent mechanical properties with relatively low costs. Since the beginning of their mass production in the 1950s, 8.3 billion tons of plastics have been produced. 5.8 billion tons or 70% of them have become waste of which the majority (4.9 billion tons) have been disposed in landfills or the environment. The majority of the produced synthetic polymers accounts to polyethylene (PE) and polypropylene (PP)[3] leading to pollution of the oceans.[4,5] Thus, 267 sea species, including 86% of all sea turtle species, 44% of all seabird

species 43% of all marine mammal species and numerous fish and crustacean species have been found to have ingested synthetic polymer.[6] Another issue are the omnipresent micro-plastics which are per definition plastic particles between 1 µm and 5 mm. In recent studies micro-plastics were found in human blood[7] and in lung tissue[8]. Since most of those plastic particles are not biodegradable, they accumulate rapidly. These problems might be intensified in the future, as the annually demand of polymers is expected to rise to above 1 billion tons by 2050.[9]

On one hand the focus is on using resources from renewable feedstock, namely for example from vegetable oils[10,11] and lipids, terpenes[12–15], lignin derivatives[16–18], carbohydrates[19–21] or proteins[22]. However, the production of biobased monomers is not always a sustainable process and may require harsh conditions to extract the targeted product or long synthesis routes and purification steps. Another disadvantage is often the low performance compared to their oil-based counterparts.[23]

Different guidelines such as the "*12 principles of green chemistry*"[24] and the "*12 principles of green engineering*"[25] were proposed to serve as guide to minimize the environmental impact of chemical products and processes. These principles have been applied to polymer production processes by Dubé et al.[26] More recently, they applied these principles to emulsion polymerization processes.[27] They concluded that the sustainability of a process goes beyond replacing oil-based educts by renewable resources. Therefore, they explored other challenges of the emulsion polymerization process, such as waste prevention, energy efficiency maximization and minimization of potential accidents. The emulsion polymerization process in general is considered a more sustainable and environmentally friendly process compared to

solvent-borne processes. Water is used instead of organic solvents, which are one of the main sources of volatile organic components (VOCs). However, polymers from emulsion polymerization make up only for a small fraction of all produced polymers. The yearly production of synthetic polymer dispersions is about 5-10% of the overall polymer consumption.[28]

The 10th of the 12 principles of green chemistry states to design chemicals and products to degrade after use; design chemicals to break down into innocuous substances after use so that they do not accumulate in the environment.[26] As mentioned above a majority of the produced polymers accounts to PE and PP. Hence, their resistance to the degrading action of living systems, due to the lack of functional groups is becoming more and more problematic in cases in which the polymeric products are only use for a limited amount of time, before they become waste.[29] Therefore, green chemistry is seeking the right balance between the stability of compounds during their shelf-life and intended use phases, and their degradability once the compounds enter the environment. The most important degradation processes are divided into biodegradation, atmospheric oxidation and hydrolysis.[24] Hydro-biodegradation is a well-known process which describes the process that gives bioassimilable products from aliphatic polyesters.[30] The hydrolytic degradation of an ester group to a carboxylic acid and an alcohol is depicted in Scheme 1.1.

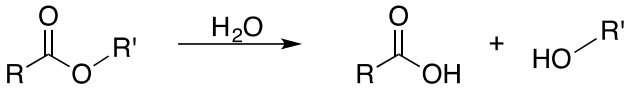

Scheme 1.1. Schematic degradation of an ester group by hydrolysis.

Aliphatic polyesters can be prepared from renewable biomass derived resources and can be recycled, composted or incinerated with low environmental impact. Furthermore, they can be synthesized to high molar masses, topological and stereo chemical control through ring opening transesterification polymerization (ROP) of cyclic monomeric esters.[31] Several metal and organic catalysts have been described for the ROP of cyclic monomeric esters.[32–37] In particular the polylactide (PLA) polymer has been widely investigated.[38] 10^8 kg $year^{-1}$ of PLA were produced industrially by ROP in 2013.[31] PLA can be produced completely amorphic or with crystalline domainsof up to 40% depending on its stereo-chemical composition. This has a huge influence on its mechanical properties, they are ranging from soft and elastic materials to stiff and high strength materials. PLA polymers are mainly used in medical chemistry and in packaging.[39]

A patent research has been carried out using IP7-Compass software. The keywords *degrad* and *ester were searched for in the IPC classifications C08 (organic macromolecular compounds) and C09 (dyes; paints; polishes; natural resins; adhesives; compositions not other provided for; applications of materials not other provided for). The star (*) indicates that anything else can be written in this position. The resulting plot of published patent families in the years from 1950 to 2019 is depicted in Figure 1.1.

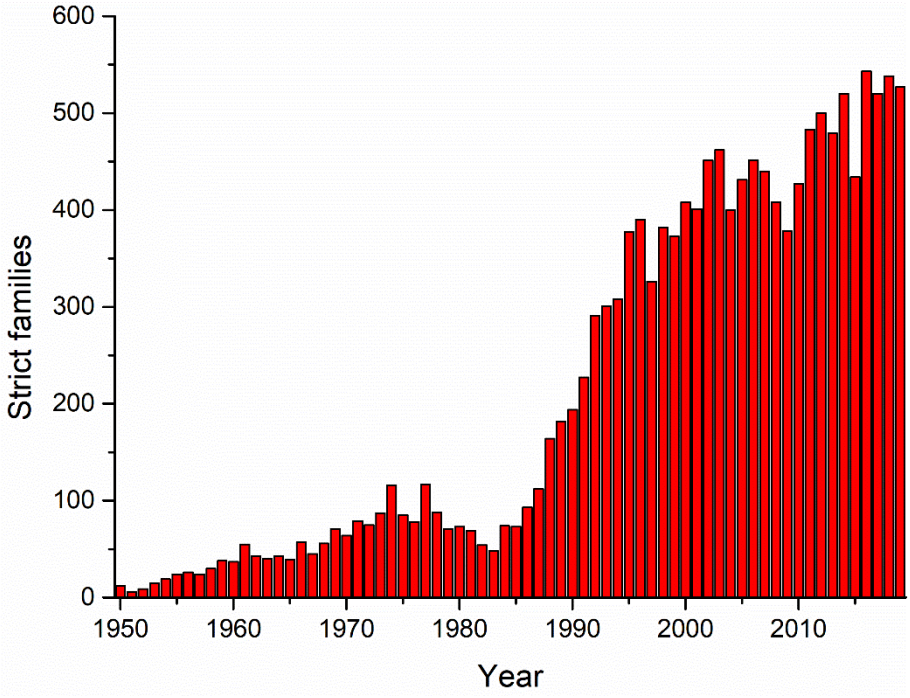

Figure 1.1. Evolution of published patents including the keywords *degrad* and *ester from 1950 to 2019 in the IPC classifications C08 and C09.

Starting from 1985 the number of published patent families with the keywords *degrad* and *ester increased drastically pointing out the importance of degradability through ester groups in the recent time. However, it has to be taken into account that also the total number of patent families in the classifications C08 and C09 is increasing over the years, but at a lower rate.

The European Union has communicated the goal to play a central role in supporting the move towards a circular economy for plastics to 2030. Setting the objective to make all plastic packaging reusable or recyclable in a cost-effective manner and a “drastic” decrease in the

leakage of plastics into the environment.[40] Hence, their most important objective are reusable and recyclable materials. However, introducing degradability into some polymers can facilitate the recycling or reusing of other materials. For example, making the coatings which are used to improve the mechanical properties and oil/grease resistance of paper used in fast-food wrappings degradable does facilitate the recycling in this kind of single-use paper products.[41] Another example is to make the pressure sensitive adhesive (PSA), which is used to adhere labels to glass bottles degradable in the washing solution that is used to clean the glass bottles for their reuse or recycling. Therefore, saving the extra step of removing the label and PSA from the glass bottle and hence reducing the energy, which is needed in the cleaning process of glass bottles.[42] This path is interesting for waterborne polymers, because they do not reach the production volume of the commodity polymers such as PE and PP.

Taking into account the facts mentioned above, the objective of this thesis is to incorporate ester groups into polymers by an emulsion polymerization process. There are different ways to incorporate degradability into a polymeric chain. One approach is to include the ester groups into the side-chain of the polymer through acrylated oligoesters, leading to degradable side-chains of the polymer. The second approach is to crosslink the polymer by diacrylated oligoesters, leading to degradable crosslinks. Finally, the third approach is to incorporate ester groups directly into the polymer backbone, leading to degradability thereof. This last approach is covered using two strategies in this work, on the one hand the thiol-ene polymerization of ester containing thiol and/or ene monomers and on the other hand the radical ring opening polymerization of cyclic ketene acetals. The three approaches are shown in Figure 1.2.

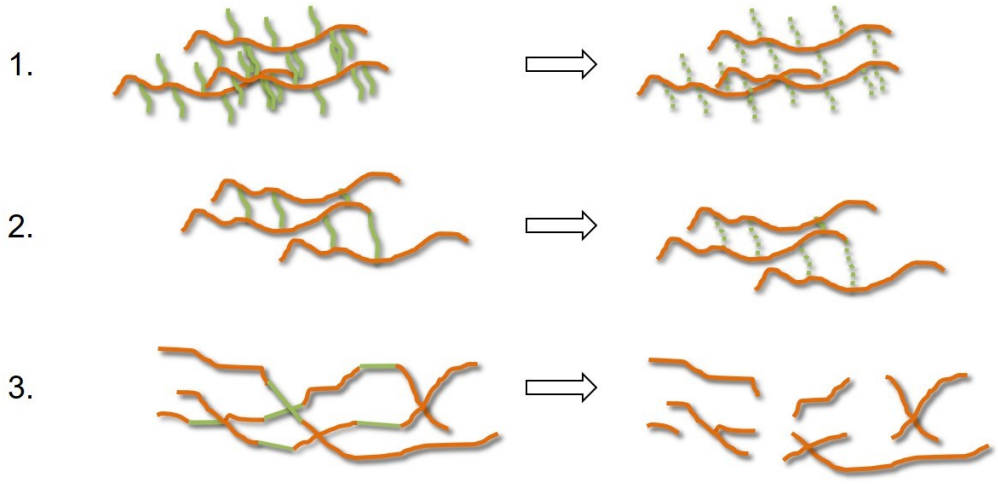

Figure 1.2. Different approaches to include degradability into polymers. Into the polymer sidechains (1.), the crosslinks (2.) and the polymer backbone (3.).

Most of the experiments have been carried out at a fundamental stage to insert degradable units, without a specific application in mind. However, some of them (especially the second approach of degradable crosslinks) have been explored for the synthesis of PSAs, with the objective to obtain a PSA that loses its adhesive properties under certain conditions due to hydrolysis of the ester groups.

The majority of the work described in this thesis has been carried out in emulsion polymerization. Therefore, a brief description of the principle of emulsion polymerization is given in the following part.

1.2. Emulsion polymerization

Emulsion polymerization is a heterogeneous free radical process, in which colloidal particles are created dispersed in a continuous medium. The resulting polymer dispersions are called latices.[28]

A mostly hydrophobic monomer is emulsified through an emulsifier in a continuous medium (mostly water). The emulsifier forms micelles above the critical micelle concentration (CMC). At the beginning of the emulsion polymerization the monomer is distributed between monomer droplets (around 1-10 µm), the water phase and micelles (around 5-10 nm). Water-soluble (i. e. potassium persulfate (KPS)) or non-water soluble (i. e. 2-2'-azobisisobutyronitrile (AIBN)) initiators are used for the initiation. Commonly used monomers are butadiene, styrene, acrylonitrile, vinyl esters, acrylic and methacrylic esters.[43]

The radicals are generated in the water phase, if water-soluble initiators are used. The generated radicals are mostly too hydrophilic to enter into the micelles. Because of this, they are growing in the water phase first, until they reach a critical length and are sufficiently hydrophobic for entering into the micelles, as shown in Figure 1.3. This process is called heterogeneous nucleation.[44]

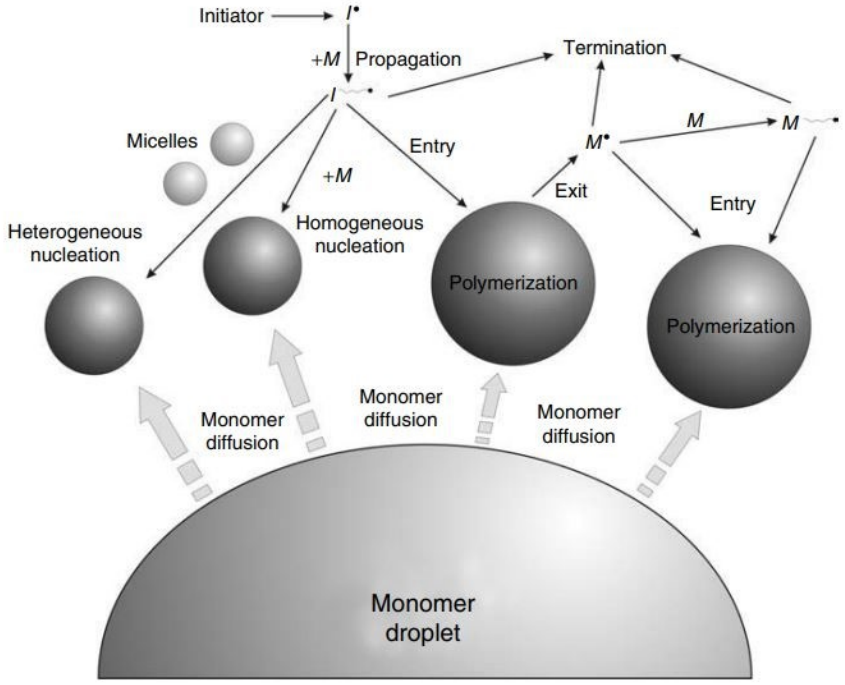

Figure 1.3. Mechanism involved in emulsion polymerization.[44]

An entry into the monomer droplets is not likely, because the surface area of these is around three magnitudes lower than the surface area of the micelles. Another possibility is the homogeneous nucleation, if the oligo-radicals exceed the critical length and reach a specific length they are not soluble in the water phase anymore. The emulsifier is adsorbed and a new micelle is formed. Depending on the water solubility of the monomers, the homogeneous (highly water-soluble monomers) or heterogeneous (water-insoluble monomers) nucleation is dominant. For control of chain architecture and distribution of molar masses in emulsion polymerization it is possible to use chain transfer agents (CTA).[45] These are defined by IUPAC as substances,

which are able to react with a chain carrier (transition species with active center), to deactivate the original chain and to generate a new chain carrier. It is a transfer of the active center.[46]

1.2.1. Emulsion polymerization – Kinetics

The first qualitative model for ab-initio emulsion polymerization was suggested by Harkins.[47] The polymerization can be divided into three phases, the nucleation phase (I), the particle growth phase (II) and the monomer depletion phase (III).

In phase I, the formation of polymer particles takes place. Monomer droplets, monomer containing micelles and polymer particles are coexisting in this phase. The number of micelles is decreasing with the time through the formation of polymer particles or emulsifier, which is provided to stabilize the growth of polymer particles. The end of the first phase is typically reached at a monomer conversion of 5-10% and around 10^{17}-10^{18} formed particles per liter. The number of particles stays constant, in case that there is no coagulation. In phase II, the polymerization rate is more or less constant. Monomer droplets and polymer particles coexist in this phase. Monomer diffuses from the monomer droplets through the water phase to the growing polymer particles where it is consumed. Phase III starts as soon as the monomer droplets are used up. The concentration of monomer in the polymer particles decreases in this phase until no monomer is left and the polymerization is ended.

The model of Harkins was upgraded by Smith and Ewart. They showed that the rate of the emulsion polymerization, which happens inside the polymer particles R_p can be described by Equation 1.1.[48] With the rate constant of propagation k_p, the monomer concentration in the

polymer particles $[M]_P$, the average number of radicals per particle $\tilde{n}$, the number of particles per volume element N_p and the Avogadro constant N_A.

$$R_p = k_p \cdot [M]_P \cdot \tilde{n} \cdot \frac{Np}{N_A} \tag{1.1}$$

The average number of radicals per particle is important for the rate of polymerization in phase II and III. Three cases can be distinguished depending on the radical entry and exit rates from the polymer particles and bimolecular termination in the particles that depend mainly on particle size,generation rate of radicals in the aqueous phase and monomer solubility.

Case 1: $\tilde{n}$ < 0.5: The average number of radicals per particle can drop below 0.5 in case that the rate of radical exit and the termination in the water phase is not negligible.

Case 2: $\tilde{n}$ = 0.5: This is the case if the radical exit is insignificant compared to the radical entry and if the particle size is too small to accommodate more than one radical at the same time. The polymerization starts if a radical enters the particle. If a second radical enters the particle the polymerization stops through termination. Accordingly, a particle either contains a radical and is active or it does not contain a radical and is inactive. This behavior is referred to as 1/0-kinetic (1 for the active state and 0 for the inactive state). This results in an average radical number per particle of 0.5. This case presumes low initiation rate and a negligible termination in the water phase.

Case 3: $\tilde{n}$ > 0.5: To reach an average radical number per particle which is above 0.5, there have to be two or more radicals in some particles because at any time there is a

significant amount of particles in an inactive state. This is the case for large particles and/or low rate constants of termination and/or large generation rate of radicals.

A predominant part of emulsion polymerization follows the mechanism described in case 2.
The polymer particle concentration N_p which is mentioned in Equation 1.1 is important for the rate of polymerization and for the degree of polymerization. As shown in Equation 1.2, Np depends on the concentration of emulsifier [*S*], the radical forming rate R_i for the concentration of initiator, (Equation 1.3) and the rate of volume increase of the polymer particles μ. k is an empiric constant. Its value is between 0.37 and 0.53 depending on the condition of the process.

$$N_p = k \cdot \left(\frac{R_i}{\mu}\right)^{\frac{2}{5}} \cdot (a_S \cdot [S])^{\frac{3}{5}} \tag{1.2}$$

For Smith-Ewart case 2 Equation 1.3, in which k_a is the entry rate coefficient, $[P_{tot}]_W$ is the concentration of radicals in the aqueous phase and w_m is the molecular weight of the repeated unit in the polymer chain, is valid.

$$\bar{M}_n^{inst} \approx \frac{k_p[M]_p}{k_a \cdot [P_{tot}]_W} w_m \tag{1.3}$$

If the radical termination in the aqueous phase is negligible, Equation 1.4 results from the balance of radicals in the aqueous phase under quasi steady-state conditions in which f is the efficiency factor of the initiator radicals, k_I is the rate coefficient for initiator decomposition, $[I]_W$ is the concentration of the thermal initiator in the aqueous phase and V_W is the volume of the aqueous phase.

$$k_a[P_{tot}]_W = 2fk_I[I]_W \frac{N_A V_W}{N_p} \quad (1.4)$$

The combination of Equation 1.3 and Equation 1.4 leads to Equation 1.5.

$$\bar{M}_n^{inst} \approx \frac{k_p[M]_p}{2fk_I[I]_W N_A} \frac{N_p w_m}{V_W} \quad (1.5)$$

Hence, the molecular weight increases with the number of polymer particles and the concentration of monomer in the polymer particles and decreases as the initiator concentration increases.[28]

According to Equations 1.1 and 1.5, in emulsion polymerization under conditions of Case 2, polymerization rate and molar masses can be simultaneously increased if the number of polymer particles is increased. This is a unique feature of the emulsion polymerization that cannot be achieved in homogeneous polymerizations.

1.2.2. Miniemulsion polymerization

Even if mainly emulsion polymerization process has been used within this manuscript, due to some limitations of it miniemulsion polymerization have been used. In the following paragraphs a brief description of it is given.

In miniemulsion polymerization, the monomer droplet size is significantly reduced to 50-1000~nm. These small monomer droplet sizes are reached by the use of an appropriate emulsifier and emulsification apparatus.[28] Miniemulsification adds complexity and costs to the

process compared to emulsion polymerization, but it enables to reach complex materials which are not possible to be produced in emulsion polymerization.[49]

A system which contains the dispersed phase, the continuous phase, a surfactant and an osmotic pressure agent, also known as costabilizer, is sheared to form a miniemulsion with small stable monomer droplets. These droplets are polymerized subsequently as shown in Figure 1.4.[50]

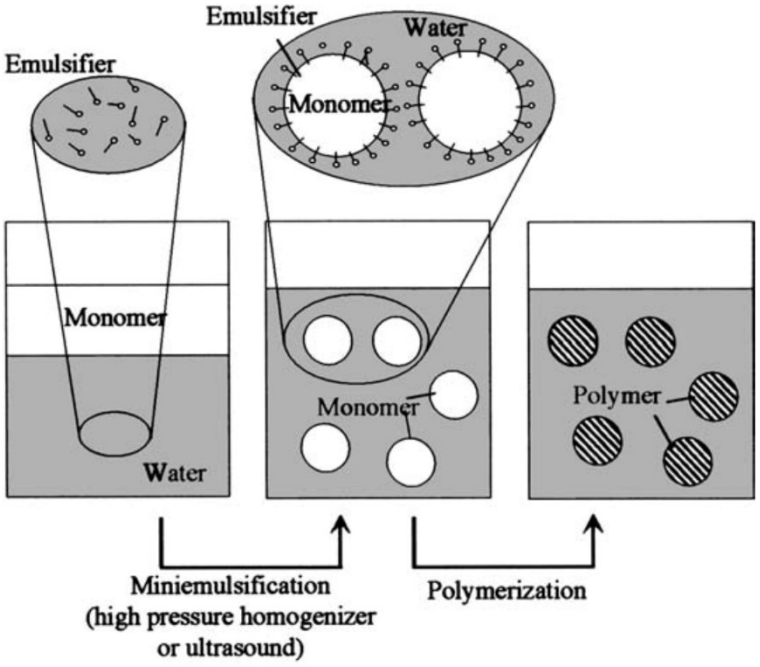

Figure 1.4. Principle of miniemulsion polymerization.[50]

A significantly higher energy than the difference in surface energy $\gamma\Delta A$ (with the surface/interface tension γ and the difference between former and newly formed interface ΔA) is required to

form small monomer droplets. During agitation a large part of the energy is absorbed by the viscous resistance. Different techniques are used for the preparation of miniemulsions depending on the requirements, such as volume of the miniemulsion and monomer droplet size. Ultrasonication for example is especially used for the homogenization of small volumes.[50] Liquids rupture to form cavities or cavitation bubbles when they are irradiated. Imploding cavitation bubbles cause shockwaves in the liquid and form jets with locally high velocities which set the liquid into a turbulent motion.[51,52] This can cause droplet disruption but the exact process is not fully understood yet. During sonication the fusing-fission rate equilibrium is depending on the amount of the emulsifier. The principle of miniemulsification through ultrasound is shown in Figure 1.5.[50]

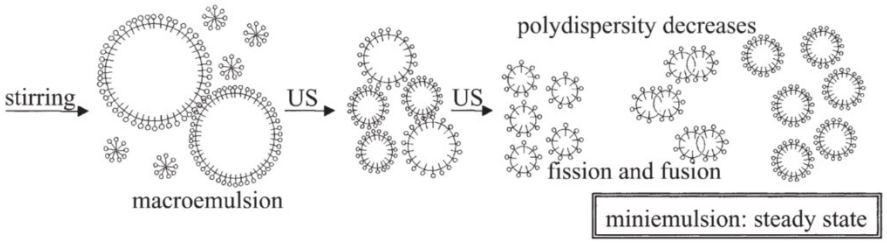

Figure 1.5. Formation of a miniemulsion through ultrasound.[50]

Another possibility for the miniemulsification are high-pressure homogenizers which can be used for higher volumes. The medium is passed to a narrow gap of a valve. The droplets are elongated by the elongational flow at the entrance as shown in Figure 1.6. Turbulences at the exit of the gap are breaking the elongated droplets. This leads to an increase in surface area of the droplets,

if the increased surface area is not covered by emulsifier, it leads to coagulation of the droplets. Hence, the broadness of the droplet size distribution and the droplet size both decrease with the number of passes.[49]

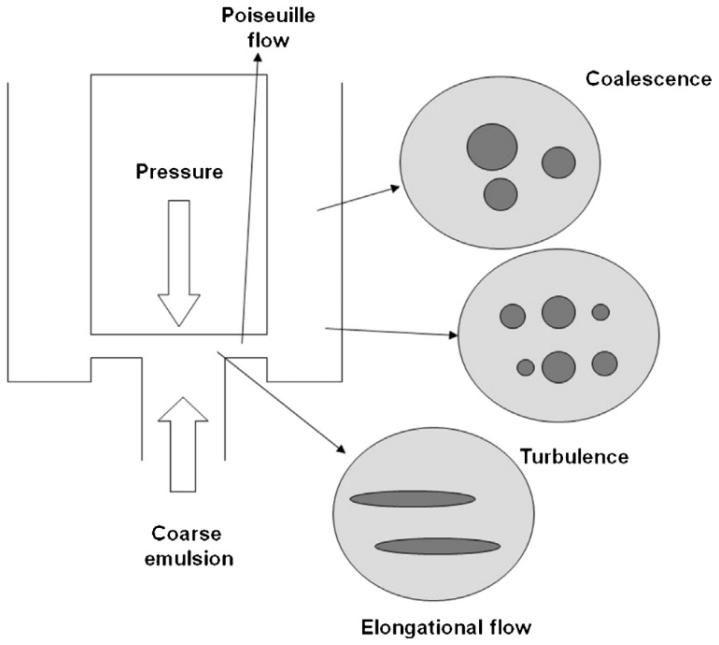

Figure 1.6. Principle of miniemulsification by high-pressure homogenization.[49]

High-pressure homogenizers seem to be attractive to applications on a industrial scale as high capacity high-pressure homogenizers with 21,000~L/h at 400~bar are available. Often one pass is not sufficient to obtain the required droplet size. Two high-pressure homogenizers can be used in series or also loop arrangements are possible to overcome this problem.[49]

A hydrophobic agent can be added to the dispersed phase to slow down the destabilization through Ostwald ripening. A steady-state of miniemulsification is reached when an efficient homogenization is applied and a sufficient amount of hydrophobe is used. Alkanes of different lengths, hydrophobic co-monomers, hydrophobic dyes, CTAs, etc. can be used at hydrophobe. After sonification the Laplace pressure is still higher than the osmotic pressure created by the hydrophobe. Hence, miniemulsification results in a system with critical stability. This miniemulsions undergo droplet growth on the timescale of hundreds of hours by collisions or hydrophobe exchange until a zero effective pressure is reached. A second dose of emulsifier which is added after the dispersion step can provide immediate long-term colloidal stability by going to the interface of the droplet and decreasing the interfacial tension between oil and water phase and also the coupled Laplace pressure.[50]

1.3. Outline of the thesis

This thesis entitled "w*aterborne degradable polyester nanoparticles*" is divided into seven chapters. A short introduction to each chapter is given below.

Chapter 1 gives a general introduction to the topic and describes the motivation and objective of this thesis.

In **Chapter 2** the synthesis of diacrylated oligester crosslinkers from macromonomers, which are synthesized by ring opening polymerization, is described. These crosslinkers were incorporated into a conventional seeded semibatch waterborne PSA formulation, leading to degradable crosslinks. Their degradability and hence loss of adhesive properties due to degradation by hydrolysis of ester groups was explored.

In **Chapter 3** the radical step-growth thiol-ene polymerization is described as a method to incorporate ester groups into the polymer backbone. Moreover, a mathematical model to obtain insight into its complex kinetics is developed.

Chapter 4 deals with the thiol-ene emulsion polymerization. Batch and semibatch polymerization processes are compared.

In **Chapter 5** an overview of the radical ring opening polymerization of the cyclic ketene acetal 2-methylene-1,3-dioxepane (MDO) is given. Additionally, reactivity ratios for the copolymerization of MDO with three sets of different monomers (vinyl, acrylate and methacrylate double bonds) are provided.

Chapter 6 explores the challenges of polymerizing MDO in waterborne systems. The kinetics of the hydrolysis of MDO in water is investigated and the emulsion copolymerization of MDO with different comonomers (acrylates and vinyl esters) is examined. The majority of this work was carried out during an Internship at *tesa SE* in the waterborne acrylic adhesives laboratory in Norderstedt, Germany.

Finally, in **Chapter 7** the most relevant conclusions of this thesis are summarized.

1.4. References

(1) Clifton, D.; Amran, A. The Stakeholder Approach: A Sustainability Perspective. *J. Bus. Ethics* **2011**, *98*, 121–136. https://doi.org/10.1007/s10551-010-0538-6.

(2) Goodland, R. The Concept of Environmental Sustainability. *Annu. Rev. Ecol. Syst.* **1995**, *26*, 1–24.

(3) De Smet, M. *A CIRCULAR ECONOMY FOR PLASTICS*; European Comission: Brussels - Belgium, 2019. https://doi.org/10.2777/269031.

(4) Eriksen, M.; Maximenko, N.; Thiel, M.; Cummins, A.; Lattin, G.; Wilson, S.; Hafner, J.; Zellers, A.; Rifman, S. Plastic Pollution in the South Pacific Subtropical Gyre. *Mar. Pollut. Bull.* **2013**, *68* (1–2), 71–76. https://doi.org/10.1016/j.marpolbul.2012.12.021.

(5) Eriksen, M.; Lebreton, L. C. M.; Carson, H. S.; Thiel, M.; Moore, C. J.; Borerro, J. C.; Galgani, F.; Ryan, P. G. Plastic Pollution in the World's Oceans: More than 5 Trillion Plastic Pieces Weighing over 250,000 Tons Afloat at Sea. *PLoS One* **2014**, 1–15. https://doi.org/10.1371/journal.pone.0111913.

(6) Laist, D. W. Impacts of Marine Debris: Entanglement of Marine Life in Marine Debris Including a Comprehensive List of Species with Entanglement and Ingestion Records. In *Marine Debris*; Coe, J. M., Rogers, D. B., Eds.; Springer, 1997; pp 99–139.

(7) Leslie, H. A.; Velzen, M. J. M. Van; Brandsma, S. H.; Vethaak, A. D.; Garcia-vallejo, J.;

Lamoree, M. H. Discovery and Quantification of Plastic Particle Pollution in Human Blood. *Environ. Int.* **2022**, *163*, 107199. https://doi.org/10.1016/j.envint.2022.107199.

(8) Jenner, L. C.; Rotchell, J. M.; Bennett, R. T.; Cowen, M. Science of the Total Environment Detection of Microplastics in Human Lung Tissue Using MFTIR Spectroscopy. *Sci. Total Environ.* **2022**, *831*, 154907. https://doi.org/10.1016/j.scitotenv.2022.154907.

(9) Hundertmark, T.; Mayer, M.; Mcnally, C.; Simons, T. J.; Witte, C. *How plastics-waste recycling could transform the chemical industry*. https://www.mckinsey.com/industries/chemicals/our-insights/how-plastics-waste-recycling-could-transform-the-chemical-industry#.

(10) Brister, E. H.; Johnston, T.; King, C. L.; Thames, S. F. New Monomers from Vegetable Oils. In *Specialty Monomers and Polymers*; Havelka, K., Ed.; American Chemical Society: Washington, DC, 2000; pp 159–169.

(11) Xia, Y.; Larock, R. C. Vegetable Oil-Based Polymeric Materials: Synthesis, Properties, and Applications. *Green Chem.* **2010**, *12*, 1893–1909. https://doi.org/10.1039/c0gc00264j.

(12) Thomsett, M. R.; Storr, T. E.; Managhan, O. R.; Stockman, R. A.; Howdle, S. M. Progress in the Synthesis of Sustainable Polymers from Terpenes and Terpenoids. *Green Mater.* **2016**, *4* (3), 115–134. https://doi.org/10.1680/jgrma.16.00009.

(13) Noppalit, S.; Simula, A.; Ballard, N.; Callies, X.; Asua, J. M.; Billon, L. Renewable Terpene Derivative as a Biosourced Elastomeric Building Block in the Design of Functional Acrylic Copolymers. *Biomacromolecules* **2019**, *20*, 2241–2251. https://doi.org/10.1021/acs.biomac.9b00185.

(14) Noppalit, S.; Simula, A.; Billon, L. Paving the Way to Sustainable Waterborne Pressure-Sensitive Adhesives Using Terpene-Based Triblock Copolymers. *ACS Sustain. Chem. Eng.* **2019**, *7*, 17990–17998. https://doi.org/10.1021/acssuschemeng.9b04820.

(15) Noppalit, S.; Simula, A.; Billon, L.; Asua, J. M. On the Nitroxide Mediated Polymerization of Methacrylates Derived from Bio-Source Terpenes in Miniemulsion, a Step towards Sustainable Products. *Polym. Chem.* **2020**, *11*, 1151–1160. https://doi.org/10.1039/c9py01667h.

(16) Deuss, P. J.; Scott, M.; Tran, F.; Westwood, N. J.; Vries, J. G. De; Barta, K. Aromatic Monomers by in Situ Conversion of Reactive Intermediates in the Acid-Catalyzed Depolymerization of Lignin. *J. Am. Chem Soc.* **2015**, *137*, 7456–7467. https://doi.org/10.1021/jacs.5b03693.

(17) Shuai, L.; Saha, B. Towards High-Yield Lignin Monomer Production. *Green Chem.* **2017**, *19*, 3752–3758. https://doi.org/10.1039/c7gc01676j.

(18) Wang, S.; Shuai, L.; Saha, B.; Vlachos, D. G.; Iii, T. H. E. From Tree to Tape: Direct Synthesis of Pressure Sensitive Adhesives from Depolymerized Raw Lignocellulosic Biomass. *ACS Cent. Sci.* **2018**, *4*, 701–708. https://doi.org/10.1021/acscentsci.8b00140.

(19) Galbis, J. A.; Garc, M. D. G.; Paz, M. V. De; Galbis, E. Synthetic Polymers from Sugar-Based Monomers. *Chem. Rev.* **2016**, *116*, 1600–1636. https://doi.org/10.1021/acs.chemrev.5b00242.

(20) Sard, H.; Desport, J. S.; Mantione, D.; Barandiaran, M. J.; Mecerreyes, D. Synthesis of Three Different Galactose-Based Methacrylate Monomers for the Production of Sugar-Based Polymers. *Carbohydr. Res.* **2016**, *432*, 50–54. https://doi.org/10.1016/j.carres.2016.06.008.

(21) Desport, J. S.; Moreno, M.; Barandiaran, J. Fructose-Based Acrylic Copolymers by Emulsion Polymerization. *Polymers (Basel).* **2018**, *10* (488). https://doi.org/10.3390/polym10050488.

(22) Xiao, J.; Tolbert, T. J. Synthesis of Polymerizable Protein Monomers for Protein-Acrylamide Hydrogel Formation. *Biomacromolecules* **2009**, *10*, 1939–1946.

(23) Aguirre, M.; Hamzehlou, S.; González, E. *Renewable Feedstocks in Emulsion Polymerization: Coating and Adhesive Applications*, 1st ed.; Elsevier Inc., 2020; Vol. 56. https://doi.org/10.1016/bs.ache.2020.07.004.

(24) Anastas, P. T.; Erythropel, H. C.; Zimmermann, J. B.; de Winter, T.; Petitjean, L. The Green ChemisTREE: 20 Years after Taking Root with 12 Principles. *Green Chem.* **2018**, *20* (9), 1929–1961. https://doi.org/10.1039/c8gc00482j.

(25) Anastas, P. T.; Zimmerman, J. B. Design through the 12 Principles of Green Engineering.

Environ. Sci. Technol. **2003**, *37*, 94–101.

(26) Salehpour, S.; Dubé, M. A. Applying the Principles of Green Chemistry to Polymer Production Technology. *Macromol. React. Eng.* **2014**, *8*, 7–28. https://doi.org/10.1002/mren.201300103.

(27) Zhang, Y.; Dubé, M. A. *Polymer Reaction Engineering of Dispersed Systems*; Pauer, W., Ed.; Springer International Publishing AG, 2017; Vol. I.

(28) Barandiaran, M. J.; de la Cal, J. C.; Asua, J. M. Emulsion Polymerization. In *Polymer Reaction Engineering*; Asua, J. M., Ed.; Blackwell Publishing: Oxford, 2007; pp 233–272.

(29) Vert, M. Aliphatic Polyesters: Great Degradable Polymers That Cannot Do Everything. *Biomacromolecules* **2005**, *6*, 538–546.

(30) Siracusa, V.; Dalla, M. Biodegradable Polymers for Food Packaging : A Review. *Trends Food Sci. Technol.* **2008**, *19* (12), 634–643. https://doi.org/10.1016/j.tifs.2008.07.003.

(31) Hillmyer, M. A.; Tolman, W. B. Aliphatic Polyester Block Polymers: Renewable, Degradable, and Sustainable. *Acc. Chem. Res.* **2014**, *47*, 2390–2396.

(32) Keefe, B. J. O.; Hillmyer, M. A.; Tolman, W. B.; Hillmyer, M. A.; Tolman, W. B. Polymerization of Lactide and Related Cyclic Esters by Discrete Metal Complexes. *J. Chem. Soc., Dalt. Trans.* **2001**, 2215–2224. https://doi.org/10.1039/b104197p.

(33) Dechy-cabaret, O.; Martin-vaca, B.; Bourissou, D. Controlled Ring-Opening

Polymerization of Lactide and Glycolide. *Chem. Rev.* **2004**, *104*, 20–23.

(34) Kamber, N. E.; Jeong, W.; Waymouth, R. M.; Pratt, R. C.; Lohmeijer, B. G. G.; Hedrick, J. L. Organocatalytic Ring-Opening Polymerization. *Chem. Rev.* **2007**, *107*, 5813–5840.

(35) Williams, C. K.; Hillmyer, M. A. Polymers from Renewable Resources: A Perspective for a Special Issue of Polymer Reviews. *Polym. Rev.* **2008**, *48*, 1–10. https://doi.org/10.1080/15583720701834133.

(36) Platel, R. H.; Hodgson, L. M.; Williams, C. K.; Platel, R. H.; Hodgson, L. M.; Williams, C. K. Biocompatible Initiators for Lactide Polymerization. *Polym. Rev.* **2008**, *48*, 11–63. https://doi.org/10.1080/15583720701834166.

(37) Stanford, M. J.; Dove, A. P. Stereocontrolled Ring-Opening Polymerisation of Lactide. *Chem. Soc. Rev.* **2010**, *39*, 486–494. https://doi.org/10.1039/b815104k.

(38) Vilela, C.; Sousa, A. F.; Fonseca, A. C.; Serra, A. C.; Coelho, J. F. J.; Freire, C. S. R.; Silvestre, A. J. D. The Quest for Sustainable Polyesters - Insights into the Future. **2014**, 3119–3141. https://doi.org/10.1039/c3py01213a.

(39) Avérous, L. Polylactic Acid : Synthesis , Properties and Applications. In *Monomers, Polymer and Composites from Renewable Resources*; Naceur Belgacem, M., Gandini, A., Eds.; Elsevier Ltd, 2008; pp 433–450.

(40) Watkins, E.; Schweitzer, J. Moving towards a Circular Economy for Plastics in the EU by

2030. *Sci. Solut. a more Sustain. Eur.* **2018**.

(41) Carter, M. C. D.; Hejl, A.; Wood, S.; Einsla, B.; Janco, M.; Defelippis, J.; Cooper, R. J.; Even, R. C. Backbone-Degradable Vinyl Acetate Latex: Coatings for Single-Use Paper Products. *ACS Macro Lett.* **2021**, *10*, 591–597. https://doi.org/10.1021/acsmacrolett.1c00172.

(42) Wenzel, F.; Agirre, A.; Aguirre, M.; Leiza, J. R. Incorporation of Novel Degradable Oligoester Crosslinkers into Waterborne Pressure Sensitive Adhesives: Towards Removable Adhesives. *Green Chem.* **2020**, *22*, 3272–3282. https://doi.org/10.1039/D0GC00463D.

(43) Chern, C. S. Emulsion Polymerization Mechanisms and Kinetics. *Prog. Polym. Sci.* **2006**, *31*, 443–486. https://doi.org/10.1016/j.progpolymsci.2006.02.001.

(44) Asua, J. M. Emulsion Polymerization: From Fundamental Mechanisms to Process Developments. *J. Polym. Sci., Part A Polym. Chem.* **2004**, *42*, 1025–1041.

(45) Plessis, C.; Arzamendi, G.; Leiza, J. R.; Alberdi, J. M.; Schoonbrood, H. A. S.; Charmot, D.; Asua, J. M. Seeded Semibatch Emulsion Polymerization of Butyl Acrylate: Effect of the Chain-Transfer Agent on the Kinetics and Structural Properties. *J. Polym. Sci. Part A Polym. Chem.* **2001**, *39*, 1106–1119.

(46) Jenkins, A. D.; Jones, R. G.; Moad, G. Terminology for Reversible-Deactivation Radical Polymerization Previously Called “Controlled” Radical or “Living” Radical Polymerization

(IUPAC Recommendations 2010)*. *Pure Appl. Chem.* **2010**, *82* (2), 483–491. https://doi.org/10.1351/PAC-REP-08-04-03.

(47) Harkins, D. A General Theory of the Mechanism of Emulsion Polymerization. *J. Am. Chem Soc.* **1946**, *69*, 1428–1444.

(48) Smith, W. V; Ewart, R. H. Kinetics of Emulsion Polymerization. *J. Chem. Phys.* **1948**, *592*, 592–599. https://doi.org/10.1063/1.1746951.

(49) Asua, J. M. Challenges for Industrialization of Miniemulsion Polymerization. *Prog. Polym. Sci.* **2014**, *39* (10), 1797–1826. https://doi.org/10.1016/j.progpolymsci.2014.02.009.

(50) Landfester, K. Miniemulsions for Nanoparticle Synthesis. *Top Curr Chem* **2003**, *227*, 75–123. https://doi.org/10.1007/b10835.

(51) Lauterborn, W.; Hentschel, W. Cavitation Bubble Dynamics Studied by High Speed Photography Holography: Part One. *Ultrasonics* **1985**, 260–268.

(52) Lauterborn, W.; Hentschel, W. Cavitation Bubble Dynamics Studied by High Speed Photography and Holography: Part Two. *Ultrasonics* **1986**, 59–65.

Chapter 2. Synthesis of degradable macromonomers and crosslinkers and their polymerization in dispersed media: degradable and removable pressure-sensitive adhesives

2.1. Introduction

One of the most important challenges of the 21st century is to diminish the amount of residues produced by humans. The World Bank predicts that the yearly-generated amount of municipal solid waste is going to increase from 1.3 billion tons up to 2.2 billion tons in the year 2025. Next to organic, paper and plastic waste, glass waste makes up for 5% of the global solid waste composition.[1] Glass bottles and jars are 100% and infinitely recyclable.[2] However, for example in the US in the year 2015 only 33.2% of the waste glass were recycled.[3] Even better than recycling, which means crushing the glass into glass cullet and manufacturing new glass from the glass cullet, would be reusing glass bottles. According to the annual worldwide production,

around 5 billion of glass bottles could be reusable. Returned bottles are cleaned in bottle cleaning machines at temperatures of around 85 ºC using additives containing a basic solution (e.g., sodium hydroxide). During the cleaning process the labels and adhesives of the glass bottles have to be removed[4] and for that the exposure to heat, jetted hot gas or sprayed hot liquid having a predetermined temperature is necessary.[5] Another method for removing bottle labels and adhesives is the usage of amidine solvents such as 1,8-diazobicyclo[5.4.0]undec-7-ene (or DBU) or fatty N,N-dialkylamides as described elsewhere.[6] All in all, the described industrial processes are either energy intensive or require the use of toxic chemicals.

In this chapter we addressed this issue by synthesizing oligoester based macromonomers and crosslinkers to be incorporated in formulations of waterborne polymer dispersions. The synthesis of acrylated oligoesters, so called macromonomers, by ring opening polymerization (ROP) and their assessment for the synthesis of polymers with degradable sidechains are described. Furthermore, the synthesis of diacrylated oligoester crosslinkers and their incorporation into a waterborne PSA formulation is investigated. The resulting PSA contains crosslinking-points which are degradable through hydrolysis and is therefore removable under aqueous basic solutions.

In the first part, the synthesis and application of macromonomers especially in the field of medical chemistry has been covered and a brief summary of the works published in the literature are summarized in the following paragraphs. Ferrari et al. reported the synthesis of degradable oligoester macromonomers[7] by ROP using 2-hydroxyethylmethacrylate (HEMA) as initiating species and lactide and *ε*-caprolactone as monomers. The degradability over time of waterborne particles obtained through emulsion homo-polymerization of the macromonomers was proven by

measurements of pH and particle size indicating a complete degradation of the particles within 6-9 months.[8] However, the solids content of the waterborne dispersions were low (5 wt%) andt they were synthesized for an application in the field of medical chemistry, especially for drug delivery[9–13]. Lactide based macromonomers were used by Ferrari et al. for the synthesis of biodegradable nanoparticles by semibatch emulsion polymerization.[14,15]

Several publications describe the production of acrylated polyethylene glycol (PEGylated) nanoparticles as promising way to deliver poorly water-soluble drugs. On one hand, the production of polyethylene glycol and polycaprolactone (PEG-PCL) based nano-medicines is described.[16] A macromonomer based on HEMA and 3 units of ε-caprolactone (CL) has been used together with a PEGylated methacrylate to produce nanoparticles in semibatch emulsion polymerization.[13,17] On the other hand, there are publications dealing with polyethylene glycol and polylactic acid (PEG-PLA) based nanoparticles. Ferrari et al. studied the effect of solvents on the synthesis of nanoparticles from lactide based macromonomers and PEG. They dissolved longer macromonomers (with more than 5 lactic acid units) in dichloromethane or ethanol before their addition to the reactor.[18] The encapsulation of hydrophobic anti-inflammatory drugs into nanoparticles based on PLA macromonomers by miniemulsion polymerization at low temperatures has been demonstrated recently.[19] Macromonomers based on ε-caprolactone and L-lactide have been synthesized by Severtson et al. with the aim to produce PSAs in co-polymerization with acrylic monomers.[20]

ROP allows not only the synthesis of macromonomers but also the synthesis of diacrylated oligoesters, which can be used as crosslinkers in free radical polymerization. They are degradable and hence, the possibility of using this crosslinkers in a PSA formulation where

typically the cohesiveness is achieved by regulating the crosslinking degree of the films is explored. The particularity sought in this case is the possibility to trigger the degradation which will open the door to degradable PSA's with potential application on beverage labels and the recycling of the glass bottles.

2.2. Synthesis of degradable macromonomers and crosslinkers

The methods for the synthesis of macromonomers and oligoester crosslinkers are described in the following part. Anaytical methods, such as Soxhlet extraction, GPC, DSC, ^{1}H-NMR and DLS are described in the Appendix of this thesis.

2.2.1. Synthesis of Macromonomers

ε-Caprolactone (CL) and L-Lactide (LA) based macromonomers (MM) and co-macromonomers (co-MM) were synthesised by ring opening polymerization (ROP) in bulk as already described in the literature (Scheme 2.1).[7,8,14,20]

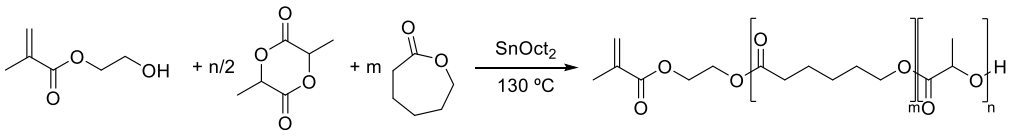

Scheme 2.1. Synthesis of macromonomers from Lactide and ε-caprolactone.

In this polymerization process tin(II) bis-(2-ethylhexanoate) ($Sn(Oct)_2$) serves as catalyst and 2-hydroxyethyl methacrylate (HEMA) as initiator. The repeating units of the macro- and co-macromonomers are controlled by the molar ratio of the monomers (L-lactide and ε-caprolactone) to the initiating species HEMA. The reactants and the catalyst (0.1% wbm) were placed in a 50 mL round-bottom flask (RBF) at 130 °C, and stirred continuously with a magnetic stirrer under N_2 flux (flow rate 15 ml/min) for 6 hours.

The results of the characterization of the macromonomers by GPC and DSC measurements are shown in Table 2.1.

Table 2.1. Characterization of the synthesized macromonomers by NMR and GPC.

Macromonomer	Theoretical Molar mass [g/mol]	Number of units (NMR)	M_n [g/mol] (GPC)	T_g [ºC]	T_m [ºC]
MCL3	472	3.9	575	-56	-
MCL6	814	6.2	837	-64	18
MCL12	1498	12.6	1566	< -60	38
MLA6	563	5.6	533	10	-
MLA12	994	11.7	972	13	-
MLA20	1570	19.4	1526	28	-
MCL4-co-LA4	874	**CL** 4.5 **LA** 4.0	931	-36	-

Repeating units determined by ^{1}H-NMR measurements and the number average molecular weight of the synthesized macromonomers are close to the theoretical values. The T_gs of the homopolymers synthesized by solution polymerization of caprolactone macromonomers decrease with an increase of the macromonomer length, from -56 ºC to below -60 ºC. Furthermore, melting peaks were observed for MCL6 (18 ºC) and MCL12 (38 ºC). T_gs spanning from 10 to 28 ºC were determined for the homopolymers of the lactide based macromonomers. Their T_g increased with their length. The homopolymer of the co-macromonomer showed a T_g of -36 ºC which is in between the values of the caprolactone and lactide based macromonomers.

The possibility to synthesize macromonomers using organocatalysts instead of $SnOct_2$ was explored. If the reaction time and concentration of catalyst were increased drastically, similar results to the catalyst $SnOct_2$ were obtained for 1,8-diazabicyclo(5.4.0)undec-7-ene (DBU). Further details are shown in the appendix.

2.2.2. Synthesis of crosslinkers

Asymmetric and symmetric oligoester crosslinkers with different target chain-lengths were synthesized by ROP using $SnOct_2$ (0.1 mol%) as a catalyst in bulk under nitrogen atmosphere. The synthesis of the crosslinkers was started either with the macromonomers (asymmetric crosslinkers) or with 1,4-butanediol (symmetric crosslinkers) as initiating species. The monomers *ε*-caprolactone and lactide were used in different ratios at a temperature of 130 ºC for 6 h. In a second step, 1.1 or 2.2 equivalents (regarding the oligoester chains) of itaconic anhydride were added, for asymmetric and symmetric crosslinkers respectively, and the temperature was kept at 90 ºC for 3 h. See Scheme 1 and 2 for more details.

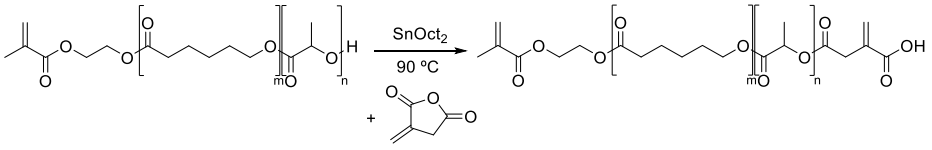

Scheme 2.2. ROP synthesis of asymmetric crosslinkers.

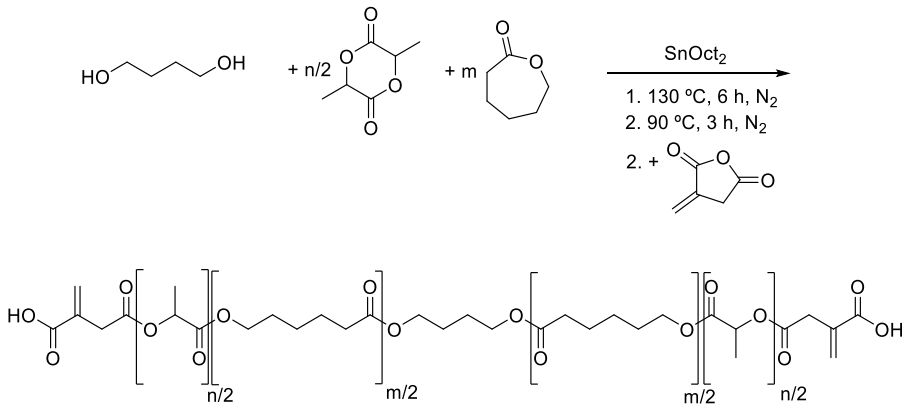

Scheme 2.3: ROP synthesis of symmetric crosslinkers.

The asymmetric and symmetric oligoester crosslinkers are referred to as ASY-LAnCLm and SY-LAnCLm in which *n* and *m* indicate the number of lactic acid units originating from lactide and *ε*-caprolactone units, respectively.

Asymmetric and symmetric crosslinkers were successfully synthesized by a one-pot ring opening polymerization process. Three different asymmetric crosslinkers and two symmetric ones were synthesized changing the ratio between lactide and *ε*-caprolactone and hence, changing the length. For all the cases, the theoretical molar mass and the experimental ones measured by either NMR or GPC were very similar confirming the desired structure of the crosslinkers (see Table 2.2 and the appendix for the NMR spectra). The number average molar masses measured by GPC show a slight deviation from the theoretical ones, which could be attributed to the polystyrene calibration used in the analyses of the data.

Table 2.2. Summary of the synthesized asymmetric and symmetric crosslinkers and their theoretical and experimental molar masses calculated from NMR and number-average molar mass (Mn) determined by GPC.

Crosslinker	*M (theo.)* [g/mol]	*M (NMR)* [g/mol]	M_n *(GPC)* [g/mol]	*PDI*
ASY-LA2CL2	598	586	503	2.0
ASY-LA4CL4	986	1118	1078	1.9
ASY-LA8CL4	1274	1274	1464	1.7
SY-LA2CL2	686	680	574	1.6
SY-LA6CL6	1486	1486	1583	1.4

2.3. Polymerization in dispersed media using degradable oligoester crosslinkers: towards easily removable waterborne PSAs

The emulsion polymerization of the macromonomers was explored with the aim of producing degradable nanoparticles with controlled particle size to be used in drug-delivery applications. The details of this part of the work have been included in the Appendix and this section will be devoted to the incorporation of the degradable cross-linkers into emulsion polymerization formulations to produce PSA's.

PSAs are viscoelastic materials that can adhere strongly to solid surfaces upon application of a light contact pressure and in short contact times.[21] They can achieve instantaneous adhesion to a surface without activation and by having sufficient internal strength not to break up before the bound between the adhesive and the surface ruptures.[22] In a typical waterborne PSA formulation,

apart from the monomers, emulsifier, initiator and water, crosslinkers and chain transfer agents (CTA) can be used to balance the cohesive and adhesive forces of the film, respectively.[23] The PSA sector is among the fastest growing ones in the adhesive market.[24] Within the different base polymers for making PSAs, waterborne acrylates are the fastest growing ones for commercial applications.[21] Therefore, new formulations with improved adhesivity, degradability or stimuli-responsive characteristics are of great interest.[25]

Different approaches to obtain degradable PSAs have been published in the literature. Sato et al. demonstrated the first strategy to obtain degradable PSAs. They synthesized two types of degradable polyperoxide PSAs. On the one hand through the synthesis of linear polyperoxides from methyl sorbate and oxygen, and on the other hand through the oxygen crosslinking of dienyl functionalized poly(ethylene glycol) to obtain peroxide groups within the crosslinks. Degradation was proved at raised temperatures and under UV-light.[26] However, due to the solvent used during the synthesis as well as the energetic conditions needed, it can be concluded that these materials do not meet the criteria of the previously mentioned environmentally friendly products.

Pu et al. demonstrated the usage of the same kind of macromonomers and co-macromonomers of lactide and *ε*-caprolactone as those described in section 2.2.1 in copolymerizations with commercial acrylates, such as *n*-butylacrylate (BA) by miniemulsion polymerization for the synthesis of PSAs.[20] Even, if they demonstrated that the PSA containing macromonomers performed as the commercial ones in terms of peel and shear properties, the loop tack was worse. Nonetheless, they did not show any degradability test of the adhesives.

Very recently, a different approach was introduced by Beharaj et al. to synthesize PSAs. They inserted CO_2 into a polyacrylic backbone forming poly(carbonate) analogues which were degraded depending on time and pH, but in all cases during large periods of time (between 4-32 days).[25] Moreover, as the molecular weights of the PSA were quite low, the final adhesive performance was not as good as the commercial ones.

On the other hand, recent patent literature describes the synthesis of (bio)degradable oligoester crosslinkers for the synthesis of degradable hydrogels.[27,28] Besides, another patent describes the synthesis of degradable PSAs by copolymerization of (meth)acrylic monomers and alkyl acryloxy glycolate monomers[29]. In this work they describe the possibility to use the degradable oligoester crosslinkers of references [30] and [31] for the synthesis of degradable PSAs. Nevertheless, these oligoester crosslinkers are produced by a multiple step synthesis, which requires purification steps of the products making it time and energy consuming.

It should be mentioned that these types of oligoester macromonomers and crosslinkers have been used in other types of applications such as in the production of graft coatings or degradable hydrogels for biomedical applications.[30,31]

In this section, the symmetric and asymmetric crosslinkers synthesized in the previous section were incorporated into a waterborne PSA formulation using a seeded semibatch emulsion polymerization process obtaining high solids content latices (of 50 wt% solids content).

2.3.1. Synthesis of PSAs using degradable crosslinkers

The incorporation of the oligoester crosslinkers was done following a typical PSA formulation (MMA/BA/AA in the weight ratio 89.1/9.9/1) and by a two-step seeded semibatch emulsion polymerization process (see Appendix Table II.2 and II.3 for the formulations of the seed and the seeded semibatch process). First, a seed with a solids content of 30% was prepared by semibatch emulsion polymerization. Surfactant (Dowfax 2A1), water and ammonium hydroxide solution were loaded into a 1 L glass reactor and heated to the reaction temperature (80 ºC). Subsequently, the initiator (KPS) was added and a preemulsion containing the monomers BA, MMA and AA (in the ratio 89.1/9.9/1), surfactant (Dowfax 2A1) and water was fed with a flow rate of 1.59 g/min for 180 min to the reactor. After finishing the feed, the reactor was maintained at 80 ºC for additional 60 minutes.

In a second step, acrylic latices with a solid content of 50 wt% were prepared by seeded semibatch emulsion polymerization at a temperature of 75 ºC and under nitrogen atmosphere. The seed and water were loaded into a 1 L glass reactor. The initiator (KPS) and the buffer (sodium bicarbonate) were added as a shot as soon as a temperature of 75 ºC was reached. Then the preemulsion containing the monomers BA, MMA, AA (in the ratio 89.1/9.9/1), oligoester crosslinkers (0.2 mol%), t-DDM, surfactant (Dowfax 2A1) and water were fed at a flow rate of 1.35 g/min in 180 min. The temperature was raised and kept at 80 ºC for 60 min after the feeding was finished.

For the sake of comparison, two more latices were synthesized, one without crosslinker and the other one using the conventional commercially available crosslinker allyl methacrylate (AMA).

The evolution of the instantaneous and overall conversions and the intensity-average particle sizes along the reaction are shown in Figure 2.1 a) and b).

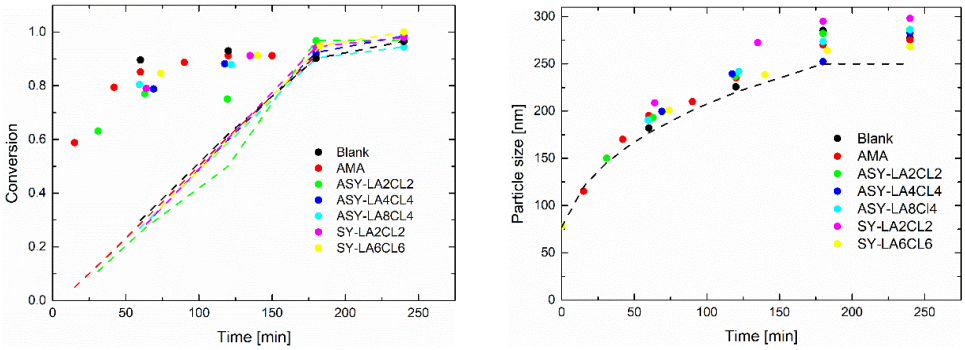

a) **b)**

Figure 2.1. a) Instantaneous (dots) and overall monomer conversions (dashed lines) of the seeded semibatch experiments containing different crosslinkers. **b)** Evolution of the intensity-average particle size (dots) measured by DLS and the theoretical evolution of particle size (dashed line) for the same experiments.

The kinetics were very similar in all the cases regardless of the type of crosslinker used. Instantaneous conversions were above 80% during most of the time and at the end almost full conversion was achieved in all the cases (see Table 2.3). Regarding the average particle size evolution, it can be seen that there were not substantial differences either, having final particle sizes between 270-300 nm. In all the cases, the average particle size was larger than the target one indicating some aggregation between particles towards the end of the polymerization process. Latexes were stable and no coagulum was detected after filtering out in a mesh.

One of the most important properties of a PSA is their T_g. As it can be seen in Table 2.3, all the synthesized latices presented similar and appropriate T_gs for the usage as PSA, between -36 ºC and -33 ºC.

2.3.2. Microstructure and adhesive performance

As for the gel content or insoluble part in THF, the blank latex showed almost no gel due to the usage of dodecanethiol as a CTA. This result was expected as it has been reported previously for the emulsion polymerization of acrylates.[32] On the other hand, the latex synthesized using AMA showed the highest gel content of 74%.

Table 2.3. Conversion, intensity-average particle size (D_p), and glass transition temperature (T_g) for PSA latices with different crosslinkers.

Crosslinker	χ [%]	D_p [nm]	T_g [ºC]
Blank	96	278	-36
AMA	98	276	-34
ASY-LA2CL2	97	295	-34
ASY-LA4CL4	99	283	-33
ASY-LA8CL4	99	286	-34
SY-LA2CL2	100	298	-34
SY-LA6CL6	100	268	-34

The gel contents of the latices with the oligoester crosslinkers are between the blank and the one containing AMA. For the asymmetric oligoester crosslinkers the shortest one ASY-LA2CL2 showed the largest gel content of 40% and increasing the length of the asymmetric oligoester crosslinker the gel content decreased. Moreover, a similar trend was found for the symmetric oligoester crosslinkers, where the longest crosslinker led to the lowest gel value of 23%. Even though the same amount of moles (0.2 mol% based on the monomers) of the oligoester crosslinkers and AMA were used, the gel content of the latices synthesized using the oligoester crosslinkers was just about half of the gel content of the AMA sample. Furthermore, the gel content decreases when increasing the length of the oligoester crosslinker. This might be due to the lower water solubility of the oligoester crosslinkers and therefore, the limited ability they may have to diffuse in the aqueous phase. The fact that the gel content decreases with an increase in the oligoester crosslinker length reinforces this hypothesis.

Table 2.4. Gel content measured by Soxhlet (GC S), weight-average molar mass (M_w) of the soluble part in THF, and dispersity index results for PSA latices with different crosslinkers.

Crosslinker	*GC S* [%]	*Sol* M_w [g/mol]	*Đ*
Blank	7 ± 7	178100	2.1
AMA	74 ± 0.3	78800	2.2
ASY-LA2CL2	40 ± 1	232600	3.4
ASY-LA4CL4	34 ± 0.5	238220	4.3
ASY-LA8CL4	31 ± 0.2	271800	4.5
SY-LA2CL2	40 ± 0.3	263600	4.1
SY-LA6CL6	23 ± 0.6	270400	3.6

Regarding the soluble M_w measured by GPC, as expected the lowest value was measured for the latex synthesized with AMA, since it had the highest amount of insoluble fraction. However, not only the M_w of the soluble part of the latices containing the oligoester crosslinkers were higher than the two references (the one without crosslinker and the one with AMA), but also the dispersity values were doubled.

In order to shed more light onto the microstructure of the different latices, the whole molar mass distribution was measured using AF4/MALS/RI technique (Figure 2.2). Broad and bimodal molar mass distributions were measured in all the cases spanning from 10^4 g/mol up to $3 \cdot 10^8$ g/mol or even $4 \cdot 10^9$ g/mol in the case of AMA. Due to the limitations of the technique, the chains with molar masses below $3 \cdot 10^4$ g/mol were not detected.

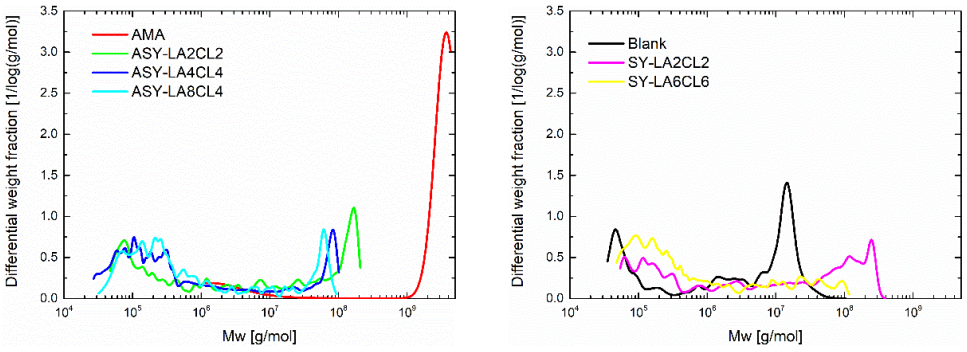

Figure 2.2. Molar mass distributions of the different PSA latices measured by AF4.

The molar mass distribution of the latex containing AMA (red) presents most of the polymer centered in a narrow peak at extremely high molar mass of $4 \cdot 10^9$ g/mol whereas the blank latex (black) shows a bimodal distribution with a peak at low molar masses $5 \cdot 10^5$ g/mol and a peak at

10^7 g/mol. The latices containing oligoester crosslinkers also present two different populations, one centered at around 10^5 g/mol (in the range of 10^4 g/mol to 10^6 g/mol that likely represents the soluble fraction) and the other one at higher molar masses above 10^7 g/mol (which can be considered as the insoluble fraction in THF). The average molar mass of the high molar mass population shifts to lower values, the longer the oligoester crosslinker is, in accordance with the lower efficiency of the longest oligoester crosslinkers as discussed above. From these molar mass distributions, the gel content can also be estimated assuming a limiting solubility. Thus, considering molecules with molar masses above 10^7 g/mol (note that the GPC analysis of the soxhlet extracted samples does not show molar masses higher than 10^7 g/mol) as gel, the gel contents were calculated from AF4 traces and are reported in Table 2.5 together with the weight-average molar mass values of the entire sample.

Table 2.5. Weight-average molar mass of the whole samples and gel content of the latices containing different crosslinkers determined from the AF4/MALS/RI analysis.

Crosslinker	M_w [kDa]	*GC AF4* [%]
Blank	10500	40
AMA	3681000	87
ASY-LA2CL2	76400	43
ASY-LA4CL4	35000	24
ASY-LA8CL4	40079	23
SY-LA2CL2	93800	48
SY-LA6CL6	30900	19

The weight-average molar masses of the entire sample indicate that the lowest molar mass was measured for the blank latex and the highest one for the AMA latex. The weight-average molar masses of the latices containing oligoester crosslinkers showed that the shorter the oligoester crosslinker chain the more efficient was the crosslinker and hence the higher were the weight-average molar masses.

The gel contents determined from AF4 results, except for the blank sample, agree reasonable well with the values and trends measured by soxhlet extraction. The blank sample showed a higher gel content, compared to the result from soxhlet extraction, of 40%. This is likely due to the fact that the high molar mass peak of the blank sample is close to the solubility criteria used to consider what is gel or not from the AF4 measurements, and this criteria might not be accurate for loosely crosslinked gels like for the blank latex. A high gel content of 87% was calculated for the AMA latex on the other hand. The gel contents determined for the latices including oligoester crosslinkers are below the value for the AMA sample and show the same trend as the one measured by soxhlet extraction.

The application of the latices synthesized in this work was to use them as removable PSAs, so they have to flow up to some point in order to make good contact with the substrates. In order to quantify this, the Dahlquist criterion is used which states that PSAs need a certain ability to flow, to be able to make full and perfect contact with a substrate. Dahlquist proposed the criterion that the storage modulus (*G'*) for measurable quick tack must be below a certain fixed value (< 0.3 MPa).[33] A typical timescale for putting a PSA onto a surface is 1 second, so the relevant *G'* for a room temperature PSA is at 1 Hz for a temperature of 25 ºC. DMA measurements were

performed using a parallel plate setup for the latices containing the different crosslinkers. The storage moduli are shown in Figure 2.3.

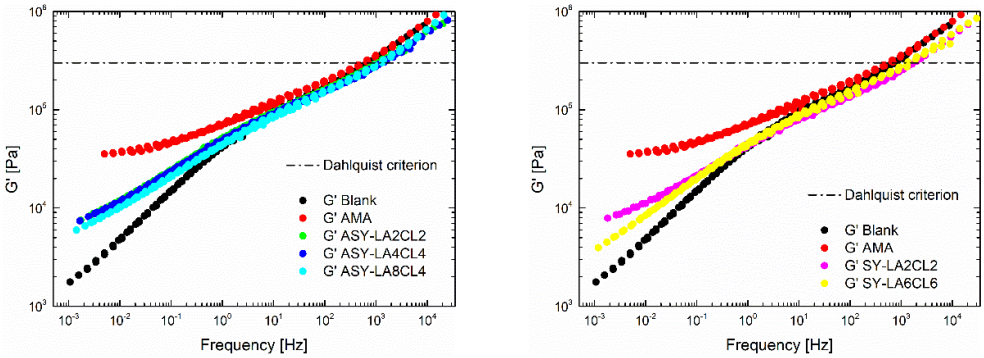

Figure 2.3. Storage moduli of the asymmetric (left) and symmetric (right) crosslinkers containing dried latices.

All the measured samples satisfied the Dahlquist criterion showing storage moduli values below 0.3 MPa at a frequency of 1 Hz. The AMA sample was the only one reaching a plateau between 10^4 and 10^5 Pa at low frequencies. On the other hand, the blank sample showed liquid like behaviour. The storage moduli of the samples containing oligoester crosslinkers were in between the AMA and the blank sample indicating a lower crosslinking density than the AMA latex which is in good agreement with the microstructure measured above (the storage moduli were higher for the samples containing the shorter oligoester crosslinkers). In the storage modulus, it can be observed that the most crosslinked system was the only one reaching a plateau and showing rubbery like performance. Furthermore, the ratio of tan(δ)/G' is related to the energy dissipation at the interface between the adhesive and substrate. An increase in the viscous modulus with respect to the elastic modulus leads to an increase in resistance to the detachment. Values

above 5 MPa^{-1} are recommended for steel substrates.[34] The tan(δ)/G' of the samples containing the different crosslinkers are plotted in Figure 2.4.

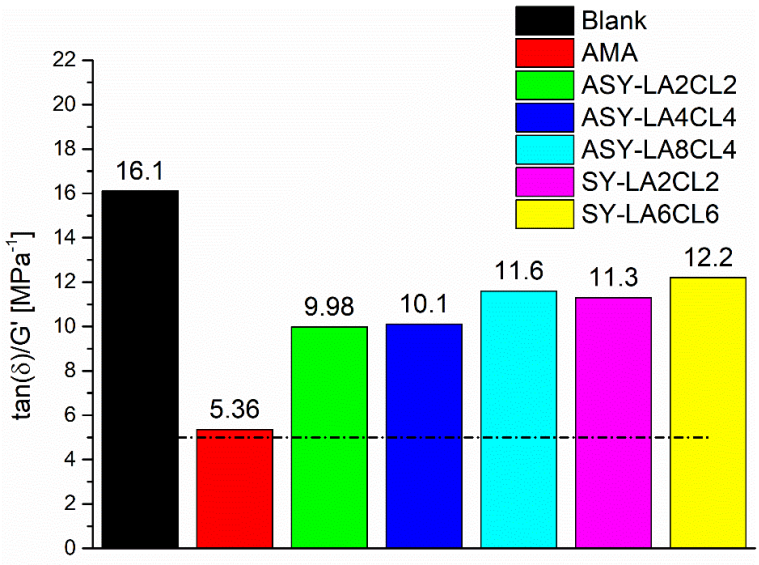

Figure 2.4. tan(δ)/G' for the polymers containing different crosslinkers at a frequency of 1 Hz and temperature of 25 ºC.

The AMA sample showed a value slightly above 5 MPa^{-1} for tan(δ)/G', whereas the blank showed a value of 16 MPa^{-1}. Values between 10 and 12 MPa^{-1} were calculated for the samples of the oligoester crosslinkers. Therefore, it can be concluded that the PSAs containing the oligoester crosslinkers are feasible to be used on steel substrates.

The performance of PSAs is characterized by adhesion required for bonding and debonding, and cohesion necessary against debonding. The character of PSAs is described by the special balance between these two properties and the challenge is to tune the microstructure of the

polymer (e.g., MMD, composition, crosslinking degree, functional groups) to meet the adhesion and cohesion requirements of the final application. The adhesion of a PSA is described by peel and tack resistances, whereas the cohesion of a PSA is characterised by shear resistance. Briefly, *peel resistance* is described as the force required to remove a PSA coated flexible material from a substrate under standard conditions (e. g. specific angle and rate). This force can be measured in different geometries (commonly peeling angle of 90º or 180º are used). *Tack* is the resistance of an adhesive film to detachment from a substrate. It measures the ability to form an instant bond (no dwell time on the contrary to the peel test) when brought into low pressure contact with a substrate. Finally, *shear resistance* is measured as the force required to pull the pressure sensitive material parallel to the surface it was attached to with a definite pressure and gives information about the cohesive performance of a PSA.

In this work, 180º Peel resistance, loop-tack, shear resistance and SAFT measurements were carried out to prove the feasibility of the synthesized latices as PSA. A detailed description of the fundamentals and the experimental procedures used to measure these properties are presented in section I.9 of the Appendix. The results of these measurements are presented in Table 2.6.

Peel values between 12 N/25mm and 21 N/25mm were measured for the different samples. These are high values compared to commercially available duct tape (approximately 10 N/25mm[35]). The AMA and SY-LA2CL2 samples showed the lowest peel value (~13 N/25mm; they are the most crosslinked samples and with lower soluble fraction) while the highest peel values of 20 N/25mm and 21 N/25mm, respectively were observed for the sample of the longest asymmetric and symmetric crosslinker, these were even higher than the peel value of the blank sample (18 N/25mm).

Table 2.6. Adhesive properties of the latices: Average peel resistance, loop-tack, shear resistance and SAFT values.

Crosslinker	Peel [N/25mm]	Loop-tack [N/25mm]	Shear [min]	SAFT [ºC]
Blank	17.7 ± 1.9	35.2 ± 1.1	11 ± 3	39 ± 3
AMA	12.6 ± 1.2	13.5 ± 2.0	10000+	128 ± 34
ASY-LA2CL2	17.0 ± 1.1	16.4 ± 0.9	2714 ± 700	100 ± 15
ASY-LA4CL4	15.4 ± 2.1	16.3 ± 3.8	826 ± 110	95 ± 12
ASY-LA8CL4	20.4 ± 3.6	18.7 ± 1.7	413 ± 114	93 ± 8
SY-LA2CL2	12.7 ± 1.1	14.4 ± 0.6	5483 ± 1050	97 ± 8
SY-LA6CL6	21.0 ± 1.7	25.5 ± 2.6	140 ± 8	71 ± 4

This could be due to the fact that peel resistance has a maximum in its dependency with the molar mass and crosslinking density[22], and likely these samples were closer to that value.

Tack on the other hand, showed the highest values for the lowest crosslinking density and/or molar mass and it decreases with increasing crosslinking density and/or molar mass. Thus, the blank sample showed by far the highest loop-tack value (35 N/25mm) followed by the SY-LA6CL6 and ASY-LA8CL4 samples (26 N/25mm and 19 N/25mm respectively) which had the lowest crosslinking density of the samples including crosslinkers. The other latices followed that trend, the lowest loop-tack values were observed for the AMA sample (14 N/25mm) and for the samples containing the two shortest asymmetric and symmetric crosslinker (16 N/25mm and 14 N/25mm, respectively). These are also high values compared to the commercial duct tape which shows a value of 7 N/25mm.[35]

Shear resistance and SAFT values also followed the trend according to the measured gel contents and molar mass distributions. The samples with the higher crosslinking density and higher molar masses (of the high molar mass mode) presented the higher times of failure. The lowest shear time of 11 minutes was observed for the blank sample and the highest of more than 10000 minutes for the AMA sample. Times of failure in between those two reference samples were observed for the asymmetric and symmetric oligoester crosslinkers containing samples. In the SAFT measurement, the blank sample failed at the lowest temperature of 39 ºC and the AMA sample at the highest temperature of 128 ºC. The longest symmetric one showed the lowest temperature of failure of 71 ºC. It is noticeable that the difference between the different crosslinkers is much more significant for the time of failure (shear resistance) than for the temperature of failure (SAFT).

Furthermore, probe tack measurements (see the section I.9.3 of the Appendix for further details) of the different crosslinkers containing PSAs were carried out on glass substrates and the stress strain curves are shown in Figure 2.5.

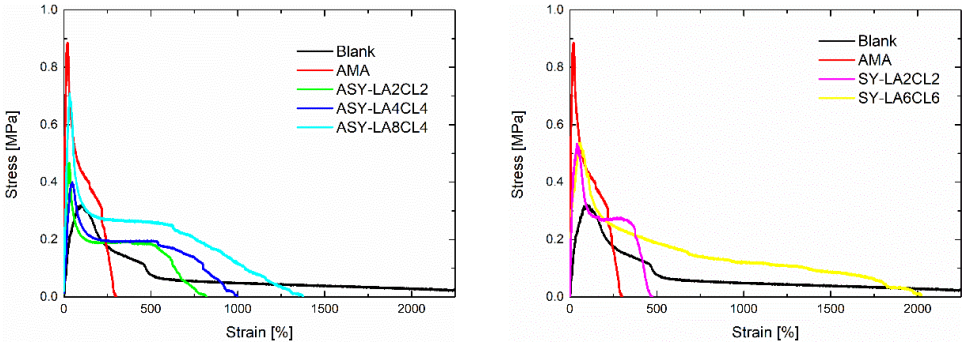

Figure 2.5. Stress strain curves obtained from probe tack measurements for the films of the latices with asymmetric (left) and symmetric (right) crosslinkers.

The curve measured for the AMA sample had no fibrillation plateau, indicating stiff behaviour, which is caused by its high degree of crosslinking (compare to Figure I.1 I) in the appendix). The blank on the other hand behaved liquid-like (compare to Figure I.1 III) in the appendix). The other samples with the oligoester crosslinkers, except for the SY-LA6CL6, which also behaved liquid-like and shows a strain up to 2000% before it broke, showed a fibrillation plateau (compare to Figure I.1 II) in the appendix). The length of the plateau increased with increasing the oligoester crosslinker length. Moreover, the fibrillation plateaus of the samples with ASY-LA2CL2 and ASY-LA4CL4 had the same stress level of 0.2 MPa. The sample containing the longest asymmetric crosslinker ASY-LA8CL4 had the longest fibrillation plateau up to a strain of 1300%, and the higher stress level of 0.3 MPa. While the short symmetric crosslinker SY-LA2CL2 showed the shortest fibrillation plateau until a strain of almost 500% at a stress level of 0.3 MPa. The length of the fibrillation plateaus of the samples is in agreement with the microstructure measured for the synthesized pressure sensitive adhesives; the fibrillation plateau increases with a decrease

in gel content and decrease in molar masses (of the high molar mass peak of the bimodal distribution in Figure 2.2.6) up to a point in which no clear plateau, but liquid like behaviour (for the blank sample and the sample containing the longest symmetric oligoester crosslinker) is observed. The samples, except the longest asymmetric and symmetric crosslinker and the blank one, showed an abrupt fall of the stress at their maximum strain, which indicates an adhesive failure. This kind of error happens if the energy for crack propagation is lower than the energy needed to elongate the fibrils.[34,36] Overall the tested samples show similar performance in the probe tack test than non degradable waterborne PSAs (having the same co-monomers of BA/MMA/AA and composition) for which maximal strains in between 500% and 2000% were observed and which show a maximal stress of approximately 0.5 MPa and a fibrillation plateau at a stress level of 0.2 MPa (see appendix Figure I.2).[37]

2.3.3. Assessment of degradability of the PSAs

The removability of the PSA's produced in this work depends on the degradation ability of the lactide/lactone oligoester crosslinkers. The degradation of polyesters and oligoesters by hydrolysis in either basic or acidic conditions has been described in the literature.[38] The mechanism and pH dependency of the degradation of PLA and PCL by hydrolysis was also investigated, and it was found that PLA degrades faster than PCL and that basic pH values lead to a higher rate of degradation than acidic pH values.[39,40] Therefore, basic conditions, similar to the pH of the washing solution used during the recycling of glass bottles, were chosen to assess the degradation of the adhesive films.

To proof that lactide and lactone moieties of the oligoester crosslinkers incorporated in polymer chains degrade under basic conditions, we first proved the concept in crosslinked copolymers synthesized by solution polymerization (see Appendix section II.4 for the synthesis, degradation and characterization of the molar mass distribution before and after the alkali treatment). The alkali treatment clearly cleaved the crosslinking points, decreasing notably the molar mass of the polymer chains.

The same analysis could not be applied to the waterborne PSA films because they were not completely soluble in THF. Therefore, to monitor the degradation it was not possible to analyse the molar mass distribution before and after the degradation (note that the molar mass distributions presented in Figure 2 were obtained by dispersing the latices directly in THF). However, an indirect proof of the degradation (and also of the removability of the adhesive film) can be obtained by monitoring the probe tack of the films during the immersion in the alkali solution.

Therefore, probe tack measurements were performed before and after immersion at different times to assess the degradation of the films. The probe tack curves of the AMA sample (left) and of the ASY-LA8CL4 sample (right) after 0 min, 15 min and 30 min of immersion time are displayed in Figure 2.6.

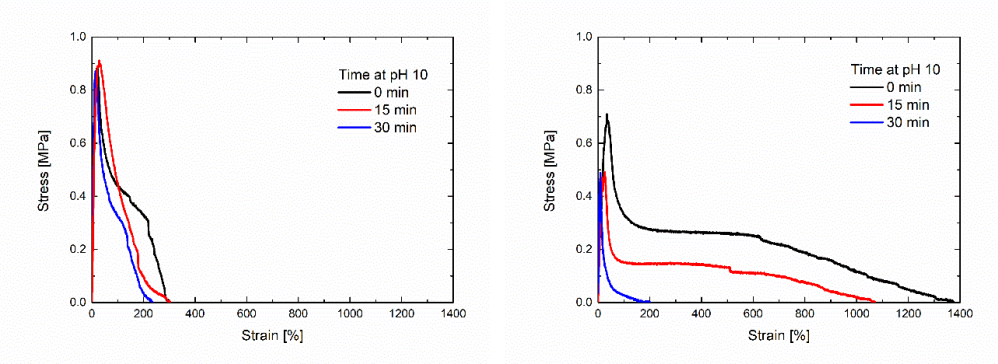

a) AMA **b) ASY-LA8CL4**

Figure 2.6. a) Probe tack measurements of the AMA sample and **b)** of the sample with ASY-LA8CL4 crosslinker after immersion of the films on a glass substrate for certain times at basic pH.

The area below the probe tack curves of the AMA sample decreased slightly with the immersion time. However, the ASY-LA8CL4 sample showed a remarkable decrease in its area after 30 min of immersion, where the fibrillation plateau completely disappeared. The work of adhesion was calculated by integration of the probe tack curves for each sample at the different immersion times. Figure 2.7 shows the calculated work of adhesion normalized to the starting value at 0 min for the asymmetric (left) and symmetric (right) crosslinkers against the immersion times.

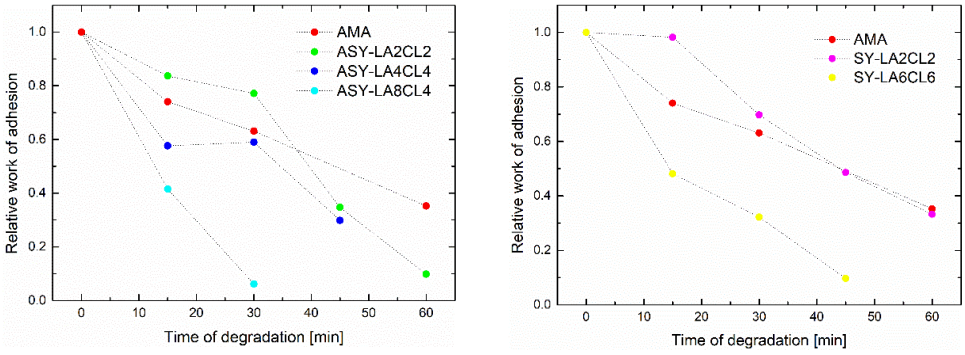

Figure 2.7. Relative work of adhesion calculated from the probe tack curves for the asymmetric (left) and symmetric (right) crosslinkers.

All of the samples showed a decrease in their relative work of adhesion with increasing time of immersion in the basic solution. Interestingly, the sample containing AMA also showed a substantial degradation up to 35% of its starting value. It has to be considered that the AMA crosslinker also contains an ester group which might also show degradation under these basic conditions. The samples of the shortest asymmetric and symmetric crosslinkers showed a similar degradation rate as the AMA sample. Nevertheless, the rate of degradation increases, increasing the length of the crosslinker, the longer the crosslinker the more ester groups in the molecule. The sample of ASY-LA8CL4 and SY-LA6CL6 showed a decrease in work of adhesion to 5% and 10% of the initial values in just 30 and 45 min, respectively.

Furthermore, as a proof of concept a film of the latex containing the ASY-LA8CL4 crosslinker, which is the sample showing the fastest rate of degradation in the probe tack measurements mentioned above, was cast onto a paper label for wine bottles. The label with the dried latex film was then attached to a glass bottle. This bottle and a commercial wine bottle with a label with a

conventional non-degradable PSA were immersed into a basic potassium hydroxide solution with a pH of 10. After 24 hours of immersion the label and the PSA containing the oligoester crosslinker could be easily removed from the glass bottle whereas the label and the PSA of the commercial wine bottle could not be removed after 24 hours of immersion into the basic solution (Figures II.5 and II.6 of the appendix).

2.4. Conclusion

A novel approach to obtain waterborne degradable and easily removable PSAs and thus, a possibility to face one of the major issues of the label removal during the recycling of glass bottles has been presented in this chapter. Symmetric and asymmetric oligoester crosslinkers have been synthesized and used to replace the conventional crosslinker AMA in a waterborne PSA formulation. The oligoester crosslinkers did not show any significant effect on the seeded semibatch emulsion polymerization regarding the kinetics and particle evolution in comparison with the two reference samples (the blank and AMA). Soxhlet extraction and AF4/MALS/RI measurements proved that the oligoester crosslinkers worked as expected in this waterborne PSA formulation, obtaining high molar masses and crosslinked samples. It is noteworthy that their efficiency is lower than that of AMA likely because of their limited solubility in the aqueous phase. In addition, their efficiency decreases with chain-length. The adhesive properties using these novel crosslinkers are in between the performance of commercial waterborne PSAs, and the length of the oligoesters allows tuning the adhesive performance. Furthermore, the degradation of the PSA films was shown by probe tack measurements. The longest asymmetric and symmetric crosslinker showed a substantial decrease in their work of adhesion in such short times as 30 min and 45 min, respectively, when immersed in basic aqueous solution at room temperature. PSA labels were applied to a glass bottle and their degradability and easy removability was demonstrated as a further proof of concept. The simplicity to implement this kind of oligoester crosslinkers into (existing) waterborne PSA formulations and the fact that the incorporation of a low amount of oligoester crosslinkers as low as 0.2 mol% is sufficient to result in a PSA with promising degradation properties make the herein reported oligoester crosslinkers

viable candidates for the production of removable PSAs. These removable PSA possess the potential to lead to a greener more sustainable way in the waste treatment, especially for the recycling of glass bottles.

2.5. References

(1) Hoornweg, D.; Bhada-Tata, P. *What a Waste - A Global Review of Solid Waste Management*, 15th ed.; The World Bank: Washington DC, 2012.

(2) Glass-Packaging-Institute. *Glass recycling facts*. http://www.gpi.org/recycling/glass-recycling-facts (accessed 2019-04-23).

(3) United-States-Environmental-Protection-Agency. *Advancing Sustainable Materials Management : 2015 Tables and Figures*; 2018.

(4) Schneck, C.; Grossmann, S.; Hackenberger, T. Process for Cleaning and Label Removal for Bottles. WO2012062372A1, 2012.

(5) Nair, H. R.; Hire, S.; Heederik, P. J. Process for the Removel of Labels from Materials. WO2015058184A1, 2015.

(6) Hunt, C. JR.; Chen, M. Solvent Application in Bottle Wash Using Amidine Based Formulas. WO2017143009A1, 2017.

(7) Yu, Y.; Ferrari, R.; Lattuada, M.; Storti, G.; Morbidelli, M.; Moscatelli, D. PLA-Based Nanoparticles with Tunable Hydrophobicity and Degradation Kinetics. *J. Polym. Sci. A* **2012**, *50*, 5191–5200. https://doi.org/10.1002/pola.26370.

(8) Ferrari, R.; Yu, Y.; Morbidelli, M.; Hutchinson, R. A.; Moscatelli, D. ????-Caprolactone-Based Macromonomers Suitable for Biodegradable Nanoparticles Synthesis Through Free Radical Polymerization. *Macromolecules* **2011**, *44* (23), 9205–9212. https://doi.org/10.1021/ma201955p.

(9) Ferrari, R.; Lupi, M.; Colombo, C.; Morbidelli, M.; Incalci, M. D.; Moscatelli, D. Colloids and Surfaces B : Biointerfaces Investigation of Size , Surface Charge , PEGylation Degree and Concentration on the Cellular Uptake of Polymer Nanoparticles. *Colloids Surfaces B Biointerfaces* **2014**, *123*, 639–647. https://doi.org/10.1016/j.colsurfb.2014.10.003.

(10) Lupi, M.; Colombo, C.; Frapolli, R.; Ferrari, R.; Sitia, L.; Dragoni, L. A Biodistribution Study of PEGylated PCL- Based Nanoparticles in C57BL / 6 Mice Bearing B16 / F10 Melanoma. *Nanotechnology* **2014**, *25*, 335706. https://doi.org/10.1088/0957-4484/25/33/335706.

(11) Rossi, F.; Ferrari, R.; Castiglione, F.; Mele, A. Polymer Hydrogel Functionalized with Biodegradable Nanoparticles as Composite System for Controlled Drug Delivery. *Nanotechnology* **2015**, *26* (1), 15602. https://doi.org/10.1088/0957-4484/26/1/015602.

(12) Colombo, C.; Gatti, S.; Ferrari, R.; Casalini, T.; Cuccato, D.; Morosi, L.; Zucchetti, M.; Moscatelli, D. Self-Assembling Amphiphilic PEGylated Block Copolymers Obtained through RAFT Polymerization for Drug-Delivery Applications. *J. Appl. Pol. Sci.* **2016**, *133* (11), 43084. https://doi.org/10.1002/app.43084.

(13) Colombo, C.; Morosi, L.; Bello, E.; Licandro, S. A.; Lupi, M.; Ubezio, P.; Morbidelli, M.; Zucchetti, M.; Incalci, M. D.; Moscatelli, D.; Frapolli, R. PEGylated Nanoparticles Obtained through Emulsion Polymerization as Paclitaxel Carriers. *Mol. Pharm.* **2016**, *13* (1), 40–46. https://doi.org/10.1021/acs.molpharmaceut.5b00383.

(14) Ferrari, R.; Colombo, C.; Dossi, M.; Moscatelli, D. Tunable PLGA-Based Nanoparticles Synthesized Through Free-Radical Polymerization. *Macromol. Mater. Eng.* **2013**, *298*, 730–739. https://doi.org/10.1002/mame.201200069.

(15) Ferrari, R.; Yu, Y.; Lattuada, M.; Storti, G.; Morbidelli, M.; Moscatelli, D. Controlled PEGylation of PLA-Based Nanoparticles. *Macromol. Chem. Phys.* **2012**, *213*, 2012–2018.

(16) Grossen, P.; Witzigmann, D.; Sieber, S.; Huwyler, J. PEG-PCL-Based Nanomedicines: A Biodegradable Drug Delivery System and Its Application. *J. Control. Release* **2017**, *260*, 46–60. https://doi.org/10.1016/j.jconrel.2017.05.028.

(17) Ferrari, R.; Colombo, C.; Casali, C.; Lupi, M.; Ubezio, P.; Falcetta, F.; Incalci, M. D.; Morbidelli, M.; Moscatelli, D. Synthesis of Surfactant Free PCL – PEG Brushed Nanoparticles with Tunable Degradation Kinetics. *Int. J. Pharm.* **2013**, *453* (2), 551–559. https://doi.org/10.1016/j.ijpharm.2013.06.020.

(18) Ferrari, R.; Cingolani, A.; Moscatelli, D. Solvent Effect in PLA-PEG Based Nanoparticles Synthesis through Surfactant Free Polymerization. *Macromol. Symp.* **2013**, *324*, 107–113. https://doi.org/10.1002/masy.201200073.

(19) San Luis, A. De; Kleinsteuber, M.; Schuett, T.; Schubert, S.; Schubert, U. S. Miniemulsion Polymerization at Low Temperature: A Strategy for One-Pot Encapsulation of Hydrophobic Anti-Inflammatory Drugs into Polyester- Containing Nanoparticles. *J. Colloid Interface Sci.* **2022**, *612*, 628–638. https://doi.org/10.1016/j.jcis.2021.12.189.

(20) Pu, G.; Dubay, M. R.; Zhang, J.; Severtson, S. J.; Houtman, C. J. Polyacrylates with High Biomass Contents for Pressure-Sensitive Adhesives Prepared via Mini-Emulsion Polymerization. *Ind. Eng. Chem. Res.* **2012**, *51* (37), 12145–12149.

https://doi.org/10.1021/ie301492v.

(21) Agirre, A.; Nase, J.; Degrandi, E.; Creton, C. Improving Adhesion of Acrylic Waterborne PSAs to Low Surface Energy Materials : Introduction of Stearyl Acrylate. *J. Polym. Sci. A* **2010**, *48*, 5030–5039. https://doi.org/10.1002/pola.24300.

(22) Benedek, I. *Pressure-Sensitive Adhesives and Applications*, Second Edi.; Marcel Dekker: New York - Basel, 2004.

(23) Chauvet, J.; Asua, J. M.; Leiza, J. R. Independent Control of Sol Molar Mass and Gel Content in Acrylate Polymer/Latexes. *Polymer (Guildf).* **2005**, *46* (23), 9555–9561. https://doi.org/10.1016/j.polymer.2005.08.061.

(24) Khan, I.; Poh, B. T. Natural Rubber-Based Pressure-Sensitive Adhesives : A Review. *J. Polym. Environ.* **2011**, *19*, 793–811. https://doi.org/10.1007/s10924-011-0299-z.

(25) Beharaj, A.; Ekladious, I.; Grinstaff, M. W. Degradable Polymers Poly (Alkyl Glycidate Carbonate) s as Degradable Pressure-Sensitive Adhesives. *Angew. Chem. Int. Ed.* **2019**, *58*, 1407–1411. https://doi.org/10.1002/anie.201811894.

(26) Sato, E.; Tamura, H.; Matsumoto, A. Cohesive Force Change Induced by Polyperoxide Degradation for Application to Dismantlable Adhesion. *ACS Appl. Mater. Interfaces* **2010**, *2* (9), 2594–2601. https://doi.org/10.1021/am1004392.

(27) Kiser, P. F.; Thomas, A. A. Biodegradable Cross-Linkers Having a Polyacid Connected to Reactive Groups for Cross-Linking Polymer Filaments. US6521431B1, 2003.

(28) Webb, C. K.; Vyavahare, N. R. Macromonomer for Preperation of a Degradable Hydrogel. US7754241B1, 2010.

(29) Lewandowski, K. M.; Lipscomb, C. E.; Janoski, J. E. Pressure-Sensitive Adhesives Prepared from Degradable Monomers and Polymers. US9334428, 2016.

(30) Okuda, T.; Ishimoto, K.; Ohara, H.; Kobayashi, S. Renewable Biobased Polymeric Materials: Facile Synthesis of Itaconic Anhydride-Based Copolymers with Poly(L-Lactic Acid) Grafts. *Macromolecules* **2012**, *45*, 4166–4174. https://doi.org/10.1021/ma300387j.

(31) Pertici, V.; Pin-barre, C.; Rivera, C.; Pellegrino, C.; Gigmes, D.; Trimaille, T. Degradable and Injectable Hydrogel for Drug Delivery in Soft Tissues. *Biomacromolecules* **2019**, *20*, 149–163. https://doi.org/10.1021/acs.biomac.8b01242.

(32) Plessis, C.; Arzamendi, G.; Leiza, J. R.; Alberdi, J. M.; Schoonbrood, H. A. S.; Charmot, D.; Asua, J. M. Seeded Semibatch Emulsion Polymerization of Butyl Acrylate: Effect of the Chain-Transfer Agent on the Kinetics and Structural Properties. *J. Polym. Sci. Part A Polym. Chem.* **2001**, *39*, 1106–1119.

(33) Dahlquist, C. A. Pressure-Sensitive Adhesives. In *Treatise on adhesion and adhesives*; Dekker: New York, 1969; pp 219–260.

(34) Deplace, F.; Mariot, S.; Chateauminois, A.; Ouzineb, K. Fine Tuning the Adhesive Properties of a Soft Nanostructured Adhesive with Rheological Measurements Fine Tuning the Adhesive Properties of a Soft Nanostructured Adhesive with Rheological Measurements. *J. Adhes.* **2009**, *85*, 18–54. https://doi.org/10.1080/00218460902727381.

(35) Lee, S.; Lee, K.; Kim, Y.; Shin, J. Preparation and Characterization of a Renewable Pressure-Sensitive Adhesive System Derived from ε - Decalactone,. *ACS Sustain. Chem. Eng.* **2015**, *3*, 2309–2320. https://doi.org/10.1021/acssuschemeng.5b00580.

(36) Daniloska, V.; Carretero, P.; Tomovska, R.; Paulis, M.; Asua, J. M. High-Performance Adhesives Resulting from Spontaneous Formation of Nanogels within Miniemulsion Particles. *Appl. Mater. Interfaces* **2014**, *6*, 3559–3567. https://doi.org/10.1021/am405752k.

(37) Aguirreurreta, Z.; Dimmer, J.; Willerich, I.; Leiza, J. R.; De, J. C. International Journal of Adhesion & Adhesives Improving the Properties of Water-Borne Pressure Sensitive Adhesives by Using Non-Migratory Surfactants. *Int. J. Adhes. Adhes.* **2016**, *70*, 287–296. https://doi.org/10.1016/j.ijadhadh.2016.07.011.

(38) Woodard, L. N.; Grunlan, M. A. Hydrolytic Degradation and Erosion of Polyester Biomaterials. *ACS Macro Lett.* **2018**, *7*, 976–982. https://doi.org/10.1021/acsmacrolett.8b00424.

(39) Jung, J. H.; Ree, M.; Kim, H. Acid- and Base-Catalyzed Hydrolyses of Aliphatic Polycarbonates and Polyesters. *Catal. Today* **2006**, *115*, 283–287. https://doi.org/10.1016/j.cattod.2006.02.060.

(40) Sailema-Palate, G. P.; Vidaurre, A.; Campillo, A. F.; Castilla-Cortazar, I. A Comparative Study on Poly (ε -Caprolactone) Fi Lm Degradation at Extreme PH Values. *Polym. Degrad. Stab.* **2016**, *130*, 118–125. https://doi.org/10.1016/j.polymdegradstab.2016.06.005.

Chapter 3. Thiol-ene polymerization

3.1. Introduction

Over more than 100 years, thiols have been used in multiple fields ranging from biochemistry to polymer science.[1] The polymerization of multifunctional thiols with multifunctional enes is a radical step-growth polymerization and is named as thiol-ene polymerization. Thiol-ene polymerization can be used to reach a broad range of applications, such as novel biomaterials[2–4], photocurable adhesives[5], dental restorative materials[6,7], clear protective or pigmented coatings[8–10], ceramics[11–13], liquid-crystalline structural materials[14,15], optical components[16] and (renewable) thermosets[17–19].

Thiol-ene chemistry has recently been claimed as a “click” reaction for the synthesis of functionalized polymers and surfaces, biofunctionalization and uniform network formation.[1,20–22]

Thiol-ene polymerization is a step-growth polymerization. Therefore, a very high conversion is necessary to achieve acceptable molar masses as described by the Carothers equation.[23] Furthermore, the ratio between the functional groups plays an important role for achieving high molar masses.[24]

A general scheme, showing the different steps involved in thiol-ene polymerization,[1] is shown in Figure 3.1. Ideally carbon centred radicals (I*) generated from initiator (photopolymerization has been commonly used) will abstract a hydrogen from a thiol functional group (R-SH) generating thiyl radicals (R-S*). These thiyl radicals add to ene functional groups (R'-C=C) producing the thio-ether coupling product (propagation). The resulting carbon centred radical abstracts a hydrogen atom from another thiol molecule (transfer reaction) generating thiyl radicals that continue propagating provided that ene functional groups are available. If only this addition/transfer reactions occur, at the end of the polymerization the concentration of thio-ether groups should be equal to the initial ene or thiol concentration for an equimolar initial ratio. A coupling efficiency of 100% will be obtained under this ideal conditions.

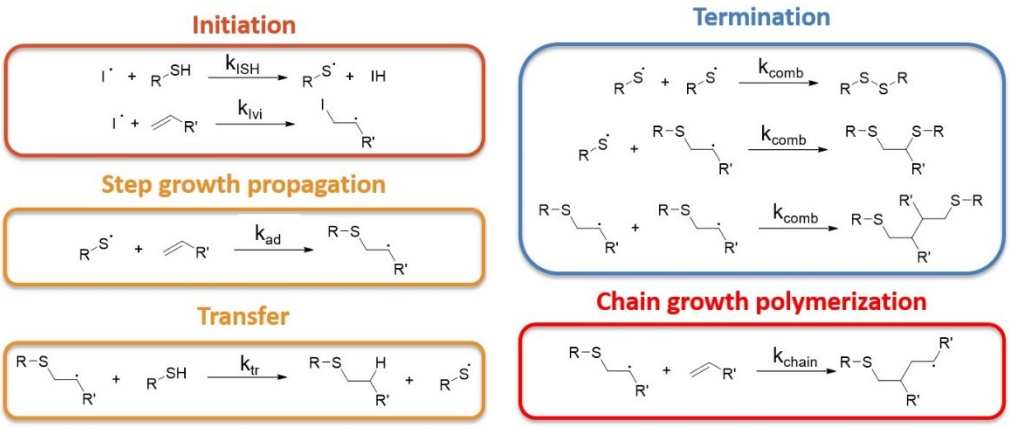

Figure 3.1. General kinetic scheme of a thiol-ene polymerization.[1]

However, many other reactions are also possible that will lead to side products and hence, a reduction of the coupling efficiency. For instance, termination reactions, which consist of the combination of radicals. The combination can occur between two thiol radicals, a thiol and a carbon radical or between two carbon radicals. A linear chain is generated in the case that the combination happens between two thiyl radicals that yield a disulphide molecule. This means that two thiyl functional groups are consumed, which would influence on the ratio between the thiol and vinyl functional groups. On the other hand, the combination of two carbon radicals, due to its midchain nature, leads to multifunctional species. This could lead to the formation of branched chains and a crosslinked network if this combination happens several times.

Another possible side reaction is the chain growth polymerization of the vinyl monomer, that is more likely when homopolymerizable monomers like acrylates are used.[25] This side reaction would influence the ratio between the thiol and ene functional groups, as only ene groups would

be consumed. Furthermore, due to the fact that in the thiol-ene polymerization multifunctional vinyl monomers are used (usually with a functionality of at least two), this side reaction would lead to the formation of a highly crosslinked network.

There are several authors that have modelled the kinetics of thiol-ene polymerization. For instance, Cramer et al. modelled different thiol-ene systems, and they found that the propagation kinetics were strongly controlled by the ratio of the propagation to the chain transfer rate coefficients (k_{ad}/k_{tr} in this article) and that the ratio was system dependent. For instance, for the thiol-allyl ether system, they found that by considering $k_{ad}/k_{tr} = 10$ in the model, the kinetics were well described. In addition, they found the overall polymerization rate to be first-order with respect to the concentration of the thiol functional groups.[26] The same authors investigated the termination mechanism, using the rotating sector method to determine the average radical life time in thiol-ene systems. Using analytical equations to calculate this average radical life-time, the authors were able to determine average radical termination rate coefficients.[27] They found that contrary to what was claimed in previous reports, the termination reactions in thiol-ene polymerization was radical-radical and that these reactions were extremely fast (with rate coefficients in the range 10^8 – 10^9 L/mol·s). Homo termination and cross termination reactions were identified.

Moreover, Bowman et al. modelled the kinetics of thiol-ene polymerization including step-growth and chain-growth aspects.[28] They showed that if no radical homopolymerization of the vinyl monomer was allowed, both the average molar masses and the gel point conversions were given by the typical equations for step-growth polymerization. However, increasing the propagation of

the vinyl monomers, high molar masses and gel points were obtained at lower conversions or shorter reaction times.

The alkene functionality has an influence to the energetics and kinetics of the radical initiated thiol-ene polymerization. Northrop and Coffey determined relative energetics computationally at the CBS-QB3 level for a series of different alkenes.[29] Interestingly, they derived values for the rate constants of the propagation (k_{ad}) and transfer (k_{tr}) steps, and for the thiol-allyl ether system they report that k_{ad}/k_{tr} could be smaller than one, against the experimental observation of Cramer et al.[26]

The importance of side reactions and diffusional limitations to the kinetics of radical thiol-ene polymerizations was studied by Derboven et al.[30] They coupled thiol-functionalized polystyrene with dodecyl vinyl ether through radical thiol-ene coupling. Termination by combination of carbon centred radicals as well as additions from radicals derived from the photoinitiator were found to be responsible for a reduced coupling efficiency.

The effects of thiol substitution on radical thiol-ene polymerizations has also been studied showing that an increase of thiol substitution from primary to tertiary lead to a 10-fold decrease of the polymerization rate.[31]

In addition to the radical thiol-ene polymerization, thiol and ene functional groups can react by the so-called thiol-Michael addition, which is catalysed by bases such as 1,8-diazobicyclo(5.4.0)undec-7-ene.[32] Kinetics for base catalysed thiol-Michael addition polymerizations were evaluated by Bowman et al. through mechanistic modeling.[33] The same

group also investigated the effect of thiol substitution on the kinetics and efficiency of the thiol-Michael reactions and polymerizations.[34]

It is worth mentioning that in all the works described above thiol-ene polymerizations were carried out with photoinitiators as a radical source (i.e. photopolymerization), and polymerization kinetics were very fast (less than one minute for almost complete conversion). The mathematical models developed have mainly considered addition/transfer reactions and side reactions, like bimolecular terminations or addition of initiator radicals to ene functional groups or even β C-S scission. Average molar masses were assessed by the moments method,[28] but neither the molar masses nor the composition of species have been measured experimentally and been compared to model predictions.

In this chapter a mathematical model for the prediction of the thiol-ene polymerization initiated by a thermal initiator is developed. In addition to the prediction of the kinetics of the polymerization (e.g., conversion of the functional ene monomer) that has been well reported in previous works[25–28,30,35], herein a detailed kinetic scheme to determine the composition of the main copolymer species formed in the polymerization has been developed. The model has been assessed by comparing the predictions with experimental data gathered during *in-situ* NMR experiments carried out at different initiator concentrations. The composition of the copolymer species have been measured for the first time by MALDI-TOF analysis revealing that up to five different species are produced during the polymerization.

3.2. Experimental part

The experimental procedures used to realize the work described within this chapter are described in this part. Further analytical methods are described in the section I of the Appendix.

3.2.1. *In situ* ^{1}H-NMR solution polymerizations

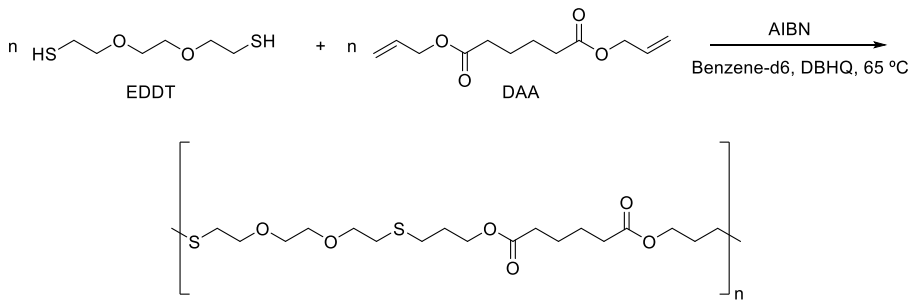

Scheme 3.1. Thiol-ene polymerization of EDDT and DAA.

In situ ^{1}H-NMR solution thiol-ene polymerizations of EDDT and DAA were carried out at atmospheric pressure in a Wilmad® NMR tube with a length of 18 cm, and a diameter of 5 mm (wall thickness of 0.43 mm) as reaction vessel. A hole was punched in the lid of the NMR tube, to prevent overpressure. The polymerizations (see Scheme 3.1) were monitored *in situ* using benzene-d_6 as solvent. DBHQ was used as inhibitor (0.02 eq.) to prevent the premature polymerization through spontaneous formation of thiyl radicals.[36–39]. Solution polymerizations

were carried out at total monomer concentration in between 40 wt% and 50 wt%. 1, 2 or 3 wbm% (weight percent based on total weight of the monomers) of the initiator AIBN were added to the NMR tube when the solution of the monomers reached the reaction temperature of 65 ºC. Two sets of experiments were carried out with almost the same ratio of functional groups (r = [-SH]/[ene]). The first set was done with r = 1.00 and the second with r = 1.02. The reactant concentrations of the different experiments are listed in Table 3.1. The detailed recipes are listed in the section III of the Appendix (Table III.1).

Table 3.1. Reactants' concentrations for the EDDT/DAA thiol-ene polymerizations monitored by in-situ NMR measurements.

Experiment	r-value	[AIBN] [mol/L]	[EDDT] [mol/L]	[DAA] [mol/L]	[DBHQ] [mol/L]
Run1	1.00	0.027	1.10	1.10	0.042
Run2	1.00	0.054	0.99	0.99	0.038
Run3	1.00	0.099	1.12	1.12	0.043
Run4	1.02	0.030	1.18	1.19	0.043
Run5	1.02	0.062	1.15	1.16	0.042
Run6	1.02	0.088	1.12	1.13	0.041

3.2.2. Mathematical model for the thermally initiated thiol-ene polymerization

A detailed kinetic scheme was developed to describe thiol-ene polymerizations and to account for the consumption of functional groups, development of the molar masses and composition of the chains based on the chain-end functionality. Figure 3.2 presents all the species considered in the thiol-ene polymerization model. P, R and S stand for polymeric species with *n* thio-ether coupling units. R and S species bear a radical whereas P species do not. R species are carbon centred radicals and S species are sulphur radicals; namely, thiyl radicals. Furthermore, the letter U describes species containing disulfides. The capital letter M stands for a monomer. The letters *a*, *b* and *I* give information about the end-groups at the terminal ends of the polymeric species. The letter *a* indicates a terminal thiol group while the letter *b* a terminal vinyl group. Letter *I* indicates an initiator fragment as the terminal end of a polymeric species. Only reactions leading to linear chains were considered in the kinetic scheme; namely functionality of the thiol and ene monomer is equal to two and the reactions that might lead to branched or crosslinked structures were not considered in the kinetic scheme. Furthermore, the assumption that the reactivity of the terminal functional groups is independent of the chain length has also been implemented. All the species in Figure 3.2 (except the monomers) also exist as disulfide containing species (see the Appendix Figure III.3 for further details).

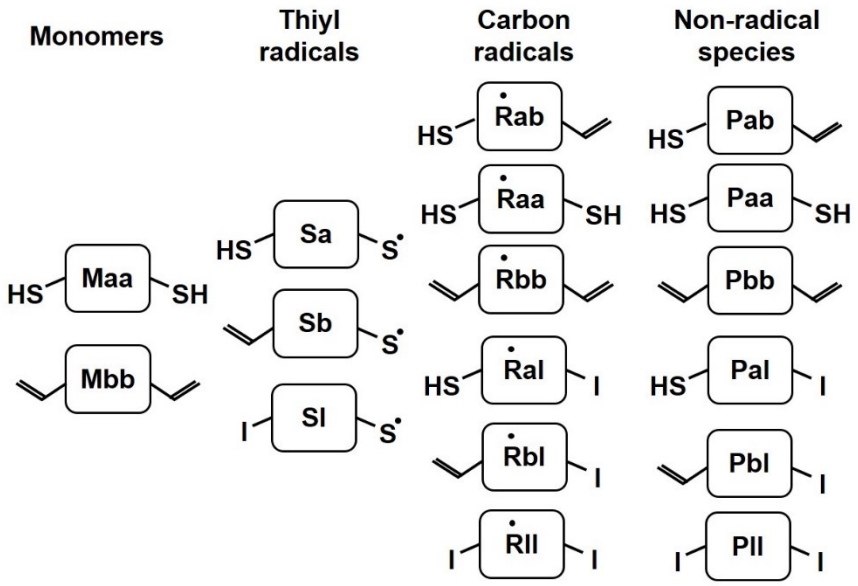

Figure 3.2. Species considered in the thiol-ene polymerization model without disulfides. The monomers Maa and Mbb, the thiyl radicals Sa, Sb and Sl, the carbon radicals Rab, Raa, Rbb, Ral, Rbl and Rll and the non-radical species Pab, Paa, Pbb, Pal, Pbl and Pll.

In addition to the main thiol-ene polymerization reactions (initiation, addition, chain transfer), the kinetic scheme consists of other side reactions such as termination by combination and inhibition. A complete list of all the reactions considered in the model is provided in section III of the Appendix. Herein examples for each of the reactions are given in Scheme 3.2-Scheme 3.6.

The initiation reactions consist of the decomposition of the initiator, the abstraction of a hydrogen from a thiol functional group by the initiator radical with the rate coefficient k_{ISH} and the addition of an initiator radical to a vinyl functional group with the rate coefficient k_{Ivi} (see Scheme 3.2). The latter reaction is considered as a side reaction, reducing the coupling efficiency of the thiol-

ene polymerization. The coupling efficiency is defined as shown in equation 3.1[30] in which $c_{thio-ether}$ is the concentration of the thio-ether product, $c_{ene,0}$ and $c_{thiol,0}$ are the initial concentrations of ene or thiol functional groups, and c_{ene} and c_{thiol} are the concentrations of ene and thiol functional groups at time t, respectively.

$$f_{coupling} = \frac{c_{thio-ether}}{c_{ene,0} - c_{ene}} \quad \text{or} \quad f_{coupling} = \frac{c_{thio-ether}}{c_{thiol,0} - c_{thiol}} \tag{3.1}$$

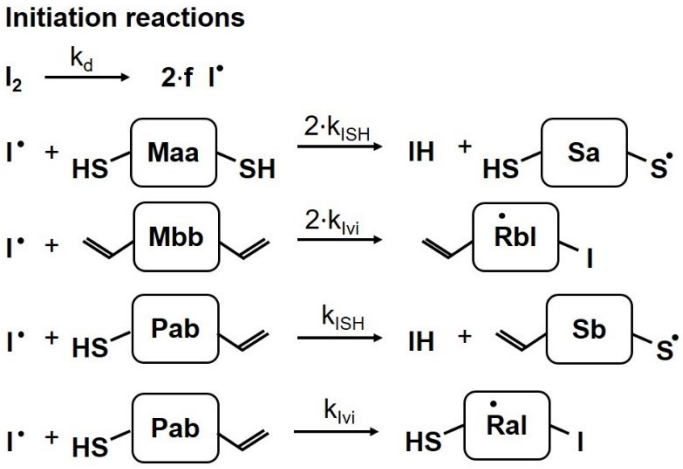

Scheme 3.2. Examples of the different initiation reactions. The decomposition of the initiator to radicals, the abstraction of a hydrogen by one initiator radical from thiol functional groups, leading to the generation of thiyl radicals, and the addition of initiator radicals to vinyl groups.

In the addition or propagation reactions (Scheme 3.3) a thiyl radical is added to a vinyl functional group forming a carbon centred radical and a thio-ether coupling unit. According to DFT calculations this reaction might be reversible[29], but there is no experimental evidence showing

that this reaction occurs. Derboven et al.[30] reported that for vinyl ether-thiol systems a mathematical model could not predict the evolution of the functional group conversion if this reaction was considered. Thus, in this work, this reaction was not included in the kinetic scheme.

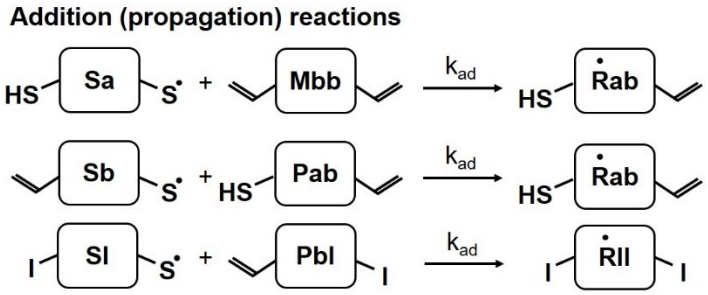

Scheme 3.3. Examples of the addition reactions, which consists of the addition of a thiyl radical to a vinyl functional group, leading to the generation of a carbon radical and a thio-ether coupling unit.

In the chain transfer reactions a carbon centred radical abstracts a hydrogen atom from a thiol functional group, so that a thiyl radical and non-radical species are formed in the chain transfer reactions (Scheme 3.4). Note that intramolecular transfer reactions were considered except those leading to cyclic species.

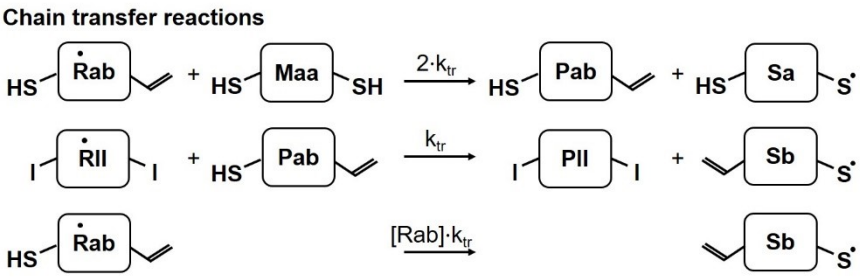

Scheme 3.4. Examples for chain transfer reactions, in which a hydrogen atom is abstracted by a carbon centred radical under the formation of a thiyl radical and non-radical species.

Termination reactions between the different radical species can occur during the polymerization. Three types of radicals are present in the reaction medium: initiator derived radicals (I*), thiyl radicals (S*) and carbon centred radicals (R*). In principle, termination reactions can occur by combination of each of them.[27,30] Nonetheless, to be consistent with the assumption that only linear chains can be formed, termination by combination of carbon centred radicals (R*+R*) and carbon centred radicals and thiyl radicals (R*+S*) is not considered because multifunctional species would be formed. Scheme 3.5 presents examples of the termination by combination reactions that have been considered. Two thiyl radicals can combine to form a disulfide, which is represented by the capital letter U in the kinetic scheme (Scheme 3.5). The rate constant for this combination is k_{comb}. Combination reactions between initiator radicals and thiyl ($k_{combISH}$) or carbon centred radicals ($k_{combIvi}$) are also considered.

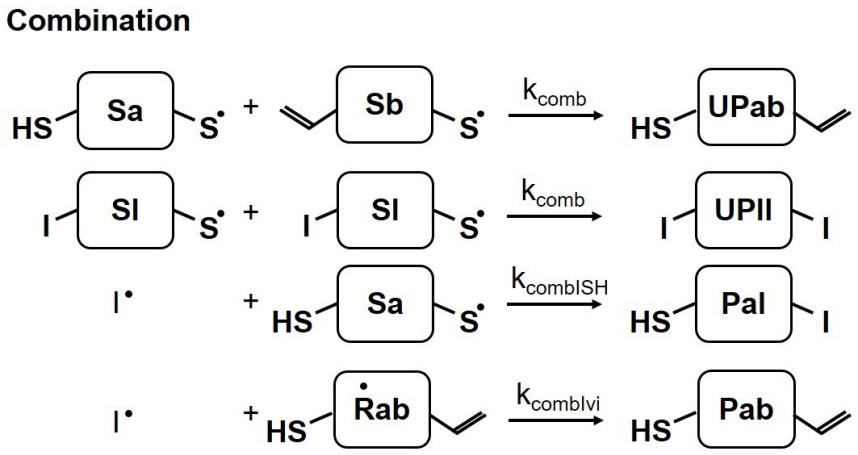

Scheme 3.5. Examples of combination reactions between two thiyl radicals, a thiyl and an initiator radical and an initiator and a carbon centred radical.

The formed disulfides can dissociate into two thiyl radicals,[41] namely the reaction can be reversible. Although there is experimental evidence of the reversibility of this reaction (e.g., disulfides have been used to synthesize self-healing polymers[42]), it has been shown that aliphatic disulfides are less likely to undergo this reaction[43] and hence this reaction was not considered in the model.

As mentioned in the experimental section, the DBHQ inhibitor was added to the monomer solutions to avoid premature reaction of the dithiol by spontaneous radical formation.[36–39] Therefore, the kinetic scheme must also consider reactions between radicals and DBHQ in order to correctly compute the experimental conditions. Admittedly, these inhibition reactions add further complexity to the predictions of the model, but there was no other way to limit the spontaneous reaction whose mechanism is unknown. All of the radical species can abstract a

hydrogen from the inhibitor that leads to the formation of a non-radical species and a non-reactive DBHQ (inhibitor) radical. Examples are shown in Scheme 3.6.

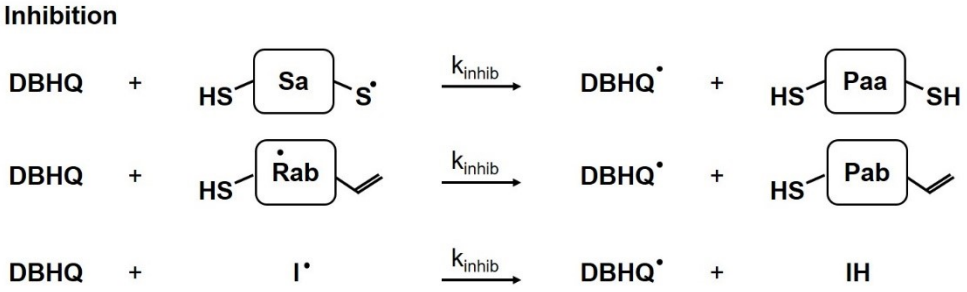

Scheme 3.6. Examples of inhibition reactions of radical species by the inhibitor DBHQ.

The kinetic scheme described above was implemented in the commercial software Predici[44]. The model outputs the conversion of the functional groups, the average molar masses and the molar fractions of the different polymeric species produced.

3.3. Results and discussion

3.3.1. Kinetics and microstructure

Thiol-ene solution polymerizations of the dithiol EDDT and the diene DAA were monitored by *in situ* ^{1}H-NMR. Polymerizations were carried out with 1, 2 and 3 wbm% of initiator. Two sets of polymerizations with a slightly different ratio between diene and dithiol functional groups (r = 1.00 and 1.02) were carried out for each of the AIBN concentrations. The evolution of the conversions of the vinyl functional groups for each of the sets is displayed in Figure 3.3.

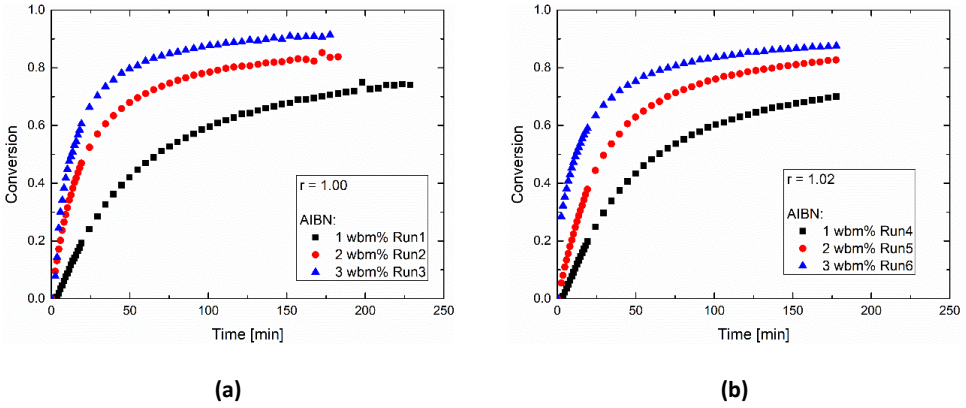

Figure 3.3. Evolution of conversion of the vinyl groups for the experiments with r = 1.00 (a) and r = 1.02 (b).

Figure 3.3 shows that small differences in the evolution of the ene conversions were obtained for the sets of experiments carried out with r=1.00 and r=1.02, specially for initiator

concentrations 2 and 3 wbm%. This should be attributed to small differences in the monomer concentrations of the experiments that slightly changed the total initiator and inhibitor concentrations of the reactions (see Table 3.1) rather than to the thiol/ene ratio. Over all, the rate of polymerization increases with increasing concentration of AIBN and also the final conversion, which is the highest for the experiments with the highest concentration of AIBN. The effect of the inhibitor is clear on the experiments because full conversion was not reached in 4 hours of reaction. In absence of the inhibitor, these reactions reach full conversion in few minutes.

The molar mass of the final sample was measured by SEC/MALS/RI. The average values and dispersities are presented in Table 3.2 as well as the final conversion of each experiment. In general, molar masses are small because full conversions were not achieved in the experiments. Furthermore, the higher the achieved conversion, the higher the molar mass is, as it is expected for a step-growth polymerization.

Table 3.2. Data measured by SEC/MALS for all of the experiments.

Experiment	r-value	Mn [kDa]	Mw [kDa]	Đ	Conversion [%]
Run1	1.00	1.8	2.5	1.4	74
Run2	1.00	1.8	3.0	1.7	84
Run3	1.00	3.4	5.6	1.7	89
Run4	1.02	1.7	2.3	1.3	70
Run5	1.02	2.2	3.7	1.7	83
Run6	1.02	3.3	5.7	1.7	88

MALDI-TOF was used to determine the nature of the copolymer chains produced and hence, to validate the kinetic scheme used in the thiol-ene polymerization model. The MALDI-TOF mass spectra for all of the experiments showed that at least five different species were present. It was observed that the molar mass difference between two consecutive peaks of the same kind was 408.10 Da, which corresponds to the mass of a thiol-ene monomer unit (see Figure 3.4). The assignment was made using MSpolycalc software,[40] considering the thiol-ene as repetitive unit and different end-groups at both chain ends. The end-groups considered were -$C_{12}H_{18}O_4$,-$C_6H_{14}S_2O_2$, -C_4H_6N, and -$C_{14}H_{21}O_2$. The -$C_{12}H_{18}O_4$ end-group stands for a terminal diene unit (b), the -$C_6H_{14}S_2O_2$ end-group for a terminal dithiol unit (a), the -C_4H_6N end-group for a terminal initiator fragment (I), and the -$C_{14}H_{21}O_2$ end-group for a terminal DBHQ fragment.

Three out of the five species could be assigned whereas two could not be assigned and remained unknown (labelled U1 and U2). The species assigned correspond to inactive species Pab, Paa and Pbb considered in the mathematical model (see Figure 3.2). The $[M+Na]^+$ adducts and their structures could be further confirmed by the good agreement between the theoretical isotopic distribution and the experimental one (Figure 3.5). Two of the detected species could not be assigned and these were labelled as U1 and U2 (Figure 3.4). The unknown species do not match with the masses of the rest of inactive species in Figure 3.2. Although species U1 might correspond to PaI $[M+Na+H]^+$ because of a good agreement with the theoretical isotopic pattern, the mass fraction of U1 species cannot be justified by the amount of initiator molecules used in the formulation (the calculation is shown in the section III.6 of the Appendix), hence this assignment was discarded.

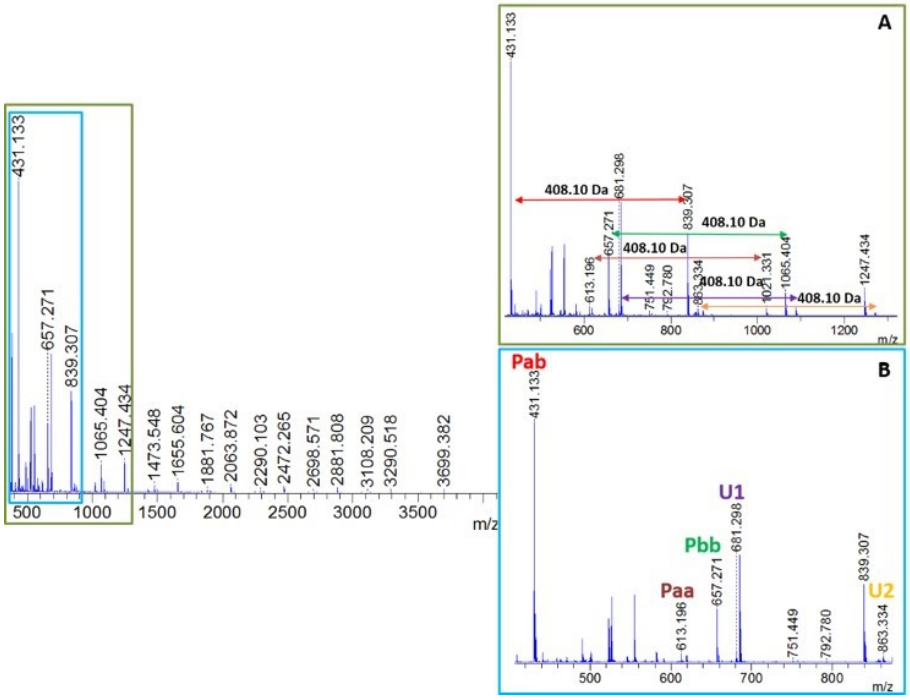

Figure 3.4. Representative MALDI-TOF mass spectra of thiol-ene polymerization using DCTB matrix and NaTFA cationization agent. Complete spectra in 500–4000 Da mass range (left). Enlargements (right) in different mass ranges (A) 400–1300 and (B) 400-900 Da, which show the different detected species Pab, Paa, Pbb, U1 and U2.

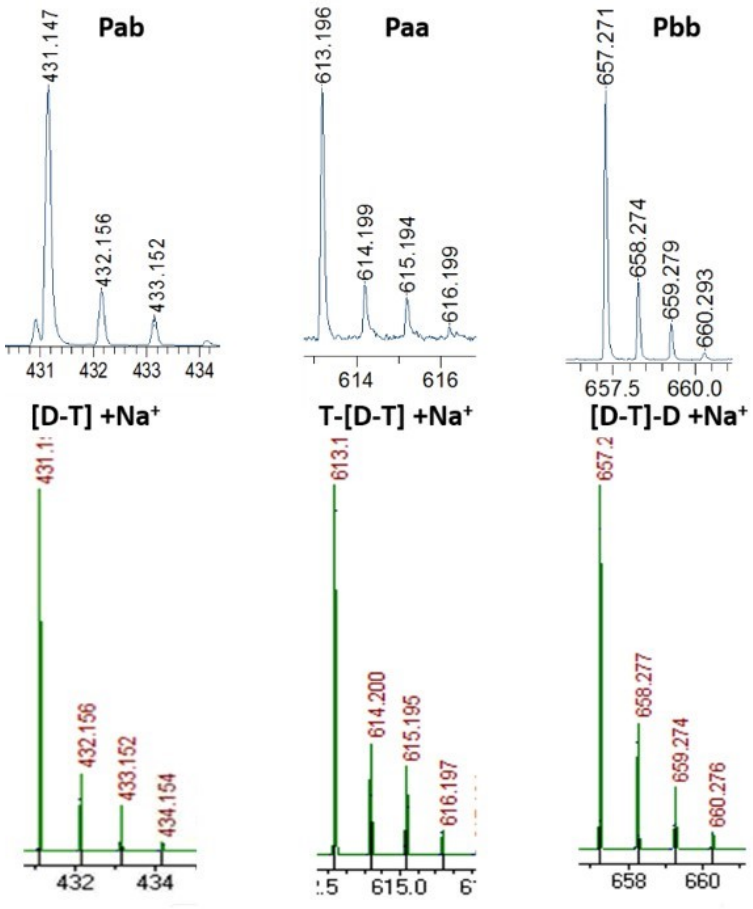

Figure 3.5. MALDI-TOF mass spectra in reflectron mode of thiol-ene copolymers compared with the isotopic pattern: observed (above) and theoretical (below).

The molar fractions of each of the species were calculated from the MALDI spectra and are displayed in Table 3.3. Pab was the most intense specie followed by Pbb and Paa. Notably, the three fractions assigned account for more than 90% of the copolymer species.

The molar fractions of the Pab specie increase with initiator concentration (final conversion) whereas the fractions of Paa and Pbb decrease. The two unknown species U1 and U2 do not show a trend for the different initiator concentrations used.

Table 3.3. Fractions calculated from MALDI-TOF mass spectra for the different species obtained from thiol-ene polymerization.

Experiment	r-value	Fractions				
		Pab	**Paa**	**Pbb**	**U1**	**U2**
Run1	1.00	0.620	0.005	0.250	0.097	0.020
Run2	1.00	0.670	0.041	0.180	0.080	0.030
Run3	1.00	0.900	0.020	0.070	0.008	0.003
Run4	1.02	0.550	0.080	0.270	0.060	0.030
Run5	1.02	0.750	0.040	0.180	0.020	0.007
Run6	1.02	0.870	0.010	0.100	0.020	0.003

3.3.2. Parameter estimation

The mathematical model described above was used to fit the experimental data (evolution of conversion of the double bonds of the diene, molar mass and composition of the copolymer species determined my MALDI-TOF). The model as described above contains a large number of rate coefficients (k_d, k_{ISH}, k_{Ivi}, k_{ad}, k_{tr}, k_{comb}, $k_{combISH}$, $k_{combIvi}$, k_{inh}) and although some of them have been already determined by other authors with sufficient accuracy, others are uncertain and likely system dependent and should be estimated.

The values of the kinetic rate coefficients taken from the literature are presented in Table 3.4.

Table 3.4. Values of parameters used in the model simulation at 65°C.

Parameter	Value	Reference
k_d (s^{-1})	$3.2 \cdot 10^{15} \exp(-131.1/RT)$	[46]
f (-)	0.6	
k_{Ivi} (L mol^{-1} s^{-1})	28.66	[45]
k_{comb} (L mol^{-1} s^{-1})	2.0×10^8	[27]
$k_{ad}=10 \times k_{tr}$ (L mol^{-1} s^{-1})		[27]
k_{ISH}^*(L mol^{-1} s^{-1})	$8.6 \times 10^3 \pm 1.2 \times 10^2$	This work
k_{tr}^*(L mol^{-1} s^{-1})	$1.1 \times 10^8 \pm 1.72 \times 10^6$	This work
k_{inhib}^*(L mol^{-1} s^{-1})	$1.7 \times 10^6 \pm 2.5 \times 10^4$	This work

**Estimated rate coefficients from parameter estimation.*

The decomposition of the AIBN initiator (k_d) and efficiency (f) are well known from free-radical polymerization studies and, hence, they were taken from literature as displayed in Table 3.4. The initiation reaction of the AIBN radical with the allyl monomer (k_{Ivi}) has not been reported. Notwithstanding, Dossi[45] carried out density functional theory, DFT, quantum computations of the addition of carbon centred radicals (from decomposition of common thermal initiators) to alkenes. He found that the addition of the initiator radical to a monomer (k_{Ivi}) was deeply affected by the initiator type; the k_{Ivi} values were much larger than the corresponding k_p values from four to nine orders of magnitude depending on the initiator considered, with the remarkable exception of the AIBN-monomer systems. AIBN was found to be the less reactive initiator because of the highest activation energy of the initiation reaction of the AIBN radical and acrylate, methacrylate, styrene or acrylonitrile monomers. The activation energy for the initiation reaction was around 10 kcal/mol for all these monomers. In absence of any other value, used the value reported by Dossi for the initiation of AIBN with styrene. It is noteworthy that this value is several orders of magnitude smaller than the values reported for the same reaction when photoinitiators like DMPA (2,2-dimethoxy-2-phenylacetophenone) are used in thiol-ene polymerizations[30].

Bowman et al. studied the kinetics of thiol-allyl photopolymerizations and they found that the chain transfer reaction was the limiting reaction and the ratio of the addition to chain transfer rate was 10. Considering this ratio they estimated the kinetic rate coefficients of chain transfer and termination reactions using the experimental measured average radical lifetimes and analytical expressions[25,27]. The thiol-ene polymerization considered in this work is also a thiol-allyl polymerization and hence, the k_{ad}/k_{tr} was set at 10 and the k_{tr} was estimated. On the other hand and for simplicity, all the termination rate coefficients were considered equal and a value of k_{tcomb}

= 2×10^8 L/mol·s was used, which is in the range of termination rate coefficients determined for the thiol-allyl systems by Bowman et al.[27]

Therefore, only three rate coefficients (k_{tr}, k_{ISH}, k_{inh}) were considered in the parameter estimation algorithm.The experimental ene conversion data, the final weight-average molar masses of each experiment, and molar fractions of the polymer species were used to estimate the unknown parameters using the parameter estimation algorithm of the Predici package.

The estimated parameters in Table 3.4 were estimated simultaneously by fitting all experimental datasets. In the parameter estimation algorithm, the relative total residual is $\boldsymbol{r_{rel}} = \frac{\mathbf{1}}{\sqrt{\boldsymbol{N}}}\sqrt{\boldsymbol{SS_E}}$, where N is the total number of data and $\boldsymbol{SS_E}$ is the weighted residual sum of squares. The lowest residual achieved in the parameter estimation algorithm yield the values displayed in Table 3.4¡Error! No se encuentra el origen de la referencia. for the three estimated rate coefficients and their confidence intervals. Note that the rate coefficients estimated in this work correspond to 65 ºC whereas the values reported in the literature are for photopolymerizations carried out at room temperature.

The estimated chain transfer coefficient ($1.1\times10^8\pm 1.72\times10^6$, L mol^{-1} s^{-1}) is one to two orders of magnitude higher than the chain transfer coefficient range found by other authors[27,30] for similar thiol-ene systems, which was reported to be in the range of 10^5-10^6L mol^{-1} s^{-1}. The k_{ISH} value is estimated to be much lower ($8.6\times10^3\pm 1.2\times10^2$, L mol^{-1} s^{-1}) than the chain transfer rate coefficient being this reaction the rate limiting one. The inhibition rate coefficient is estimated to be $1.7\times10^6\pm 2.5\times10^4$ (L mol^{-1} s^{-1}), which is reasonable for a termination reaction. It is worth mentioning that the constants of k_{ISH} and k_{inhib} are correlated.

Figures 3.6-3.10 show the comparison of experimental ene conversion, weight-average molar masses and molar fractions of polymer species with the model prediction using the estimated parameters of Table 3.4. Figure 3.6 reveals that the model predicts reasonably well the overall rate of polymerization and the effect of initiator concentration. The sensitivity of the model prediction to the initiator concentration is weaker than what it is observed experimentally, and this leads to worst predictions for the highest initiator concentrations.

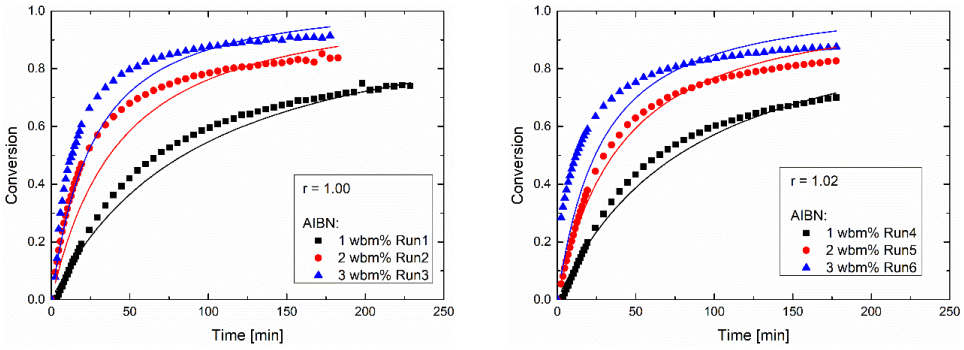

Figure 3.6. Comparison between the predicted (lines) and experimental ene conversions (symbols) for the experiments with r = 1.00 (a) and r = 1.02 (b).

Figure 3.7 displays the comparison of the weight-average molar mass measured at the end of each reaction with the values predicted by the model at the same time. Molar masses in the range of 2300 – 5700 g/mol were determined, which will be chains between 6 to14 repeating units. The model captures well the increase of the molar masses by increasing initiator concentration and predicts reasonably well the weight-average molar masses of different experiments. However, in step-growth polymerization the molar masses are a direct function of

the conversion of the functional groups (well-known Carothers equation). Therefore, it is worth plotting all the molar masses achieved in the experiments as a function of the conversion and compare with the model predictions and the Carothers equation (Equation 3.1).

$$M_w = (1 + X/1 - X)w_{RU} \quad (3.1)$$

In which X is conversion and w_{RU} (g/mol) is the molar mass of the repeating unit). Figure 3.8 shows that the experimental molar masses are higher than the predicted ones and also higher than the predicted by the Carothers equation. Note that the predictions of the model developed in this work collapse in a single line.

The deviation between the experimental and predicted values (developed model or Carothers equation) is an indication that side reactions occur that lead to higher molar masses than predicted by the models. The Carothers equation assume no side reactions at all and the model developed in this work considers only bimolecular terminations by combination between thiyl radicals. As discussed in the mathematical model section, this assumption avoids the formation of trifunctional species and hence, the formation of branched and crosslinked chains with higher molar masses, which likely causes the observed deviation.

A similar deviation was found by Chemtob et al.[36] for the same thiol-ene polymerization system when comparing experimental molar masses and the Carothers equation for polymers produced in thiol-ene emulsion polymerization. Chemtob et al.[36] hypothesized that such deviations have been observed in other step-growth polymerizations with fast kinetics and separation of

monomers in two phases[47,48]. However, this hypothesis is very unlikely in solution polymerization reactions.

On the other hand, the model prediction and the prediction of the Carothers equation are very close except at conversions below 0.7. This is an indication that the side reactions considered in the model (initiation of vinyl groups, and termination between thiyl radicals and inhibition reactions) are not significant in the outcome of the polymerization. This is in agreement with the high coupling efficiency calculated in the model predictions that reach values of 0.97.

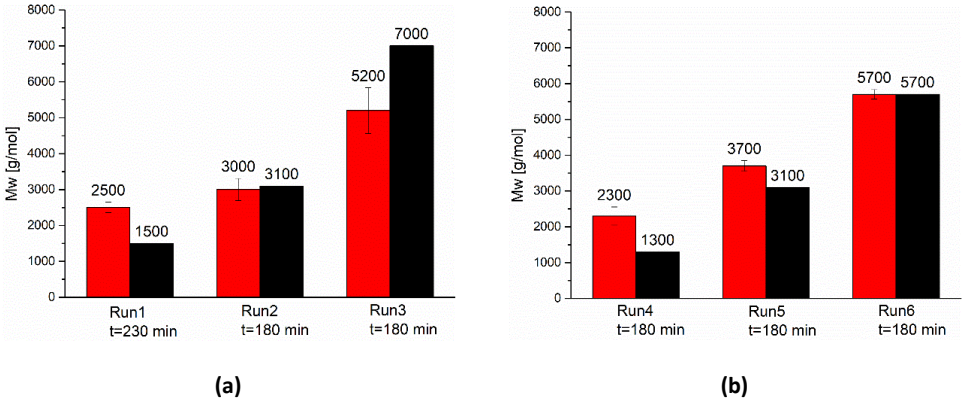

Figure 3.7. Comparison of weight-average molar masses measured by SEC/MALS (red) and model predictions (black) at the reaction time indicated in the Figure.

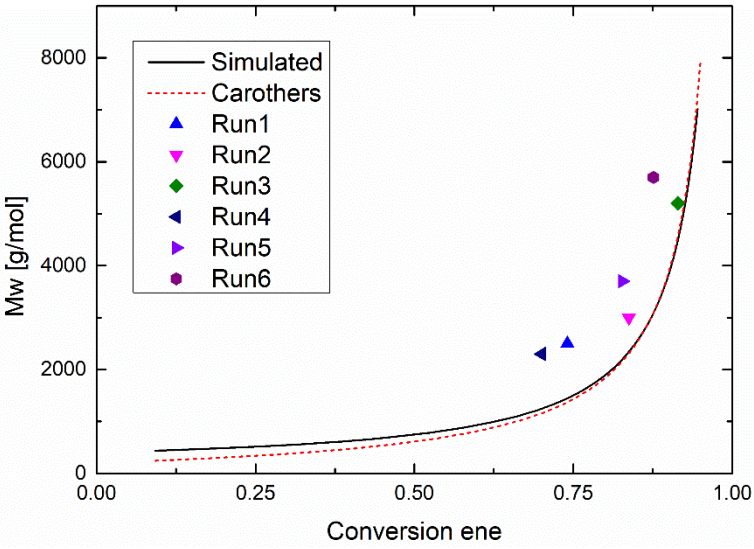

Figure 3.8. Carothers equation (red dashed line), experimental (dots) and predictions of the mathematical model (black line) developed in this work for the weight-average molar masses.

Figure 3.9 and 3.10 show the comparison between the molar fractions of polymer species (Pab, Paa and Pbb) measured experimentally by MALDI-TOF with model predictions at final time of each experiment. The model captured well that the main species are those identified in the MALDI-TOF analysis; namely, Pab, Paa and Pab. However, these fractions account for more than 99% of the species in the model prediction whereas experimentally they accounted for approximately 90% of the polymer species (there were two species detected in the MALDI-TOF that could not be identified). This is in agreement with the differences found in the molar masses for the model predictions and the experimental values; namely, the unknown species that represent circa 10% of the polymer cannot be justified by the side reactions considered in the

model and other side reactions should be considered (combination reactions leading to non-linear species) to fill this gap.

On the other hand, it is noteworthy that the model predicts well that the main species is Pab. However, the effect of initiator concentration on the molar fractions of the species is not captured by the model. Experimentally, Pab species increase with initiator concentration whereas the fractions of Paa and Pbb decrease, while in the model Pab species decrease with increasing the initiator concentration and Paa and Pbb increase. Note that this trend predicted by the model for the effect of initiator concentration on composition of the species has been found insensitive to any parameter included in the model.

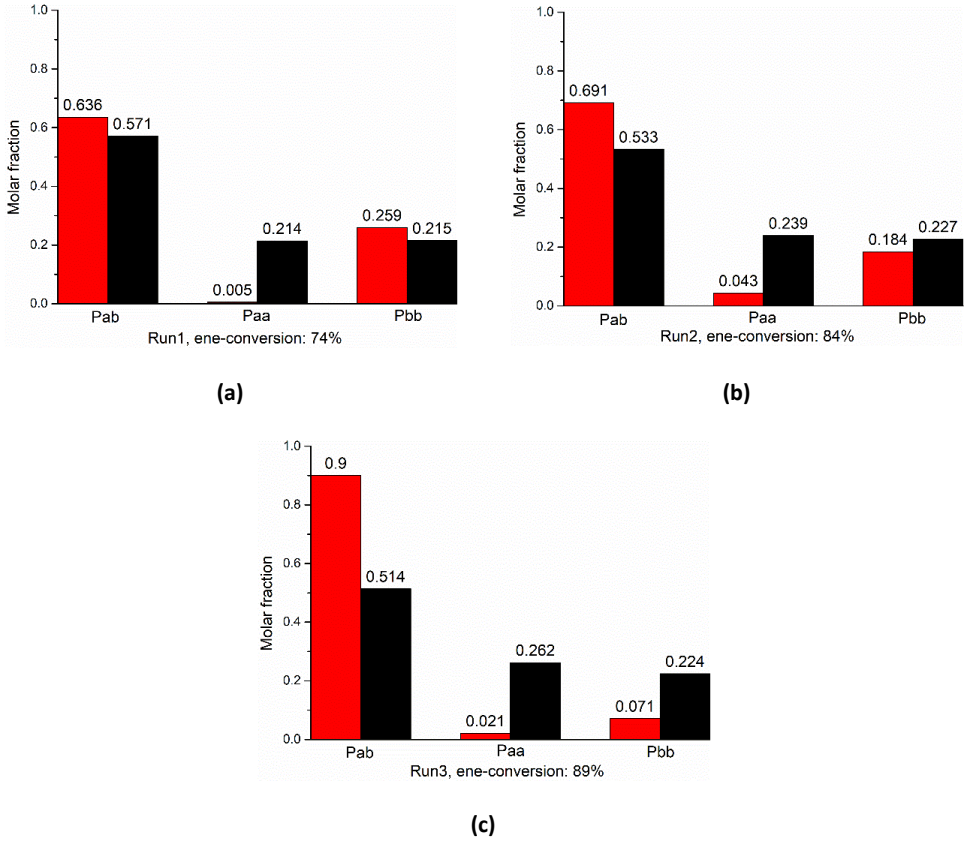

Figure 3.9. Comparison between the experimental fractions of the species Pab, Paa and Pbb measured by MALDI-TOF (red) and simulated (black) for the experiments with r = 1.00.

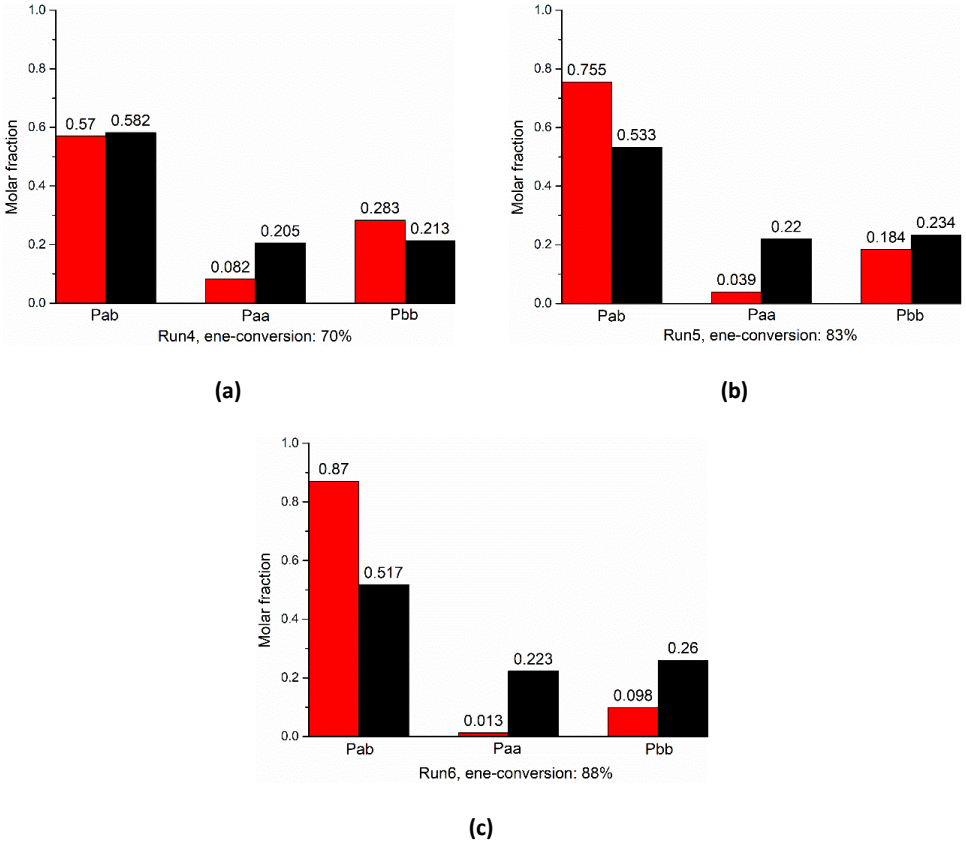

Figure 3.10. Comparison between the experimental fractions of the species Pab, Paa and Pbb measured by MALDI-TOF (red) and simulated (black) for the experiments with r = 1.02.

Overall, the prediction of the model is in relative good agreement with the experimental functional group conversion and molar masses although there are notable differences in the composition of the polymer species. This has been achieved using estimated rate coefficients that are substantially different to those reported by other authors for similar thiol-ene system (although the reported values were at room temperature and herein at 65ºC) and hence, their validity may

be questionable. A simulation using the rate coefficients reported in the literature for the thiol-allyl ether system[30] and only estimating the unknown rate coefficient of inhibition reaction was carried out for comparison purposes. The rate coefficients used are listed in the section III of the Appendix (Table III.3) and the comparison between model predictions and experimental data are displayed in Figures III.3-III.7 in the Appendix. The predictions for these set of parameters show that the kinetics are not captured by the model i.e. the rate of polymerization is underestimated and the prediction of the molar masses at final time of the reaction is also poorer. On the other hand, the molar fractions of polymer species show little sensitivity to the model parameters while as mentioned also above, the trend predicted by the model for the effect of initiator concentration shows to be insensitive to the model parameters.

3.4. Conclusion

A mathematical model for the thermally initiated thiol-ene polymerization was developed. The model considers the generation of initiator radicals by thermal decomposition, the abstraction of hydrogen atoms of these radicals in thiol functional groups generating thiyl radicals (R-S*), the addition of thiyl radicals to ene functional groups generating the thio-ether coupling and the chain transfer of these radicals with thiol functional groups. In addition to these reactions, the model considers side reactions (reaction of initiator radicals with ene functional groups, termination reactions between thiyl radicals and thiyl radicals and initiator radicals, and inhibition reactions of all radical species with DBHQ molecules) that reduce the ideal 100% coupling efficiency. The model was used to predict the thiol-ene solution polymerization of EDDT (dithiol) and DAA (diene) initiated by AIBN. The time evolution of the ene conversions achieved for different initiator concentrations was reasonable well fitted by the model using three estimated rate coefficients; k_{ISH}, k_{tr} and k_{inhib} together with parameters from the literature for this thiol-ene system. The molar masses predicted by the model are slightly smaller than those measured experimentally likely because side reactions leading to branched chains were not considered (e.g. termination between carbon centred radicals and carbon centred radicals and thiyl radicals). The model predicts that three polymeric species (Paa, Pab and Pbb) account for 99% of the polymer produced in the polymerizations. Experimentally these three species account for up to 90% of the polymer. Notably, the model is able to predict that the main species is Pab although the effect of the initiator concentration on the molar fractions is not captured. The estimated values for k_{ISH} and k_{tr} are not in agreement with reported data for similar systems, but it was found that using the values from literature yield substantially worse predictions of the molar masses and ene

conversions although no noticeable changes in the prediction of the composition of the polymer species.

The model predictions of species produced in a thiol-ene polymerization are compared with experimental data. As discussed above there is a 10% of species that has not been recognized and in addition the model, although roughly identifies well the main polymeric species formed, it is not able to capture correctly their distribution and the trends in their distribution when initiator concentration is increased. These discrepancies need to be addressed by carrying out more experiments and including additional side reactions in the model to cope with the complexity of thiol-ene polymerizations.

3.5. References

(1) Hoyle, C. E.; Lee, T. Y.; Roper, T. Thiol-Enes: Chemistry of the Past with Promise for the Future. *J. Polym. Sci. Part A Polym. Chem.* **2004**, *42* (21), 5301–5338. https://doi.org/10.1002/pola.20366.

(2) Machado, T. O.; Sayer, C.; Araujo, P. H. H. Thiol-Ene Polymerisation : A Promising Technique to Obtain Novel Biomaterials. *Eur. Polym. J.* **2017**, *86*, 200–215. https://doi.org/10.1016/j.eurpolymj.2016.02.025.

(3) Cardoso, P. B.; Machado, T. O.; Feuser, P. E.; Sayer, C.; Meier, M. A. R.; Araújo, P. H. H. Biocompatible Polymeric Nanoparticles From Castor Oil Derivatives via Thiol-Ene Miniemulsion Polymerization. *Eur. J. Lipid Sci. Technol.* **2018**, *120* (1), 1–8. https://doi.org/10.1002/ejlt.201700212.

(4) Machado, T. O.; Cardoso, P. B.; Feuser, P. E.; Sayer, C.; Araújo, P. H. H. Thiol-Ene Miniemulsion Polymerization of a Biobased Monomer for Biomedical Applications. *Colloids Surfaces B Biointerfaces* **2017**, *159*, 509–517. https://doi.org/10.1016/j.colsurfb.2017.07.043.

(5) Donovan, B. R.; Cobb, J. S.; Ho, E. F. T.; Patton, D. L. Thiol-Ene Adhesives from Clove Oil Derivates. *RSC Adv.* **2014**, *4*, 61927–61935. https://doi.org/10.1039/c4ra12020e.

(6) Lu, H.; Carioscia, J. A.; Stansbury, J. W.; Bowman, C. N. Investigations of Step-Growth Thiol-Ene Polymerizations for Novel Dental Restoratives. *Dent Mater.* **2005**, *21*, 1129–

1136. https://doi.org/10.1016/j.dental.2005.04.001.

(7) Cramer, N. B.; Couch, C. L.; Schreck, K. M.; Carioscia, J. A.; Boulden, E.; Stansbury, J. W.; Bowman, C. N. Investigation of Thiol-Ene and Thiol-Ene-Methacrylate Based Resins as Dental Restorative Materials. *Dent Mater.* **2011**, *26* (1), 21–28. https://doi.org/10.1016/j.dental.2009.08.004.Investigation.

(8) Black, M.; Rawlins, J. W. Thiol – Ene UV-Curable Coatings Using Vegetable Oil Macromonomers. *Eur. Polym. J.* **2009**, *45* (5), 1433–1441. https://doi.org/10.1016/j.eurpolymj.2009.02.007.

(9) Chen, Z.; Chisholm, B. J.; Patani, R.; Wu, J. F.; Fernando, S.; Jogodzinski, K.; Webster, D. C. Soy-Based UV-Curable Thiol – Ene Coatings. *J. Coat. Technol. Res.* **2010**, *7* (5), 603–613. https://doi.org/10.1007/s11998-010-9241-x.

(10) Resetco, C.; Hendriks, B.; Badi, N.; Prez, F. Du. Materials Horizons Thiol – Ene Chemistry for Polymer Coatings and Surface Modification – Building in Sustainability. *Mater. Horiz.* **2017**, *4*, 1041–1053. https://doi.org/10.1039/c7mh00488e.

(11) Reddy, S. K.; Cramer, N. B.; Cross, T.; Raj, R.; Bowman, C. N. Polymer-Derived Ceramic Materials from Thiol-Ene Photopolymerizations. *Chem. Mater.Mater.* **2003**, *15*, 4257–4261.

(12) Wang, X.; Schmidt, F.; Hanaor, D.; Kamm, P. H.; Li, S. Additive Manufacturing of Ceramics from Preceramic Polymers : A Versatile Stereolithographic Approach Assisted

by Thiol-Ene Click Chemistry. *Addit. Manuf.* **2019**, *27* (February), 80–90. https://doi.org/10.1016/j.addma.2019.02.012.

(13) Wang, X.; Schmidt, F.; Gurlo, A. Fabrication of Polymer-Derived Ceramics with Hierarchical Porosities by Freeze Casting Assisted by Thiol-Ene Click Chemistry and HF Etching. *J. Eur. Ceram. Soc.* **2020**, *40* (2), 315–323. https://doi.org/10.1016/j.jeurceramsoc.2019.09.038.

(14) Natarajan, L. V; Shepherd, C. K.; Brandelik, D. M.; Sutherland, R. L.; Chandra, S.; Tondiglia, V. P.; Tomlin, D.; Bunning, T. J. Switchable Holographic Polymer-Dispersed Liquid Crystal Reflection Gratings Based on Thiol - Ene Photopolymerization. *Chem. Mater.* **2003**, *15*, 2477–2484.

(15) Ware, T. H.; Perry, Z. P.; Middleton, C. M.; Iacono, S. T.; White, T. J. Programmable Liquid Crystal Elastomers Prepared by Thiol − Ene Photopolymerization. *ACS Macro Lett.* **2015**, *4*, 942–946. https://doi.org/10.1021/acsmacrolett.5b00511.

(16) Matsukawa, K.; Fukuda, T.; Watase, S.; Goda, H. Preperation of Photo-Curable Thiol-Ene Hybrids and Their Application for Optical Materials. *J. Photopolym. Sci. Technol.* **2010**, *23*, 115–119.

(17) Jawerth, M.; Johansson, M.; Lundmark, S.; Gioia, C.; Lawoko, M. Renewable Thiol−Ene Thermosets Based on Refined and Selectively Allylated Industrial Lignin. *ACS Sustain. Chem. Eng.* **2017**, *5*, 10918–10925. https://doi.org/10.1021/acssuschemeng.7b02822.

(18) Li, C.; Johansson, M.; Sablong, R. J.; Koning, C. E. High Performance Thiol-Ene Thermosets Based on Fully Bio-Based Poly(Limonene Carbonate)S. *Eur. Polym. J.* **2017**, *96* (August), 337–349. https://doi.org/10.1016/j.eurpolymj.2017.09.034.

(19) Tian, Y.; Wang, Q.; Cheng, J.; Zhang, J. A Fully Biomass Based Monomer from Itaconic Acid and Eugenol to Build Degradable Thermosets via Thiol-Ene Click Chemistry. *Green Chem.* **2020**, *22*, 921–932. https://doi.org/10.1039/c9gc03931g.

(20) Hoyle, C. E.; Bowman, C. N. Thiol-Ene Click Chemistry. *Angew. Chem. Int. Ed.* **2010**, *49*, 1540–1573. https://doi.org/10.1002/anie.200903924.

(21) Kade, M. J.; Burke, D. J.; Hawker, C. J. The Power of Thiol-Ene Chemistry. *J. Polym. Sci., Part A Polym. Chem.* **2010**, *48*, 743–750. https://doi.org/10.1002/POLA.

(22) Hoyle, C. E.; Lowe, A. B.; Bowman, C. N. Thiol-Click Chemistry: A Multifaceted Toolbox for Small Molecule and Polymer Synthesis. *Chem. Soc. Rev.* **2010**, *39*, 1355–1387. https://doi.org/10.1039/b901979k.

(23) Carothers, H. Polymers and Polyfunctionality. *Trans. Faraday Soc.* **1935**, *32*, 39–49.

(24) Stille, J. K. Step-Growth Polymerization. *J. Chem. Educ.* **1981**, *58* (11), 862–866.

(25) Reddy, S. K.; Cramer, N. B.; Bowman, C. N. Thiol-Vinyl Mechanisms. 2. Kinetic Modeling of Ternary Thiol-Vinyl Photopolymerizations. *Macromolecules* **2006**, *39*, 3681–3687. https://doi.org/10.1021/ma0600097.

(26) Cramer, N. B.; Davies, T.; Brien, A. K. O.; Bowman, C. N. Mechanism and Modeling of a Thiol - Ene Photopolymerization. *Macromolecules* **2003**, *36*, 4631–4636. https://doi.org/10.1021/ma034072x.

(27) Reddy, S. K.; Cramer, N. B.; Bowman, C. N. Thiol - Vinyl Mechanisms . 1 . Termination and Propagation Kinetics in Thiol - Ene Photopolymerizations. *Macromolecules* **2006**, *39*, 3673–3680. https://doi.org/10.1021/ma060008e.

(28) Okay, O.; Bowman, C. N. Kinetic Modeling of Thiol-Ene Reactions with Both Step and Chain Growth Aspects. *Macromol. Theory Simulations* **2005**, *14* (4), 267–277. https://doi.org/10.1002/mats.200500002.

(29) Northrop, B. H.; Coffey, R. N. Thiol−Ene Click Chemistry: Computational and Kinetic Analysis of the Influence of Alkene Functionality. *Am. Chem. Soc.* **2012**, *134*, 13804–13817. https://doi.org/10.1021/ja305441d.

(30) Derboven, P.; Dagmar, R. D.; Stamenovic, M. M.; Espeel, P.; Marin, G. B.; Prez, F. E. Du. Kinetic Modeling of Radical Thiol−Ene Chemistry for Macromolecular Design: Importance of Side Reactions and Diffusional Limitations. *Macromolecules* **2013**, *46*, 1732–1742. https://doi.org/10.1021/ma302619k.

(31) Long, K. F.; Bongiardina, N. J.; Mayordomo, P.; Olin, M. J.; Ortega, A. D.; Bowman, C. N. Effects of 1°, 2°, and 3° Thiols on Thiol–Ene Reactions: Polymerization Kinetics and Mechanical Behavior. *Macromolecules* **2020**, *53*, 5805–5815. https://doi.org/10.1021/acs.macromol.0c00369.

(32) Nguyen, L. T.; Gokmen, T.; Du Prez, F. Kinetic Comparison of 13 Homogeneous Thiol-X Reactions. *Polym. Chem.* **2013**, *4* (5527). https://doi.org/10.1039/b000000x.

(33) Zhang, X.; Claudino, M.; Bowman, C. N. Mechanistic Modeling of the Thiol−Michael Addition Polymerization Kinetics: Structural Effects of the Thiol and Vinyl Monomers´. *Macromolecules* **2018**, *51*, 5979–5988. https://doi.org/10.1021/acs.macromol.8b01264.

(34) Long, K. F.; Wang, H.; Dimos, T. T.; Bowman, C. N. Effects of Thiol Substitution on the Kinetics and Efficiency of Thiol-Michael Reactions and Polymerizations. *Macromolecules* **2021**, *54*, 3093–3100. https://doi.org/10.1021/acs.macromol.0c02677.

(35) Cramer, N. B.; Bowman, C. N. Thiol – Ene Chemistry. In *Chemoselective and Bioorthogonal Ligation Reactions: Concepts and Applications*; WILEY-VCH, 2017; Vol. First edit, pp 117–145.

(36) Minh, C.; Le, Q.; Schmutz, M.; Chemtob, A. Ab Initio Batch Emulsion Thiol − Ene Photopolymerization. *Macromolecules* **2020**, *53*, 2369–2379. https://doi.org/10.1021/acs.macromol.0c00265.

(37) Esfandiari, P.; Ligon, S. C.; Lagref, J. J.; Frantz, R.; Cherkaoui, Z.; Liska, R. Efficient Stabilization of Thiol-Ene Formulations in Radical Photopolymerization. *J. Polym. Sci., Part A Polym. Chem.* **2013**, *51*, 4261–4266. https://doi.org/10.1002/pola.26848.

(38) Edler, M.; Mostegel, F. H.; Roth, M.; Oesterreicher, A.; Kappaun, S.; Griesser, T. Enhancing the Stability of UV-Curable Thiol/Vinyl Carbonate Resins. *J. Appl. Pol. Sci.*

2017, *134*. https://doi.org/10.1002/app.44934.

(39) Cramer, N. B.; Reddy, S. K.; Cole, M.; Hoyle, C.; Bowman, C. N. Initiation and Kinetics of Thiol – Ene Photopolymerizations without Photoinitiators. *J. Polym. Sci., Part A Polym. Chem.* **2004**, *42*, 5817–5826. https://doi.org/10.1002/pola.20419.

(40) Desport, J. S.; Frache, G. MSPolyCalc : A Web - Based App for Polymer Mass Spectrometry Data Interpretation . The Case Study of a Pharmaceutical Excipient. *Rapid Commun. Mass Spectrom.* **2020**, *34* (52). https://doi.org/10.1002/rcm.8652.

(41) Ruiperez, F.; Galdeano, M.; Gimenez, E.; Matxain, J. M. Sulfenamides as Building Blocks for Efficient Disulfide- Based Self-Healing Materials . A Quantum Chemical Study. *ChemistryOpen* **2018**, *7*, 248–255. https://doi.org/10.1002/open.201800003.

(42) Rekondo, A.; Martin, R.; de Luzuriaga, A. R.; Cabañero, G.; Grande, H. J.; Odriozola, I. Catalyst-Free Room-Temperature Self-Healing Elastomers Based on Aromatic Disulfide Metathesis. *Mater. Horiz.* **2014**, *1*, 237–240. https://doi.org/10.1039/c3mh00061c.

(43) Matxain, J. M.; Asua, M.; Ruipe, F. Design of New Disulfide-Based Organic Compounds for the Improvement of Self-Healing Materials. *Phys. Chem. Chem. Phys.* **2016**, *18*, 1758–1770. https://doi.org/10.1039/c5cp06660c.

(44) Wulkow, M. Computer Aided Modeling of Polymer Reaction Engineering-The Status of Predici, I-Simulation. *Macromol. React. Eng.* **2008**, *2* (6), 461–494. https://doi.org/10.1002/mren.200800024.

(45) Dossi, M. Quantum Chemistry Study of Free-Radical Polymerization Kinetics, Politecnico de Milano, 2011.

(46) Korolev, G. V; Bubnova, M. L.; Makhonina, L. I. Free-Radical Copolymerization of Binary Mixtures of Vinyl Monomers of Various Compositions : Initiation Rate Constants 1. *Polym. Sci. Part A Polym. Chem.* **2007**, *49* (3), 242–248. https://doi.org/10.1134/S0965545X07030029.

(47) Piradashvili, K.; Alexandrino, E. M.; Wurm, F. R.; Landfester, K. Reactions and Polymerizations at the Liquid − Liquid Interface. *Chem. Rev.* **2016**, *116*, 2141–2169. https://doi.org/10.1021/acs.chemrev.5b00567.

(48) Song, Y.; Fan, J.; Wang, S. Recent Progress in Interfacial Polymerization. *Mater. Chem. Front.* **2017**, *1*, 1028–1040. https://doi.org/10.1039/c6qm00325g.

Chapter 4. Thermally initiated Thiol-Ene Polymerization in dispersed media

4.1. Introduction

The general features of thiol-ene radical step-growth polymerization were discussed in Chapter 4 and a mathematical model was developed. However, the radical step-growth polymerizations carried out so far were either in bulk or in solution. In this Chapter, the results obtained for thermally initiated thiol-ene polymerizations in waterborne systems as a method to incorporate ester groups into the polymer backbone are presented.

Step-growth polymerizations are far less commonly used in dispersed systems than radical-mediated chain-growth reactions.[1] Thus different kinetic factors such as for example the number of radicals per particle or the nucleation mechanism is not well studied for these systems.

The major amount of waterborne thiol-ene polymerizations described in the literature are carried out in miniemulsion polymerizations. Thiol-ene miniemulsion photopolymerizations have been described for the synthesis of biomaterials,[2–4] synthesis of semicrystalline polysulfide nanoparticles[5,6] and synthesis of functional sub-100 nm polymer nanoparticles.[7] In addition,

droplet nucleation during miniemulsion photopolymerization was investigated recently by Chemtob et al.[8]. They found out that using water-soluble photoinitiator, substantial homogeneous nucleation was occurring even for very water-insoluble monomers. However, at small enough droplet diameters (~100 nm), droplet nucleation was the dominant mechanism. On the other hand, thermally initiated thiol-ene minimemulsion polymerizations were used to encapsulate different concentrations of magnetic nanoparticles for the synthesis of superparamagnetic biobased poly(thioether-ester)[9]. The encapsulation efficiency was increased by 30% through the substitution of the dithiol 1.4-butanedithiol for the tetrathiol pentaerythritol tetra(3-mercaptopropionate) (PETMP) due to the crosslinking in these nanoparticles. The nanoparticles with sizes between 95 and 260 nm presented superparamagnetic behaviour.

There are few reports of thiol-ene radical step-growth polymerization performed in emulsion polymerization. Shipp et al. demonstrated that, despite the relatively small molar masses which are typically obtained from step-growth polymerizations, emulsion polymerization of thiol-ene monomers is possible to achieve by typical emulsion polymerization reaction conditions.[1] Their polymerizations were carried out in batch at a scale of 10 mL and a solid content of 10 wt%. SDS was used as surfactant and KPS as thermal initiator at 60 ºC. Furthermore, bi- and trifunctional enes as well as bi- and tetrafunctional thiols were used. The effect of surfactant and initiator concentration on particle sizes was studied and an empiric correlation was obtained to predict the particle size as a function of KPS and SDS concentrations. Over all particle sizes between 70-1000 nm with narrow particle size distributions were synthesized and the correlation shown in Equation 4.1 was proposed for systems consisting of a trifunctional ene and a tetrafunctional thiol monomer.

$$\mathbf{d_Z = (1090 \pm 80)[KPS]^{-(0.53\pm0.04)}[SDS]^{-(0.44\pm0.03)}} \quad \text{(Eq. 4.1)}$$

The orders of dependence of the particle diameter (d_Z) on surfactant (-0.44) and initiator concentrations (-0.53) are higher than the ones predicted by the Smith-Ewart kinetics for conventional emulsion polymerizations, which are -0.2 for the surfactant concentration and -0.13 for the initiator concentration.[1]

In a more recent publication, Chemtob et al. studied *ab-initio* batch emulsion thiol-ene photopolymerization of the dithiol EDDT and the diene DAP at solid contents up to 40 wt% using DBHQ as inhibitor to prevent preliminary polymerization.[10] Emulsions were prepared using a magnetic stirrer or an Ultra-Turrax homogenizer and photopolymerizations were carried out immediately after the preparation of the emulsion. Particle sizes in a range from 90-500 nm with relatively high polydispersities of the particle size distribution were obtained. Additionally, they found out that polymer particle formation mainly proceeded through the precipitation of oligo-radicals (*homogeneous nucleation*) even if the concentration of the emulsifier exceeded the CMC. Another publication of Chemtob et al. describes the photocatalytic thiol-ene emulsion polymerization of the dithiol 2,2'-dimercaptodiethyl sulphide with various dienes.[11] These emulsion polymerizations were carried out at a solid content of 10%. They obtained particle sizes in the range of 70-230 nm and number-average molar masses in between 7500-11000 g/mol.

In this Chapter, the results obtained for thermally initiated miniemulsion and emulsion thiol-ene polymerizations are presented and discussed. The structures of the used diene monomers are shown in Figure 4.1 and the thiol monomers are shown in Figure 4.2.

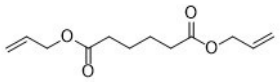

Diallyl adipate (DAA)

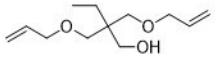

Trimethylolpropane diallyl ether
(TMPDAE)

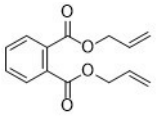

Diallyl phthalate (DAP)

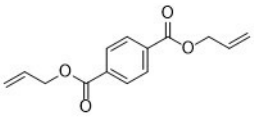

Diallyl terephthalate
(DATP)

Figure 4.1. Structures of the different diene monomers used within this work.

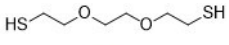

2,2'-
(Ethylenedioxy)
diethanthiol
(EDDT)

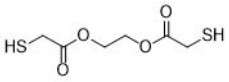

Glycol
dimercaptoacetate
(GDMA)

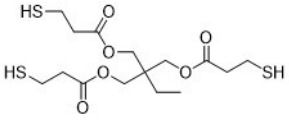

Pentaerythritol tetrakis(3-
mercaptopropionate)
(TMPMP)

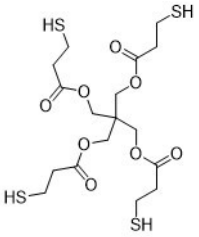

Pentaerythritol
tetra(3-
mercaptopropionate)
(PETMP)

Figure 4.2. Structures of thiol monomers with different functionalities used in this work.

Due to the low glass transition temperatures of the polymers obtained by thiol-ene polymerization, they are interesting candidates for the synthesis of PSAs. A recent publication by Sardon et al. describes the synthesis of PSAs via a photo-polymerization process which is

carried out in bulk.[12] Therefore, the feasibility to synthesize PSAs with ester groups in their polymeric backbone by thiol-ene polymerization in dispersed media is discussed in this chapter.

4.2. Experimental part

The experimental procedures are described in this part. Descriptions of the characterization methods such as GPC, NMR, DLS, DSC and AF4 are given in the appendix.

4.2.1. Thermally initiated thiol-ene miniemulsion polymerizations

Miniemulsions with 25 wt% monomer phase (based on the total weight) were prepared. The ratio between the thiol functional groups of the thiol-monomers and the vinyl functional groups of the diene-monomers (DAA; DAP and TMPDAE were used as diene monomers) was set to be 1 in all cases. Mostly, linear thiol- and ene-monomers were used. Nevertheless, in some cases, also up to 4 mol% of the tetrafunctional thiol PETMP was used. The 4 mol% was calculated with respect to the total amount of thiol functional groups, to keep the ratio of thiol- and ene-functional groups at 1. 4 wbm% of hexadecane was added to the oil phase as co-stabilizer. The aqueous phase consisted of 3 wbm% of the surfactant Dowfax 2A1 and distilled water. The formulation is shown in Table 4.1. Each of the two phases were stirred with a magnetic stirrer at 800 rpm, first individually for 15 min and after that, they were mixed and stirred for further 15 min. The mixture was then sonicated in an ice bath with a Hielscher sonicator (operating at 80% amplitude and 80% cycle). The miniemulsion was then transferred to a 50 mL round bottom flask, stirred with a magnetic stirrer at 700 rpm and heated to 75 ºC under nitrogen atmosphere. The initiator KPS was added as a shot when the reaction temperature was reached.

Table 4.1. General miniemulsion formulation.

Component		
Oil Phase	Diene	0.012 mol
	EDDT	0.012 mol
	TMPMP/PETMP*	0-4 mol%
	Hexadecane	4 wbm%
Water Phase	Dowfax 2A1	3 wbm%
	Deionized water	75 wt%
Initiator	KPS	0.5 wbm%

*With respect to the total amount of thiol functional groups (mol%)

4.2.2. Thermally initiated thiol-ene emulsion polymerizations

Thiol-ene emulsion polymerizations were carried out at a solid content of 25% either in a batch or in a semibatch process. For batch polymerizations, the diene (DAP, TMPDAE) and the dithiol EDDT were mixed with Dowfax 2A1 as surfactant and distilled water in a 50 mL round bottom flask and under nitrogen atmosphere. The thermal initiator KPS was added when the reaction temperature of 75 ºC was reached. On the other hand, for the semibatch emulsion thiol-ene polymerizations the surfactant Dowfax 2A1 and distilled water were mixed at first in a 50 mL round bottom flask, stirred with a magnetic stirrer at 700 rpm under nitrogen atmosphere. Furthermore, two feed streams, one with the thiol component (dithiol and trifunctional thiol in some cases) and one with the diene component (DAP or DATP) were prepared. When the reaction temperature of 75 ºC was reached, the complete amount of the thermal initiator KPS

was added as a shot and the feeding of the thiol and ene monomers was started at an equimolar ratio with respect to the total amount of thiol and ene functional groups. The total feeding time was three hours. Upon finishing the monomer addition, the reaction was kept for one more hour at the same reaction temperature. The general formulation for emulsion polymerizations is shown in Table 4.2.

Table 4.2. Formulation for the thiol-ene emulsion polymerizations.

Component	
Diene	0.012 mol
Dithiol	0.012 mol
TMPMP/PETMP*	0-4 mol%
Dowfax 2A1	2 wbm%
Deionized water	75 wt%
KPS	1 wbm%

4.2.3. Degradation studies of thiol-ene polymers obtained by emulsion polymerization

100 mg of thiol-ene polymer synthesized by emulsion polymerization of bifunctional enes and thiols were immersed into 5 mL of a potassium hydroxide solution with a pH of ~11 for 24 h. Afterwards the solution was neutralized by the addition of a hydrochloride solution (0.1 mol/L).

The samples were dried, dissolved in THF and the molar mass distribution was determined by GPC measurements.

4.3. Thiol-ene miniemulsion polymerizations

Thiol-ene miniemulsion polymerizations were carried out between the diene DAA, DAP or DAP/TMPDAE (molar ratio 1/1) and the dithiol EDDT. The different runs that were carried out in thiol-ene miniemulsion polymerization are shown in Table 4.3.

Table 4.3. List of diene and dithiol monomers and tetrafunctional thiol PETMP that were used in the runs of miniemulsion polymerization.

Run	Diene	Dithiol	PETMP [%]
ME1.1	DAA	EDDT	-
ME1.2	DAA	EDDT	1.3
ME1.3	DAA	EDDT	2.5
ME2.1	DAP	EDDT	-
ME2.2	DAP	EDDT	1.3
ME3.1	DAP/TMPDAE	EDDT	1.3
ME3.2	DAP/TMPDAE	EDDT	2.5
ME3.3	DAP/TMPDAE	EDDT	4.1

Final conversions were above 97% in all of the cases and particle sizes of 185 to 260 nm were obtained (Table 4.4). Relatively low weight-average molar masses of 14.8 kDa and 19.0 kDa were obtained for the thiol-ene polymerization of only linear monomers (ME1.1 and ME2.1). Therefore, to increase the molar masses, different concentrations of the tetra-functional thiol

PETMP were used in some of the miniemulsion polymerization runs. An increase to 85.6 kDa of weight-average molar mass was observed for ME1.2, which includes 1.3% of PETMP. All the other samples of runs with the tetrafunctional thiol PETMP were not completely soluble in THF and therefore, molar masses could not be determined by GPC measurements.

Table 4.4. Summary of the analysis for the final latices of DAA and EDDT with different concentrations of PETMP.

Run	*X* [%]	*dp* [nm]	PDI	Mw [kDa]	Đ	Tg [ºC]
ME1.1	98	202	0.079	14.8	2.6	-64
ME1.2	99	232	0.042	85.6	16	-60
ME1.3	98	189	0.047	-	-	-56
ME2.1	99	235	0.050	19.0	2.8	-37
ME2.2	99	257	0.116	-	-	-34
ME3.1	99	192	0.062	-	-	-48
ME3.2	99	201	0.141	-	-	-44
ME3.3	98	218	0.100	-	-	-41

Particle sizes were comparable to the particle sizes obtained by Chemtob et al.[8] who investigated the droplet nucleation in miniemulsion thiol-ene photo-polymerization. They used the same diene DAP and the dithiol EDDT monomers. Furthermore, they used two different photo-initiators at a surfactant concentration below the CMC so that no micelles were present during the miniemulsion polymerization. The water-soluble photo-initiator lithium phenyl(2,4,6-trimethylbenzoyl)phosphinate (TPO-Li) and the oil-soluble photo-initiator phenyl(2,4,6-trimethylbenzoyl)phosphine oxide (TPO) were used. Relatively similar particles sizes were

obtained for both photo-initiators, ranging from 100 nm to 225 nm depending on the surfactant concentration. They found out that the nucleation mechanism was completely different for the two photo-initiators of different solubility. For the system with the water-soluble initiator TPO-Li the monomer droplets were significantly bigger than the particles. Therefore, they concluded that homogeneous nucleation was the dominant nucleation mechanism and nucleation of the monomer droplets was negligible. If the oil-soluble initiator TPO was used, they observed that monomer droplets and particles were more or less of the same size and therefore, droplet nucleation was considered as the predominant nucleation mechanism.[8] KPS, which was used as thermal initiator for the thiol-ene miniemulsion polymerizations presented in this work, is water-soluble pointing towards homogeneous nucleation. Furthermore, the concentration of Dowfax 2A1 was above the CMC. Therefore, additionally heterogeneous nucleation could be a possibility.

Glass transition temperatures were very low for the polymers obtained by miniemulsion polymerizations with the diene DAA, and increasing the PETMP concentration (ME1.1 to ME1.3) the Tg was raised from -64 ºC to -56 ºC. The glass transition temperature increased by almost 30 ºC if DAP was used as diene monomer (ME2.1 and ME2.2). When the diene component was changed to 50 mol% DAP and 50 mol% TMPDAE, while the dithiol EDDT with different concentrations of PETMP was maintained (ME3.1, ME3.2 and ME3.3), the determined glass transition temperatures were in between the values for the polymers obtained using DAA + EDDT and DAP + EDDT (ME1.2 and ME 2.1).

The latex of run ME3.2 was analysed by Transmission electron microscopy (TEM) (Figure 4.3). The size distribution of the polymer particles was broad; particles between 100 and 1500 nm

could be observed. However, in the TEM images (see Figure 4.3), due to the low Tg of the particles, the big aggregates might come from the sample preparation in which the particles tend to aggregate, since in the DLS there was not evidence of having such big particles.

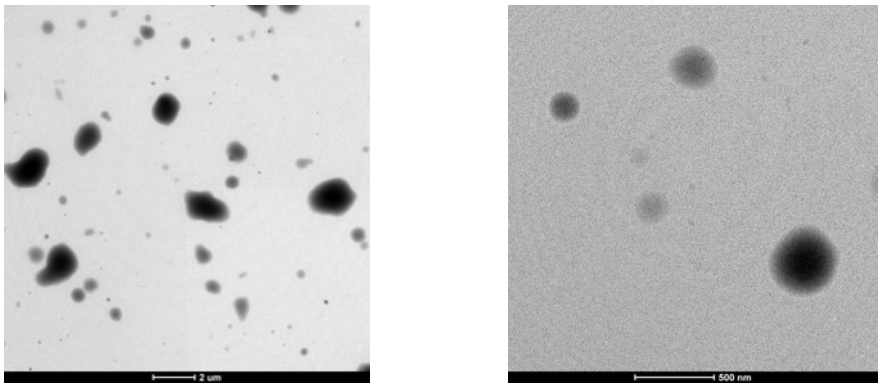

(a) **(b)**

Figure 4.3. TEM micrographs of the EDDT + DAP + TMPDAE + PETMP (2.5 mol%) latex (ME3.2).

As it has been mentioned previously, Tg values in the range of -50 ºC to -20 ºC are characteristic of polymers used as PSAs. Nevertheless, the wettability of the latices ME2.1 and ME2.2 was poor and it was not possible to cast films, not even if 1 wt% of the wetting agent Silwet L-77 was used. However, the wettability of the latices from the runs ME3.1 to ME3.3 was better, likely due to the hydroxyl groups which are introduced to the thiol-ene polymer by the usage of TMPDAE as a part of the diene monomer component (see Figure 4.1). Films with a thickness of 100 μm of the synthesized latices were cast on a glass substrate and probe tack measurements were carried out (Figure 4.4). As it was already explained in Chapter 2, in order to have a good PSA material the right balance between viscous and elastic properties is

needed.[13] Though, in this case none of the latexes presented a fibrillation plateau and furthermore, the film with 1.3 mol% of PETMP (ME3.1) showed liquid like behaviour.

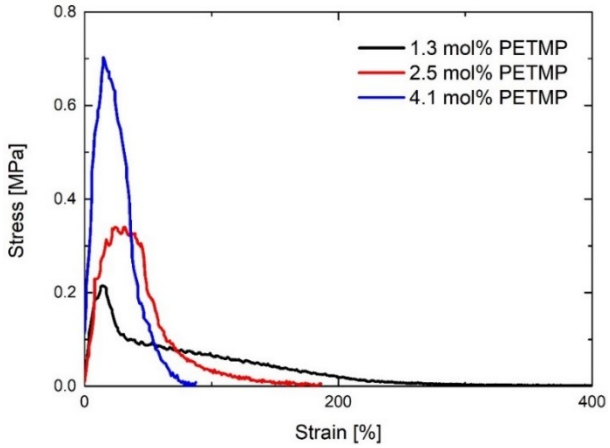

Figure 4.4. Probe tack measurements for the films of the latices from the miniemulsion polymerization of DAP and TMPDAE with different concentrations of PETMP.

Over all, it has been demonstrated that it was challenging to obtain films from latices produced by miniemulsion polymerization even if different thiol-ene monomers were used. Furthermore, the properties of the few films that could be casted were poor and the particle size distribution of the polymer particles was broad which could be related to how the polymerization proceed and also to the nucleation process of the monomer droplets. In the following section, the thiol-ene emulsion polymerization is explored as an alternative to the miniemulsion polymerization.

4.4. Thiol-ene emulsion polymerization

Different experiments were carried out in emulsion polymerization following either a batch or a semibatch process. The different parameters which were used during each of the different runs are shown in Table 4.5.

Table 4.5. List of the diene and dithiol monomers, of the trifunctional thiol TMPMP and the process (batch or semibatch) that was used in each of the runs for the experiments in emulsion polymerization.

Run	Diene	Dithiol	TMPMP [%]	Process
B1	TMPDAE	GDMA	-	Batch
B2	DAP	EDDT	-	Batch
SB1.1	DAP	EDDT	-	Semibatch
SB1.2	DAP	EDDT	10	Semibatch
SB1.3	DAP	EDDT	20	Semibatch
SB2.1	DATP	EDDT	-	Semibatch
SB2.2	DATP	EDDT	10	Semibatch
SB2.3	DATP	EDDT	20	Semibatch

Initially, two batch emulsion polymerizations were carried out with two different combinations of diene and dithiol. The first run B1, contained the diene TMPDAE, which was also used by Shipp et al.[1] and the dithiol GDMA. The second batch emulsion polymerization was carried out between the diene DAP and the dithiol EDDT under very similar conditions as in the work of Chemtob et al.[10] (B2). In B1 the ester groups were provided by the dithiol whereas in B2

by the diene. The results of those two batch emulsion polymerizations are summarized in Table 4.6.

Table 4.6. Final conversions and particle sizes measured for the two experiments carried out in batch emulsion polymerization.

Run	*X* [%]	*dp* [nm]	PDI
B1	99	989	0.3
B2	95	472	0.2

Nearly complete conversion of vinylic functional groups were obtained within short timeframes. Furthermore, particles with sizes in between 470 to 1000 nm with a broad, multimodal particle size distribution characterized by a high dispersity of the particle size distribution of ~ 0.3 measured by DLS were obtained. The evolution of conversion of the vinylic functional groups and particle size for run B1 are shown in Figure 4.5.a and the size distribution of the final sample of this run is shown in Figure 4.5.b.

As it has been mentioned, similar systems were described in the literature[1,14]. Shipp et al. observed narrow particle size distributions for a system of the diene TMPDAE and the dithiol EDDT. However, they observed aggregation of their particles over time despite their relatively high zeta-potential. On the other hand, they describe significant batch-to-batch variations for the PDI of a system of the monomers TMPDAE and 1,6-hexanedithiol (HDT), which indicate a colloidally unstable latex.

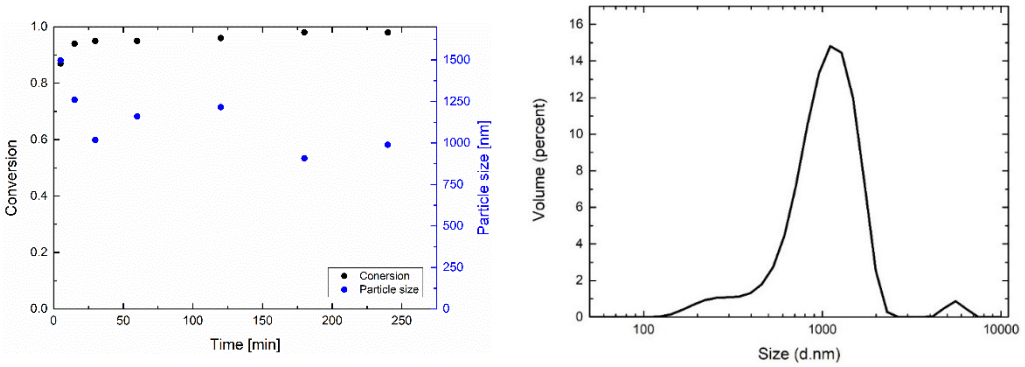

Figure 4.5. Particle sizes measured by DLS and conversion of vinylic functional groups calculated from ^{1}H-NMR spectra for the batch emulsion polymerization of TMPDAE and GDMA (**a**). And particle size distribution of the final sample (**b**).

They showed that the droplet size is significantly lower for the TMPDAE/EDDT system (500 nm) compared to the TMPDAE/HDT system (20 µm). This is due to the water-soluble nature of EDDT. Therefore, the majority of EDDT is present in the aqueous phase, leaving mostly TMPDAE in the monomer droplets. Whereas, in the case of TMPDAE/HDT both monomers are mostly present in the monomer droplet phase, leading to larger monomer droplets. These differences of distributions of the monomers between aqueous and monomer droplet phase would have a strong effect on the copolymer growth and the particle nucleation.[1] GDMA which was used as dithiol in the run B1 has a slightly lower water-solubility than EDDT.

A similar system to run B2 is described by Chemtob et al. They also used DAP and EDDT as monomers, the only difference being that they were using a redox initiator system at a temperature of 25 ºC compared to KPS which was used at 75 ºC in run B2. The particle sizes

they measured were similar and comparable to the ones obtained in run B2. However, when they use a photoinitiator for the same system, the size of the polymer particles decreased significantly to 100 nm with a PDI of 0.17 which seems that the fast nucleation of the particles prevents the broad particle size distribution.[10]

Considering this last idea, further thiol-ene emulsion polymerizations were carried but this time in a semibatch procedure feeding both components at the same time. Two different feeds were used, *feed 1* including the diene component (DAP or DATP) and *feed 2* including the thiol component consisting of EDDT (and TMPMP for the runs in which the trifunctional thiol was used). The feeding of the monomers was done for 180 min. The initial charge was water and the surfactant Dowfax 2A1. Figure 4.6 shows the set-up used for the semibatch thiol-ene emulsion polymerizations.

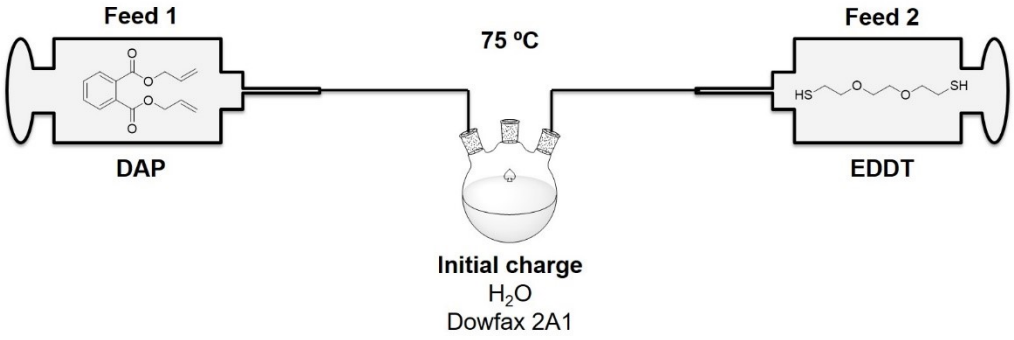

Figure 4.6. Polymerization process scheme for the semibatch thiol-ene emulsion polymerizations with two different feeds.

The instantaneous conversion of the vinyl functional groups and the evolution of particle size for run SB1.1 are shown in Figure 4.7. Instantaneous conversions are above 60% during the whole polymerization and after 240 min a vinyl functional group conversion of 99% was reached.

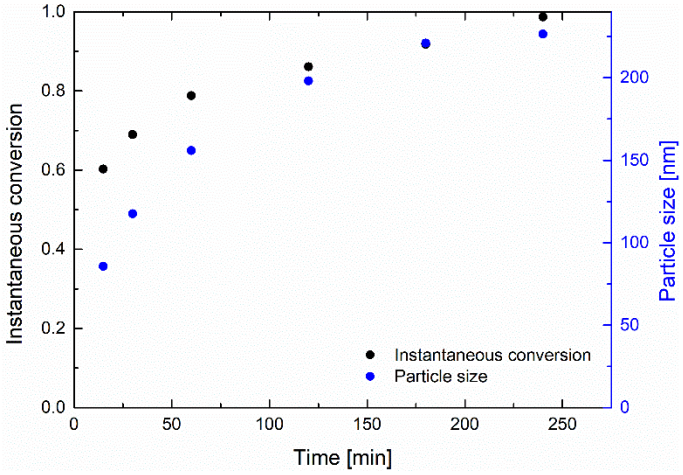

Figure 4.7. Evolution of particle size (blue) and instantaneous conversion of vinyl functional groups (black) during the semibatch emulsion polymerization of EDDT and DAP.

The particle sizes increased during the whole polymerization process. To check if the nucleation of the particles happened only at the beginning of the process or throughout the whole polymerization process the number of particles N_p was determined (see Appendix section I.2) and the evolution of the number of particles over the reaction time is plotted in Figure 4.8.a. It can be seen that up to 60 min of reaction, the number of particles is decreasing slightly which might be due to aggregation of the so far relatively small particles. From this point on, the number of particles stays constant, which confirms that the particle nucleation occurs during the first

stages of the emulsion polymerization process and then, this particles grow on size[15]. Chemtob et al. observed for the batch photo-emulsion polymerization of DAP/EDDT that the number of particles is rapidly increasing up to conversions of ~80%, after that the rate of formation of new particles decreases quickly until conversions of ~97% to almost reach a steady-state value during the last percent of conversion (Figure 4.8.b). From this the conclusion is drawn that, due to the high propagation rates for the thiol-ene polymerization (see Chapter 3) during the semibatch thiol-ene emulsion polymerization. Particle nucleation is limited to the first ~60 min of the polymerization in which the instantaneous conversions are below 50%. Afterwards, the thiol and ene monomers polymerize in the already formed particles, which is an indication that they transfer through the aqueous phase is fast and their partition into the polymer particles is favoured.

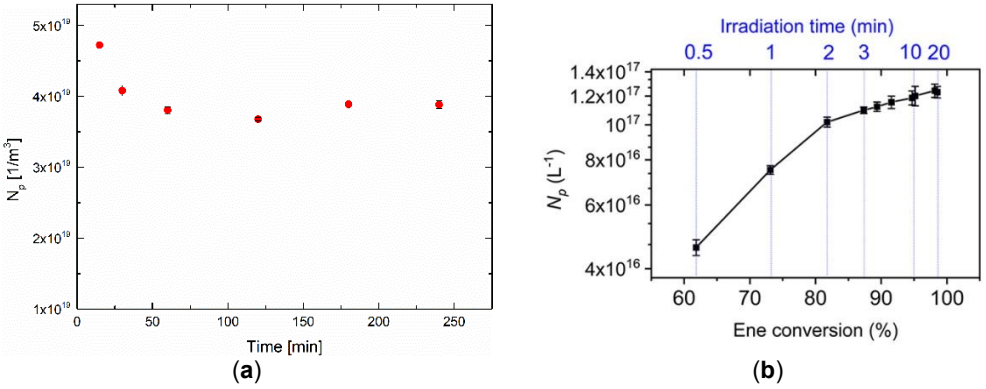

Figure 4.8. Number of particles over the reaction time of the semibatch emulsion polymerization of DAP and EDDT (**a**) and evolution of Np over conversion (or reaction time) for the batch emulsion photo-polymerization carried out by Chemtob et al.[10] (**b**).

CHDF technique was used to compare the particle size distribution of the lattices containing DAP and EDDT synthesized in batch (run B2) and semibatch process (run SB1.1) (Figure 4.9). The results agreed with the DLS measurements. The sample from semibatch emulsion polymerization of DAP and EDDT showed a narrow particle size distribution whereas the polymer dispersion carried out in batch showed a multimodal distribution with particles ranging between 100-800 nm.

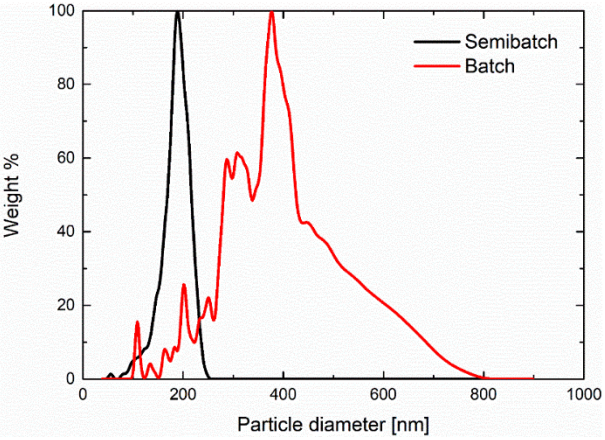

Figure 4.9. CHDF characterization of the latices obtained by batch (red) and semibatch (black) emulsion polymerization of DAP and EDDT.

In order to improve the mechanical properties of the DAP and EDDT latex, the same formulation and process was used with the only exception of including the trifunctional thiol TMPMP, which was fed in the same stream of the thiol component. However, the ratio of vinylic and thiol functional groups was kept at 1:1. Three different experiments were carried out, varying

the TMPMP content (in mol% based on the functional groups of the thiol component) 0, 10 and 20% (run SB1.1, SB1.2 and SB1.3). The same was done for the polymerization of DATP and EDDT (run SB2.1, SB2.2 and SB2.3) and the results are shown in Table 4.7. High monomer conversions were obtained in all of the cases. The final particle sizes remained constant for the runs SB1 no matter the amount of TMPMP used. This confirms that nucleation of polymer particles took place first, and that once polymer particles were produced the remaining dithiol and diene monomers polymerized inside the particles increasing their size, as for experiment SB1.1. Unexpectedly, for the SB2 series (using DATP as diene) increasing the TMPMP concentration significantly decreases the particle sizes (from 237 to 115 nm). Figure 4.10 shows the evolution of particle sizes during the semibatch emulsion polymerization of DAP and EDDT (a) and DATP and EDDT (b) with different amounts of the TMPMP.

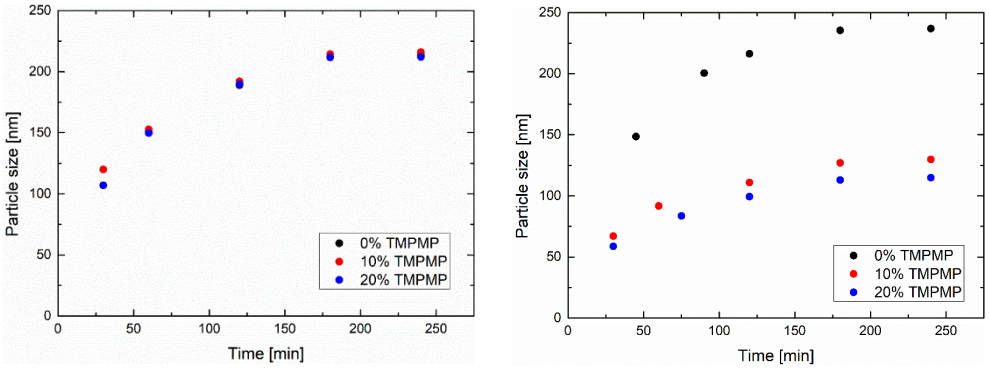

(**a**) (**b**)

Figure 4.10. Evolution of particle sizes during the semibatch emulsion polymerization of DAP and EDDT (**a**) and DATP and EDDT (**b**) with different amounts of the trifunctional thiol TMPMP (0% in black, 10% in red and 20% in blue).

Admittedly, there is no explanation yet for the effect of TMPMP in the particle nucleation of the DATP/EDDT system. The number of particles generated with TMPMP are substantially higher (particle sizes are half with respect to those obtained in experiment SB2.1).

Table 4.7. Characteristics for the latices synthesized by semibatch emulsion polymerization of DAP and EDDT.

Run	*X* [%]	*dp* [nm]	PDI	Mw [kDa]	Tg [ºC]	Tm [ºC]
SB1.1	99	213	0.015	13.2	-40	-
SB1.2	99	216	0.035	-	-34	-
SB1.3	98	215	0.011	-	-32	-
SB2.1	99	237	0.019	12.7	-36	51
SB2.2	98	130	0.068	-	-32	53
SB2.3	97	115	0.025	-	-31	49

The weight average molar mass could be only measured for the latices without trifunctional thiol, because the dried polymer of the latices with 10 and 20% of TMPMP was not completely soluble in THF. As expected (see Chapter 3) a relatively low weight-average molar mass of 13200 g/mol and 12700 g/mol was measured for the latices with only linear dienes and dithiols. The glass transition temperatures on the other hand showed a trend depending on the concentration of TMPMP, they increase from -40 ºC to -32 ºC with increasing TMPMP concentration for runs of SB1 and from -36 ºC to -31 ºC for runs of SB2. Furthermore, melting peaks were observed for the polymer of DATP and EDDT (runs SB2).

All the latices obtained by the semibatch process were also analysed by Soxhlet extraction, SEC/MALS of the soluble part and AF4/MALS/RI to obtain further information about the molar mass distribution. The determined molar mass averages, dispersity of the molar mass distribution (by SEC/MALS of the soluble part) and gel content (determined by AF4 and Soxhlet extraction) are listed in Table 4.8. The resolution of the data obtained by AF4, especially for the high molecular weight peak was poor. Therefore, only the fraction of this high molecular weight peak (gel content) is reported and confirmed by the results of the Soxhlet extraction.

Table 4.8. Molar weight averages determined by SEC/MALS of the soluble part and gel contents determined by AF4 measurements and Soxhlet extraction.

Sample	Mn [kDa]	Mw [kDa]	PDI	GC S [%]	GC AF4 [%]
SB1.1	23	34	1.5	0	10
SB1.2	9	50	5.8	21	67
SB1.3	33	241	7.2	11	48
SB2.1	21	39	1.9	0	2.4
SB2.2	7	21	3.2	24	61
SB2.3	5	11	2.1	38	79

The data from the AF4 measurements shows a fraction of gel content even for the polymerizations in which only linear dienes and dithiols were used, 10% for SB1.1 and 2.4% for SB2.1. Higher gel contents of between 50% and 80% were determined for the polymerizations in which the trifunctional thiol TMPMP was used. The gel contents determined by Soxhlet extractions were over all lower than the data from AF4 but follow the same trend (Figure 4.11).

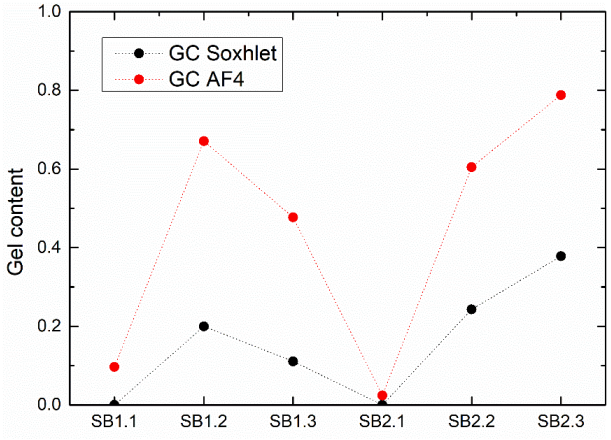

Figure 4.11. Gel contents determined by Soxhlet extraction (black) and by AF4 (red).

The dried polymer of the latex without TMPMP showed liquid like properties. However, the dried polymer with 10% of TMPMP seemed to be tacky. Hence, films of a thickness of 100 µm were prepared on a glass substrate and probe tack measurements of this film were performed (Figure 4.12). The dried film of this latex was heterogeneous; therefore, probe tack measurements were carried out in different locations of the film. Each curve in Figure 4.12 belongs to a measurement in a different position of the film. The measured strains are very different depending on the location of the measurement (between 1800% and 2500%). This might be due to different thicknesses distributed over the area of the heterogeneous film. Over all the mentioned strain is high and the curves present a plateau, which is characteristic of the fibrillation process. Therefore, this type of material would be appropriate for a PSA.

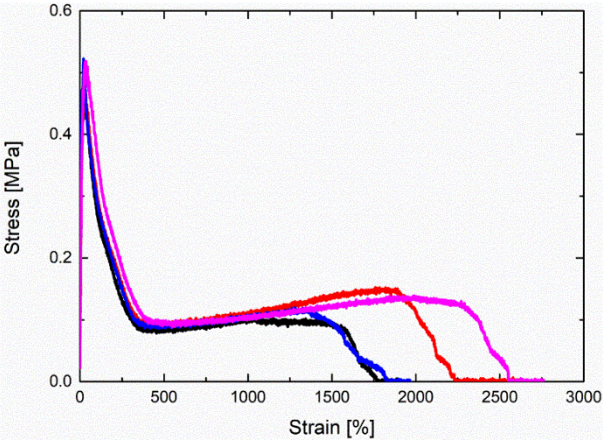

Figure 4.12. Probe tack curves of the dried film of the latex of DAP and EDDT with 10% of TMPMP.

Dried polymers of the latices with DATP as diene were not tacky due to the different substitution of the diene which might induce crystallization in the *para*-substituted monomer, which could be attributed to the more linear polymer structure formed with this *para*-substitution. DSC measurements were carried out to confirm this assumption and the thermogram for the dried polymer of DATP and EDDT is depicted in Figure 4.13 in which both heating cycles are shown. The melting peak is only visible in the first cycle and therefore, the second-order transition of the glass transition temperature is more pronounced in the second heating cycle. These results indicate that the polymer contained crystalline domains during the first cycle and behaved completely as an amorphous polymer in the second heating cycle. The crystallisation kinetics were slow because of the rigidity of the polymer chains provided by the phenyl group, therefore, once the crystalline domain was molten after the first heating cycle in the DSC, the polymer did not recrystallize within the time of the cooling ramp.

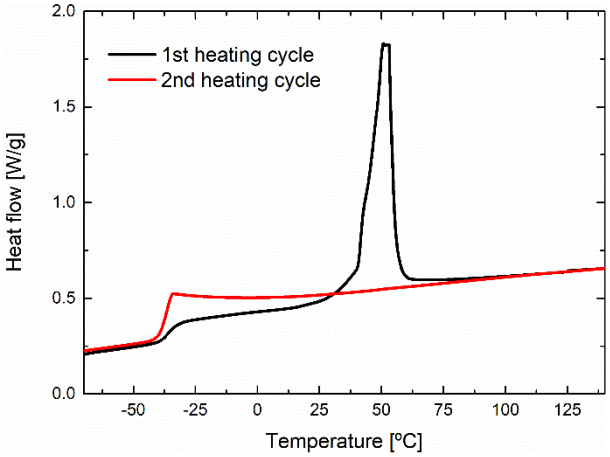

Figure 4.13. DSC of the dried polymer of the latex with DATP and EDDT. First cycle in black and third cycle in red.

A similar behaviour was found for all of the samples containing DATP, in which the melting peak was only visible in the first DSC cycle. The first heating cycle for all of the samples containing DATP is shown in Figure 4.14. The glass transition temperature shifted with increasing TMPMP content to slightly higher temperatures. However, the melting temperature did not show a trend depending on the TMPMP content, in all of the cases it was approximately 50 ºC.

TEM micrographs of the latices carried out by thiol-ene semibatch emulsion polymerization of DAP and EDDT and DATP and EDDT without the addition of trifunctional monomers are shown in Figure 4.15.

In both lattices, narrow particles size distribution of the polymer particles were seen. This further confirms the observations which were made by DLS and CHDF measurements, confirming that

thermal semibatch thiol-ene emulsion polymerization is leading to particles with a narrow particle size distribution (see Figure 4.3).

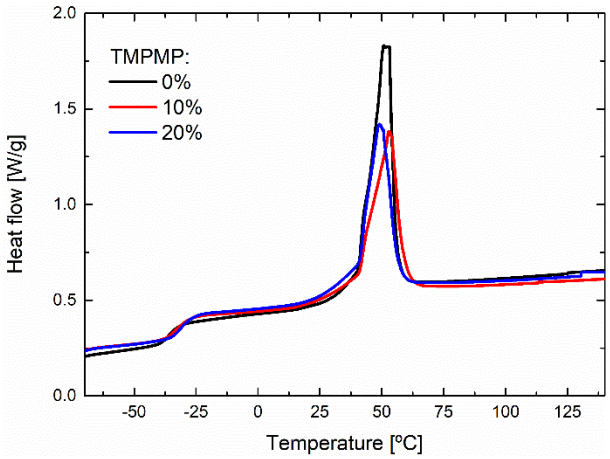

Figure 4.14. First cycles of the DSC measurements for the samples of DATP and EDDT, containing different amounts of TMPMP.

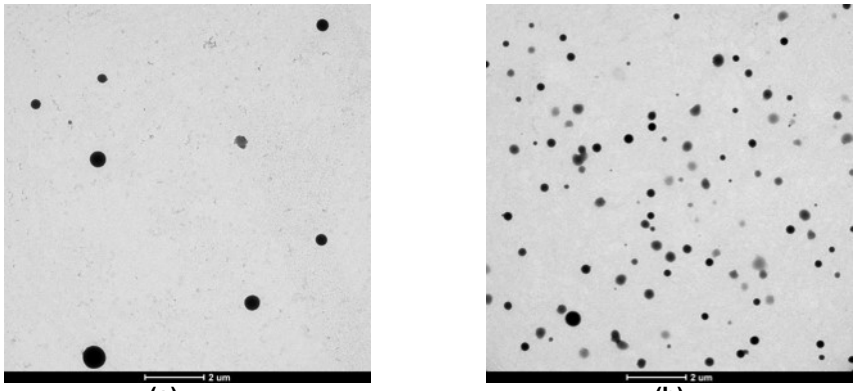

(a) **(b)**

Figure 4.15. TEM micrographs of two lattices obtained by thiol-ene emulsion polymerization of EDDT with either DAP **(a)** or DATP **(b)**.

4.5. Degradation studies of polymers obtained by thiol-ene emulsion polymerization

Dried polymers of SB1.1 and SB2.1 were immersed into KOH-solution with a pH value of approx. 11 for 24 h. After that the samples were neutralized and dried. Figure 4.16 shows the molar mass distributions for the dried samples (before and after immersion into the KOH solution).

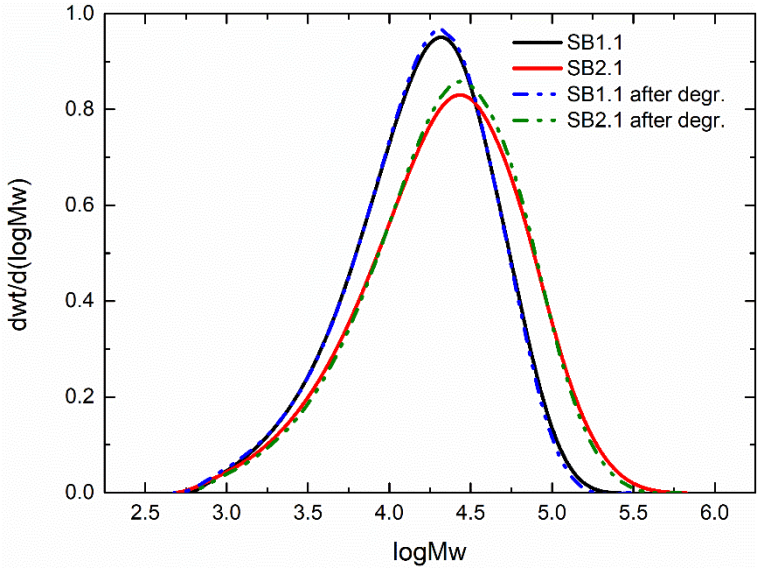

Figure 4.16. Molar weight distributions of the dried polymers of SB1.1 and SB2.1 before and after immersion into KOH solution (degr.).

The molar weight distributions of the samples before and after immersion into KOH solution are overlapping. Therefore, it can be assumed that the ester groups in the backbone of the thiol-ene polymer did not hydrolyse after 24 hoursof treatment in a basic aqueous solution. Number and weight averages as well as the dispersity of the molar weight distributions are listed in Table 4.9.

Table 4.9. Number and weight averaged molar masses for the polymers of SB1.1 and SB2.1 before and after immersion into KOH solution.

Sample	Mn [g/mol]	Mw [g/mol]	PDI
SB1.1	9200	24200	2.6
SB2.1	10600	36900	3.5
SB1.1 degr.	8900	23400	2.6
SB2.1 degr.	11200	35800	3.2

The measured molar masses are far above the molar masses measured before for the same polymers (compared to the data for SB1.1 and SB2.1 in Table 4.7). The weight average molar mass of the polymer SB1.1 is twofold higher and for SB2.1 threefold higher. The degradation experiments were carried out one year after the synthesis of the lattices which were stored at room temperature. Therefore, the explanation could be that further radicals were generated from the remaining thiol groups, so that the polymerization continued during the storage time leading to the increased molar masses. However, it can be concluded that the ester groups of the thiol-ene polymer do not degrade under the conditions that were used in this degradation study. It should be mentioned that the degradation studies were carried out within a timeframe of 24 hours. Whereas other authors studied much longer timeframes of up to 80 weeks[16] to observe

the degradation of ester groups. Therefore, further studies are necessary to evaluate the degradability of ester containing polymers from thiol-ene emulsion polymerization.

4.6. Conclusions

The objective of the work presented in this chapter was to incorporate ester groups into the polymer backbone through thiol-ene polymerization in dispersed media. Most of the literature regarding thiol-ene polymermization in dispersed media refers to miniemulsion polymerization and only a few articles about thiol-ene emulsion polymerization are published.[1,10] Thermally initiated miniemulsion polymerizations were carried out with a variety of diene monomers and the dithiol EDDT and the tetra-functional thiol PETMP to increase molar masses and mechanical properties. It was not possible to obtain a good film from the latices obtained by miniemulsion polymerization. Furthermore, the particle size distribution of the polymer particles was broad and multimodal. Therefore, the emulsion thiol-ene polymerization was investigated. Batch emulsion polymerization experiments led to latices with a large and broad particle size distribution as those obtained by miniemulsion polymerization. On the other hand, semibatch emulsion polymerization yielded a significantly narrower particle size distribution. Furthermore, the particle size of the dispersion can be better controlled. Depending on the used diene and on the amount of multi-functional thiol, it was possible to tune the gel content and therefore, to influence the properties of the resulting polymer. The thiol-ene polymer from semibatch emulsion polymerization of DAP and EDDT showed weak PSA properties in the probe tack test. Whereas the polymer from DATP and EDDT was not tacky and rather brittle due to its crystallinity. First degradation studies of the linear polymers obtained from semibatch emulsion polymerization did give no evidence for the

hydrolysis of the ester groups in the backbone of the thiol-ene polymer during the immersion in basic aqueous solution in 24 hours.

This work can serve as a starting point for the synthesis of PSAs by semibatch thiol-ene emulsion polymerization process. Compared to the miniemulsion polymerization process, the emulsion polymerization has several advantages, for example the ability to scale-up the process, industrial application of miniemulsion polymerization processes is still scarce. [17] It has been demonstrated that thiol-ene polymerizations can be carried out without the need of adding inhibitors, which affects the kinetics of the polymerization. However, research is still necessary to better understand and control the nucleation of polymer particles and its growth in batch and semibatch emulsion polymerizations. Additionally, the microstructure of the latexes should be optimized to produce PSA with balance adhesive and cohesive performance.

4.7. References

(1) Durham, O. Z.; Chapman, D. V.; Krishnan, S.; Shipp, D. A. Radical Mediated Thiol-Ene Emulsion Polymerizations. *Macromolecules* **2017**, *50* (3), 775–783. https://doi.org/10.1021/acs.macromol.6b02228.

(2) Machado, T. O.; Sayer, C.; Araujo, P. H. H. Thiol-Ene Polymerisation : A Promising Technique to Obtain Novel Biomaterials. *Eur. Polym. J.* **2017**, *86*, 200–215. https://doi.org/10.1016/j.eurpolymj.2016.02.025.

(3) Machado, T. O.; Cardoso, P. B.; Feuser, P. E.; Sayer, C.; Araújo, P. H. H. Thiol-Ene Miniemulsion Polymerization of a Biobased Monomer for Biomedical Applications. *Colloids Surfaces B Biointerfaces* **2017**, *159*, 509–517. https://doi.org/10.1016/j.colsurfb.2017.07.043.

(4) Cardoso, P. B.; Machado, T. O.; Feuser, P. E.; Sayer, C.; Meier, M. A. R.; Araújo, P. H. H. Biocompatible Polymeric Nanoparticles From Castor Oil Derivatives via Thiol-Ene Miniemulsion Polymerization. *Eur. J. Lipid Sci. Technol.* **2018**, *120* (1), 1–8. https://doi.org/10.1002/ejlt.201700212.

(5) Jasinski, F.; Lobry, E.; Tarablsi, B.; Chemtob, A.; Nouen, D. Le; Criqui, A. Light-Mediated Thiol−Ene Polymerization in Miniemulsion: A Fast Route to Semicrystalline Polysul Fi de Nanoparticles. *ACS Macro Lett.* **2014**, *3*, 958–962.

(6) Jasinski, F.; Rannée, A.; Schweitzer, J.; Fischer, D.; Lobry, E.; Croutxé-Barghorn, C.; Schmutz, M.; Le Nouen, D.; Criqui, A.; Chemtob, A. Thiol-Ene Linear Step-Growth Photopolymerization in Miniemulsion: Fast Rates, Redox-Responsive Particles, and Semicrystalline Films. *Macromolecules* **2016**, *49* (4), 1143–1153. https://doi.org/10.1021/acs.macromol.5b02512.

(7) Amato, D. V; Amato, D. N.; Flynt, A. S.; Patton, D. L. Functional, Sub-100 Nm Polymer Nanoparticles via Thiol-Ene Miniemulsion Photopolymerization. *Polym. Chem.* **2015**, *6*, 5625–5632. https://doi.org/10.1039/c4py01449a.

(8) Minh, C.; Le, Q.; Vidal, L.; Schmutz, M.; Chemtob, A. Droplet Nucleation in Miniemulsion Thiol-Ene Step Polymerization. *Polym. Chem.* **2021**, *12*, 2084–2094. https://doi.org/10.1039/d1py00139f.

(9) dos Santos, P. C. M.; Machado, T. O.; Santin, J. V. C.; Feuser, P. E.; Córneo, E. S.; Avila, R. A. M.-; Sayer, C.; Araujo, P. H. H. Superparamagnetic Biobased Poly (Thioether-Ester) via Thiol-Ene Polymerization in Miniemulsion for Hyperthermia. *J.*

Appl. Pol. Sci. **2021**, 1–10. https://doi.org/10.1002/app.49741.

(10) Minh, C.; Le, Q.; Schmutz, M.; Chemtob, A. Ab Initio Batch Emulsion Thiol − Ene Photopolymerization. *Macromolecules* **2020**, *53*, 2369–2379. https://doi.org/10.1021/acs.macromol.0c00265.

(11) Minh, C.; Le, Q.; Schrodj, G.; Ndao, I.; Bessif, B.; Heck, B.; Pfohl, T.; Reiter, G.; Elgoyhen, J.; Tomovska, R. Semi-Crystalline Poly(Thioether) Prepared by Visible-Light-Induced Organocatalyzed Thiol-Ene Polymerization in Emulsion. *Macromol. Rapid Commun.* **2021**, *2100740*, 1–6. https://doi.org/10.1002/marc.202100740.

(12) Llorente, O.; Agirre, A.; Calvo, I.; Olaso, M.; Tomovska, R.; Sardon, H. Exploring the Advantages of Oxygen-Tolerant Thiol-Ene Polymerization over Conventional Acrylate Free Radical Photopolymerization Processes for Pressure-Sensitive Adhesives. *Polym. J.* **2021**, 1195–1204. https://doi.org/10.1038/s41428-021-00520-z.

(13) Badia, A.; Movellan, J.; Barandiaran, M. J.; Leiza, J. R. Of Sustainable Pressure Sensitive Adhesives High Biobased Content Latexes for Development of Sustainable Pressure Sensitive Adhesives . *Ind. Eng. Chem. Res.* **2018**, *57* (43), 14509–14516. https://doi.org/10.1021/acs.iecr.8b03354.

(14) Quoc Le, C. M.; Schmutz, M.; Chemtob, A. Ab Initio Batch Emulsion Thiol-Ene Photopolymerization. *Macromolecules* **2020**, *53* (7), 2369–2379. https://doi.org/10.1021/acs.macromol.0c00265.

(15) Asua, J. M. Emulsion Polymerization: From Fundamental Mechanisms to Process Developments. *J. Polym. Sci., Part A Polym. Chem.* **2004**, *42*, 1025–1041.

(16) Woodard, L. N.; Grunlan, M. A. Hydrolytic Degradation and Erosion of Polyester Biomaterials. *ACS Macro Lett.* **2018**, *7*, 976–982. https://doi.org/10.1021/acsmacrolett.8b00424.

(17) Asua, J. M. Challenges for Industrialization of Miniemulsion Polymerization. *Prog. Polym. Sci.* **2014**, *39* (10), 1797–1826. https://doi.org/10.1016/j.progpolymsci.2014.02.009.

Chapter 5. Radical ring opening polymerization of the cyclic ketene acetal 2-methylene-1,3-dioxepane with vinyl monomers

5.1. Introduction

In this chapter the radical ring opening polymerization (rROP) of 2-methylene-1,3-dioxepane (MDO) with vinyl monomers will be explored.

The rROP of cyclic ketene acetals such as MDO enables the incorporation of ester groups into the polymeric backbone. Therefore, obtaining a broad range of (bio)degradable materials comparable to those from ring opening polymerization (ROP) of lactones and lactides,[1] or from polycondensation processes, is a desirable goal. Since chain mobility is an important factor in

biodegradation, the biodegradability of polyethylene terephthalate (PET) and polybutylene terephthalate (PBT), for example, is limited by the aromatic substituents present in these polymers.[2] rROP combines the advantages of ROP, which is the ability to synthesize polymers with a heteroatom/functional group in the main chain, and radical polymerization, which are its robustness, ease of operation, mild polymerization conditions compared to other techniques, as well as the ability to reach high molar masses and therefore, desirable mechanical properties.[1] The radical polymerization of cyclic ketenes can follow two different routes; on the one hand, the ring opening producing a polyester and on the other, the ring retention producing a polyacetal.[3]

MDO is the most frequently used cyclic ketene acetal in rROP.[4] The mechanism of the rROP of MDO is shown in Scheme 1.1. The homopolymerization of MDO leads to the complete ring opening of its seven-membered ring to form poly(*ε*-caprolactone) in the presence of radical initiators.[5] However, the presence of branched structures is reported between 20%-30%,[3,6] due to an intramolecular hydrogen transfer during the radical propagation.[3,7] These short branches can disturb the chain regularity and influence the crystallinity of the resulting polymer. Jin *et al*. reported a conversion of 70% within 48 h of homopolymerization of MDO at 50 ºC and with 2 mol% of AIBN as initiator, which shows the slow rate of the MDO homopolymerization, particularly compared to vinyl monomers.[7] Through a pulsed-laser polymerization (PLP) experiment it was not possible to obtain a propagation rate coefficient value for the homopolymerization of MDO due to high chain transfer rates to polymer and monomer.[8]

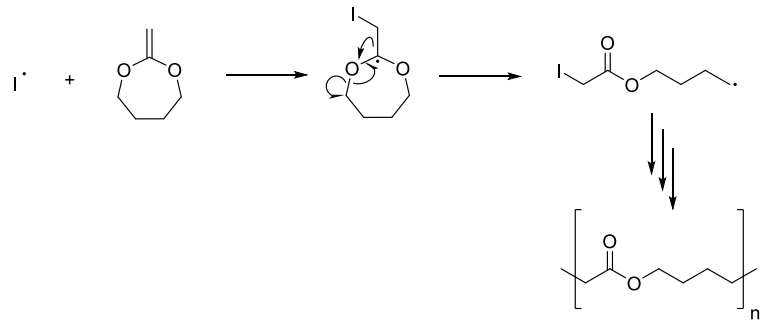

Scheme 1.1. Mechanism of the rROP of MDO in the presence of a radical initiator (I*).[8]

Due to the relatively low incorporation rates of cyclic ketenes in copolymerizations with common vinyl monomers caused by the unfavourable reactivity ratios, the radical copolymerization of MDO with vinyl monomers is challenging in general.[1] First copolymerizations were carried out using ethylene and styrene as comonomers.[9,10] An incorporation of 10% of ester units was observed for the copolymerization between 20 mol% of styrene and 80 mol% of MDO carried out at 120 ºC in bulk with di-*tert*-butyl peroxide (DTBP) as initiator.[9] In a later study a semibatch process was used, in which MDO was charged into the reaction vessel and styrene was added slowly when the reaction temperature of 130 ºC was reached and DTBP served as initiator. This copolymerization showed the incorporation of 19% of ester units (determined by elemental analysis) for the copolymerization of 50 mol% of MDO and 50 mol% of styrene.[11] Similar results were obtained for the copolymerization of MDO with ethylene with an incorporation of 10% of ester units for a mixture of 78% of ethylene and 22% of MDO.[10]

Further insights into the copolymerization kinetics can be obtained by studying reactivity ratios.[8,12–19] Copolymerizations of MDO and their reactivity ratios have been studied for some

comonomer systems such as MDO with acrylic monomers (e.g. methyl acrylate (MA)), MDO with methacrylic monomers (e.g. methyl methacrylate (MMA)) and MDO with VAc. The PLP experiment of MDO and MMA at 40 ºC showed very low incorporation of MDO into the polymer chains.[8] The reactivity ratios, estimated by assuming a terminal copolymerization model and using a nonlinear regression, led to a very low reactivity ratio of MDO (r_{MDO} = 0.057) compared to that of MMA (r_{MMA} = 34.12).[8] Nevertheless, under conventional polymerization conditions with DTBP as initiator and at a temperature of 120 ºC, it was possible to incorporate up to 57% of ester units into the copolymer (with 78% MDO in the starting monomer mixture). In this study the reactivity ratios were estimated by the Kelen-Tüdos method, which led to a ten-fold decrease in reactivity ratio of MMA (r_{MDO} = 0.4 and r_{MMA} = 3.5).[12]

For copolymerizations with acrylates like methyl acrylate (MA) the incorporation of MDO units into the copolymer was also low. Copolymerizations of MDO with MA were carried out with benzene as solvent either at 50 ºC with AIBN as the initiator or at 115 ºC with DTBP as the initiator. Reactivity ratios for this copolymerization system were estimated to be r_{MDO} = 0.0235 and r_{MA} = 26.535[13], but the copolymer compositions used were taken at high conversions limiting the accuracy of the calculated reactivity ratios. Lena and van Herk[18] re-evaluated the reactivity ratios for different cyclic ketene acetals and vinyl monomer systems published in the literature using a non-linear least-square (NLLS) method taking into account the error in the ^{1}H-NMR data used to determine the compositions. More recently, the same authors[14] reported reactivity ratios of MDO with methyl acrylate (MA), *n*-butyl acrylate (BA), 2-ethylhexyl acrylate (2EHA) and dodecyl acrylate (DA) within a broader study that attempted the uniform incorporation of MDO into (meth)acrylate copolymers. These copolymerizations were carried out at 70 ºC in

cyclohexane with 5 wt% of AIBN as initiator. They estimated the reactivity ratios using the same method as Lena *et al*.[18]. For the monomer couple MA/MDO a substantially lower reactivity ratio for MA was estimated compared to the reactivity ratio estimated by Sun et al.,[13] likely because a lower conversion polymer was used to measure the composition and this is less affected by the composition drift. Even lower reactivity ratios have been estimated for BA and 2EHA, but in these two cases also a lower reactivity ratio of MDO was estimated. The highest reactivity ratio for MDO was estimated for the DA/MDO system. Using the estimated reactivity ratios and a semibatch feeding profile it was possible to improve the homogeneity of the MDO insertion into the copolymer.[14] The reported reactivity ratios for copolymerizations of MDO with different acrylates are summarized in Table IV.1 in section IV of the Appendix.

Several studies have been carried out intending to copolymerize VAc with MDO.[15–19] Albertsson et al.[15] incorporated up to 70% of MDO units into the copolymer of VAc and MDO. First copolymerizations were carried out in bulk at 60 ºC with AIBN as initiator. The reactivity ratios were determined by the Finemann-Ross method. Only a slightly higher reactivity ratio was determined for the copolymerization of VAc than for that of MDO (r_{MDO} = 0.93, r_{VAc} = 1.71), which led to copolymers with more randomized distribution of MDO units.[15] A re-evaluation of this data estimated similar reactivity ratios by NLLS method (r_{MDO} = 0.95 and r_{VAc} = 1.71).[18] Similar results were found in other works. A summary is provided in Table IV.2 in the Appendix.

The homogeneous incorporation of MDO into copolymerization requires accurate knowledge of the reactivity ratios and application of optimal addition profiles as recently shown by Lena et al.[14] for the production of degradable acrylate copolymers by solution polymerization. Furthermore, accurate reactivity ratios enable the simulation of the degradation at a molecular level. The

composition drift has a huge impact to the material properties after degradation. A system with no composition drift leads to shorter and more homogeneous chains after degradation than a system with higher composition drift.[20]

Literature reports on vinyl monomers as discussed are scarce. Additionally, the studied monomer systems are limited and in some cases the copolymer compositions used in the estimation algorithm were not appropriate because samples taken at high conversion were used, which are prone to have a composition drift. In other words, they do not correspond to the instantaneous copolymer composition produced at the feed ratio used in the experiment. The aim of this chapter is to shed light on the copolymerization of MDO/VAc, MDO/2OA and MDO/LMA. VAc was chosen as a monomer because the use of MDO/VAc is reported to be one of the best working systems with only slight composition drift (see above). However, the data presented in this manuscript was not free of composition drift. Hydrophobic and biobased (meth)acrylates were selected as they can be excellent candidates for high biobased content degradable materials made by copolymerization with MDO or other similar cyclic ketene acetal monomers. *In situ* ^{1}H-NMR spectroscopy was used to monitor the rROP solution copolymerizations and a non-linear parameter estimation approach was used to estimate the reactivity ratios of the three sets of monomers.

5.2. Experimental part

The three different sets of co-polymerization experiments of MDO with different co-monomers carried out within this chapter are described in this part. Procedures of the used analytical methods are described in section I of the Appendix.

5.2.1. *In situ* ^{1}H-NMR solution polymerizations

In situ ^{1}H-NMR solution rROP copolymerizations of MDO with VAc, 2OA or LMA were carried out in a Wilmad® NMR tube with a length of 18 cm, and a diameter of 5 mm (wall thickness of 0.43 mm) as reaction vessel. A hole was punched in the lid of the NMR tube, to prevent overpressure. The copolymerizations were monitored *in situ* using benzene-d_6 as solvent at atmospheric pressure. Solution polymerizations were carried out at a total monomer concentration of 50 wt%. 2 mol% (based on the monomers) of the initiator AIBN was added to the NMR tube when the solution of the monomers reached the reaction temperature of 65 ºC. Four experiments with different comonomer compositions were carried out for each of the monomer couples. The molar monomer ratios used for each copolymerization system are presented in the next section.

The liquid ^{1}H-NMR spectra were acquired via NMR measurements with a 500 MHz Bruker Avance NMR instrument equipped with a Z gradient broadband observe (BBO) probe. Scans were performed every 10 min for the first 3 h and every 30 min for the next 11 h for the MDO/VAc

and MDO/LMA systems. For the MDO/2OA system scans were performed every minute for the first 15 min and every 10 min for the next 3.5 h because of the faster propagation rate of 2OA compared to the other comonomers. The number of scans was one for each of the measurements with a relaxation delay of 10.00 s, a pulse width of 14 μs and an acquisition time of 2.23 s. The signals which were tracked to calculate conversions from the NMR spectra are assigned to their protons (Figure IV.1, IV.2 and IV.3 of the Appendix). Absolute integrals were used for the calculation of monomer conversions.

5.2.2. Determination of reactivity ratios

Reactivity ratios were calculated according to the non-linear least square method developed by de la Cal et al.[21] and Garcia.[22] This method is described in detail for a copolymerization of monomers *A* and *B* assuming the terminal copolymerization model in section IV.1 of the Appendix. Here, we briefly describe the estimation approach. The reactivity ratios have been estimated using the evolution of the individual comonomer conversion over the overall conversion as shown in Equation 5.1, with X_A the conversion of monomer *A*, X_T the overall conversion, R_{pi} the polymerization rate of monomer *i* [mol/L·s], [*i*] the monomer concentration [mol/L] and $[i]_0$ the initial concentration of monomer *i* [mol/L], and r_i the reactivity ratio of monomer *i*:

$$\frac{dX_A}{dX_T} = \frac{[A]_0 + [B]_0}{[A]_0} \cdot \frac{R_{pA}}{R_{pA} + R_{pB}} = \frac{[A]_0 + [B]_0}{[A]_0} \cdot \left(\frac{1 + r_A \cdot \frac{[A]}{[B]}}{2 + r_A \cdot \frac{[A]}{[B]} + r_B \cdot \frac{[B]}{[A]}} \right) \tag{5.1}$$

where:

$$\frac{[A]}{[B]} = \frac{[A]_0 \cdot (1 - X_A)}{[B]_0 - X_T \cdot ([A]_0 + [B]_0) + [A]_0 \cdot X_A} \tag{5.2}$$

The cumulative copolymer composition (Y_i, cumulative copolymer composition with respect to monomer i) is calculated knowing the individual and overall conversion as shown in Equation 5.3.

$$Y_A = \frac{[A]_0 \cdot X_A}{([A]_0 + [B]_0) \cdot X_T} \tag{5.3}$$

A parameter estimation algorithm in which the objective function presented in Equation 5.4 is minimized was used. Y_{MDOexp} is the experimental cumulative composition with respect to MDO determined by ^{1}H-NMR measurements and Y_{MDOcal} is the calculated cumulative composition using Equations 5.1 to 5.3. The reactivity ratios are the only parameters of this model. Subscript *i* refers to the experiment and subscript *j* to the sample number of each of the experiments used for the estimation procedure.

$$J = \left[\sum_{i=1}^{N}\sum_{j=1}^{P_i}\left(Y_{MDOexp} - Y_{MDOcal}\right)^2\right] \tag{5.4}$$

The parameter estimation algorithm was coded in Matlab using the ODE45 solver to solve ordinary differential equations and LSQNONLIN for nonlinear data fitting. 95% confidence

intervals were calculated using nonlinear regression parameter confidence intervals function (NLPARCI).

5.3. Results and discussion

The solution copolymerization of three different systems was studied: MDO/VAc, MDO/2OA and MDO/LMA. Examples of the evolution of the NMR spectra over time for each of the three studied systems are shown in the appendix (Figure IV.1, IV.2 and IV.3).

5.3.1. Copolymerization of MDO and VAc

Copolymerizations of MDO and VAc were performed in NMR tubes at different molar comonomer ratios (MDO/VAc: 0.32/0.68; 0.25/0.75; 0.20/0.80 and 0.05/0.95). Figure 5.1 shows the time evolution of conversions of both comonomers for the four experiments carried out using different feed comonomer ratios, as well as the time evolution of the overall conversion.

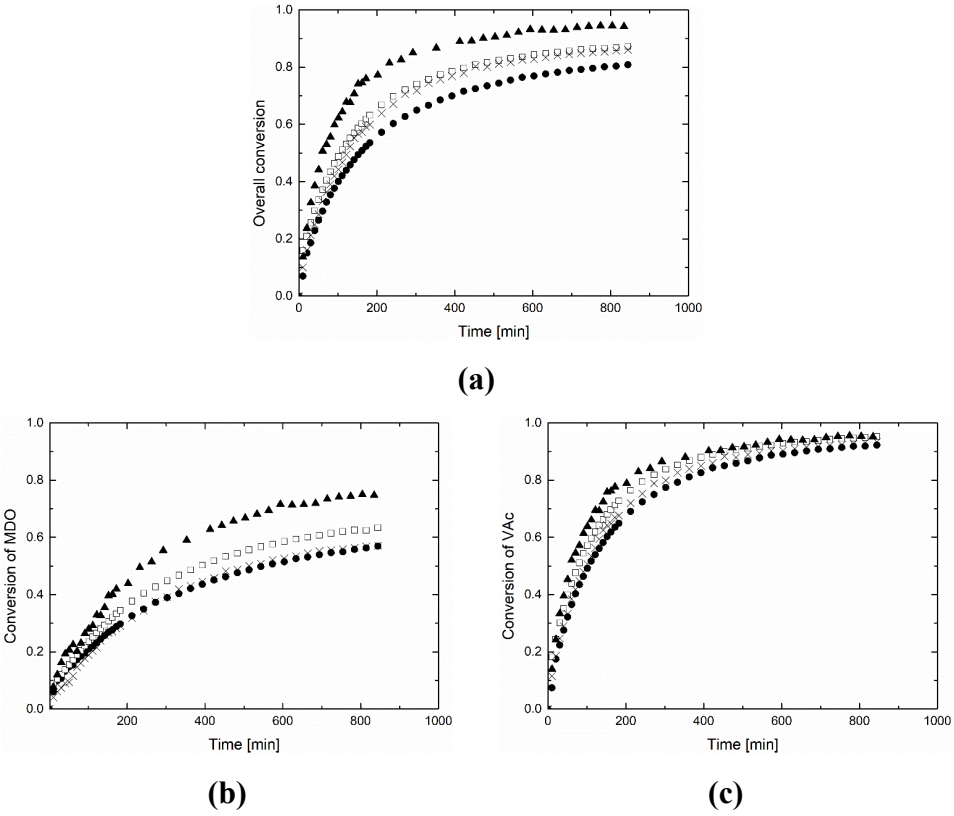

Figure 5.1. Evolution of (a) overall conversion and individual conversions of (b) MDO and (c) VAc during the copolymerization of MDO and VAc with the different feed molar ratios of MDO/VAc: 0.32/0.68 (circle), 0.25/0.75 (square), 0.20/0.80 (X) and 0.05/0.95 (triangle).

It can be seen that the overall rate of polymerization decreases by increasing the MDO fraction in the feed.

Overall, VAc monomer polymerized faster than MDO. At 500 minutes, VAc reached a conversion higher than 80% for all monomer ratios, whereas MDO achieved conversions between 50% and 70% by the end of the experiment and even at low feed monomer ratio of MDO, the incorporation of MDO in the copolymer was not complete. The reactivity ratios for the MDO/VAc system were estimated according to the non-linear least square method explained above (using all the experimental data). Figure 5.2 shows the comparison between the cumulative copolymer composition with respect to MDO determined experimentally by NMR analysis (points) and the calculated cumulative copolymer composition (lines) using the estimated reactivity ratios. The fitting of the experimental cumulative copolymer composition by the model using the estimated reactivity ratios is reasonably good.

The reactivity ratios of each monomer with the 95% confidence intervals are: r_{MDO} =0.43 ± 0.06 and r_{VAc} = 3.25 ± 0.12. This was expected because, firstly, VAc copolymerized faster than MDO (Figure 4) and, secondly, all the reported reactivity ratios of this comonomer system in the literature presented higher reactivity ratios for VAc (see Appendix Table IV.2). Nonetheless, notably the reactivity ratio estimated for VAc in this work is higher than that reported in previous works.

In order to shed light on the impact of the different reactivity ratios the Mayo-Lewis equation[23] was used to plot the instantaneous copolymer composition, F_{MDO}, as a function of the feed ratio, f_{MDO}, for different sets of reactivity ratios and experimental data. The reactivity ratios estimated in this work and those estimated by Lena et al.[18] and Agarwal et al.[16] were plotted in Figure 5.3. Furthermore, the experimental instantaneous copolymer compositions (when available) were included. For this work, the instantaneous copolymer compositions with respect to MDO, F_{MDO},

were calculated from the evolution of the individual monomer conversions of MDO and VAc (see Appendix section IV.3 for details). The noise of the data is present due to the time derivatives of the individual conversions that were not filtered. The “instantaneous” copolymer composition data used by Lena et al.[18] were taken from Undin et al.[15] and the copolymer compositions were measured from samples taken at high conversions (> 65% for all feed compositions). The instantaneous copolymer compositions used by Agarwal et al.[16] were measured at samples taken at conversions between 15-20%, but unfortunately were not reported. However, the authors reported the copolymer compositions at high conversions for these experiments and they have been plotted in the Mayo-Lewis plot shown in Figure 5.3.

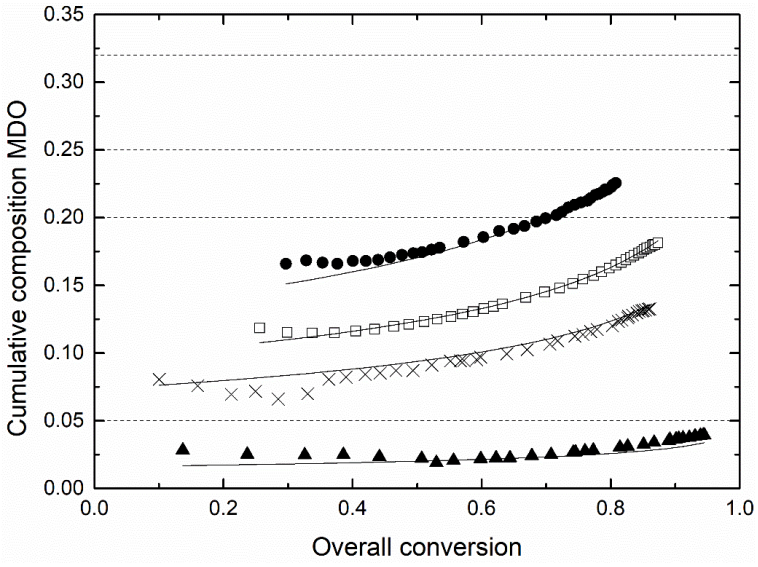

Figure 5.2. Conversion evolution of the cumulative composition of MDO for the in situ NMR experiments. (Dashed lines) Feed monomer composition, (scatter) experimental results and (lines) model predictions with the estimated reactivity ratios. Molar ratios of MDO and VAc: 0.32/0.68 (circle), 0.25/0.75 (square), 0.20/0.80 (X) and 0.05/0.95 (triangle).

Figure 5.3 shows clear differences between the three sets of reactivity ratios. It is worth noting that these three sets have been included because all copolymerization experiments were carried out under bulk conditions using AIBN as initiator and the temperatures were very close (between 60 and 70ºC). Therefore, the impact of the experimental conditions on the estimated reactivity ratios should be low. Thus, the discrepancies found between the works should only arise from the quality and quantity of the copolymer compositions measured in each approach and the parameter estimation algorithm employed to get the reactivity ratios.

An interesting observation in the plot is that the copolymer compositions obtained at high conversions (red squares, gathered in the work of Undin et al.[15] and used by Lena et al.[18] and the green triangles, gathered by Agarwal et al.[16]) are in very good agreement and fit reasonable well with the composition estimated with the reactivity ratios using the NLLS method of Lena et al.[18] (which were almost the same as those obtained by Undin et al.[15] with a linear estimation method). Interestingly, the low conversion copolymer compositions used by Agarwal et al.[16] to get the reactivity ratios (dashed green-line) do not match with the high conversion data (green triangles) clearly indicating the impact of using high conversion copolymer compositions in estimating the reactivity ratios.

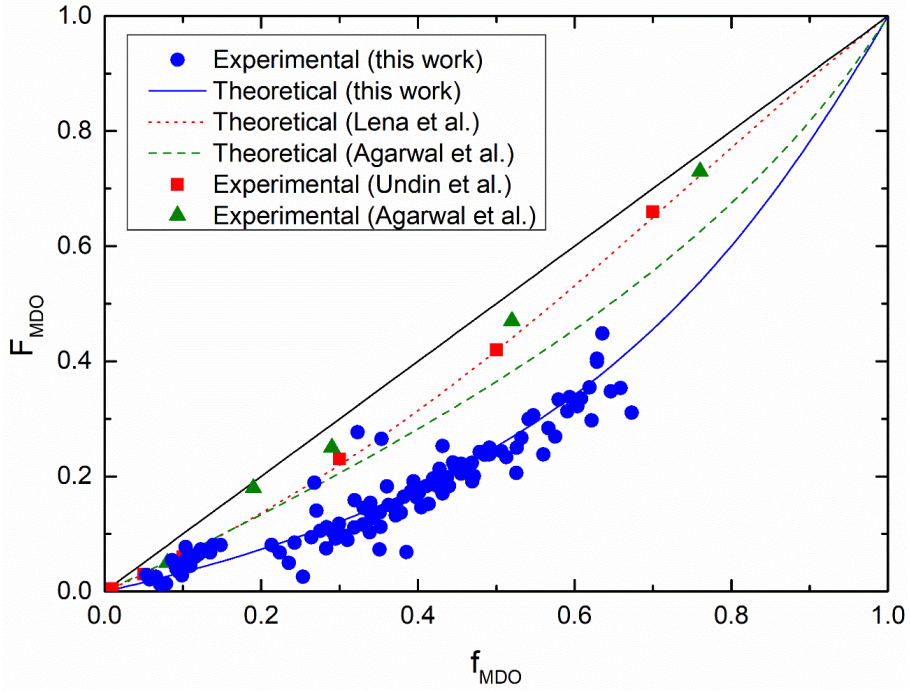

Figure 5.3. Mayo-Lewis plot for the copolymerization of MDO and VAc. The experimental instantaneous cumulative copolymer composition calculated from the evolution of the individual monomer conversions (blue circles); the theoretical instantaneous copolymer composition calculated using the reactivity ratios published in this article (blue line); the theoretical instantaneous copolymer composition calculated using the reactivity ratios of Lena et al.[18] (red, dotted line); the experimentally determined copolymer composition by Undin et al.[15] obtained at high conversions (red square), and Agarwal et al.[16] (green, dashed line); and the high conversion experimental data gathered from their work (green triangle) for the sake of comparison.

Notably, the instantaneous copolymer compositions determined in this work are more abundant because each experiment at each feed composition provides data large number of data points from the individual monomer conversions. In addition, the estimated reactivity ratios fit well both

the cumulative copolymer compositions (Figure 5.2) as well as the instantaneous copolymer compositions of the Mayo-Lewis plot.

5.3.2. Copolymerzation of MDO and 2OA

2-Octyl acrylate is a biobased monomer (with a bio-content of 73% derived from castor oil) that has been recently used in all acrylic waterborne dispersions for applications in pressure sensitive adhesives and coatings.[24,25] Therefore, it is an interesting acrylic monomer candidate for the incorporation of degradable polyester units by copolymerization with MDO or other cyclic ketene acetals. In order to determine the reactivity ratios of this comonomer system copolymerizations were carried out at different molar ratios of MDO and 2OA (MDO/2OA: 0.42/0.58; 0.22/0.78; 0.12/0.88 and 0.05/0.95). The evolution of overall and individual monomer conversions during these copolymerizations are displayed in Figure 5.4.

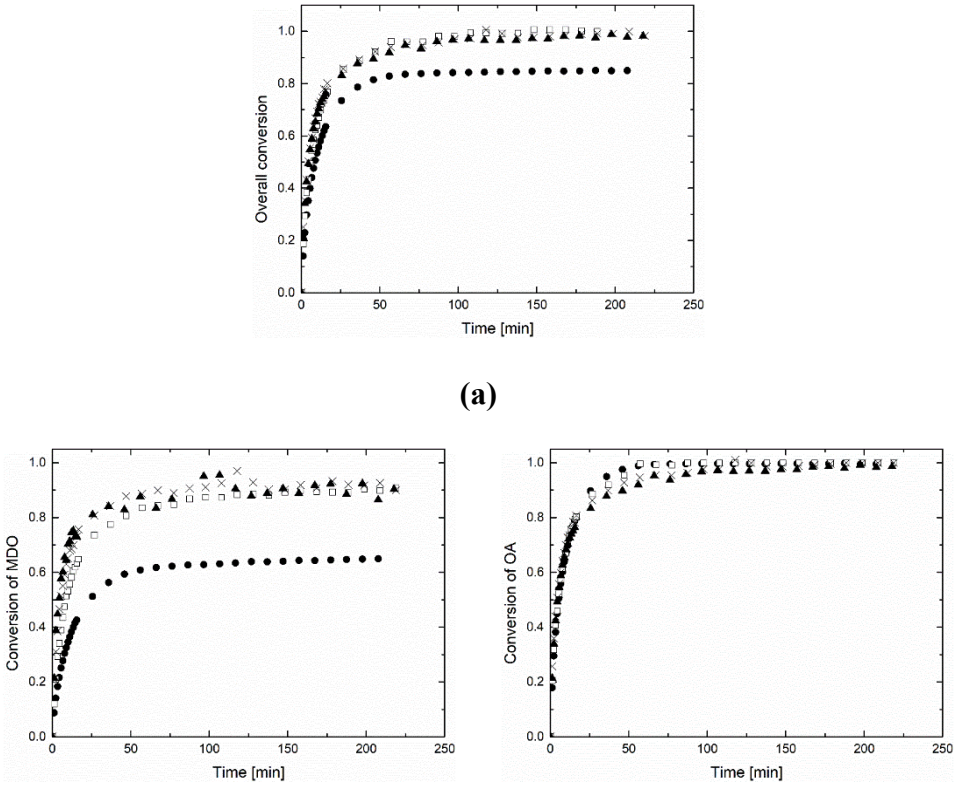

Figure 5.4. Evolution of (a) overall conversion and individual conversions for (b) MDO and (c) 2OA during their copolymerization at the different molar feed ratios of MDO/2OA: 0.42/0.58 (circle); 0.22/0.78 (square); 0.12/0.88 (X) and 0.05/0.95 (triangle).

It can be seen that this system copolymerizes faster than the MDO/VAc; this is due to the higher rate of polymerization of acrylates compared to VAc.[26] Complete conversions for 2OA were reached within a shorter timeframe (around 125 minutes). On the other hand, limited conversions for MDO between 60% and 85% were achieved. The conversion of 2OA was not significantly

affected by the feed monomer ratio. However, the polymerization rate of MDO decreased by increasing the MDO fraction in the feed. The copolymerization with the highest MDO concentration (molar ratio MDO/2OA: 0.42/0.58) presented the lowest final conversion of 60%. Furthermore, the conversion of MDO did not increase significantly when all the 2OA was consumed. This is likely due to the extremely low homo-propagation rate of MDO, in agreement with previous studies.[8]

The estimated reactivity ratios for MDO (r_{MDO}) and 2OA (r_{2OA}) are with a 95% confidence interval: r_{MDO} = 0.0 + 0.0003 and r_{2OA} = 1.293 ± 0.053. The estimated reactivity ratio for MDO appears to be zero for this system. This result indicates that the MDO cross-propagation rate coefficient with 2OA is much higher than its homopolymerization propagation constant. On the other hand, the reactivity ratio of 2OA (slightly above 1) indicates that 2OA is homo- and copolymerizing almost equally. The estimated reactivity ratio of 2OA in the MDO/2OA copolymerization is far lower than the value for methyl acrylate (r_{MDO} = 0.0235 and r_{MA} = 26.535) reported in literature.[13] Figure 5.5 shows the comparison between the experimentally determined (points) and the calculated (lines) cumulative copolymer compositions. It can be seen that, up to a certain concentration of MDO in the feed (< 0.12), the composition drift is not substantial and therefore, it should be possible to obtain relatively homogeneous MDO-co-2OA copolymers without the need for optimizing monomer addition profiles. However, the agreement between the experimental data and the model prediction is poorer in this case (compared to the MDO/VAc and MDO/LMA system). Admittedly, we do not have an explanation for the poorer fitting that cannot be directly attributed to the range of the feed compositions used to get the experimental data, which was broader that for the VAc/MDO comonomer system.

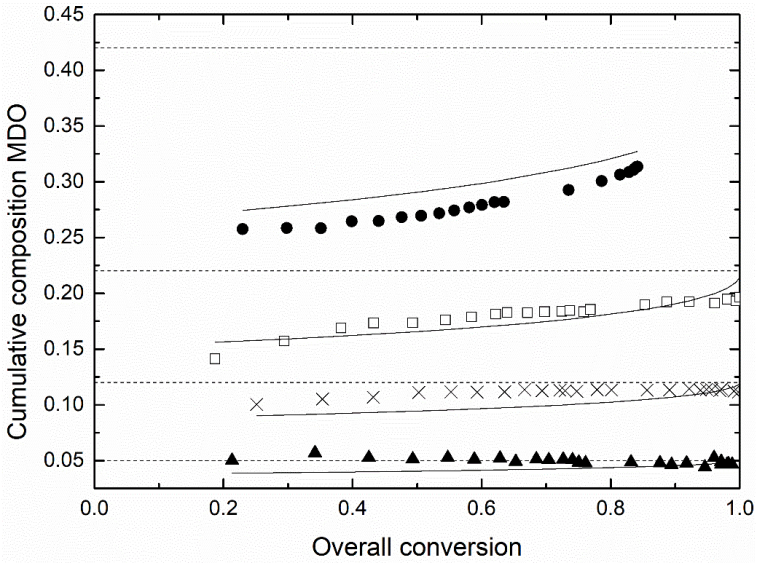

Figure 5.5. Conversion evolution of the cumulative composition of MDO for the in situ NMR experiments. Feed composition (dashed lines), experimental values (scatter) and model predictions (continuous lines) with the estimated reactivity ratios for the copolymerization with the different molar ratios of MDO and 2OA (MDO/2OA: 0.42/0.58 (circle); 0.22/0.78 (square); 0.12/0.88 (X) and 0.05/0.95 (triangle)).

The reactivity ratios estimated for this acrylate and MDO are in relatively good agreement with those estimated by Lena et al.[14] for MA, *n*-BA, 2EHA and DA. For all systems, the reactivity ratio of the MDO monomer is close to zero and that of the acrylate close to or higher than one with no clear trend based on the length of the side chain of the acrylate. The Mayo-Lewis copolymer composition plot for this system is presented in the appendix (Figure IV.4). For comparison purposes the experimental data for the 2EHA/MDO system (2EHA and 2OA are isomers) obtained by Lena et al.[14] is included in the same plot. Up to a MDO feed fraction of 0.8 the instantaneous copolymer compositions calculated from the reactivity ratios for the 2OA/MDO

system and the 2EHA/MDO system show relatively similar evolutions confirming the good agreement between the two sets of reactivity ratios. The discrepancy at higher feed ratios (f_{MDO}>0.8) is likely due the fact that very little data were obtained in this range in the four monomer ratios used in this work that led to a r_{MDO} = 0.

5.3.3. Copolymerzation of MDO and LMA

Lauryl methacrylate is another biobased monomer with a bio-content of 75% derived from lauryl alcohol, which is prepared from fatty acids.[27] Therefore, it is another interesting candidate for the production of degradable high biobased copolymers together with MDO or other cyclic ketene acetals. Copolymerizations were carried out at 4 different molar ratios of MDO and LMA, MDO/LMA: 0.52/0.48; 0.30/0.70; 0.23/0.77 and 0.09/0.91. The time evolution of the overall and individual monomer conversions of MDO and LMA for these copolymerizations are shown in Figure 5.6.

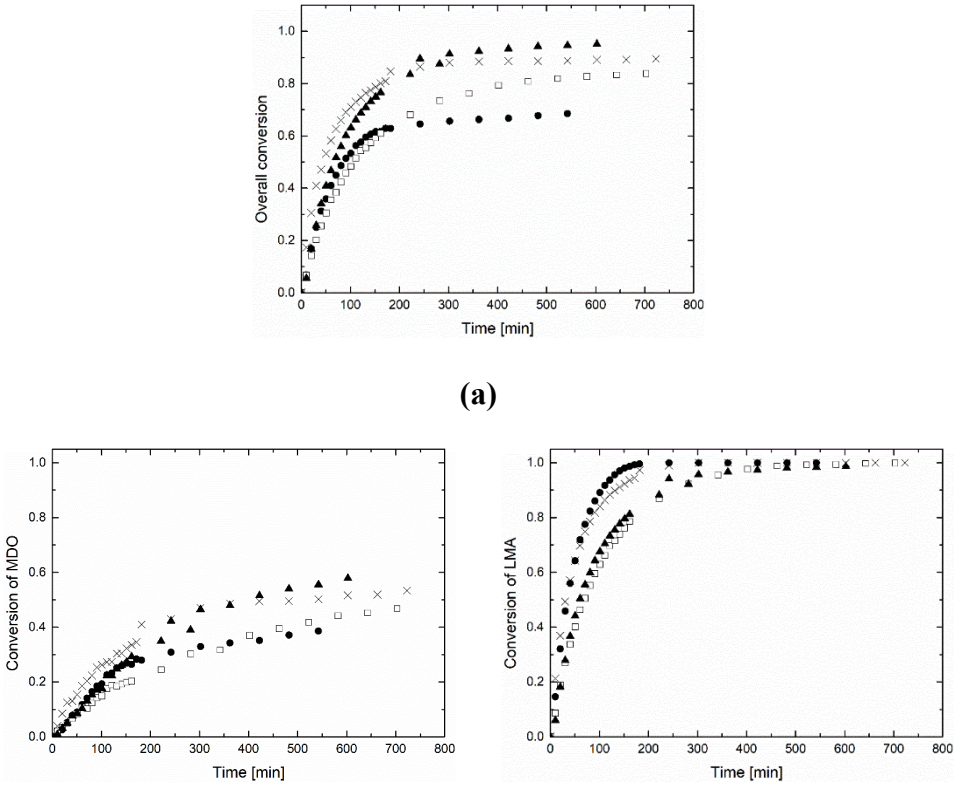

Figure 5.6. Evolution of (a) overall conversion and individual monomer conversions for (b) MDO and (c) LMA for the copolymerization of those two monomers in different molar ratios of MDO/LMA: 0.52/0.48 (circle); 0.30/0.70 (square); 0.23/0.77 (X) and 0.09/0.91 (triangle).

The copolymerization of LMA and MDO is slower than for MDO/2OA, but faster than for MDO/VAc and the polymerization rate decreases by increasing the MDO molar ratio in the feed, which is a common feature for all studied systems. Complete conversions for LMA were obtained after 200-400 min depending on the comonomer ratio used. Up to this point, MDO reached

conversions between 20% and 40% and from here on, the polymerization rate of MDO decreased significantly so that no full conversions of MDO were obtained at the end of the copolymerizations. After 600-700 min the conversions of MDO were between 35% and 60%. This is due to the lower homopolymerization rate of MDO as discussed above. The polymerization rate of LMA does not show a clear trend as a function of the monomer feed ratio. On the contrary, the polymerization rate of MDO increases by decreasing the amount of MDO in the feed.

The reactivity ratios for both monomers with the 95% confidence intervals are r_{MDO}= 0.022 ± 0.002 and r_{LMA}=8.471 ± 0.028. As for VAc and 2OA the reactivity ratio of MDO is close to zero, indicating a preference of the MDO radical to crosspropagate with the methacrylate monomer. The reactivity ratio of LMA (r_{LMA} = 8.5) is higher than those found for VAc and 2OA; namely, that homopropagation of the LMA monomer is favoured over the crosspropagation with MDO, which makes the incorporation of MDO in the copolymer chains challenging.

The experimental cumulative copolymer compositions determined by ^{1}H-NMR (points) and the calculated cumulative compositions using the estimated reactivity ratios (lines) are shown in Figure 5.7. The fitting of the experimental cumulative composition, carried out at different monomer feeds, is reasonably good and the data shows a substantial composition drift along the experiments. The estimated reactivity ratios are in reasonable agreement with the reactivity ratios of MDO (and other cyclic ketene acetals) with other methacrylates like MMA. The r_{MDO} values are close to zero but there are substantial discrepancies in the r_{MMA} values (as discussed in the introduction of this chapter). Agarwal[12] reported a value of r_{MMA} = 3.5 (a ratio of 87.5 between them) for bulk polymerizations carried out at 120 ºC and Roberts et al.[8] reported a

value of r_{MMA} = 34 (a ratio of 599 between them) for bulk copolymerizations at 40 ºC. The value r_{LMA} = 8.5 gives a ratio between the two reactivity ratios of 385, which is in between the two reported values.

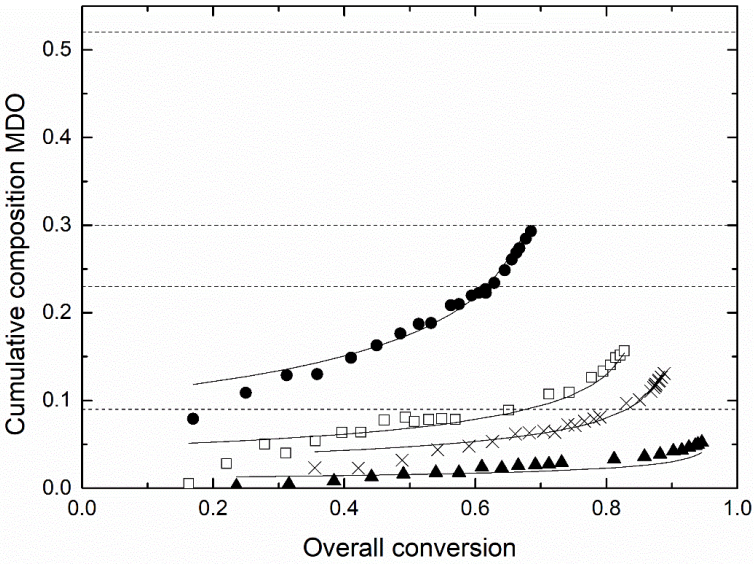

Figure 5.7. Conversion evolution of the cumulative composition of MDO for the co-polymerization of MDO and LMA. Comparison between monomer feed composition (dashed lines), experimental values (scatter) and calculated values by estimation of the reactivity ratios (line). With the different molar ratios of MDO/LMA: 0.52/0.48 (dot); 0.30/0.70 (square); 0.23/0.77 (X) and 0.09/0.91 (triangle).

The Mayo-Lewis copolymer composition plot for the MDO/LMA system is presented in the appendix (Figure IV.5). The agreement between the experimentally determined instantaneous copolymer composition and theoretically calculated one is reasonable even though the experimental data presents substantial signal noise that, as noted above, is a result of the time derivatives of the data on Figure 5.6 b and c that is not filtered.

5.4. Conclusion

The copolymerizations of the cyclic ketene MDO with the vinylic monomers VAc, 2OA and LMA in different molar ratios were monitored by *in situ* ^{1}H-NMR spectroscopy. In all of the three comonomer systems, a much lower consumption rate of MDO compared to the other comonomers was observed. The estimated reactivity ratio of MDO was the highest for the copolymerization system MDO/VAc. However, for the copolymerizations with 2OA and LMA it was close to zero. This means that crosspropagation of MDO terminated growing chains was substantially higher than homopropagation. The estimated reactivity ratio for 2OA was only slightly above one, making the MDO/2OA system viable for the incorporation of significant fractions of MDO into the copolymer. On the other hand, the estimated reactivity ratios for VAc and LMA for their copolymerization with MDO were far higher than one, making these systems less viable for the incorporation of MDO into the resulting copolymer. In the latter cases, the homogeneous incorporation of MDO in the copolymers requires appropriate feeding strategies of the monomers to avoid the intrinsic composition drift of the comonomer pairs.

5.5. References

[1] A. Tardy, J. Nicolas, D. Gigmes, C. Lefay, Y. Guillaneuf, *Chem. Rev.* **2017**, *117*, 1319–1406.

[2] R. Mueller, *Process Biochem.* **2006**, *41*, 2124–2128.

[3] S. Jin, K. E. Gonsalvez, *Macromolecules* **1997**, *30*, 3104–3106.

[4] J. Undin, A. Finne-Wistrand, A. Albertsson, *Biomacromolecules* **2013**, *14*, 2095–2102.

[5] W. J. Bailey, Z. Ni, *J. Polym. Sci., Polym. Chem. Ed.* **1982**, *20*, 3021–3030.

[6] A. Tardy, J. Honoré, D. Siri, J. Nicolas, D. Gigmes, C. Lefay, Y. Guillaneuf, *Polym. Chem.* **2017**, *8*, 5139–5147.

[7] S. Jin, K. E. Gonsalves, *Macromolecules* **1998**, *31*, 1010–1015.

[8] G. E. Roberts, M. L. Coote, J. P. A. Heuts, L. M. Morris, T. P. Davis, *Macromolecules* **1999**, *32*, 1332–1340.

[9] W. J. Bailey, T. Endo, Y. Lin, Z. Ni, *J. Macromol. Sci. Chem.* **1984**, *21*, 979–995.

[10] W. J. Bailey, B. Gapud, *Polym. Stab. Degrad.* **1985**, *280*, 423–431.

[11] B. Wu, R. W. Lenz, *J. Environ. Polym. Degrad.* **1998**, *6*, 23–29.

[12] S. Agarwal, *Polym. J.* **2007**, *39*, 163–174.

[13] L. F. Sun, R. X. Zhuo, Z. L. Liu, *J. Polym. Sci., Part A Polym. Chem.* **2003**, *41*, 2898–2904.

[14] J. Lena, A. W. Jackson, L. R. Chennamaneni, C. T. Wong, F. Lim, Y. Andriani, P. Thoniyot, A. M. Van Herk, *Macromolecules* **2020**, *53*, 3994–4011.

[15] J. Undin, T. Illanes, A. Finne-wistrand, A. Albertsson, *Polym. Chem.* **2012**, *3*, 1260–1266.

[16] S. Agarwal, R. Kumar, T. Kissel, R. Reul, *Polym. J.* **2009**, *41*, 650–660.

[17] G. G. Hedir, C. A. Bell, N. S. Ieong, E. Chapman, I. R. Collins, R. K. O. Reilly, A. P. Dove, *Macromolecules* **2014**, *47*, 2847–2852.

[18] J. Lena, A. M. Van Herk, *Ind. Eng. Chem. Res.* **2019**, *58*, 20923–20931.

[19] D. Ding, X. Pan, Z. Zhang, N. Li, J. Zhu, X. Zhu, *Polym. Chem.* **2016**, *7*, 5258–5264.

[20] D. Gigmes, P. H. M. Van Steenberge, D. Siri, R. D. Dagmar, Y. Guillaneuf, C. Lefay, *Macromol. Rapid Commun.* **2018**, *39*, 1800193.

[21] J. C. de la Cal, J. R. Leiza, J. M. Asua, *J. Polym. Sci., Part A Polym. Chem.* **1991**, *29*, 155–167.

[22] G. Garcia, Sintesis de Floculantes Catonicos En Reactores Continuos, University of the

Basque Country, **2009**.

[23] F. R. Mayo, F. M. Lewis, *J. Am. Chem Soc.* **1944**, *66*, 1594–1601.

[24] A. Badia, J. Movellan, M. J. Barandiaran, J. R. Leiza, *Ind. Eng. Chem. Res.* **2018**, *57*, 14509–14516.

[25] A. Badía, M. Kastelijn, J. Scheerder, J. R. Leiza, *Prog. Org. Coatings* **2020**, *147*, 105708.

[26] R. Jovanovic, M. A. Dube, *J. Appl. Polym. Sci.* **2004**, *94*, 871–876.

[27] S. Cousinet, A. Ghadban, E. Fleury, F. Lortie, J. Pascault, D. Portinha, *Eur. Polym. J.* **2015**, *67*, 539–550.

Chapter 6. Copolymerization of MDO in waterborne systems

6.1. Introduction

In this chapter, the emulsion copolymerization of the cyclic ketene acetal MDO together with other monomers will be described. The aim is to synthesize latices with backbone degradable polymer particles. However, the polymerization of cyclic ketenes in waterborne systems is challenging due to their high water sensitivity, which leads to rapid hydrolysis.[1] Furthermore, MDO polymerizes either by ring opening or by ring retention (see Scheme 6.1). The MDO unit that undergoes ring opening is incorporated into the polymer backbone with an ester unit, providing the polymeric chain with a degradable unit. However, when the MDO unit is incorporated as ring retention, an acetal unit is added to the polymer chain without adding any degradable unit. The ratio of ring opening to ring retention is strongly influenced by the polymerization parameters, mainly by the temperature.[2,3]

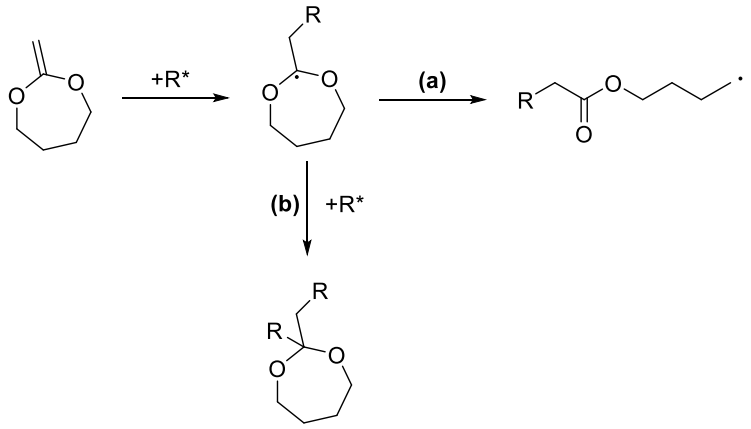

Scheme 6.1. MDO is incorporated to a polymer either by RROP (a) or by ring retention (b).

It is reported in the literature, that increasing the temperature increases the ratio of ring opening to ring retention. At 70 ºC 28% of the MDO was incorporated into a *n*BA/MDO-copolymer (by solution polymerization in cyclohexane) as ring opened units, whereas at 90 ºC 34% were incorporated as ring opened units. Furthermore, it is also stated that large alkyl acrylates also favor ring opening.[3]

In the literature, there are different attempts reported to incorporate MDO into a polymeric backbone. Landfester et al.[4] were the first ones copolymerizing the cyclic ketene acetal 5,6-benzo-2-methylene-1,3-dioxepane (BMDO) with MMA and styrene in miniemulsion to obtain biodegradable drug carriers. They showed that depending on the amount of BMDO in the copolymer a significant decrease of the weight average molar mass of the copolymer after treatment with either the enzyme *Lipase PS* or concentrated potassium hydroxide solution (50%

- 5% residual Mw after 48 h). Furthermore, the feasibility of the nanoparticles to act as drug carriers was proven by the incorporation and release of the cytostatic drug paclitaxel.

Apart from the medical application as drug carrier, latices with backbone degradable particles are also of interest for other fields.[5] One of them is the usage as coatings for single use paper products, which are often used for the packaging of food, such as paper boxes, wrappers, etc. These are in many cases coated to increase the mechanical properties and the oil/grease resistance. However, when these food-packaging products are contaminated, it becomes difficult to recover and recycle the underlying fibers. Preventing potential pathways for degradation[6] sustainability could be increased by coatings made of biodegradable latices. With this motivation Carter et al. described the emulsion copolymerization of MDO with vinyl acetate.[7] They reported that mildly basic conditions (pH: 8) and low temperatures (40 ºC) are essential to prevent the rapid hydrolysis of MDO. Furthermore, they demonstrated the degradability of the MDO units containing co-polymers by hydrolysis of the ester groups in a basic aqueous solution with a bicarbonate buffer and a pH value of 10. Within 50 days they observed a mass loss of ~50% for films of the dried VAc-co-MDO copolymer.

Very recently D'Agosto et al. reported the emulsion copolymerization of the thionolactone monomer dibenzo[c,e]oxepane-5-thione (DOT), which was first proposed by Roth et al.[8] and Gutekunst et al.[9], with butyl acrylate and/or styrene. DOT similar to MDO also undergoes rROP leading to in-chain thioester functions.[10] Unlike MDO, DOT is assumed to present favorable reactivity ratios with styrene or (meth)acrylates and do undergo complete ring opening (no ring retention). Low contents of DOT of ~2-5 mol% were sufficient to obtain degradable copolymers.

Degradation through isopropylamine and 1,5,7-triazobicyclo[4.4.0]dec-5-ene (TBD) was demonstrated.

Due to the growing interest in industry to produce more sustainable polymer latexes, the synthesis of waterborne degradable copolymers is a hot topic and the research on the synthesis of new monomers able to polymerize by emulsion polymerization and that will readily copolymerize with common oil-based or novel biobased monomers and the understanding and process optimization of already described monomers is of paramount importance in the field. In this context, this chapter assesses the copolymerization of MDO in emulsion polymerization. From the current understanding of the polymerization of MDO in aqueous media it is clear that to achieve waterborne polymer particles with a degradable backbone from the emulsion copolymerization of MDO with other monomers, it is necessary that the rate of consumption of MDO by polymerization is higher than the rate of its hydrolysis. In this Chapter we assess the kinetics of the hydrolysis of MDO in aqueous media under different conditions in an attempt to find the optimal conditions for its incorporation in emulsion polymerization. Then, different approaches to copolymerize MDO with other comonomers in dispersed media are presented.

6.2. Experimental part

In the following part, the experiments for the copolymerization of MDO in waterborne systems are described. The analysis by ^{1}H- and ^{13}C-NMR spectroscopy, the characterization of particle sizes by disc centrifuge, the determination of pH-values through pH-meter and the measurement of solid contents by a thermo-balance for the calculation of conversions are described in the appendix.

6.2.1. Hydrolysis studies of MDO

The hydrolysis studies of MDO were done adding 100 mg of D_2O and 600 mg of an aqueous KOH solution adjusted to pH: 10 or pH: 8 into a Wilmad® NMR tube with a length of 18 cm, and a diameter of 5 mm (wall thickness of 0.43 mm). The tube was then heated to the desired temperature (30, 40 or 50 ºC), when the temperature was stable, 50 µL of MDO were added to the NMR tube with an Eppendorf pipette. The liquid ^{1}H-NMR spectra were acquired via NMR measurements with a 500 MHz Bruker Avance NMR instrument equipped with a Z gradient broadband observe (BBO) probe. Scans were performed every 5 min. The number of scans was one for each of the measurements with a relaxation delay of 10.00 s, a pulse width of 14 µs and an acquisition time of 2.23 s.

6.2.2. Emulsion copolymerization of MDO

6.2.2.1. Batch emulsion copolymerization of MDO and vinyl acetate (VAc)

Two different approaches were studied to incorporate the MDO in the polymeric backbone by batch emulsion polymerization. First of all, conventional emulsion polymerization approach was used whereas in the second one, a prepolymer was prepared first and then the copolymerization was carried out.

The conditions of the experiments and results from different measurements are listed in Table 6.1. The ratio between VAc and MDO was 80/20 in all of the experiments. In some of the cases, MDO was diluted first in Chloroform before the addition to the emulsion, with the objective to protect MDO from hydrolysis. Sodium hydrogencarbonate ($NaHCO_3$) was used as buffer to keep the pH at a neutral value. Except for the experiment in which triethylamine was used as a base to set the pH to a slightly basic value. KPS or AIBN were used as initiator at reaction temperatures in between 60-70 °C and the solid content was around 20%. Experiment MEP was carried out in miniemulsion polymerization. In all the other experiments EPn were carried out batchwise.

Table 6.1. Conditions for emulsion and miniemulsion co-polymerizations of VAc and MDO.

Ref	EP1	EP2	EP3	EP4	MEP*
VAc/MDO	80/20	80/20	80/20	80/20	80/20
Solvent	-	$CHCl_3$	$CHCl_3$	$CHCl_3$	$CHCl_3$
Buffer	$NaHCO_3$	$NaHCO_3$	Et_3N	$NaHCO_3$	$NaHCO_3$
Initiator	KPS	KPS	AIBN	AIBN	KPS
Temperature	65 ºC	70 ºC	60 ºC	60 ºC	60 ºC
SC	20%	18%	18%	19%	17%

*2 wbm% of hexadecane were used as co-stabilizer in the miniemulsion polymerization MEP.

In another attempt to copolymerize MDO, VAc and lauryl methacrylate (LMA) co-monomers were used, but these monomers were at first prepolymerized in bulk. More precisely, MDO/VAc or MDO/LMA in the weight ratio 20/80 were polymerized in a vial under nitrogen atmosphere and magnetic stirring. Polymerizations were carried out at temperatures of 65 ºC with 2 mol% of AIBN as initiator. The reaction temperature was kept for 10-20 min and then cooled down to room temperature. Then, 12.5 wbm% of hexadecane were added to the pre-polymer to complete the organic phase. Furthermore, an aqueous solution of 99.8 wt% destilled water and 0.2 wt% Dowfax 2A1 was prepared. The organic phase was poured into the aqueous phase under magnetic stirring and was further stirred for 60 min. The mixture was then sonicated in an ice bath with a Hielscher sonicator (operating at 80% amplitude and 50% cycle). After which the miniemulsion was degassed for 15 min and then polymerized at 72 ºC for 12 h.

6.2.2.2. Seeded semibatch emulsion copolymerization of MDO

Other attemps were done to incorporate MDO by emulsion co-polymerization this time by seeded semi batch process and with the co-monomers BA, 2OA, Veova 10 and Veova EH, in a 1 l glass reactor with an anchor type stirrer (200 rpm) and under nitrogen atmosphere.

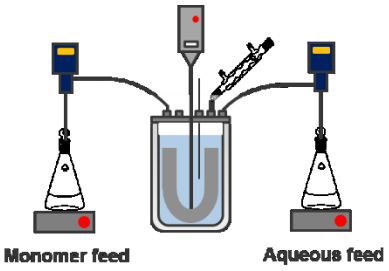

Figure 6.1. Scheme of the set-up, which was used to carry out the seeded semibatch emulsion polymerizations.

Firstly, a commercial acrylic seed (Acronal A508, BASF) with a particle size of 65 nm was used as the initial charge together with distilled water, ammonia to adjust the pH and EDTA as one part of the catalyst for the redox initiator system. The redox initiator system consisted of FF6, APS, EDTA and Iron(II)sulfate ($FeSO_4$) in ratios that were already described by Kohut-Svelko et al.[11] When the reaction temperature of 20, 30, 40 or 50 ºC was reached APS, Iron(II)sulfate and FF6 were added as shots, each of them dissolved in distilled water. Subsequently two feeding streams were started. One containing neat monomer (which was nBA, 2OA, Veova 10 or Veova EH) and the other one an aqueous solution consisted of surfactants Dowfax 2A1 and Disponil AFX1080, further FF6 and distilled water. The feedings were carried out over a timeframe of

180 min. Afterwards the reaction temperature was kept for further 30 min. Then the reaction temperature was raised to 80 ºC for 30 min. Finally, the reactor was cooled down to 25 ºC. The detailed formulation of the seeded semibatch emulsion polymerization is shown in Table 6.2.

Table 6.2. Formulation for the seeded semibatch emulsion polymerization in presence of MDO.

	Component	Amount [wbm%]
Initial charge	Acronal A508	14
	EDTA	0.02
	Ammonia	0.36
	Water	78.57
Shot at reaction temperature	APS	0.60
	FF6	0.15
	$FeSO_4$	0.01
	Water	14.29
Monomer feed	MDO	5/10
	Co-monomer	90/95
Aqueous solution	Dowfax 2A1	2.22
	Disponil AFX1080	0.31
	FF6	0.45
	Ammonia	0.46
	Water	50

For the seeded semibatch emulsion polymerizations of MDO with the vinyl esters Veova 10 and Veova EH a third feeding stream was used and only 25% of the APS was added as a shot at the reaction temperature and the remaining 75% were fed over the reaction time.

6.3. Results and discussion

6.3.1. Kinetics of the hydrolysis of MDO

At first, the hydrolysis of MDO to 4-hydroxybutyl acetate (4-HBA) (Scheme 6.2) under different conditions was studied to find the best parameters for its prevention and therefore, for the emulsion polymerization of MDO.

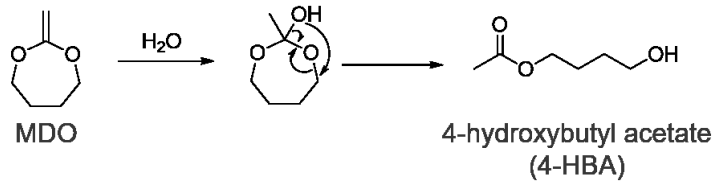

Scheme 6.2. Hydrolysis of MDO to 4-HBA.

Hydrolysis experiments were carried out by *in situ* ^{1}H-NMR to track the disappearance of the MDO protons and the appearance of the protons of the hydrolysis product 4-HBA (Figure 6.2). In the first spectra during the *in situ* hydrolysis experiment it seems that the peaks of MDO get split into two separated peaks The reason for this is not clear, it might be caused by the generation of intermediate products. Another explanation could be the presence of MDO on the one hand in the water phase and on the other hand in a formed MDO phase, due to its low water-solubility. Hence, the appearance of the peaks belonging to the protons of 4-HBA was tracked and their integral was divided over the integral of 4-HBA plus the integral of the MDO peaks to calculate the molar fraction of 4-HBA, which can be seen as hydrolysis percentage.

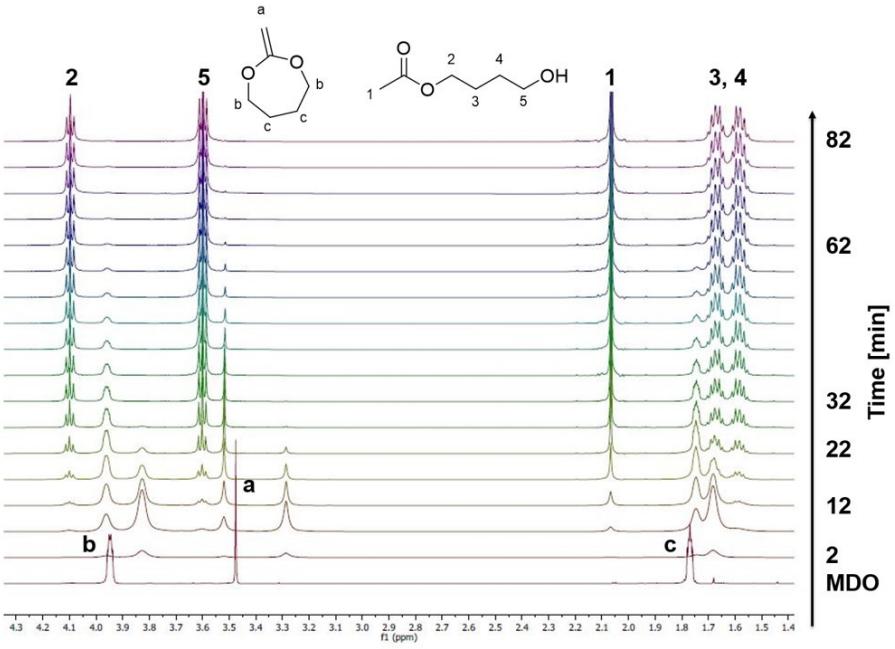

Figure 6.2. ^{1}H-NMR spectra for one of the *in situ* hydrolysis experiments of MDO (pH: 8 and 30 ºC). With assignment of the protons of MDO and 4-HBA to the signals.

Different conditions were investigated to observe the effects of temperature and pH-values, for instance, the temperature was varied from 30-40 ºC and the pH between 8 and 10. The results are shown in Figure 6.3. It can be seen that after one hour, at pH=8 and 30 ºC, all the MDO was converted to 4-HBA, or in other words, all the MDO was hydrolysed. On the other hand, for the cases in which pH=8 and 40 ºC and pH=10 and 30 ºC, the appearance of 4-HBA is much faster. Therefore, the conditions in which the hydrolysis is slower are considered as the most promising to polymerize MDO in water-based systems.

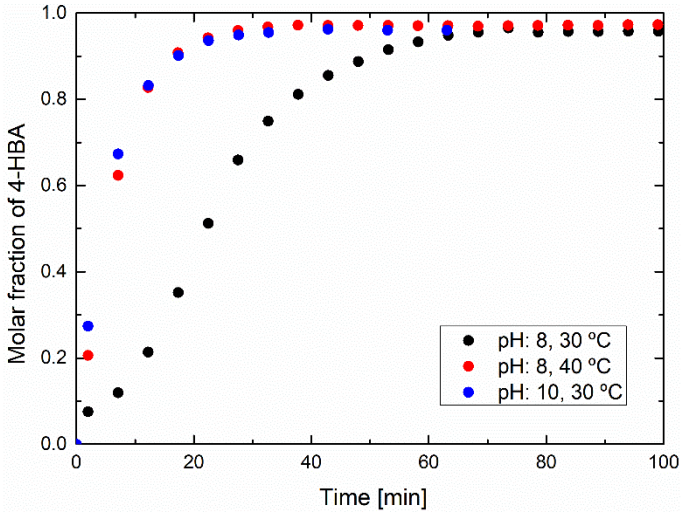

Figure 6.3. Evolution of the molar fraction of 4-HBA determined by ^{1}H-NMR spectra during the hydrolysis experiment of MDO at different conditions.

Compared to the findings of Carter et al.[7] the hydrolysis seems to be much faster. They observed complete hydrolysis within 3-5 hours, whereas in the presents experiments complete hydrolysis was reached in 30-60 min. It needs to be mentioned that the conditions for the hydrolysis experiment of MDO by Carter et al. were different. They dissolved MDO first in DMSO-d_6 and did the experiments changing the ratios of DMSO-d_6 /D_2O solutions between 10/1, 100/1 and 1000/1. They found out that the rate of hydrolysis of MDO was increasing with the fraction of water in the solution.

6.3.2. Emulsion copolymerization of MDO

6.3.2.1. Batch (mini)emulsion polymerization

First experiments were carried out in batch emulsion copolymerization of MDO and the acrylate LMA or the vinyl ester VAc to incorporate pMDO units into the copolymer. These experiments were done before the results of the hydrolysis studies were known, therefore not much attention was paid neither to the pH of the dispersion nor to the temperature of reaction. Preliminary experiments to incorporate ester units into the polymer backbone through (mini)emulsion co-polymerization were carried out with MDO and VAc. VAc was chosen due to its more favorable reactivity ratios for the co-polymerization with MDO, compared to other common monomers as it was already discussed in Chapter 5. The experimental results obtained for the different experiments are listed in Table 6.3.

Table 6.3. Emulsion and miniemulsion co-polymerization of VAc and MDO.

Ref	**EP1**	**EP2**	**EP3**	**EP4**	**MEP**
dp	155 nm	125 nm	876 nm	-	154 nm
Conversion	71%	51%	50%	41%	40%
VAc/MDO	**100/0**	**100/0**	**100/0**	**-**	**100/0**
Coagulation	No	Yes	Creaming	Yes	No

In the experiments in which KPS was used as an initiator (EP1, EP2 and MEP) particle sizes between 125-155 nm were determined and the conversions were in the range between 40-70%. In all the cases, the final polymer consisted only of VAc units (confirmed by NMR measurements) and hence, no incorporation of MDO into the polymer was observed. Additionally, the hydrolysis product 4-HBA was found in the aqueous phase. Moreover, for the experiment EP4 coagulation

was observed so that it was stopped after 60 min. For the other experiment in which AIBN was used as initiator, creaming and a relatively high particle size of almost 900 nm were observed. Therefore, it can be concluded that the temperatures and the pH-value at which these experiments were carried out are not appropriate for the emulsion polymerization of MDO. This is in agreement with the results from the hydrolysis study (Figure 6.3), which was carried out after these first preliminary experiments.

Another strategy was followed to incorporate MDO by batch miniemulsion polymerization. It was demonstrated in Chapter 5, that the copolymerization of MDO with different monomers was possible in bulk polymerization. This is why, in the following attempts it was thought to first, synthesize a co-polymer of MDO with VAc or with LMA as a hydrophobic monomer in bulk up to low conversions ~20% and then, in a second step this pre-polymer was dispersed with surfactant, stabilizer and water and polymerized by miniemulsion polymerization. The mixture was then sonified, and the initiator was added to the miniemulsion to carry out the polymerization and to complete the reactions of the remaining comonomers with the expectation that MDO will be less prone to contact with water. Conversions for the bulk co-polymerizations were determined by ^{1}H-NMR measurements. Three different experiments were carried out following this strategy (Table 6.4). One with LMA and the other two with VAc.

Table 6.4. Conversions of the bulk co-polymerization of VAc or LMA and MDO.

Comonomer	AIBN [wbm%]	Time [min]	Conversion [%]
LMA	1	20	~10
VAc	1	15	~20
VAc	2	20	~50

Furthermore, the miniemulsification step of the pre-polymer was challenging due to the high viscosities reached by the prepolymer. Hence, not the whole prepolymer got dispersed during the sonification step, a solid remained which seemed to contain polyMDO units. The usage of chain transfer agent in the bulk pre-polymerization step might be a solution to reduce the molar mass of the prepolymer and hence, decrease the viscosity of the pre-polymer solution and therefore facilitate its dispersion by sonication. Nevertheless, after the miniemulsion polymerization the ^{1}H-NMR spectra of the water soluble part of the latex in D_2O showed the presence of the hydrolysis product 4-HBA. Therefore, this route to incorporate MDO turned unsuccessful and due to lack of time we did not continue.

6.3.2.2. Seeded semibatch emulsion polymerization

According to the hydrolysis experiments carried out in the previous section, it is possible to slow down the hydrolysis of MDO in water by adjusting the pH to a slightly basic value (pH: 8) and at lower temperatures (30 ºC). In the case of the emulsion polymerization of MDO, the consumption of MDO is a competition between its hydrolysis (once in contact with water) and its

consumption through polymerization (that occurs in the polymer particles). Therefore, in order to favor the polymerization, it was tried to increase the polymerization rate of MDO. According to equation 6.1 the polymerization rate of MDO is proportional to the rate constant (k_{pni}), the monomer concentration in the particles ($[M]_P$), the average number of radicals in the particles ($\tilde{n}$), Avogadros constant (N_A) and the total number of particles (N_P).

$$R_{pi} = (k_{pAi}P_A^p + k_{pBi}P_B^p)[i]_P \frac{\tilde{n}}{N_A} N_P \tag{6.1}$$

Thus, high numbers of polymer particles were used during the seeded semibatch emulsion polymerization process. The number of particles was set by the amount of seed used in the initial charge. Furthermore, different feeding rates of the monomer feed stream were tried, to check the effect of different monomer concentrations.

First experiments were carried out with a monomer feed stream consisting of 5 wt% MDO and 95 wt% of BA with feeding times of 60 or 180 min and at temperatures between 20 ºC and 50 ºC. Conversions were determined by the measurement of the solid content with a thermo-balance. The evolution of instantaneous conversions for the experiments with 180 min and 60 min of monomer feeding time are shown in Figure 6.4 (a). Instantaneous conversions are ~95% over the reaction time, with a final conversion of 97% for the experiment at 30 ºC with a feeding time of 180 min. In the experiments with a feeding time of 60 min, the instantaneous conversions were lower during the feeding period, likely due to monomer accumulation, but high final conversions of ~97% were obtained at the end of the process. It is concluded that the redox initiator system (APS/FF6) was feasible for temperatures as low as 20 ºC. For comparison

purposes a polymerization without MDO was also carried out at 30 ºC and 180 min of BA monomer feeding time.

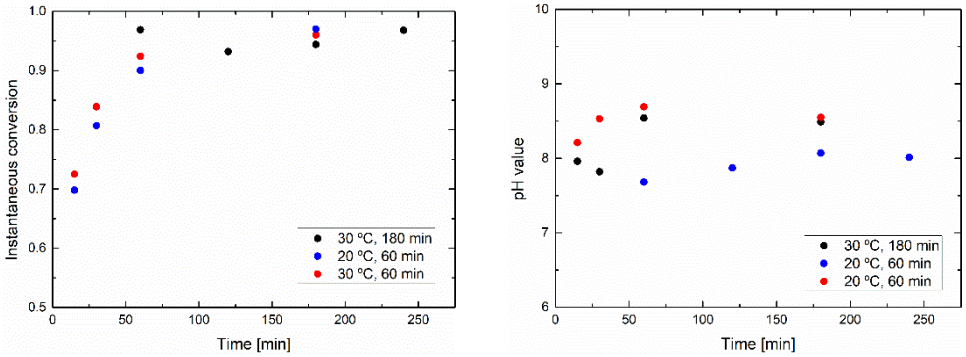

Figure 6.4. Evolution of instantaneous conversions **(a)** and pH value **(b)** for the seeded semibatch emulsion copolymerizations of MDO and BA with feeding times of 180 min and 60 min.

The pH value was adjusted by the addition of ammonia to the latex (a part of it was added initially and another part was fed in the aqueous solution) and the evolution of the pH value over the reaction time measured by a pH-meter is plotted in Figure 6.4 (b). The pH in all of the measured samples was in between 7.7 – 8.7.

Particle size distributions of the latices were measured by a disc centrifuge. Average particles sizes and final conversions for all of the carried out experiments are listed in Table 6.5. Knowing the initial size and amount of the seed of 65 nm and the amount of monomer fed to the reactor, it is possible to calculate the theoretical particle diameter, which is 150 nm. The obtained particle sizes are below this value with average values in the range of 120-135 nm. This deviation might be due to secondary nucleation happening during the feeding period.

Table 6.5. Reaction temperature, feeding time, final conversion, average particle for the carried out seeded semibatch polymerizations between acrylates and MDO.

Co-monomer ratio	T [ºC]	Feeding time [min]	Conversion [%]	d_p [nm]
BA/MDO 95/5	30	180	97	123
BA/MDO 95/5	30	60	97	121
BA/MDO 95/5	20	60	96	132
BA/MDO 95/5	40	60	98	126
BA/MDO 95/5	50	60	98	134
BA/MDO 90/10	30	60	95	116
BA/2OA 95/5	40	180	94	160

^{13}C-NMR measurements were used to investigate if the MDO was incorporated into the copolymer. An example for the ^{13}C-NMR spectra is shown in Figure 6.6.

As it can be seen in Figure 6.6, peaks 1-6 indicate the generation of the hydrolysis product 4-HBA and peaks a-f belong to the BA units of the polymer. Additionally, the fact that the ratio of the intensities between peak 1,4 and 5 is 1:1:1 is indicating that there are no ring-opened MDO units present in the co-polymer. Peak 1 exists only in the hydrolysis product, whereas, peak 4 and 5 would also correspond to the ring-opened ester units within the co-polymer. The appearance of peaks x and y in the two spectra for the experiments in which MDO was used, indicates the incorporation of MDO into the copolymer in a ring retained form, this possible way of MDO incorporation is shown in the introduction of this chapter (see Scheme 6.1).

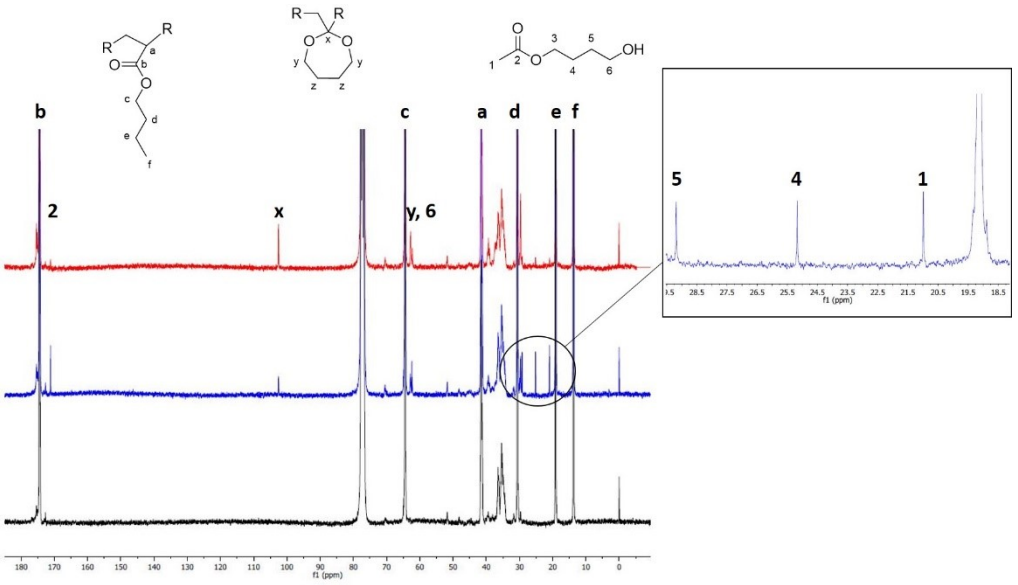

Figure 6.6. ^{13}C-NMR spectra of the dried polymers from the seeded semibatch emulsion copolymerization of MDO and BA. The polymerization of 100% BA at 30 ºC with a feeding time of 180 min (black spectrum), the polymerization of 95 wt% BA and 5 wt% MDO at 30 ºC with a feeding time of 180 min (blue spectrum) and polymerization of 95 wt% BA and 5 wt% MDO at 20 ºC with a feeding time of 60 min (red spectrum).

Therefore, the MDO is present in the BA/MDO co-polymer as acetal units and not as ester units. The four different pathways, which MDO can undergo in the copolymerization with the monomer *n*BA as an example are shown in Scheme 6.3. Pathway (a) shows the hydrolysis of MDO to 4-HBA. In all the other cases a radical is added to the MDO monomer at first, generating a MDO radical. The radical then has the possibility to undergo ring opening to form an ester group in the main chain of the active radical (b). According to the ^{13}C-NMR data discussed previously, there were no ring-opened MDO units present in the co-polymer. Therefore, MDO did not undergo

pathway (a) in the carried out polymerizations. In the other two possibilities, the MDO radical is not able to open before another vinyl group, in this case either of another MDO molecule (c) or a molecule of the co-monomer (BA), (d) is added to it. This polymeric backbone is the one called ring retention.

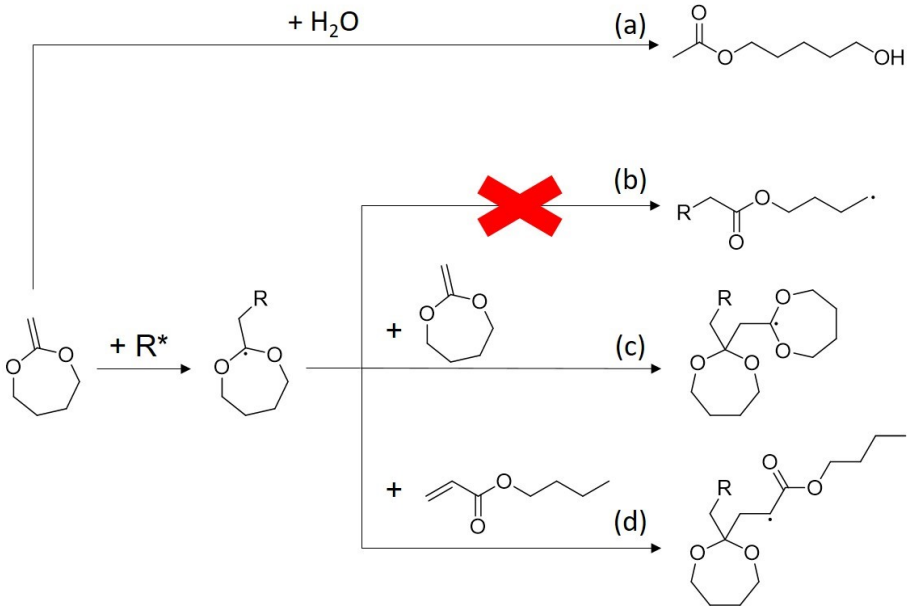

Scheme 6.3. Possible pathways which MDO can undergo in the co-polymerization with *n*BA.

As discussed in the introduction, the ratio of ring opening to ring retention of the MDO radical depends on different parameters. Having this in mind, the temperature of the emulsion polymerizations was varied from 20-50 ºC, the feeding time was changed and different acrylates (*n*BA and 2OA) were used.

There was no evidence that MDO has been incorporated into the copolymer as ring-opened ester units. Hence, MDO has either undergone hydrolysis to the hydrolysis product 4-HBA or has been incorporated into the co-polymer as ring-retained acetal units. The amount of hydrolysis and incorporation as acetal units are shown in Table 6.6.

Table 6.6. Amount of MDO incorporated into the co-polymer as acetal unit and amount hydrolysed to 4-HBA determined by ^{13}C-NMR.

Co-monomer ratio	T [ºC]	Feeding time [min]	Acetal units [mol%]	4-HBA [mol%]
BA/MDO 95/5	30	180	26	74
BA/MDO 95/5	30	60	76	24
BA/MDO 95/5	20	60	86	14
BA/MDO 95/5	40	60	16	84
BA/MDO 95/5	50	60	8	92
BA/MDO 90/10	30	60	56	44
BA/2OA 95/5	40	180	0	100

The NMR spectra showed, that MDO was either incorporated in the ring retained form as an acetal unit or did hydrolyze. Furthermore, the addition of the monomer in a shorter feeding time seemed to increase the incorporation ratio in relation to hydrolysis. Additionally temperature showed an effect, for the lower temperatures higher incorporation rates of up to 86% of the used MDO (for the experiment carried out at 20 ºC) were observed. On the other side, at higher temperatures such as 40 ºC (16% of MDO incorporated) and 50 ºC (8% of MDO incorporated) the incorporation rate of MDO decreased, so that most of it hydrolyzed. The experiment with the

co-monomers MDO and 2OA was carried out to study the effect of using larger acrylates. However, it seems that the MDO completely hydrolyzed in this experiment and there is no evidence for MDO incorporated into the polymer.

In addition to the so far studied effects of temperature and nature of the acrylate, also the kind of co-monomer has an influence on the ratio of ring opening to ring retention. MDO is reported to undergo 100% ring opening in its homopolymerization at all of the investigated temperatures (50-120 ºC).[12] Hence, the usage of acrylates as co-monomer might be responsible for the ring retention of the MDO radical, due to their fast polymerization rates, which might cause the addition of an acrylate monomer to the MDO radical before it is able to rearrange to its ring opened form. For the copolymerization of MDO with VAc as co-monomer, it seems to undergo quantitative ring opening.[7] Therefore, the following experiments were carried out with the vinyl esters Veova 10 or Veova EH as co-monomers (Scheme 6.4).

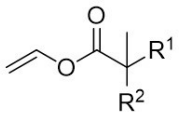

$R^1 + R^2$ = 7 carbon atoms

Veova 10

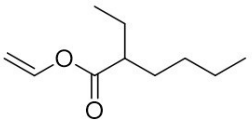

vinyl 2-ethylhexanoate (Veova EH)

Scheme 6.4. Structures of Veova 10 and Veova EH.

Experiments were carried out following the same procedure as the seeded semibatch emulsion polymerizations described above.

The temperature was set to 40 ºC as it was described by Carter et al.[7] for the semibatch emulsion polymerization of the vinyl ester VAc with MDO. The feeding of monomer was carried out within

180 min of feeding time. Final conversions and particle sizes for the experiments carried out are shown in Table 6.7.

Table 6.7. Conversions and particle sizes measured for the co-polymerization of MDO with the vinyl esters Veova 10 and Veova EH.

Co-monomer ratio	Conversion [%]	d_p [nm]
Veova 10/MDO 95/5	72	182
Veova EH/MDO 95/5	89	173

The dried polymers were analysed by ^{13}C-NMR measurements to investigate if MDO was incorporated into the polymer. For the polymer of Veova 10 and MDO it was not possible to find peaks belonging to MDO. Furthermore, high amounts of unreacted Veova 10 were visible, a conversion of 72% was calculated for the copolymerization of Veova 10 and MDO. It was visible by the jacket and reactor temperature that the reaction was not running smooth. Therefore, for the following experiments a third feeding stream to feed the APS over the feeding time (instead of addition as a shot before feeding of the monomer was started) was added.

The ^{13}C-NMR spectrum and the assignment of its carbon atoms for the dried polymer of the seeded semibatch emulsion polymerization of Veova EH and MDO is shown in Figure 6.5.

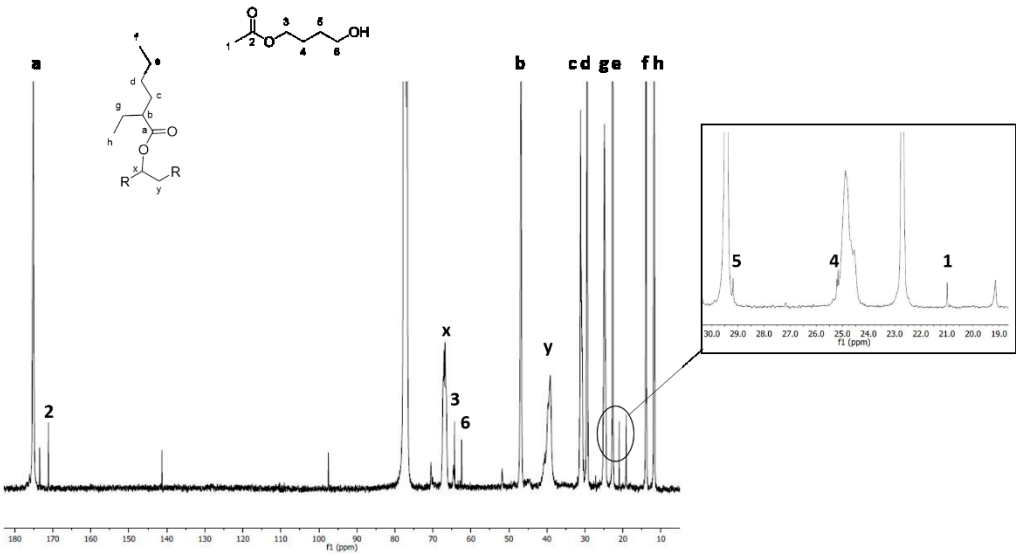

Figure 6.5. ^{13}C-NMR spectrum of the dried polymer from the seeded semibatch emulsion polymerization of Veova EH and MDO.

The two peaks at 141 and 98 ppm correspond to the vinyl carbons of unreacted Veova EH and the peak at 19 ppm belongs to BA, most likely from the used seed (Acronal A508). The peak at 173.5 ppm could belong to the carbonyl carbon atom of MDO that has been incorporated to the polymer by ring opening, however this could not be completely clarified. Furthermore, peaks belonging to the hydrolysis product 4-HBA and the Veova EH polymer could be identified. The ^{1}H-NMR spectrum also shows the sharp peaks (3 and 6) of the hydrolysis product 4-HBA (Figure 6.6).

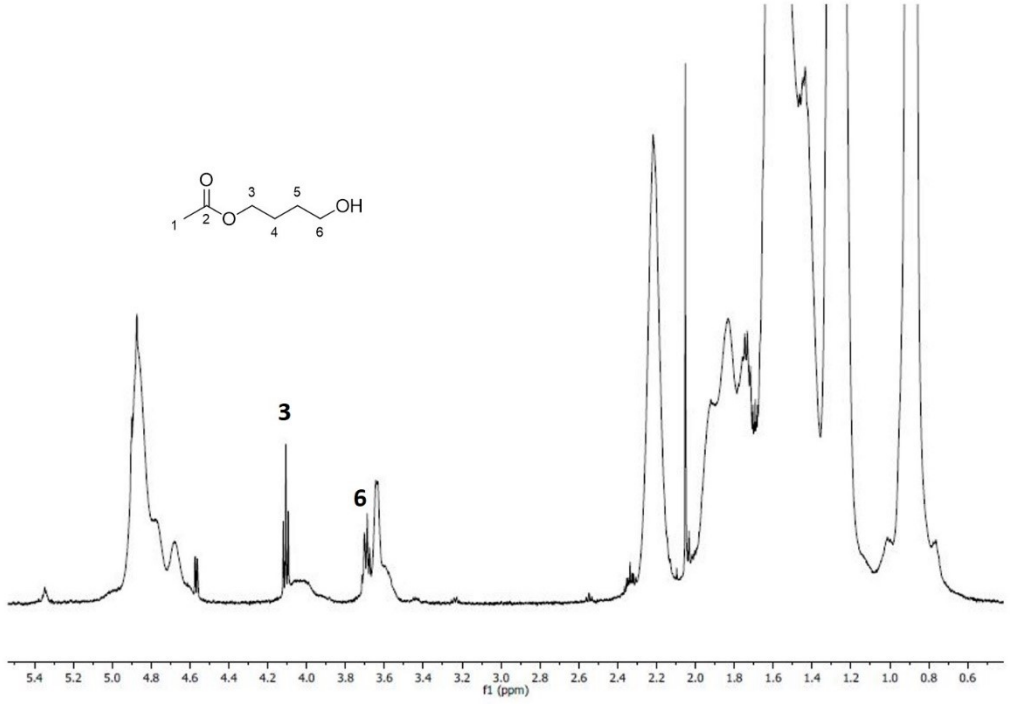

Figure 6.6. ^{1}H-NMR spectrum of the dried polymer synthesized by seeded semibatch emulsion polymerization of Veova EH and MDO.

No clear evidence for the incorporation of MDO into copolymers with Veova 10 or Veova EH as ring opened units was observed. However, the absence of a signal at 100 ppm leads to the conclusion that no MDO has been incorporated into the polymer as ring retained acetal units. Most likely the MDO did hydrolyze to 4-HBA before it was able to polymerize.

6.4. Conclusion

This chapter addresses the copolymerization of MDO in dispersions with the aim to produce a waterborne polymer with ester groups in its main chain, which should therefore be degradable. Different strategies have been pursued. In the first trials the co-polymerizations of MDO with VAc in emulsion and miniemulsion polymerizations at relatively high temperatures and neutral pH yielded VAc homo-polymers and complete hydrolysis of MDO. Pre-polymerizing MDO together with VAc or LMA up to low overall conversions in bulk and miniemulsification of this organic phase with an aqueous solution containing surfactant and subsequent polymerization also yielded homo-polymers of VAc or LMA and hydrolyzed MDO.

Studying the hydrolysis of MDO in water clarified the importance of the conditions for the polymerization of MDO in waterborne systems. Slightly basic pH values of around 8 and low temperatures of 30 ºC were found to be the best conditions in order to slow down the hydrolysis of MDO. Employing these conditions in a seeded semibatch emulsion polymerization of MDO with acrylates enabled the incorporation of up to 85% of the fed MDO into the copolymer. However, the polymerized MDO got exclusively incorporated following the ring retention pathway, leading to acetal units in the backbone which are not degradable. The low temperatures, which are crucial to extend the lifetime of MDO in the water-phase, promote on the other hand ring retention over ring opening of MDO. The seeded semibatch emulsion polymerization of MDO with the vinyl esters Veova 10 and Veova EH did not show a clear evidence that MDO got incorporated into the main chain of the polymer. Further studies are necessary to find a way to incorporate MDO into waterborne co-polymers synthesized by

emulsion polymerization. Likely, other co-monomers with appropriate reactivity ratios should be investigated and chemistries to avoid the hydrolysis of MDO should be discovered.

6.5. References

(1) Kresge, A. J.; Straub, T. S. Kinetics of Hydrolysis of Some Sterically Hindered Ketene Acetals. *J. Am. Chem Soc.* **1983**, *105*, 3957–3961.

(2) Undin, J.; Plikk, P.; Finne-wistrand, A.; Albertsson, A. Synthesis of Amorphous Aliphatic Polyester-Ether Homo- and Copolymers by Radical Polymerization of Ketene Acetals. *J. Polym. Sci., Part A Polym. Chem.* **2010**, *48*, 4965–4973. https://doi.org/10.1002/POLA.

(3) Lena, J.; Jackson, A. W.; Chennamaneni, L. R.; Wong, C. T.; Lim, F.; Andriani, Y.; Thoniyot, P.; Herk, A. M. Van. Degradable Poly(Alkyl Acrylates) with Uniform Insertion of Ester Bonds, Comparing Batch and Semibatch Copolymerizations. *Macromolecules* **2020**, *53* (10), 3994–4011. https://doi.org/10.1021/acs.macromol.0c00207.

(4) Siebert, J. M.; Baumann, D.; Zeller, A.; Mailänder, V.; Landfester, K. Synthesis of Polyester Nanoparticles in Miniemulsion Obtained by Radical Ring-Opening of BMDO and Their Potential as Biodegradable Drug Carriers. *Macromol. Biosci.* **2012**, *12* (2), 165–175. https://doi.org/10.1002/mabi.201100236.

(5) Delplace, V.; Nicolas, J. Degradable Vinyl Polymers for Biomedical Applications. *Nat. Chemiistry* **2015**, *7*, 771–784. https://doi.org/10.1038/NCHEM.2343.

(6) Häußler, M.; Eck, M.; Rothauer, D.; Mecking, S. Closed-Loop Recycling of Polyethylene-like Materials. *Nature* **2021**, *590*, 423–427. https://doi.org/10.1038/s41586-020-03149-9.

(7) Carter, M. C. D.; Hejl, A.; Wood, S.; Einsla, B.; Janco, M.; Defelippis, J.; Cooper, R. J.; Even, R. C. Backbone-Degradable Vinyl Acetate Latex: Coatings for Single-Use Paper Products. *ACS Macro Lett.* **2021**, *10*, 591–597. https://doi.org/10.1021/acsmacrolett.1c00172.

(8) Bingham, N. M.; Roth, P. J. Degradable Vinyl Copolymers through Thiocarbonyl Addition-Ring-Opening (TARO) Polymerization. *Chem. Commun.* **2019**, *55* (1), 55–58. https://doi.org/10.1039/c8cc08287a.

(9) Smith, R. A.; Fu, G.; McAteer, O.; Xu, M.; Gutekunst, W. R. Radical Approach to Thioester-Containing Polymers. *J. Am. Chem Soc.* **2019**, *141*, 1446–1451.

(10) Galanopoulo, P.; Gil, N.; Gigmes, D.; Guillaneuf, Y.; Lages, M.; Nicolas, J.; Lansalot, M.; Agosto, F. D. One-Step Synthesis of Degradable Vinylic Polymer-Based Latexes via Aqueos Radical Emulsion Polymerization. *Angew. Chem. Int. Ed.* **2022**.

https://doi.org/10.1002/anie.202117498.

(11) Kohut-Svelko, N.; Pirri, R.; Asua, J. M.; Leiza, J. R. Redox Initiator Systems for Emulsion Polymerization of Acrylates. *J. Polym. Sci. Part A Polym. Chem.* **2009**, 2917–2927. https://doi.org/10.1002/pola.

(12) Tardy, A.; Gil, N.; Plummer, C. M.; Siri, D.; Gigmes, D.; Lefay, C.; Guillaneuf, Y. Polyesters by a Radical Pathway: Rationalization of the Cyclic Ketene Acetal Efficiency. *Angew. Chemie Int. Ed.* **2020**. https://doi.org/10.1002/anie.202005114.

Chapter 7. Conclusion and future perspectives

7.1. Conclusion

The main objective of this thesis was to develop waterborne degradable nanoparticles through the usage of ester groups. Therefore, three different approaches have been followed (Figure 7.1). The first approach was the synthesis of acrylated oligoesters (macromonomers) by ring opening polymerization and their polymerization in dispersed systems, leading to waterborne polymers with degradable side-chain. The second approach included the synthesis of diacrylated oligoester crosslinkers from macromonomers and their incorporation into a waterborne PSA formulation, leading to polymers with degradable crosslinking points. Two possibilities for the realization of the approach of a degradable polymer backbone were explored. On one hand the thiol-ene polymerization of ester groups containing dienes or/and dithiols and on the other hand the radical ring opening polymerization of the cyclic ketene acetal MDO.

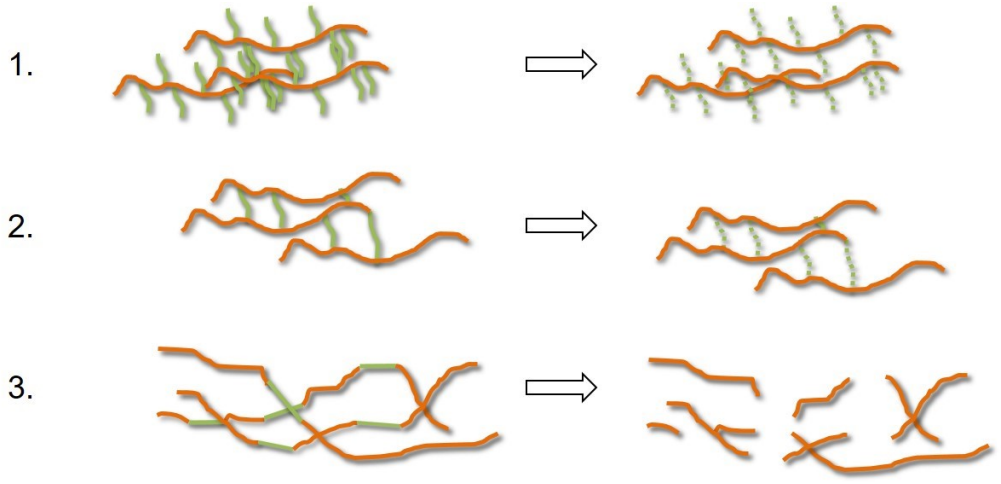

Figure 7.1. Different approaches for the incorporation of ester groups into waterborne polymers. Leading to degradable side-chains (1.), degradable crosslinking (2.) and a degradable polymer backbone (3.).

Macromonomers of different length and composition were synthesized from the monomers lactide or/and ε-caprolactone. Preliminary experiments to obtain particles of these macromonomers were carried out using acrylated polyethylene glycols as stabilizer. Solvent-borne co-polymers of macromonomers and acrylated polyethylene glycols showed that over all degradation rate seemed to be dependent of the polymer composition, making this approach useful in medical chemistry, especially in the field of drug delivery.

Asymmetric and symmetric crosslinkers of different length were synthesized by ring opening polymerization, of macromonomers and itaconic anhydride. These oligoester crosslinkers and allyl methacrylate, as a reference, were used to synthesize waterborne PSAs close to formulations used in industry by seeded semibatch emulsion polymerization of nBA, MMA and AA. Soxhlet (gel content) and AF4/MALS/RI (molar mass distributions) measurements showed

that the oligoester crosslinkers were less effective compared to allyl methacrylate. However, by the usage of these crosslinkers and chain transfer agent it was possible to tune the adhesive properties and comparable performance to common waterborne PSAs was reached. Probe tack measurements after immersion into basic potassium hydroxide solution showed that the PSA properties were lost in timeframes as short as 30 minutes, depending on the length of the used oligoester crosslinkers (See Figure 7.2). The longest crosslinkers showed a faster degradation compared to the shorter ones. All in all the longest asymmetric crosslinker showed the best balance between PSA properties and fast degradation rate. As a proof of concept, paper labels were attached to glass bottles by films made out of the PSA with the longest asymmetric oligoester crosslinker. After immersion into potassium hydroxide solution, with a comparable pH to that of the washing solutions for glass bottles, the label and PSA film could be removed easily from the glass bottle (Figure 7.2).

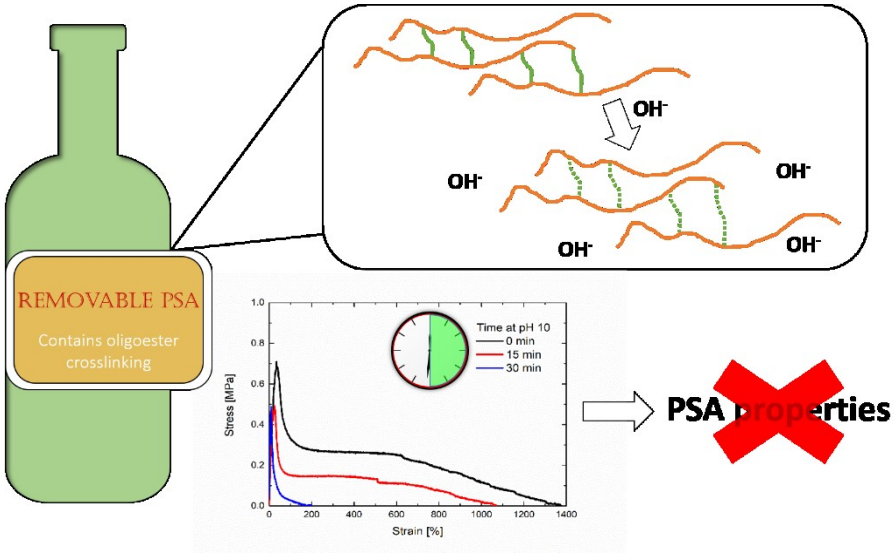

Figure 7.2. Schematic depiction of the approach of degradable crosslinks in waterborne PSAs and loss of adhesive properties over inmersion of the PSA film in basic aqueous media.

The approach of a degradable polymer backbone was divided into two different strategies. The first one was thiol-ene polymerization of ester containing dienes or/and dithiols. Thiol-ene polymerization, being a radical step-growth polymerization, it is challenging to obtain high molecular weights. Therefore, a mathematical model was developed to improve the understanding of the kinetics of the thermally initiated thiol-ene polymerization. The fitting was compared to kinetics and microstructural characteristics of the thiol-ene polymerization measured by *in situ* ^{1}H-NMR, MALDI-TOF and SEC/MALS/RI (Figure 7.3). The time evolution of the ene conversions achieved for different initiator concentrations was reasonable well fitted by the model using three estimated rate coefficients; together with parameters from the literature.

The molar masses predicted by the model are slightly smaller than those measured experimentally likely because side reactions leading to branched chains were not considered (e.g. termination between carbon centred radicals and carbon centred radicals and thiyl radicals). The model predicts that three polymeric species (Paa, Pab and Pbb) account for 99% of the polymer produced in the polymerizations. Experimentally these three species account for up to 90% of the polymer.

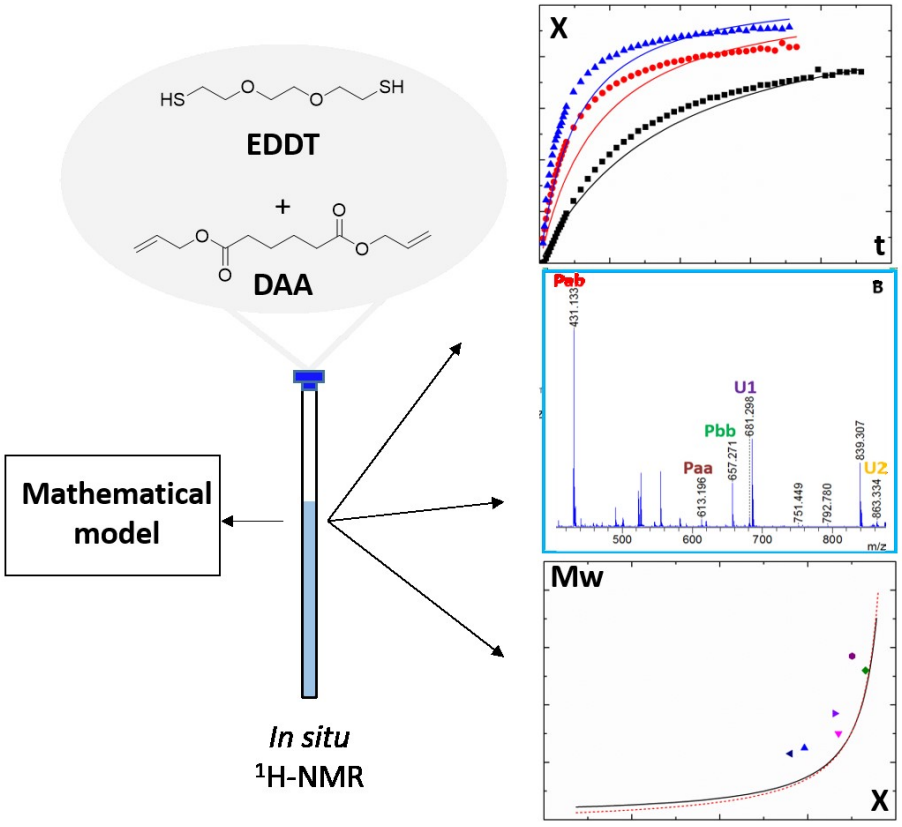

Figure 7.3. *In situ* ^{1}H-NMR thiol-ene polymerization of the dithiol EDDT and the diene DAA were fitted by data generated by the developed mathematical model.

Different (mini)emulsion polymerization methods to produce waterborne thiol-ene polymers with ester groups in the polymer backbone were tried. The best results were obtained for a semibatch emulsion polymerization process, in which the thiol and the diene component were fed in separated feeding streams. The evolution of particle sizes was better controlled and more narrow compared to a batch process. Depending on the used diene, different properties of the polymer

were observed. The diene DAP led to a polymer showing PSA properties. Changing the diene to DATP, stiff and relatively brittle polymers with crystalline domains were obtained. However, preliminary degradation studies did not show a decrease in molecular weight after immersion into a basic aqueous solution. Therefore, further experiments would be necessary to evaluate the degradability of thiol-ene polymers obtained by this process.

The second strategy to produce a waterborne polymer with ester groups in the polymer backbone was the radical ring opening polymerization of the cyclic ketene acetal MDO. As a first step, the reactivity ratios of MDO with three different sets of co-monomers were determined. Vinyl acetate, 2-octyl acrylate and lauryl methacrylate were used as co-monomers (Figure 7.4).

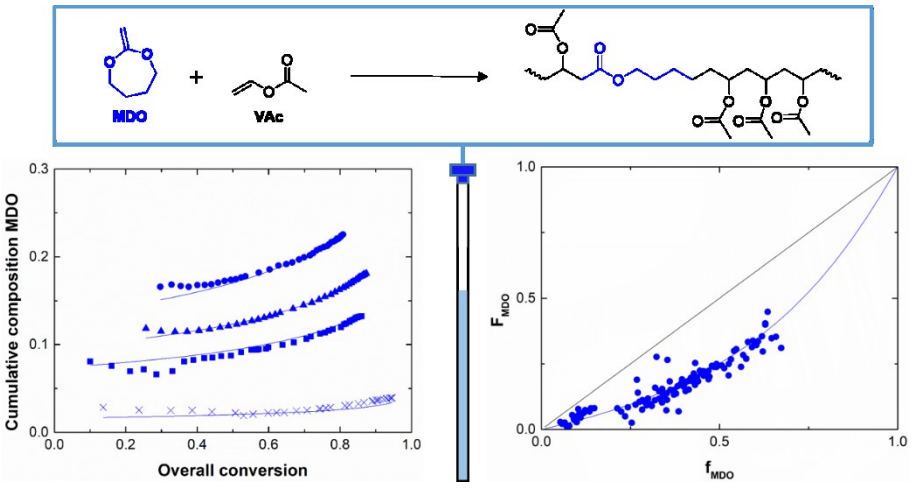

Figure 7.4. Determination of reactivity ratios of co-polymerizations of MDO with different co-monomers (e. g. vinyl acetate in this figure) by *in situ* ^{1}H-NMR solution polymerization.

The most favourable reactivity ratios were calculated for the co-polymerization of MDO with vinyl acetate and the co-polymerization of MDO with 2-octyl acrylate.

However, the incorporation of MDO into waterborne systems is challenging due to its high water-sensitivity (or to any protic reagent, which reacts opening the ring and yielding the hydroxybutirate alcohol). Therefore, the hydrolysis reaction of MDO in water was carefully studied under different conditions. It was concluded that a slighlty basic pH of 8 and a low temperature of 30 ºC are the best conditions to slow down the rate of the hydrolisis of MDO. Under these conditions, it was possible to incorporate MDO into co-polymers by seeded semibatch emulsion polymerization of MDO and butyl acrylate. However, MDO got exclusively incorporated into the co-polymer by ring retention. Thus, no ester groups have been incorporated into the co-polymer backbone by this approach.

These three different approaches have been explored up to different levels of depth. The approach of degradable crosslinking was developed the furthest, targeted to a specific application as degradable PSAs for the labels for glass bottles. The other approaches require further research, this is described in the following section.

7.2. Future perspectives

Three different approaches to incorporate ester groups into waterborne polymers with the aim to make them degradable have been elaborated in this work. Different levels of extend of progress were reached for each approach.

For the approach of degradable sidechains, only preliminary works were carried out. Further studies to observe the degradation of the polymer sidechains depending on macromonomer length and composition as well as studying the incorporation and release of a drug are necessary to link this approach to the application field of drug delivery.

Another approach was using thiol-ene polymerization, to incorporate ester groups in the backbone of the waterborne polymer. The model that was developed to describe the kinetics of thiol-ene polymerization can only correctly track linear species. Developing a model, which can also track branched species, which can be formed in thiol-ene polymerization due to side reactions, perhaps by Monte Carlo simulation would be interesting. Additionally, the by semibatch emulsion polymerization produced polymers require further studies of their nucleation and degradation behaviour. The effects of different diene and dithiol monomers should be studied therefore.

The emulsion co-polymerization of the cyclic ketene acetal MDO did not yield ester containing units in the polymer backbone. Other monomers with more favourable reactivity ratios might be a possibility to overcome this issue. Furthermore, the biphenylic cyclic thionolactone

dibenzo[c,e]oxepane-5-thione (DOT) was reported by D'Agosto et al. to be used in emulsion polymerization to synthesize degradable vinylic polymers (Scheme 7.1)[1].

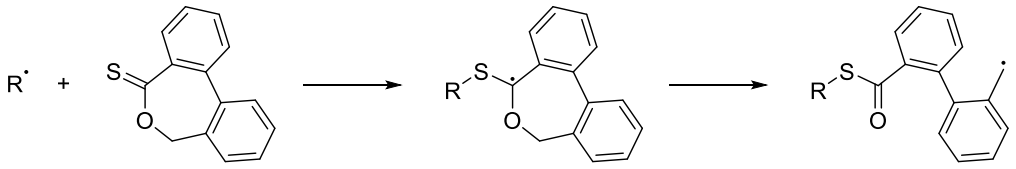

Scheme 7.1. Radical ring opening mechanism of DOT.[1]

DOT is compared to MDO reported to be less likely to undergo hydrolysis and to be incorporated into polymers exclusively in the ring-opened way. This monomer is an interesting starting point to solve the problems which were experienced with MDO within this work.

7.3. References

(1) Galanopoulo, P.; Gil, N.; Gigmes, D.; Guillaneuf, Y.; Lages, M.; Nicolas, J.; Lansalot, M.; Agosto, F. D. One-Step Synthesis of Degradable Vinylic Polymer-Based Latexes via Aqueos Radical Emulsion Polymerization. *Angew. Chem. Int. Ed.* **2022**. https://doi.org/10.1002/anie.202117498.

Resumen y conclusiones

El objetivo principal de esta tesis ha sido sintetitzar nanopartículas polímericas en fase acuosa que fueran degradables mediante el uso de grupos éster. Para ello, se han seguido tres enfoques diferentes. El primero consistió en la síntesis de oligoésteres acrílicos (macromonómeros) mediante polimerización de apertura de anillo y su polimerización en sistemas dispersos, dando lugar a polímeros de base acuosa con cadena lateral degradable. El segundo enfoque incluía la síntesis de oligoésteres diacrílicos a partir de los macromonómeros y su incorporación a una formulación de adhesivos sensibles a la presión (PSA) de base acuosa, dando lugar a polímeros con puntos de reticulación degradables. Por último, se exploraron dos posibilidades para la realización del planteamiento de obtener la degradabilidad en la cadena polimérica principal. Por un lado, la polimerización tiol-eno de grupos de ésteres que contienen dienos o/y ditioles y, por otro lado, la polimerización radical de apertura de anillo del acetal ceteno cíclico MDO.

Para conseguir degradabilidad en las cadenas laterales, se sintetizaron macromonómeros de diferente longitud y composición a partir de los monómeros lactida y/o ε-caprolactona. Se llevaron a cabo experimentos preliminares para obtener partículas de estos macromonómeros utilizando polietilenglicoles acrilados como estabilizantes. Los copolímeros de

macromonómeros y de polietilenglicoles acrilados, que se obtienen con disolventes, mostraron que la tasa de degradación global parece depender de la composición del polímero, lo que hace que este enfoque sea útil en aplicaciones médicas, especialmente en el campo de la administración de fármacos.

Por otro lado, se sintetizaron macromonómeros difuncionales asimétricos y simétricos de diferente longitud mediante la polimerización de apertura de anillo de la lactida y ε-caprolactona. Estos oligoésteres tiene capacidad de reticulación puesto que tienen dos grupos acrílicos y junto con el metacrilato de aliloque se usó como agente reticulante de referencia, se sintetizaron PSAs de base acuosa cercanos a las formulaciones utilizadas en la industria mediante la polimerización en emulsión de nBA, MMA y AA. Estas polimerizaciones se sintetizaron de forma semi-continua. Los resultados obtenidos mediante Soxhlet (contenido de gel) y AF4/MALS/RI (distribuciones de masa molar) mostraron que los agentes reticulantes oligoésteres eran menos eficaces en comparación con el metacrilato de alilo. Sin embargo, mediante el uso de estos reticulantes y el agente de transferencia de cadena fue posible ajustar las propiedades adhesivas y se alcanzó un rendimiento comparable al de los PSAs comunes en base agua. Se formaron películas de los adhesivos en sustartos de vidrio y se estudió la evolución de las propiedades adhesivas sumergiendo las películas en soluciones acuosas básicas. Los diacrilatos reticuladores más largos mostraron una degradación más rápida en comparación con los más cortos. En general, el reticulador asimétrico más largo mostró el mejor equilibrio entre las propiedades de PSA y la velocidad de degradación. Como prueba de concepto, se adhirieron etiquetas de papel a botellas de vidrio con películas hechas de PSA con el reticulante oligoéster asimétrico más largo. Tras la inmersión en una solución de hidróxido de potasio, con un pH

comparable al de las soluciones que se usan durante el lavado de las botellas de vidrio en la industria, la etiqueta y la película de PSA pudieron retirarse fácilmente de la botella de vidrio.

En la última estrategia para producir nanopartículas degradables, se querían introducir los grupos ésteres en la cadena polimérica principal se utilizaron dos vías diferentes. La primera fue la polimerización tiol-eno de dienos que contienen ésteres y/o ditioles. La polimerización tiol-eno, al ser una polimerización radical por etapas, supone un reto a la hora de obtener altos pesos moleculares. Por lo tanto, se desarrolló un modelo matemático para mejorar la comprensión de la cinética de la polimerización de tiol-eno iniciada térmicamente. El ajuste se comparó con la cinética y las características microestructurales de la polimerización del tiol-eno medidas por *in situ* ^{1}H-NMR, MALDI-TOF y SEC/MALS/RI. La evolución temporal de las conversiones de los grupos vinílicos alcanzadas para diferentes concentraciones de iniciador fue razonablemente bien ajustada por el modelo estimando tres coeficientes de velocidad; junto con parámetros que se obtuvieron de la literatura. Las masas molares predichas por el modelo son ligeramente menores que las medidas experimentalmente, probablemente porque no se consideraron las reacciones laterales que producen a cadenas ramificadas (por ejemplo, la terminación entre radicales centrados en el carbono y radicales centrados en el carbono y radicales tiilo). El modelo predice que tres especies poliméricas (Paa, Pab y Pbb) representan el 99% del polímero producido en las polimerizaciones. Experimentalmente, estas tres especies representan hasta el 90% del polímero.

Se probaron diferentes métodos de polimerización tanto en miniemulsión como en emulsión para producir polímeros de tiol-eno en base agua para introducir grupos éster en la cadena principal polimérica. Los mejores resultados se obtuvieron con un proceso semicontinuo de polimerización en emulsión , en el que el tiol y el componente de dieno se alimentaron en flujos separados. La evolución del tamaño de las partículas se pudo controlar mejor y fue más homogenea. Dependiendo del dieno utilizado, se observaron diferentes propiedades del polímero. El dieno DAP dio lugar a un polímero con propiedades de PSA. Cambiando el dieno a DATP, se obtuvieron polímeros rígidos y relativamente frágiles con dominios cristalinos. Sin embargo, los estudios preliminares de degradación no mostraron una disminución del peso molecular tras la inmersión en una solución acuosa básica. Por lo tanto, serían necesarios más experimentos para evaluar la degradabilidad de los polímeros de tiol-eno obtenidos por este proceso.

La segunda estrategia para producir un polímero de base acuosa con grupos éster en la cadena principal fue la polimerización mediante apertura de anillo radical del acetal ceteno cíclico MDO. Como primer paso, se determinaron las relaciones de reactividad del MDO con tres conjuntos diferentes de comonómeros. Se utilizaron como comonómeros el acetato de vinilo, el 2-acrilato de octilo y el metacrilato de laurilo.

Las relaciones de reactividad más favorables se calcularon para la copolimerización de MDO con el acetato de vinilo y la copolimerización de MDO con 2- acrilato de octilo.

Sin embargo, la incorporación del MDO en sistemas acuosos es un reto debido a su alta sensibilidad al agua (o a cualquier reactivo prótico, que reacciona abriendo el anillo y dando

lugar al alcohol hidroxibutírico). Por lo tanto, se estudió cuidadosamente la reacción de hidrólisis del MDO en agua en diferentes condiciones. Se llegó a la conclusión de que un pH ligeramente básico de 8 y una temperatura baja de 30 ºC son las mejores condiciones para frenar la velocidad de hidrólisis del MDO. En estas condiciones, fue posible incorporar MDO a los copolímeros mediante unapolimerización en emulsión semicontinuade MDO y acrilato de butilo. Sin embargo, el MDO se incorporó exclusivamente al copolímero por retención de anillos. Por lo tanto, no se llegaron a incorporar grupos de éster en la columna principal del copolímero mediante este enfoque.

Estos tres enfoques diferentes se han explorado hasta diferentes niveles de profundidad. El enfoque de reticulación degradable fue el que más se desarrolló, dirigido a una aplicación específica como PSA degradable para las etiquetas de las botellas de vidrio.

List of publications and conference presentations

Parts of this Thesis have been published. The process to produce easily removable PSAs with degradable crosslinks using oligoester crosslinkers has been presented in a patent application. The list of publications from this work is presented below:

"Method for producing a polymeric composition and polymeric composition thus produced as well as applications thereof, especially as or in pressure-sensitive adhesives" F. Wenzel, M. Aguirre, J. R. Leiza, WO2021058122A1, 2019.

"Incorporation of novel degradable oligoester crosslinkers into waterborne pressure sensitive adhesives: towards removable adhesives" F. Wenzel, A. Agirre, M. Aguirre, J. R. Leiza, *Green Chem*, 2020, *22*, 3272-3282.

"Kinetics of radical ring opening polymerization of the cyclic ketene acetal 2-methylene-1,3-dioxepane with vinyl monomers" F. Wenzel, S. Hamzehlou, L. Pardo, M. Aguirre, J. R. Leiza, *Ind. Eng. Chem. Res.* 2021, 60, 29, 10479-10488.

"Modeling the kinetics and microstructure of a thermally initiated thiol-ene polymerization" F. Wenzel, S. Hamzehlou, E. Gonzalez de San Roman, M. Aguirre, J. R. Leiza, *Macromol. React. Eng.* 2021, *15*, 2100034.

Parts of this work have been presented in international conferences as well as in meetings of the Industrial Liaison Program (ILP) of Polymat.

Oral Presentations

"Synthesis of waterborne degradable polyester nanoparticles" F. Wenzel, M. Aguirre, J. R. Leiza, WPPRE, Prague, Czech Republic, 2018.

"Waterborne nanoparticles by thiol-ene (mini)emulsion polymerization" F. Wenzel, M. Aguirre, J. R. Leiza, WPPRE, Hamburg, Germany, 2019.

"Degradable crosslinking in waterborne pressure-sensitive adhesives" F. Wenzel, M. Aguirre, J. R. Leiza, POLYMAT, 19th Industrial Liaison Program (ILP) Meeting, Donostia-San Sebastian, Spain, 2019.

"Insights into thiol-ene polymerization: kinetics of the radical step-growth polymerization and application in waterborne systems" F. Wenzel, M. Aguirre, J. R. Leiza, POLYMAT, 21st Industrial Liaison Program (ILP) Meeting, Donostia-San Sebastian, Spain, 2021.

Poster presentations

"Waterborne degradable polyester nanoparticles" F. Wenzel, M. Aguirre, J. R. Leiza, PRE X, Punta Cana, Dominican Republic, 2018.

"Waterborne nanoparticles by thiol-ene (mini)emulsion polymerization" F. Wenzel, M. Aguirre, J. R. Leiza, PRE 2019, Hamburg, Germany, 2019.

Appendix

I. General characterization Methods

I.1. Solids content and monomer conversion

Approximately 2mL of the latex were withdrawn from the reactor during the polymerization process, placed in a pre-weighed aluminum pan and immediately thereafter a drop of a 1 wt% hydroquinone solution was added to stop the reaction. The pan was dried until constant weight was achieved. The solids content (SC) was obtained gravimetrically and is given by:

$$SC = \frac{weight\ of\ the\ solid\ dried\ material}{weight\ of\ the\ latex} \qquad (I.1)$$

The instantaneous conversion (X) was determined by the following equation,

$$X(t) = \frac{Polymerized\ Monomer}{Total\ Monomer} = \frac{(SC \cdot Latex) - NPS}{MW} \qquad (I.2)$$

Where, NPS is the non-polymerizable materials (surfactants, costabilizers and initiators) and MW is the amount of monomer plus polymer at each time.

I.2. N_p calculations

Polymer particle sizes were measured by dynamic light scattering (DLS) using a Malvern Zetasizer Nano ZS (laser: 4mw, He-Ne, λ=633 nm, angle 173º). The equipment determines the particle size by measuring the rate of fluctuations in light intensity scattered by particles as they diffuse through a fluid.

Samples were prepared by diluting a fraction of the latex with deionized water. The analyses were carried out at 25 °C and each run consisted in 1 minute of temperature equilibration followed by 2 size measurements per sample.

Results obtained from DLS were used to determine the number of particles (N_p).

$$N_p = \frac{V_p}{V_t} = \frac{6 \cdot (W_{pol}/\rho_{pol}) \cdot X}{\pi \cdot d_p{}^3} \qquad (I.3)$$

N_p was determined following Equation I.4. W_{pol} corresponds to the amount of polymer (g) at each time, and it was calculated from the monomer conversion (*X*). ρ_{polym} refers to the polymer density and d_p to the average particle size.

I.3. Molecular weight

The molecular weight of the soluble fraction (obtained by Soxhlet extraction) was determined by Size Exclusion Chromatography/ Gel Permeation Chromatography (SEC/GPC).

The samples taken out from the Soxhlet were first dried, redisolved in THF to achieve a concentration of about 0.1 % (g/ml) and filtered (polyamide Φ=45 μm) before injection into the SEC instrument. The set up consisted of a pump (LC-20A, Shimadzu), an autosampler (Waters 717), a differential refractometer (Waters 2410) and three columns in series (Styragel HR2, HR4 and HR6, with pore sizes ranging from 10^2 to 10^6 Å). Chromatograms were obtained at 35 ºC using THF flow rate of 1 ml/min. The equipment was calibrated using polystyrene standards (5^{th} order universal calibration) and therefore, the molecular weight was referred to PS.

I.4. Gel content

The gel content by definition is the fraction of polymer that is not soluble in a good common solvent such as tetrahydrofuran (THF). The gel fraction was determined by Soxhlet extraction.

To measure the gel content glass fiber square pads (CEM) were used as backing. A few drops of latex were placed on the filter (filter weight=W_1) and dried under vacuum overnight at room temperature. The filter together with the dried polymer was weighed (W_2) and a continuous extraction with THF under reflux in the Soxhlet for 24 hours was done afterwards (Figure I.1). After this period of time, the wet filter was weighed (W_3) and dried overnight. Finally, the weight of the dry sample was taken (W_4). Gel content was calculated as the ratio between the weight of the insoluble polymer fraction and that of the initial sample, as Equation I.4 shows.

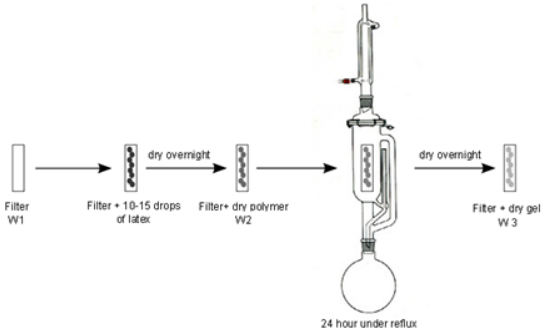

Figure I.1. Scheme of Soxhlet extraction method for gel content measurements.

$$\text{Gel content } (\%) = \frac{W_4 - W_1}{W_2 - W_1} \times 100 \qquad (I.4)$$

I.5. Capillary hydrodynamic fractionation chromatography (CHDF)

To determine the PSD of multimodal latexes, the Capillary Hydrodynamic Fractionation chromatography technique was used (CHDF-2000 from Matec Applied Sciences). It was operating at a flow rate of 1.4 mL/min, at 35 °C and the detector wavelength was set at 200 nm. The carrier fluid was 1/4X-GR500 (Matec). The samples were diluted to 0.6 wt% using the carrier fluid and they were analyzed using Matec software v.2.3.

I.6. Dynamic scanning calorimetry (DSC)

The glass transition temperature (T_g) was determined by differential scanning calorimetry (DSC, Q1000, TA Instruments) of dry polymers from the final latexes using hermetic pans.

I.7. Asymmetric flow field flow fractionation (AF4)

The entire molar mass distributions of the latices were determined by asymmetric-flow field-flow fractionation (AF4, Wyatt Eclipse 3) using a multi-angle light scattering (MALS) and a refractive index (RI) detector and THF as solvent. A pump (LC-20, Shimadzu) coupled to a DAWN Helios multiangle light scattering laser photometer (MALS, Wyatt) equipped with a HE-Ne laser (λ = 658 nm) and an Optilab Rex differential refractometer (λ = 658 nm) (RI, Wyatt Technology). ASTRA 6 software (Wyatt Technology) was used for the data collection and treatment. 10 mg of the latices were dispersed in 1 mL of THF for the preparation of the samples. 50 µL of this solution were injected for the measurement. The Debye plot with second-order Berry formalism was used to calculate the molar mass from the RI/MALS data.

I.8. Dynamic mechanical analysis (DMA)

As for the rheological behaviour of the latices, dynamic mechanical analysis (DMA) was performed with an Anton Paar rheometer using parallel plate geometry. Frequency sweeps (0.3-120 rad s^{-1}) with an applied strain between 0.5% and 2% were made on 500 µm thick samples of 8 mm as diameter at 23 ºC.

I.9. Adhesive properties

The performance of PSAs is characterized by adhesion, required for bonding and debonding, and cohesion necessary against debonding. The character of PSAs is described by the special balance between these two properties. The adhesion of a PSA is described by peel and tack, whereas the cohesion of a PSA is characterised by shear resistance.[1] In this section the basic principles for the characterization of PSAs are explained and a detailed description for the within this work conducted methods to measure PSA properties is provided.

Tests were performed at 23ºC and 50% humidity. Four samples were tested for each formulation and the average values were reported. The peel, loop tack and probe tack tests were performed with a TA.HDPlus Texture Analyzer (Texture Technologies, Hamilton, MA, USA).

I.9.1 Film preparation

Adhesive films were prepared by casting the latex on a flame treated polyethylene terephthalate (PET) sheet (29 µm thick) using a stainless steel film applicator. The film applicator was used with a gap of 120 µm to produce films with a thickness of approximately 60 µm. For the probe tack measurements, films with a final thickness of 100 µm were casted over a glass substrate. In all the cases, films were dried at 23 ºC and 50% humidity for 12 h.

I.9.2 Peel adhesion

In order to achieve peel adhesion the bonding stage must allow some dwell time. In this time the adhesive flows in absence of any externally applied forces to maximize the contact with the substrate. Peel adhesion is one of the most important parameters to evaluate PSA properties.[2] It is the force required to remove a PSA coated flexible material from a substrate under standard conditions (e. g. specific angle and rate). This force can be measured in different geometries. Common tests are carried out with a peeling angle of 90º or 180º. The determination of peel strength at an angle of 90º is advantageous for samples with low flexibility, which would suffer the risk of cracking, breaking or delamination at an angle of 180º.[3] Peel measurements in this work were carried out at an angle of 180º.

The 180º Peel strength test was performed according to ASTM-D3330. PSA tapes with a width of 25 mm were applied to steel plates. Pressure was applied by rolling a 2 kg rubber coated weight 4 times over the steel plate. The applied tapes were left to dwell for 10 min. The tapes were then peeled off at a crosshead speed of 5 mm/sec. The average value of peel strength in N/25mm was obtained for peeling 6 cm of the tape specimens.

I.9.3 Tack tests

Tack is the resistance of an adhesive film to detachment from a substrate. It measures the ability to form an instant bond (no dwell time on the contrary to the peel test) when brought into low pressure contact with a substrate. The American Society for Testing and Materials defines tack

as the force required to separate an adherent and an adhesive at the interface, shortly after they were brought rapidly into contact under a light pressure of short duration (ASTM-1878-6). Tack can be measured quantitatively by a loop tack tester or by contact mechanics such as probe tack tests.[1]

Loop tack

Loop tack defines the force that is required to separate a loop of material at a specific speed from a specific area of a standard surface with which it was brought into contact with for a certain contact time (without applying a significant pressure).[1]

The loop tack test was carried out according to ASTM-D6195. PSA tapes with a length of 100 mm and a width of 25 mm were attached in the shape of a loop with the PSA facing to the outside of the loop to the upper grip of the equipment. The loop was then moved downwards with the speed of 0.100 mm/s until it came into full contact with a stainless steel plate (width 25 mm) in an area of 25 mm x 25 mm. After a contact time of 0.1 s the loop was moved upwards with a speed of 0.055 mm/s. The force required to peel off the loop was measured in N/25mm and the average value was reported.

Probe tack

The probe tack test is a powerful tool to gain information about the debonding mechanism of an adhesive. The parameters influencing the results of the probe tack test are the rheological properties of the adhesive layer and the nature of its interaction with the surfaces of the substrate and the probe.[4] The adhesive performance is characterized by three parameters obtained from

the force-displacement curve: the maximal nominal stress (σ_{max}), the strain at break (ϵ_{max}) and the adhesion energy, which is defined as the area below the stress strain curve from the probe tack experiment (equation I.5).

$$W_{adh} = h_0 \int_0^{\epsilon max} \sigma(\epsilon) \mathrm{d}\epsilon \quad \text{(I.5)}$$

Also, the shape of the stress strain curve provides information of the nature of the adhesive. Four different types of probe tack curves were distinguished for different adhesives (Figure I.1). The first type of these curves is defined by a sharp maximum in stress at relatively low strains and a low total area below the curve (Figure I.1, I), this kind of behaviour is usually related to samples with high glass transition temperatures or/and high crosslinking density or/and high molar mass. The other extreme type is liquid like behaviour as shown in Figure I.1, III. This type of curves is observed for adhesives with a low glass transition temperature or/and low crosslinking density or/and low molar mass. This kind of behaviour is dictated by the viscous flow of the adhesive, leading to a breakage within the adhesive itself, leading to a cohesive failure, which can be observed by residues of the adhesive, which stay at the probe after the breakage. Most adhesives show a behaviour in between these two extremes (Figure I.1, II). In this case, the curves are defined by reaching a sharp peak of the maximum of the stress, followed by a pronounced shoulder and finally reaching zero. In this case, the detachment happens between the probe and the adhesive layer, the so called adhesive failure. For this kind of behaviour the

adhesive completely debonds from the probe so that no macroscopic residues are left over at the probe. This type of curve represents a typical stress-strain curve for a probe tack experiment with an adhesive. Within this curve, it is possible to distinguish between different stages of the debonding mechanism. At first, in the linear elastic domain, the adhesive layer is homogenously deformed, then cavities start to form in the adhesive film, the deformation is becoming non-linear, inhomogeneous and non-reversible. The stress then stabilizes at a lower, nearly constant value, which is caused by the formation (from the walls between the cavities) and elongation of fibrils. The stress reaches zero when the fibrils break.[5]

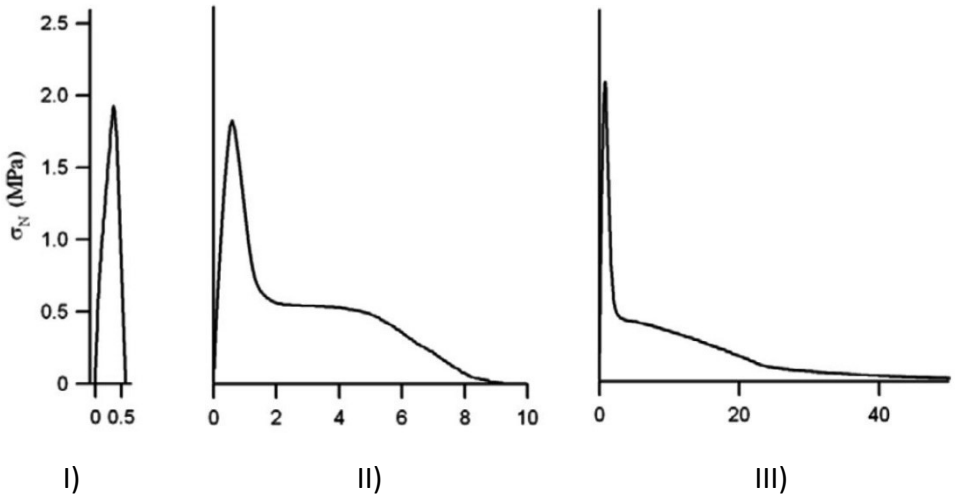

Figure I.1. Different stress-strain curves for the probe tack experiment. I) Brittle failure, II) adhesive debonding with hardening in the case of II b), III) cohesive debonding of a liquid like behaving adhesive.[5]

The probe tack tests were performed on glass plates according to ASTM-D2979. Films were casted from the latices and dried for 12 h before the measurements were carried out. A 1 inch stainless steel ball was moved downwards to the film with a speed of 0.1 mm/s and brought into contact with the PSA film for a contact time of 1 s. Thereafter, the stainless steel ball was moved upwards at a speed of 0.055 mm/s until either a cohesive or adhesive error was observed, so that the probe was completely separated from the PSA film.

Figure I.2 shows probe tack curves for non degradable waterborne PSA with a similar formulation as the PSAs synthesized in this work (Chapter 2), also with the monomers BA/MMA/AA in the same composition as for the PSA synthesized within this work but without using any kind of crosslinker or chain transfer agent. Each of the curves represent a latex following this formulation but different surfactants are used. The sample Dowfax-3 represents a latex using the surfactant Dowfax 2A1 as it is also used within this work.

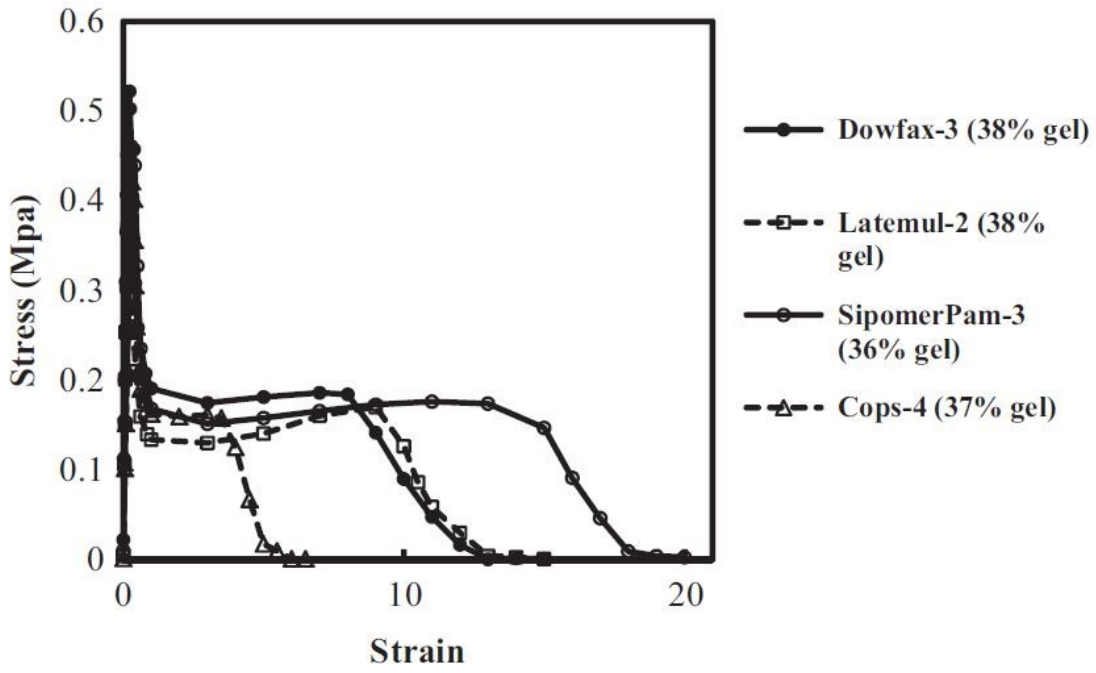

Figure I.2. Stress-strain curves of the probe tack curves obtained for a conventional non degradable waterborne PSA formulations with the monomers BA/MMA/AA. The difference between the curves being the used surfactants. Reprinted from Int. J. Adhes. Adhes. with permission from Elsevier.[6]

I.9.4 Shear and SAFT tests

Shear resistance is measured as a force required to pull the pressure sensitive material parallel to the surface it was attached to with a definite pressure and gives information about the cohesive performance of a PSA. Usually the holding time is measured under standard conditions. The

holding power is basically a viscosity effect. The adhesive should not break under debonding forces (mainly shear and peel forces). This requirement is inverse to Dahlquist's criterion which states that the storage modulus has to be below a certain value for measurable quick tack.[1]

Shear tests were carried out on steel plates using SAFT equipment (Sneep industries) according to ASTM-D3654. PSA tapes were attached within an area of 25 mm x 25 mm of the steel plate. Pressure was applied by rolling 1 kg weight 4 times over the steel plate attached to the PSA tape. The attached PSA tapes were left for 10 min to dwell. A weight of 1 kg was then attached to the PSA tape. The steel plates with the attached tapes were held by a test stand at an angle of 1º relative to the vertical and at a temperature of 23 ºC. The time from the attachment of the weight until the complete separation of the tape from the steel plate is recorded and reported as time of failure, which is an indication for the shear strength of the PSA tapes. The SAFT tests were prepared similarly. The difference being that a temperature ramp from 23 ºC to 200 ºC with a rate of 1 ºC/min was applied as soon as the weight was attached. For this test, the temperature of failure is reported.

II. Additional information for Chapter 2

II.1 Analysis of synthesized oligoester crosslinkers by proton nuclear magnetic resonance spectroscopy (NMR)

Proton NMR was carried out to characterize the synthesized oligoester crosslinkers. The spectrum of one asymmetric oligoester crosslinker (ASY-LA4CL4) is shown in Figure II.1 and the spectrum of one symmetric oligoester crosslinkers is shown in Figure II.2 for each of them the protons of the molecules are assigned to the signals of the spectra.

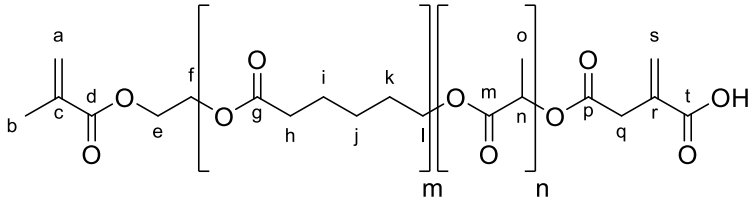

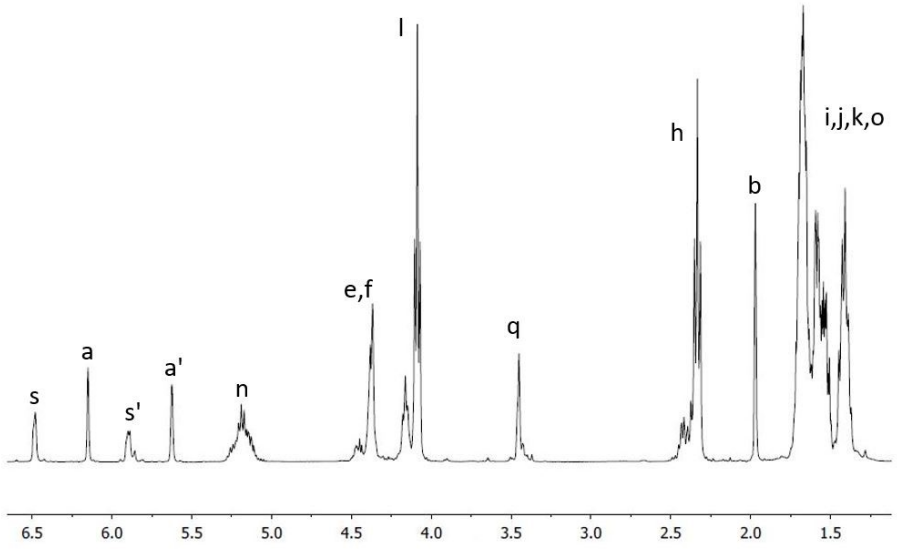

Figure II.1. ^{1}H-NMR spectrum of the synthesized ASY-LA4CL4 oligoester crosslinker with assignment of the signals.

The number of lactic acid (*n*(LA)) and *ε*-caprolactone (*n*(CL)) units for each of the asymmetric oligoester crosslinkers was calculated as shown in equation II.1 and II.2. In which *I*(a) is the integral of proton a, *I*(n) is the integral of proton n and *I*(h) is the integral of proton h.

$$n(\mathrm{LA}) = \frac{I(\mathrm{n})}{I(\mathrm{a})} \qquad \text{(II.1)}$$

$$n(\mathrm{CL}) = \frac{I(\mathrm{h})}{I(\mathrm{a}) \cdot 2} \qquad \text{(II.2)}$$

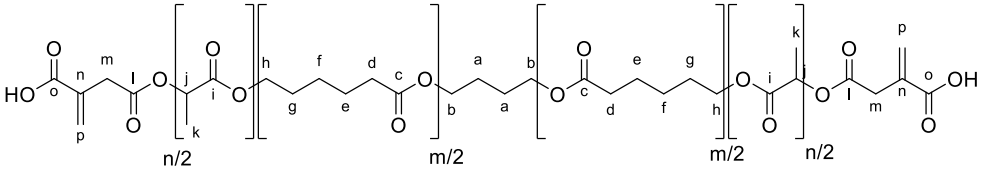

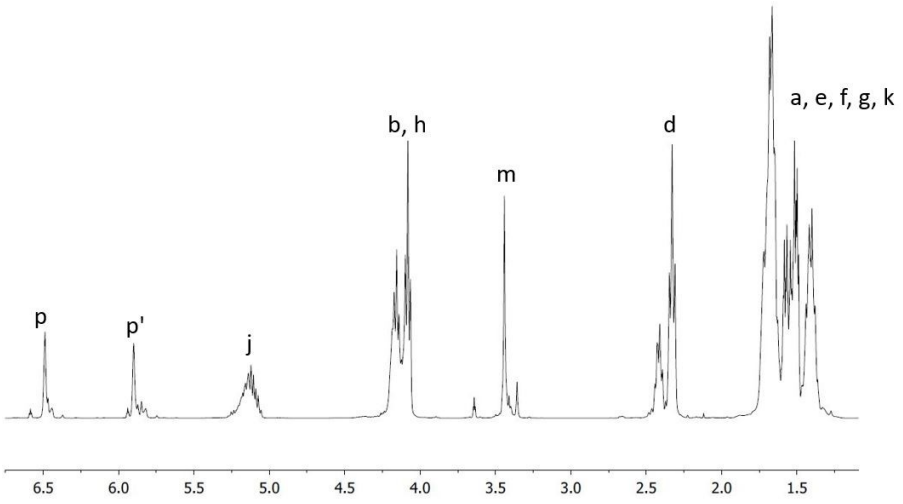

Figure II.2. ^{1}H-NMR spectrum of the synthesized SY-LA6CL6 oligoester crosslinker with assignment of the signals.

The number of lactic acid (*n*(LA)) and ε-caprolactone (*n*(CL)) units for each of the symmetric oligoester crosslinkers was calculated as shown in equation II.3 and II.4. In which *I*(p) is the integral of proton p, *I*(j) is the integral of proton j and *I*(d) is the integral of proton d.

$$n(\mathrm{LA}) = \frac{I(\mathrm{j}) \cdot 2}{I(\mathrm{p})} \quad \text{(II.3)}$$

$$n(\mathrm{CL}) = \frac{I(\mathrm{d})}{I(\mathrm{p})} \quad \text{(II.4)}$$

Following these equations (Equation II.1, II.2, II.3 and II.4) it is possible to calculate the molar masses of each of the crosslinker through the number of units and their molar masses.

II.2. Degradation studies

100 µm films were prepared on glass substrates and immersed into a potassium hydroxide solution with a pH of 10. Every 15 min they were taken out of the potassium hydroxide solution, excess potassium hydroxide solution was carefully removed without touching or damaging the PSA films, the films were then left to dry for approximately 1 h at 30 ºC and probe tack measurements were performed. The sufficiency of this drying method was confirmed by carrying out probe tack measurements 24 h after the PSA films were taken out of the potassium hydroxide solution, which led to no significant change in the results compared to the results after drying for

1 h. The work of adhesion was calculated by integration of the probe tack curves. The average value of 4 measurements for each immersion time is reported.

30 µm films were prepared on a paper label substrate. The paper label with the film was then attached to a glass bottle. The glass bottle with the attached label and PSA film was immersed for 24 h into a potassium hydroxide solution at a pH of approximately 10. As a reference sample, the same procedure was carried out with a commercial wine bottle with its label and commercial PSA. After the immersion time, the removal of the labels was tried, by peeling of the labels by hand.

II.3. Free radical polymerization of macromonomers

The macromonomers were co-polymerized with and stabilized by methacrylated polyethylene glycols (PEGMAs) of different lengths either in emulsion or dispersion polymerization. The shorter macromonomers could be polymerized in emulsion polymerization, whereas the longer macromonomers were too hydrophobic to be polymerized in conventional emulsion polymerization and were therefore polymerized in dispersion polymerization, by adding 30 wt% of ethanol to the aqueous phase (the procedures and the results are described and discussed in the appendix).

Due to the difficulties found to produce a reproducible waterborne dispersion using the macromonomers, degradation studies were carried out with solvent-borne copolymers of the macromonomers and PEGMA. Degrees of polymerizations differ between emulsion and solution polymerization. However, for the degradation study this is not crucial, as the degradation of the

polymer sidechains is monitored. The dried co-polymers were immersed into a phosphate buffered saline (PBS) solution with a pH of 7.3. Samples were withdrawn over a timeframe of 71 days and absolute and relative weight average molar masses were monitored over 71 days are plotted in Figure II.3.

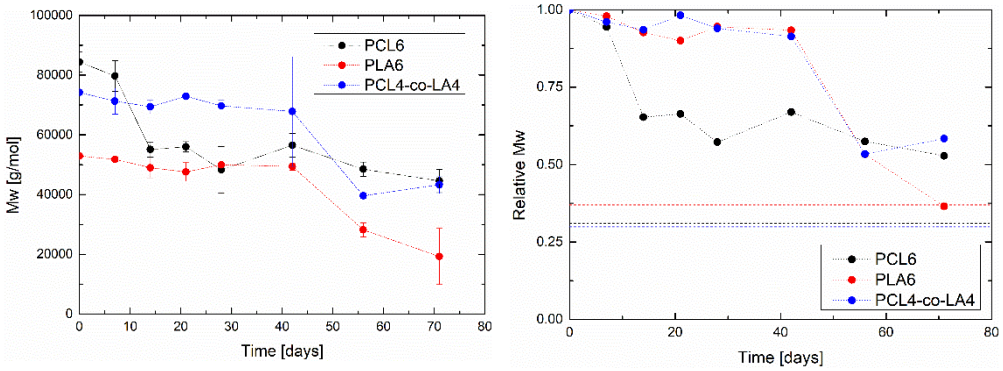

(a) **(b)**

Figure II.3. Evolution of absolute **(a)** and relative **(b)** weight average molar mass over time of PCL6 (black), PLA6 (red) and PCL4-co-LA4 (blue) in the buffer solution. The dashed lines represent the theoretical mass loss for each of the polymers if all of the ester groups would hydrolyse.

Different degradation behaviours of the polymers of different macromonomers have been observed. The majority of the degradation of PCL6 happens in the first two weeks of immersion into the PBS buffer solution (35% of the initial weight average molar mass are lost within this timeframe). Thereafter, the mass loss slows down significantly. Finally, a mass loss of 47% was determined for PCL6. PLA6 and PCL4-co-PLA4 are showing a relatively similar evolution of weight average molar masses. However, they show a reverse behaviour compared to PCL6. During the first 40 days, barely any degradation happens (below 10%). In the last 30 days a

drastic decrease of weight average molar masses (final mass loss of 64% for PLA6 and 42% for PCL4-co-LA4) was observed. PLA6 exactly reaches this value within 71 days. Whereas, the ester groups of PCL6 and PCL4-co-LA4 do not seem to hydrolyse completely. This behaviour was not expected, as PLA is reported to degrade faster, due to self-catalysis by its carboxylic end-groups, than PCL.[7]

II.4 Degradation of PSA copolymers synthesized by solution polymerization

To proof that lactide and lactone moieties of the oligoester crosslinkers incorporated in polymer chains degrade under basic conditions, we first proved the concept in crosslinked copolymers synthesized by solution polymerization.

The monomers BA/MMA/AA (in the ratio 89.1/9.9/1) were polymerized in a solution polymerization with a solid content of 30% in toluene, using 1 mol% of the oligoester crosslinkers. 5 wbm% of AIBN were added after the polymerization temperature was reached. The solution polymerizations were carried out for 4 hours at 70 ºC and under nitrogen atmosphere.

The oligoester crosslinkers ASY-LA4CL4 and SY-LA6CL6 were used in a solution polymerization with the monomers BA/MMA/AA (89.1/9.9/1) and compared to the blank (without using a crosslinker). The dried polymer was immersed for 24 h in a potassium hydroxide solution to degrade. The molar mass distributions measured by Gel Permeation Chromatography (GPC) before and after degradation are shown in Figure II.4.

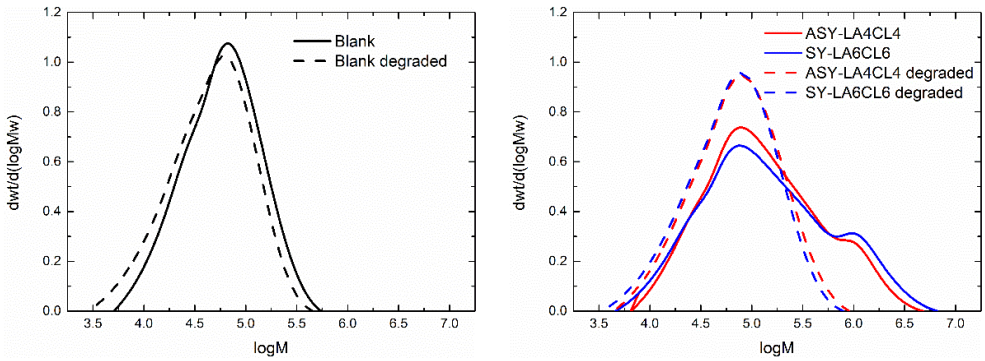

Figure II.4. Molar mass distribution of the polymers obtained from solution polymerization before (straight line) and after degradation (dashed line) at basic pH.

The molar mass distribution of the polymers with oligoester crosslinkers is broader compared to the molar mass distribution of the blank polymer clearly showing the crosslinking reactions in the presence of the oligoester crosslinkers. The distribution of the blank after immersing it into a basic solution had a negligible effect on the molar mass distribution, whereas the distribution of the oligoester containing polymers gets much narrower and almost like the blank after the degradation.

The weight average molar masses and the dispersity index of the polymers obtained by solution polymerization are displayed in Table II.1.

Table II.1. Weight average molar mass and dispersity index of the polymers from solution polymerization before and after degradation at basic pH.

	M_W [g/mol]	PDI
Blank	80800	2.0
Blank degraded	65000	2.2
ASY-LA4CL4	297600	4.7
ASY-LA4CL4 degraded	96000	2.5
SY-LA6CL6	375400	6.4
SY-LA6CL6 degraded	108000	2.5

The weight-average molar mass of the blank decreases around 20% after degradation, whereas the weight average molar mass of the polymers with the synthesized oligoester crosslinkers is around one third of the initial value after degradation. Furthermore, the polydispersity of the polymer including the asymmetric oligoester crosslinker decreases from 4.7 to 2.5 and of the polymer including the symmetric crosslinker from 6.4 to 2.5. On the other hand the blank polymer shows a slight increase in dispersity from 2.0 to 2.2 after degradation. These results prove that the synthesized oligoester crosslinkers are able to act as crosslinkers in a co-polymerization with acrylate monomers and that the crosslinks are degradable in basic media.

II.5. PSA synthesis by seeded semibatch emulsion polymerization

The PSAs were produced in two step seeded emulsion polymerization procedure. First, the seed was produced following the recipe shown in Table II.2.

Table II.2. Formulation of the synthesized by semibatch emulsion polymerization.

Ingredient	Amount [g]	Percentage [wbm%]
BA	185.18	89.1
MMA	20.67	9.9
AA	2.09	1.0
Dowfax 2A1	11.53	2.5
Water	353.06	170.0
Ammonia	8.36	4.0
KPS	0.52	0.25

Reaction temperature: 80 ºC; Agitation: 200 rpm.

In the second step the seed was grown in a semibatch emulsion polymerization process following the recipe shown in Table II.3.

Table II.3. Formulation of the seeded semibatch emulsion polymerizations.

Ingredient	Amount [g]	Percentage [wbm%]
Seed	18.00	9.0
BA	178.80	89.1
MMA	19.90	9.9
AA	2.02	1.0
Dowfax 2A1	2.78	0.6
Water	182.50	58.9
Crosslinker*	0.46-5.61	0.2 mol%
t-DDM	0.30	0.15
KPS	0.49	0.25
Sodium bicarbonate	0.49	0.25

*The percentage of the crosslinkers is reported in mol% (based on the monomers) instead of wbm% due to the different molar masses of the used crosslinkers.

Reaction temperature: 75 ºC; Agitation: 200 rpm.

II.6. Removability test of PSA labels from glass bottles

The glass bottles and their labels were immersed into a basic aqueous solution for 24 h and it was tried to peel the labels off from the bottles by hand. The label from the commercial wine bottle could not be removed (Figure II.5).

Figure II.5. Commercial wine bottle with commercial label and PSA after immersion into basic aqueous solution for 24 h.

On the other hand, the label which was attached with the oligoester crosslinker (ASY-LA8CL4) containing latex could be removed easily after an immersion into the basic aqueous solution for 24 h (Figure II.6).

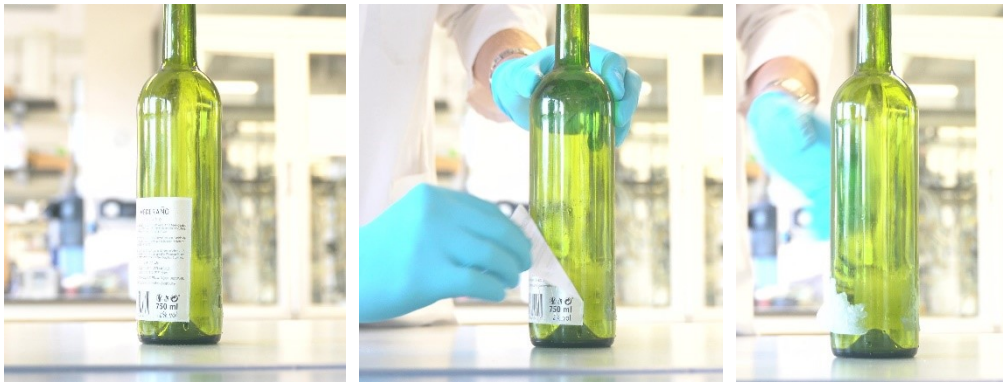

Figure II.6. Paper label attached to a glass bottle with PSA which includes a synthesized oligoester crosslinker (ASY-LA8CL4) after immersion into a basic aqueous solution for 24 h.

III. Additional information for Chapter 3

III.1. Recipes

The detailed recipes for all of the runs are listed in Table III.1.

Table III.1. Recipes for all of the carried out solution polymerizations.

Run	DBHQ [g]	Benzene-d6 [g]	AIBN [g]	EDDT [g]	DAA [g]
1	0.0077	0.435	0.0037	0.165	0.205
2	0.0062	0.415	0.0066	0.135	0.167
3	0.0072	0.390	0.0125	0.157	0.194
4	0.0060	0.311	0.0031	0.135	0.168
5	0.0057	0.307	0.0062	0.128	0.159
6	0.0058	0.325	0.0092	0.131	0.163

III.2. ^{1}H-NMR Analysis

The signals at 5.8-5.7 ppm ($I_{vinylic1}$) and 5.2-4.9 ppm ($I_{vinylic2}$) were used to track the decrease of vinyl functional groups and the signal at 4.0 ppm ($I_{polymeric}$) to determine the amount of polymerized vinyl functional groups (Figure III.1). The equation for the determination of the ene functional group conversion (X_{ene}) is shown in equation III.1.

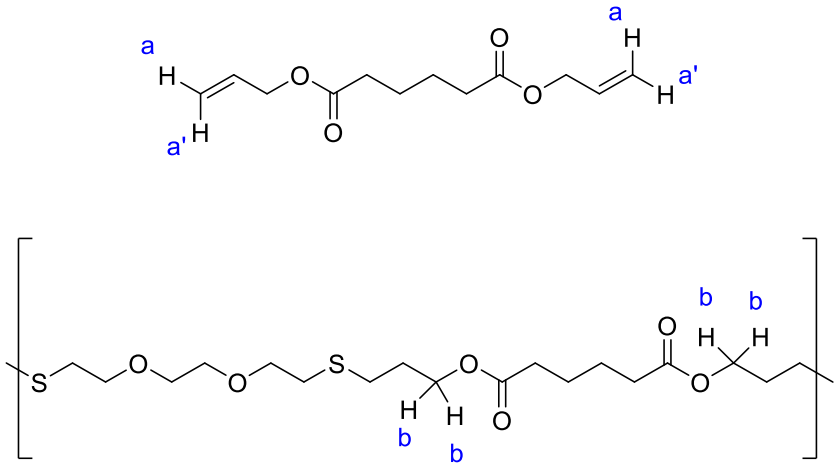

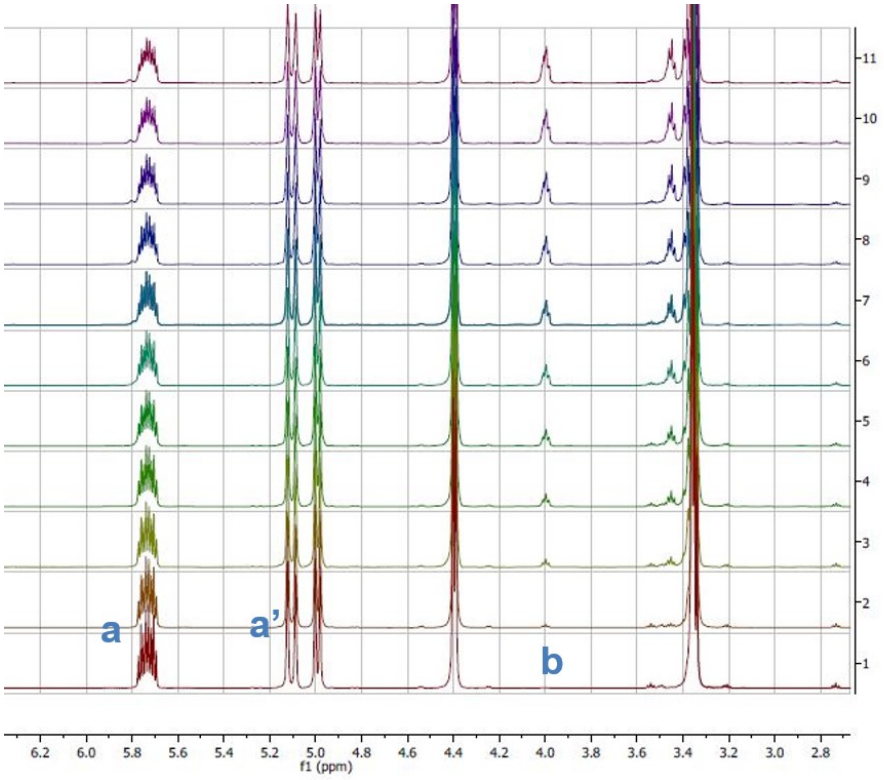

Figure III.1. Example of the in situ ^{1}H-NMR spectra taken during thiol-ene polymerization with r=1.00 and 1 wbm% of AIBN (first 10 spectra taken during the first 10 min of the polymerization).

$$X_{ene} = \frac{I_{polymeric}}{I_{polymeric} + I_{vinylic1} + I_{vinylic2}} \quad \text{(III.1)}$$

III.3. SEC/MALS/RI

The dn/dc for the thiol-ene copolymers was determined measuring the refractive index of a thiol-ene copolymer that was synthesized in solution polymerization (Polymer from Run3) at different concentrations. The slope of these values (Figure III.2) gives the dn/dc. The used concentrations are listed in Table III.2.

Table III.2. Concentrations used for the determination of the dn/dc.

	Concentrations [mg/mL]
1	0.532
2	1.069
3	2.124
4	3.133
5	3.976
6	4.861

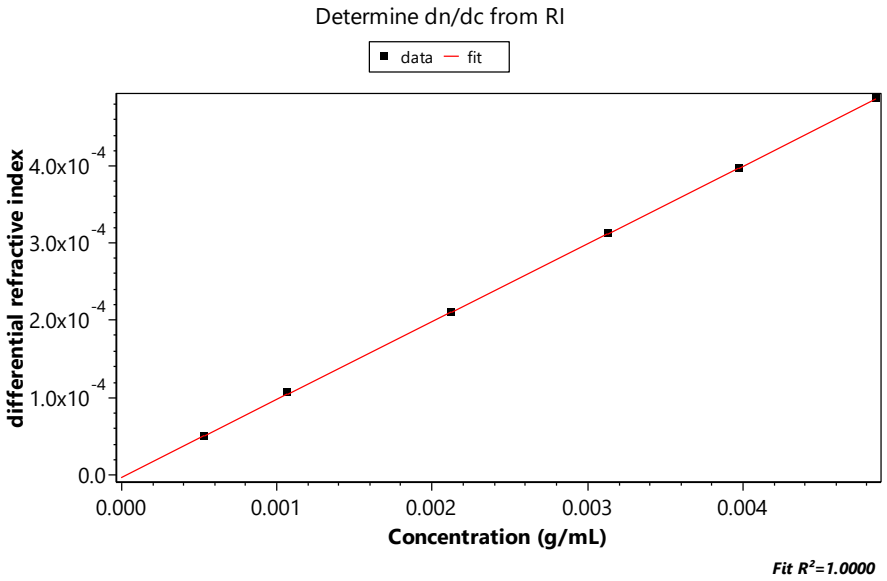

Figure III.2. Determination of the dn/dc for a thiol-ene copolymer from the monomers DAA and EDDT.

III.4. Mathematical model for thiol-ene polymerization

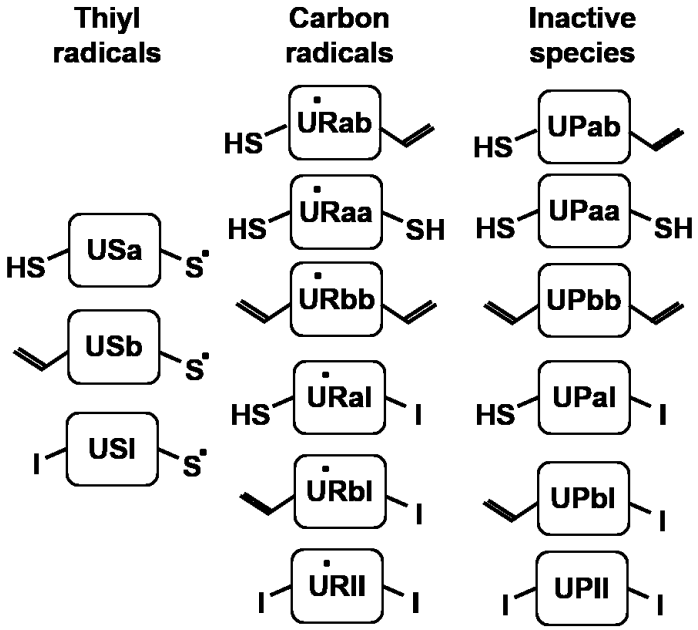

Figure III.3. Species with at least one disulfide in the chain, signalized by the letter U. The thiyl radicals USa, USb and USI, the carbon radicals URab, URaa, URbb, URaI, URbI and URII and the inactive species UPab, UPaa, UPbb, UPaI, UPbI and UPII.

III.5. Kinetic steps

All the steps of the kinetic scheme are displayed below.

Initiation reactions		
1.	I_2 → 2*f I*	kd
2.	I* + Maa → IH + Sa	2*kISH
3.	I* + Mbb → RbI	2*kIvi
4.	I* + Paa → IH + Sa	2*kISH
5.	I* + UPaa → IH + USa	2*kISH
6.	I* + Pab → IH + Sb	kISH
7.	I* + UPab → IH + Sb	kISH
8.	I* + PaI → IH + SI	kISH
9.	I* + UPaI → IH + USI	kISH
10.	I* + Pab → RaI	kIvi
11.	I* UPab → URaI	kIvi
12.	I* + Pbb → RbI	2*kIvi
13.	I* + UPbb → URbI	2*kIvi
14.	I* + PbI → RII	kIvi
15.	I* + UPbI → URII	kIvi

Addition (propagation) reactions		
16.	SI + Mbb → RbI	2*kad
17.	USI + Mbb → URbI	2*kad
18.	SI + Pab → RaI	kad
19.	USI + Pab → URaI	kad
20.	SI + UPab → URaI	kad
21.	USI + UPab → URaI	kad
22.	SI + Pbb → RbI	2*kad
23.	USI + Pbb → URbI	2*kad
24.	SI + UPbb → URbI	2*kad
25.	USI + Pbb → URbI	2*kad
26.	SI + PbI → RII	kad
27.	USI + PbI → URII	kad
28.	SI + UPbI → URII	kad
29.	USI + UPbI → URII	kad
30.	Sa + Mbb → Rab	2*kad
31.	USa + Mbb → URab	2*kad
32.	Sa + Pbb → Rab	2*kad
33.	USa + Pbb → URab	2*kad
34.	Sa + UPbb → URab	2*kad
35.	USa + UPbb → URab	2*kad

36.	Sa + Pab → Raa	kad
37.	USa + Pab → URaa	kad
38.	Sa + UPab → URaa	kad
39.	USa + UPab → URaa	kad
40.	Sa + PbI → RaI	kad
41.	USa + PbI → URaI	kad
42.	Sa + UPbI → URaI	kad
43.	USa + UPbI → URaI	kad
44.	Sb + Mbb → Rbb	2*kad
45.	USb + Mbb → URbb	2*kad
46.	Sb + Pbb → Rbb	2*kad
47.	USb + Pbb → URbb	2*kad
48.	Sb + UPbb → URbb	2*kad
49.	USb + UPbb	2*kad
50.	Sb + Pab → Rab	kad
51.	USb + Pab → URab	kad
52.	Sb + UPab → URab	kad
53.	USb + UPab → URab	kad
54.	Sb + PbI → RbI	kad
55.	USb + PbI → URbI	kad
56.	Sb + UPbI → URbI	kad

57.	USb + UPbI → URbI	kad

Chain transfer reactions		
58.	Rab + Paa → Pab + Sa	2*ktr
59.	URab + Paa → UPab + Sa	2*ktr
60.	Rab + UPaa → Pab + USa	2*ktr
61.	URab + UPaa → UPab + USa	2*ktr
62.	Rab + Maa → Pab + Sa	2*ktr
63.	URab + Maa → UPab + Sa	2*ktr
64.	Rab + Pab → Pab + Sb	ktr
65.	URab + Pab → UPab + Sb	ktr
66.	Rab + UPab → Pab + USb	ktr
67.	URab + UPab → UPab + USb	ktr
68.	Rab + PaI → Pab + SI	ktr
69.	URab + PaI → UPab + SI	ktr
70.	Rab + UPaI → Pab + USI	ktr
71.	URab + UPaI → UPab + USI	ktr
72.	Rab → Sb	ktr*[Rab]
73.	URab → USb	ktr*[URab]
74.	Rbb + Maa → Pbb + Sa	2*ktr

75.	URbb + Maa → UPbb + Sa	2*ktr
76.	Rbb + Paa → Pbb + Sa	2*ktr
77.	URbb + Paa → UPbb + Sa	2*ktr
78.	Rbb + UPaa → Pbb + USa	2*ktr
79.	URbb + UPaa → UPbb USa	2*ktr
80.	Rbb + Pab → Pbb + Sb	ktr
81.	URbb + Pab → UPbb + +Sb	ktr
82.	Rbb + UPab → Pbb + USb	ktr
83.	URbb + UPab → UPbb + USb	ktr
84.	Rbb + PaI → Pbb + SI	ktr
85.	Rbb + UPaI → Pbb + USI	ktr
86.	URbb + PaI → UPbb + SI	ktr
87.	URbb + UPaI → UPbb + USI	ktr
88.	RbI + Maa → PbI + Sa	2*ktr
89.	URbI + Maa → UPbI + Sa	2*ktr
90.	RbI + Paa → PbI + Sa	2*ktr
91.	URbI + Paa → UPbI + Sa	2*ktr
92.	RbI + UPaa → PbI + USa	2*ktr
93.	URbI + UPaa → UPbI + USa	2*ktr
94.	RbI + Pab → PbI + Sb	ktr
95.	URbI + Pab → UPbI + Sb	ktr

96.	RbI + UPab → PbI + USb	ktr
97.	URbI + UPab → UPbI + USb	ktr
98.	RbI + PaI → PbI + SI	ktr
99.	URbI + PaI → UPbI + SI	ktr
100.	RbI + UPaI → PbI + USI	ktr
101.	URbI + UPaI → UPbI + USI	ktr
102.	RaI + Maa → PaI + Sa	2*ktr
103.	URaI + Maa → UPaI + Sa	2*ktr
104.	RaI + Paa → PaI + Sa	2*ktr
105.	URaI + Paa → UPaI + Sa	2*ktr
106.	RaI + UPaa → PaI + USa	2*ktr
107.	URaI + UPaa → UPaI + USa	2*ktr
108.	RaI + Pab → PaI + Sb	ktr
109.	URaI + Pab → UPaI + Sb	ktr
110.	RaI + UPab → UPaI + USb	ktr
111.	URaI + UPab → UPaI + USb	ktr
112.	RaI + PaI → PaI + SI	ktr
113.	URaI + PaI → UPaI + SI	ktr
114.	RaI + UPaI → PaI + USI	ktr
115.	URaI + UPaI → UPaI + USI	ktr
116.	RaI → SI	ktr*[RaI]

117.	URaI → USI	ktr*[URaI]
118.	RII + Maa → PII + Sa	2*ktr
119.	URII + Maa → UPII + Sa	2*ktr
120.	RII + Paa → PII + Sa	2*ktr
121.	URII + Paa → UPII + Sa	2*ktr
122.	RII + UPaa → PII + USa	2*ktr
123.	URII + UPaa → UPII + USa	2*ktr
124.	RII + Pab → PII + Sb	ktr
125.	URII + Pab → UPII + Sb	ktr
126.	RII + UPab → PII + USb	ktr
127.	URII + UPab → UPII + USb	ktr
128.	RII + PaI → PII + SI	ktr
129.	URII + PaI → UPII + SI	ktr
130.	RII + UPaI → PII + USI	ktr
131.	URII + UPaI → UPII + USI	ktr
132.	Raa + Maa → Paa + Sa	2*ktr
133.	URaa + Maa → UPaa + Sa	2*ktr
134.	Raa + Paa → Paa + Sa	2*ktr
135.	URaa + Paa → UPaa + Sa	2*ktr
136.	Raa + UPaa → Paa + USa	2*ktr
137.	URaa + UPaa → UPaa + USa	2*ktr

138.	Raa + Pab → Paa + Sb	ktr
139.	URaa + Pab → UPaa +Sb	ktr
140.	Raa + UPab → Paa + USb	ktr
141.	URaa + UPab → UPaa + USb	ktr
142.	Raa + PaI → Paa + SI	ktr
143.	URaa + PaI → UPaa + SI	ktr
144.	Raa + UPaI → Paa + USI	ktr
145.	URaa + UPaI → UPaa + USI	ktr

Combination reactions		
146.	Sb + SI → UPbI	kcomb
147.	Sb + USI → UPbI	kcomb
148.	USb + USI → UPbI	kcomb
149.	USb + SI → UPbI	kcomb
150.	Sb + Sb → UPbb	kcomb
151.	USb + Sb → UPbb	kcomb
152.	USb + USb → UPbb	kcomb
153.	SI + SI → UPII	kcomb
154.	USI + SI → UPII	kcomb
155.	USI + USI → UPII	kcomb

156.	Sa + Sa → UPaa	kcomb
157.	USa + Sa → UPaa	kcomb
158.	USa + USa → UPaa	kcomb
159.	Sa + Sb → UPab	kcomb
160.	Sa + USb → UPab	kcomb
161.	USa + Sb → UPab	kcomb
162.	USa + USb → UPab	kcomb
163.	Sa + SI → UPaI	kcomb
164.	Sa + USI → UPaI	kcomb
165.	USa + SI → UPaI	kcomb
166.	USa + USI → UPaI	kcomb
167.	Sa + I* → PaI	kcombSI
168.	Sb + I* → PbI	kcombSI
169.	SI + I* → PII	kcombSI
170.	USa + I* → UPaI	kcombSI
171.	USb + I* → UPbI	kcombSI
172.	USI + I* → UPII	kcombSI
173.	RbI + I* → PbI	kcombIvi
174.	RaI + I* → PaI	kcombIvi
175.	RII + I* → PII	kcombIvi
176.	Rab + I* → Pab	kcombIvi

177.	Raa + I* → Paa	kcomblvi
178.	Rbb + I* → Pbb	kcomblvi
179.	URbI + I* → UPbI	kcomblvi
180.	URaI + I* → UPaI	kcomblvi
181.	URII + I* → UPII	kcomblvi
182.	URbb + I* → UPbb	kcomblvi
183.	URab + I* → UPab	kcomblvi
184.	URaa + I* → UPaa	kcomblvi

Inhibition reactions		
185.	I* + DBHQ → IH + DBHQ*	kinhib
186.	Rab + DBHQ → Pab + DBHQ*	kinhib
187.	URab + DBHQ → UPab + DBHQ*	kinhib
188.	Raa + DBHQ → Paa + DBHQ*	kinhib
189.	URaa + DBHQ → UPaa + DBHQ*	kinhib
190.	Rbb + DBHQ → Pbb + DBHQ*	kinhib
191.	URbb + DBHQ → UPbb + DBHQ*	kinhib
192.	RaI + DBHQ → PaI + DBHQ*	kinhib
193.	URaI + DBHQ → UPaI +DBHQ*	kinhib
194.	RbI + DBHQ → PbI + DBHQ*	kinhib

195.	URbI + DBHQ → UPbI + DBHQ*	kinihib
196.	RII + DBHQ → PII + DBHQ*	kinhib
197.	URII + DBHQ → UPII + DBHQ*	kinhib
198.	Sa + DBHQ → Paa + DBHQ*	kinhib
199.	USa + DBHQ → UPaa + DBHQ*	kinhib
200.	Sb + DBHQ → Pab + DBHQ*	kinhib
201.	USb + DBHQ → UPab + DBHQ*	kinhib
202.	SI + DBHQ → PaI + DBHQ*	kinhib
203.	USI + DBHQ → UPaI + DBHQ*	kinhib

III.6. Non-assigned fractions detected in MALDI-TOF analysis

At first it was assumed that one distribution observed in the MALDI-TOF spectra could account for the species PaI, which are formed by combination reactions of initiator derived radicals and carbon centred species. For the polymerization with the ratio [DAA]/[EDDT] = 1.00 and the experiment with 1 wbm% of AIBN, the fraction of this distribution is 10%. Taking into account the total mass of monomer Maa and Mbb used for this experiment (0.37 g) and dividing this mass by the Mn determined by SEC/MALS (1800 g/mol), this leads to $2.05 \cdot 10^{-5}$ mol of PaI chains.

The amount of initiator radicals generated during the reaction time (13716 s) can be calculated following the first order equation resulting from the integration of the material balance of the

initiator (equation III.2). With the total volume of 0.83 mL and a concentration of 4.5 g/L of AIBN, it follows that $1.06 \cdot 10^{-5}$ mol of initiator radicals (I*) are generated over the complete reaction time. And this is assuming an efficiency factor (f) of 1. Therefore, it can be concluded, that the unknown species in the MALDI-TOF do not belong to the PaI species.

$$[I_2]_t = [I_2]_0 \cdot e^{-k \cdot t} \quad \text{(III.2)}$$

Prediction of the model using literature rate coefficients

Table III.3: Values of parameters used in the model simulation using the rate coefficients reported in the literature for the thiol-allyl ether system.

Parameter	Value	Reference
k_d (s^{-1})	$3.2 \cdot 10^{15} \exp(-131.1/RT)$	[8]
f (-)	0.6	
k_{lvi} (L mol^{-1} s^{-1})	28.66	[9]
k_{comb} (L mol^{-1} s^{-1})	2.0×10^8	[10]
$k_{ad}=10 \times k_{tr}$ (L mol^{-1} s^{-1})		[10]
k_{lSH}(L mol^{-1} s^{-1})	1.8×10^7	[11]
k_{tr}(L mol^{-1} s^{-1})	1.1×10^6	[11]
k_{inhib}^*(L mol^{-1} s^{-1})	$2.7 \times 10^5 \pm 61$	This work

**Estimated rate coefficients from parameter estimation.*

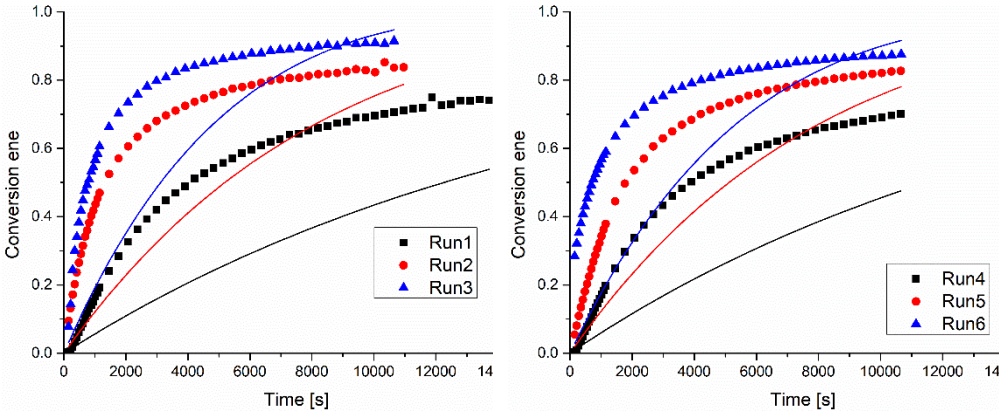

Figure III.3. Plot of simulated data with experimental data for the conversions of ene functional groups for runs 1,2 and 3 **(a)** and runs 4,5 and 6 **(b)**.

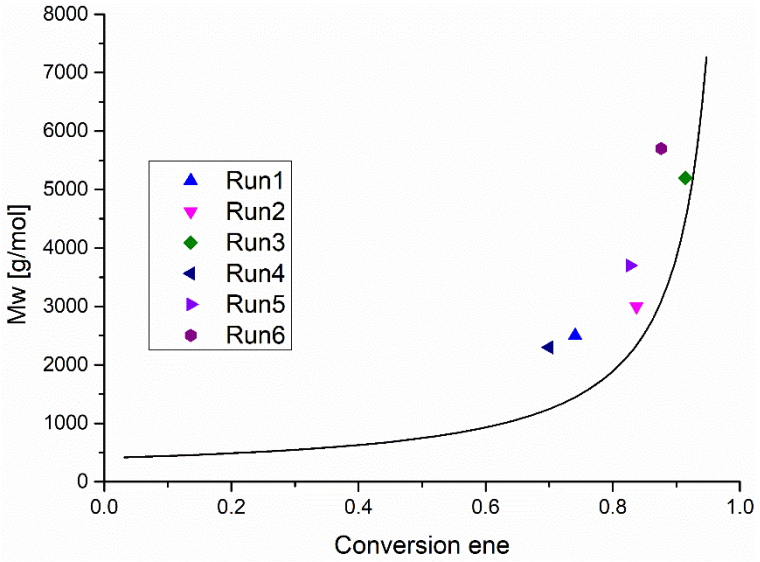

Figure III.4. Experimental (dots) and predictions of the mathematical model (black line) developed in this work for the weight-average molar masses.

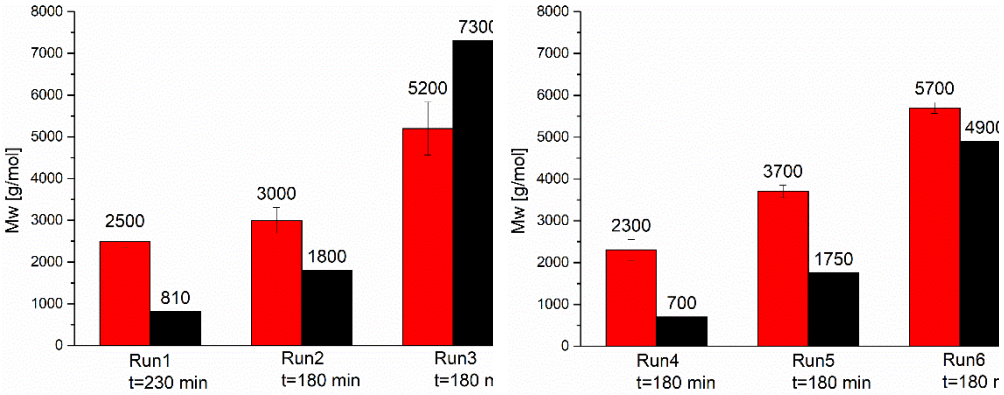

Figure III.5. Comparison of weight-average molar masses measured by SEC/MALS (red) and model predictions (black) at the reaction time indicated in the Figure.

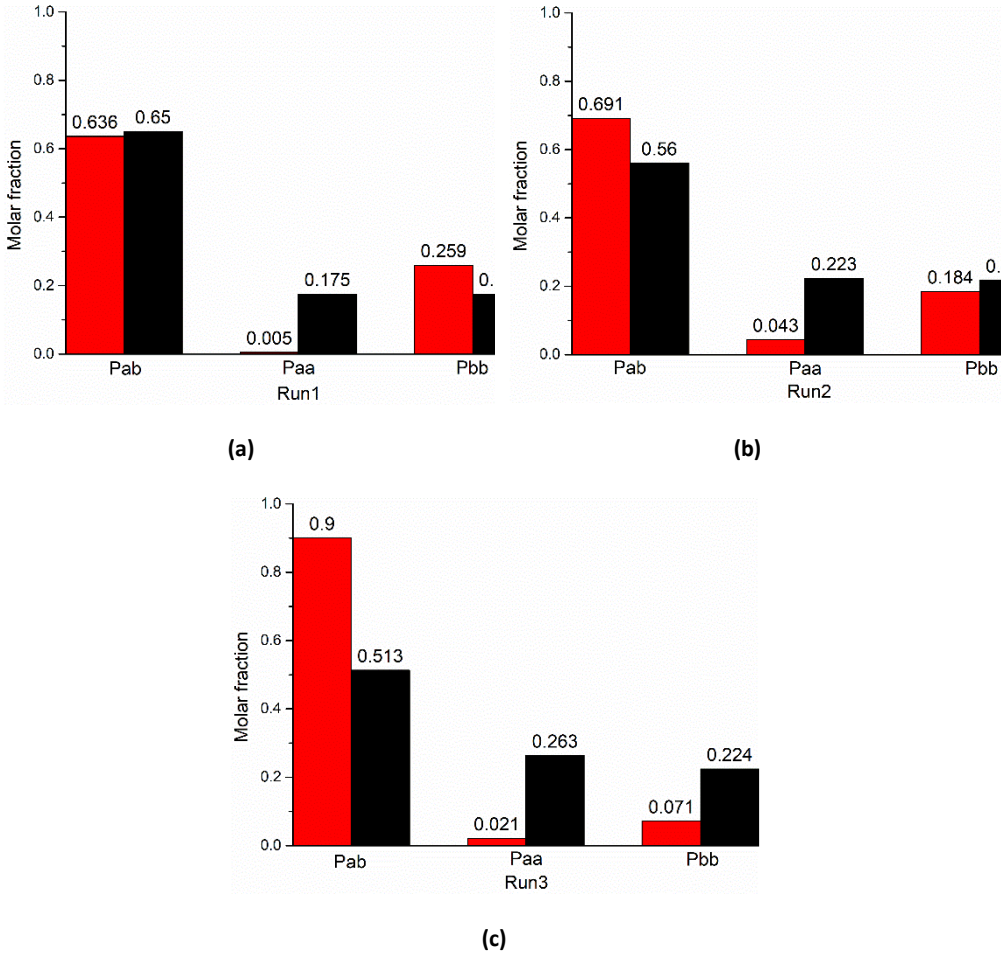

Figure III.6. Comparison between the experimental fractions of the species Pab, Paa and Pbb measured by MALDI-TOF (red) and simulated (black) for the experiments with r = 1.00.

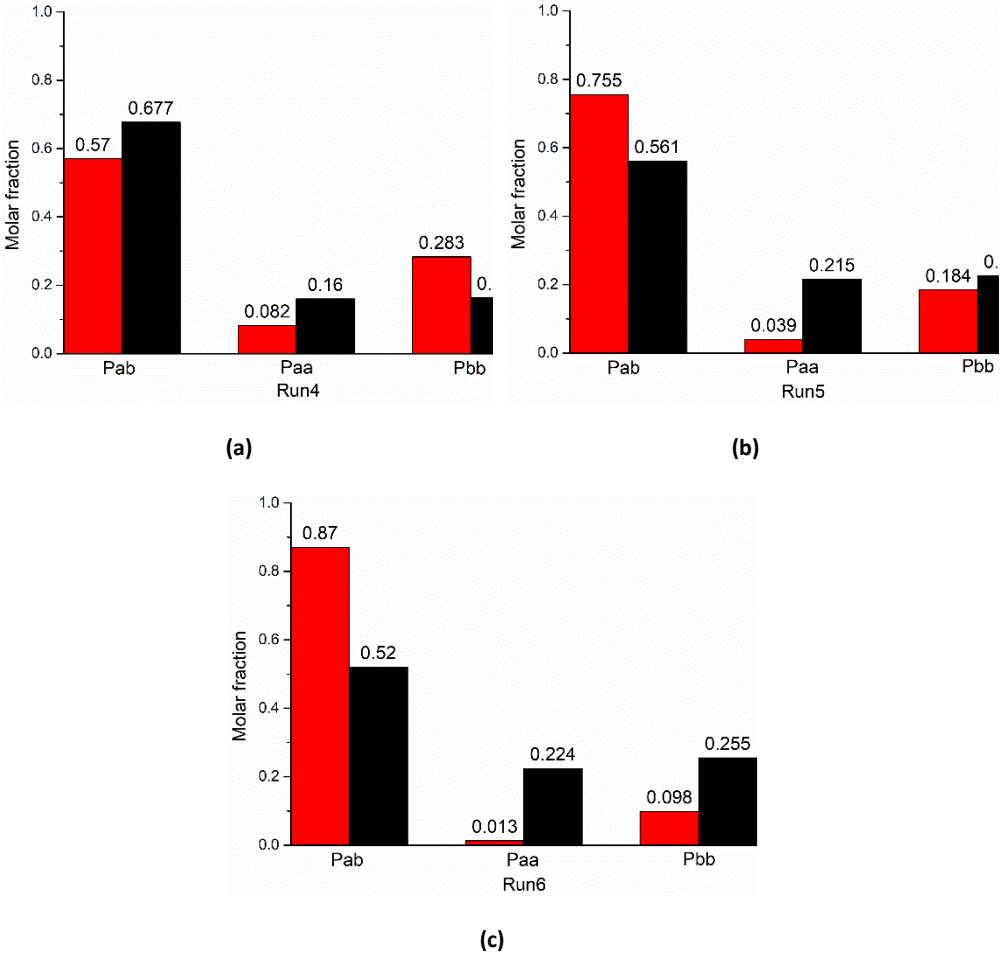

Figure III.7. Comparison between the experimental fractions of the species Pab, Paa and Pbb measured by MALDI-TOF (red) and simulated (black) for the experiments with r = 1.00.

IV. Additional information for Chapter 5

Table IV.1. summarizes reactivity ratios of the copolymerization of MDO with different acrylates reported in literature.

Table IV.1. Reactivity ratios for the copolymerization of MDO with different acrylates. AIBN was used as initiator in all of the cases.

System	Method	Solvent	T [º C]	r_{MDO}	$r_{acrylate}$	Reference
MA/MDO		Benzene	50/115	0.024	26.54	[12]
MA/MDO	NLLS	Cyclohexane	70	0.168 (-0.141, +0.250)	3.354 (-0.954, +2.382)	[13]
BA/MDO	NLLS	Cyclohexane	70	0.044 (-0.083, +0.391)	1.761 (-0.445, +0.761)	[13]
2EHA/MDO	NLLS	Cyclohexane	70	0.002 (-0.116, +0.171)	1.507 (-0.434, +0.854)	[13]
DA/MDO	NLLS	Cyclohexane	70	0.339 (-0.319, +3.108)	2.257 (-0.943, +10.707)	[13]

Table IV.2. summarizes reactivity ratios for the copolymerizatin of MDO with VAc reported in literature.

Table IV.2. Reactivity ratios for the copolymerization of MDO and VAc reported in the literature.

Method	Solvent	Initiator	T [ºC]	r_{MDO}	r_{VAc}	Reference
Kelen-Tüdos	Bulk	AIBN	70	0.47	1.56	[14]
Finemann-Ross	Bulk	AIBN	60	0.93	1.71	[15]
NLLS	Bulk	AIBN	60	1.03	1.22	[16]
NLLS	Bulk	AIBN	60	0.95	1.71	[17]
Kelen-Tüdos & Finemann-Ross	Bulk	TPO/$Co(acac)_2$*	30	0.14	1.89	[18]

*(2,4,6-trimethylbenzoyl)diphenylphosphin (TPO) as photo-induced initiator and cobalt acetylacetonate ($Co(acac)_2$) as mediator.

IV.1. Determination of reactivity ratios

The material balances for each monomer for the case of a copolymerization (assuming terminal model kinetics) in batch are shown in Equation IV.1 and IV.2 in which [i] is the concentration of monomer i [mol/L], R_{pi} is the polymerization rate of monomer i [mol/L·s], k_{pij} the propagation rate constant of a radical with the terminal unit i with monomer j [mol/L·s], P_i the probability to find a radical with the ultimate unit i and $[R^*]$ the total concentration of radicals.

$$\frac{d[A]}{dt} = -R_{pA} = -(k_{pAA}P_A + k_{pBA}P_B)[A][R^*] \quad \text{(IV.1)}$$

$$\frac{d[B]}{dt} = -R_{pB} = -(k_{pAB}P_A + k_{pBB}P_B)[B][R^*] \quad \text{(IV.2)}$$

The definition of probabilities shown in Equation IV.3 and IV.4 follows from Equation IV.1 and IV.2 if the Quasi-Steady-State assumption (QSSA) is fulfilled.

$$P_A = \frac{k_{pBA}[A]}{k_{pBA}[A] + k_{pAB}[B]} \quad \text{(IV.3)}$$

$$P_B = 1 - P_A \quad \text{(IV.4)}$$

Equation IV.5 defines the conversion of monomer A (X_A) and Equation IV.6 defines the overall conversion (X_T). $[i]_0$ is the initial concentration of monomer i in these two equations.

$$X_A = \frac{[A]_0 - [A]}{[A]_0} \quad \text{(IV.5)}$$

$$X_T = \frac{([A]_0 - [A]) + ([B]_0 - [B])}{[A]_0 + [B]_0} \tag{IV.6}$$

Differentiation of Equation IV.5 and IV.6 leads to Equation IV.7, IV.8 and IV.9.

$$dX_A = -\frac{d[A]}{[A]_0} \tag{IV.7}$$

$$dX_T = \frac{-d[A] - d[B]}{[A]_0 + [B]_0} \tag{IV.8}$$

$$\frac{dX_A}{dX_T} = \frac{[A]_0 + [B]_0}{[A]_0} \cdot \frac{R_{pA}}{R_{pA} + R_{pB}} = \frac{[A]_0 + [B]_0}{[A]_0} \cdot \left(\frac{1 + r_A \cdot \frac{[A]}{[B]}}{2 + r_A \cdot \frac{[A]}{[B]} + r_B \cdot \frac{[B]}{[A]}} \right) \tag{IV.9}$$

In which r_A and r_B are the reactivity ratios of monomer A and B defined as shown in Equation IV.10 and IV.11.

$$r_A = \frac{k_{pAA}}{k_{pAB}} \quad \text{(IV.10)}$$

$$r_B = \frac{k_{pBB}}{k_{pBA}} \quad \text{(IV.11)}$$

Concentrations can be defined as function of X_A and X_T as depicted in Equation IV.12, to enable the integration of Equation IV.9.

$$\frac{[A]}{[B]} = \frac{[A]_0 \cdot (1 - X_A)}{[B]_0 - X_T \cdot ([A]_0 + [B]_0) + [A]_0 \cdot X_A} \quad \text{(IV.12)}$$

The cumulative copolymer composition (Y_i, cumulative copolymer composition referred to monomer i) is defined as shown in Equation IV.13.

$$Y_A = \frac{[A]_0 \cdot X_A}{([A]_0 + [B]_0) \cdot X_T} \quad \text{(IV.13)}$$

The molar monomer ratios of the experiments for each of the monomer couples are listed in Table IV.3.

Table IV.3. Molar monomer ratios of the experiments for each of the monomer couples.

	Experiment 1	Experiment 2	Experiment 3	Experiment 4
MDO/VAc	0.32/0.68	0.25/0.75	0.20/0.80	0.05/0.95
MDO/2OA	0.42/0.58	0.22/0.78	0.12/0.88	0.05/0.95
MDO/LMA	0.52/0.48	0.30/0.70	0.23/0.77	0.09/0.91

IV.2. NMR spectra

The monomer conversions of MDO and VAc were measured following the evolution of the peaks of the protons at the carbon atoms *a* and *c* of MDO (δ [ppm] = 3.50-3.40 and 3.70-3.60) and VAc (protons at carbon atom (1) at δ [ppm] = 4.75-4.60 and (1') at δ [ppm] = 4.40-4.25) as indicated in Figure IV.1. The VAc and MDO monomer structures as well as the NMR spectra for the copolymerization of MDO/VAc and the change of intensity of the peaks over polymerization time can be seen in Figure IV.1.

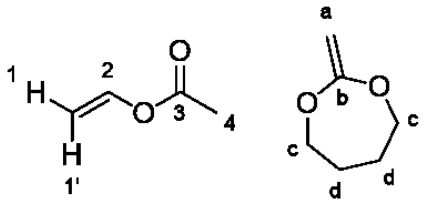

VAc MDO

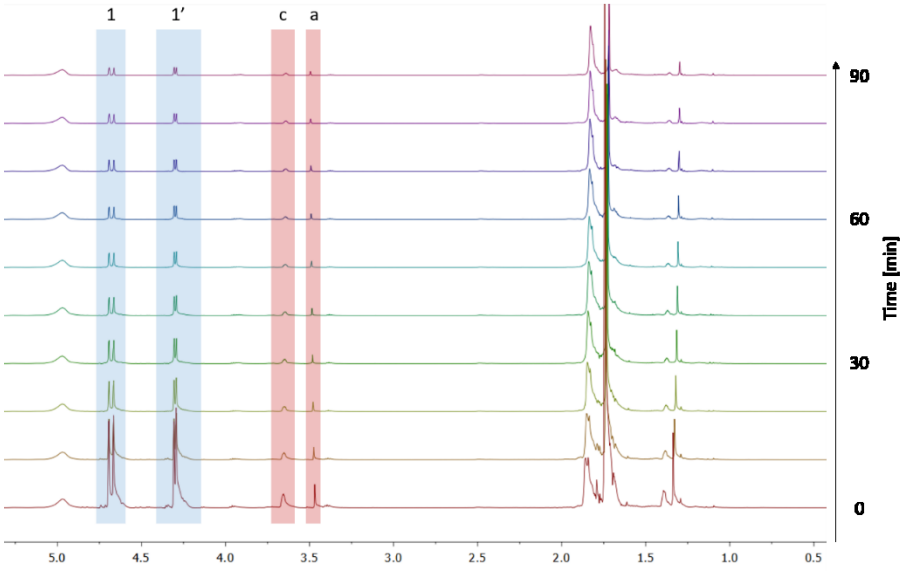

Figure IV.1. First 10 ^{1}H NMR spectra for the copolymerization of MDO/VAc with the molar ratio of 0.25/0.75. The peaks that were tracked to follow the conversion of VAc are marked in blue and the ones for MDO are marked in red.

The monomer conversions for the copolymerizations of 2OA/MDO were measured following the evolution of the peaks of the protons (1 and 1´) and (2) of 2OA ((1) at δ [ppm] = 6.25-6.10, (2) at δ [ppm] = 6.00-5.80 and (1') at δ [ppm] = 5.45-5.30) and (c) of MDO (δ [ppm] = 3.70-3.60). The

used peaks are assigned in Figure IV.2 and an example of the evolution of the peaks for the copolymerization of MDO and 2OA is also shown. The used peaks are assigned in Figure IV. and an example of the evolution of the peaks for the copolymerization of MDO and 2OA is also shown.

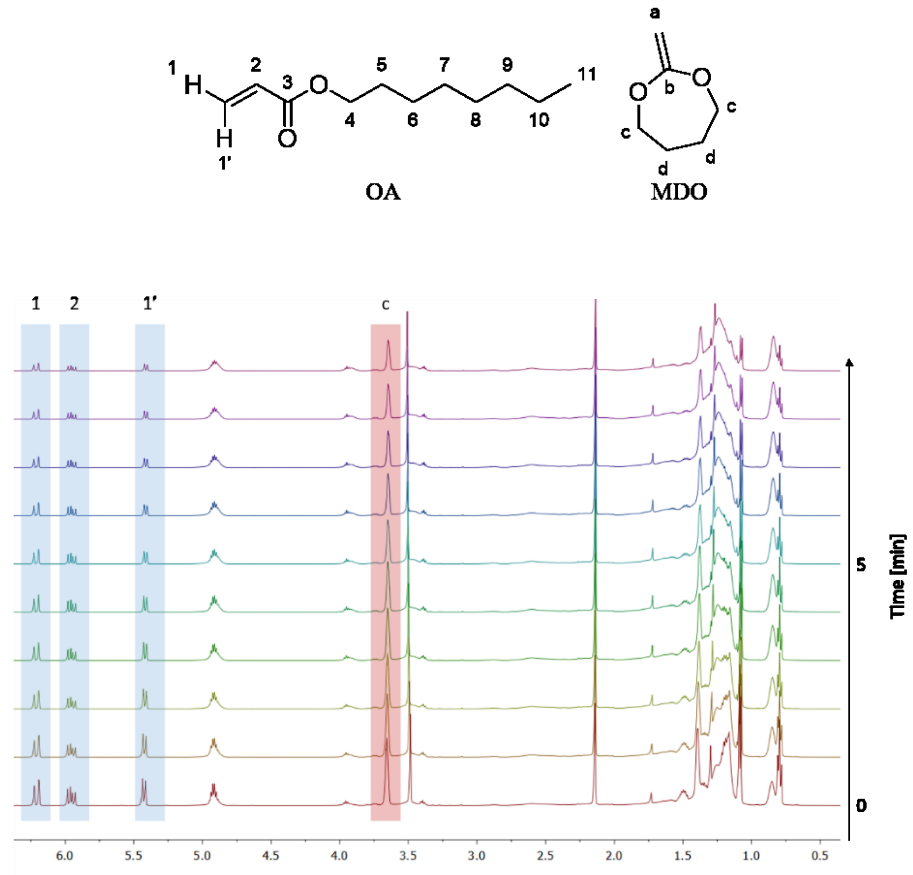

Figure IV.2. First 10 ^{1}H NMR spectra for the copolymerization of MDO/2OA in the molar ratio 0.42/0.58. The peaks used to calculate the conversion of 2OA are marked in blue and the one for MDO in red.

The monomer conversions for the copolymerization of MDO with LMA were measured by following the evolution of the peaks of the protons attached to the carbon atom 1 of LMA ((1) at

δ [ppm] = 6.10-6.00 and (1') at δ [ppm] = 5.35-5.25) and the protons at the carbon atoms (a) and (c) of MDO ((a) at δ [ppm] = 3.50-3.40 and (c) at δ [ppm] = 3.70-3.60). Figure IV.3 shows an example of NMR spectra for the copolymerizations of MDO/LMA, the signals used for the determination of conversions are assigned to the carbon atoms of the monomers.

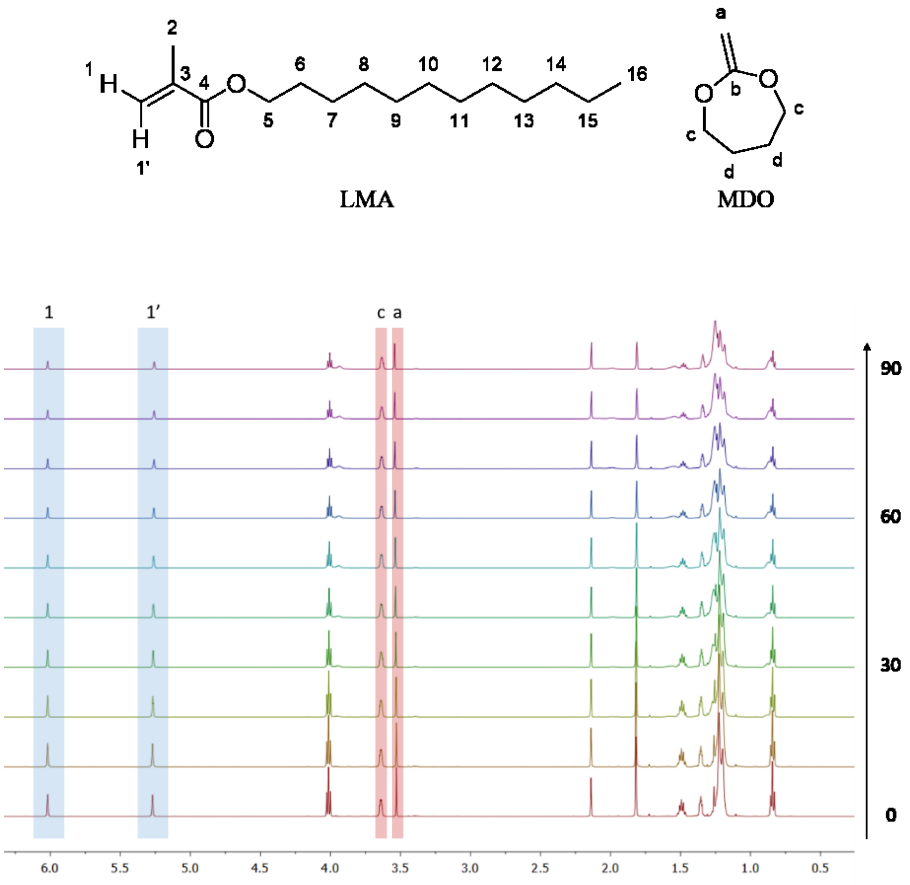

Figure IV.3. First 10 recorded ^{1}H NMR spectra for the copolymerization of MDO/LMA with the molar ratio 0.30/0.70. The peaks used to calculate the conversion of LMA are marked in blue and the ones for MDO in red.

IV.3. Mayo-Lewis plots

The theoretical instantaneous copolymer composition, F_A of a monomer A has been calculated from the reactivity ratios r_A and r_B of the comonomers A and B and the instantaneous fraction of the feed f_A and f_B of the monomers A and B using the Mayo-Lewis equation (Equation IV.14).[19]

$$F_A = \frac{r_A \cdot f_A^2 + f_A \cdot f_B}{r_A \cdot f_A^2 + 2 \cdot f_A \cdot f_B + r_B \cdot f_B^2} \quad \text{(IV.14)}$$

where f_A and f_B are readily obtained from the evolution of the fractional conversions of each monomer. The experimental instantaneous copolymer compositions have been calculated from the time evolution of the fractional conversions of each of the monomers, A and B. The derivative of fractional conversions of each monomer yields, the polymerization rate of each monomer at each sampling time; $R_{p,i}$. The instantaneous copolymer composition, F_A, is then readily calculated as follow:

$$F_A = \frac{R_{p,A}}{R_{p,A} + R_{p,B}} \quad \text{(IV.15)}$$

The Mayo-Lewis plot for the MDO/2OA system is shown in Figure IV.4. The theoretical evolution of instantaneous copolymer composition for the MDO/2EHA system is plotted as well using the reactivity ratios estimated by Lena et al.[13]

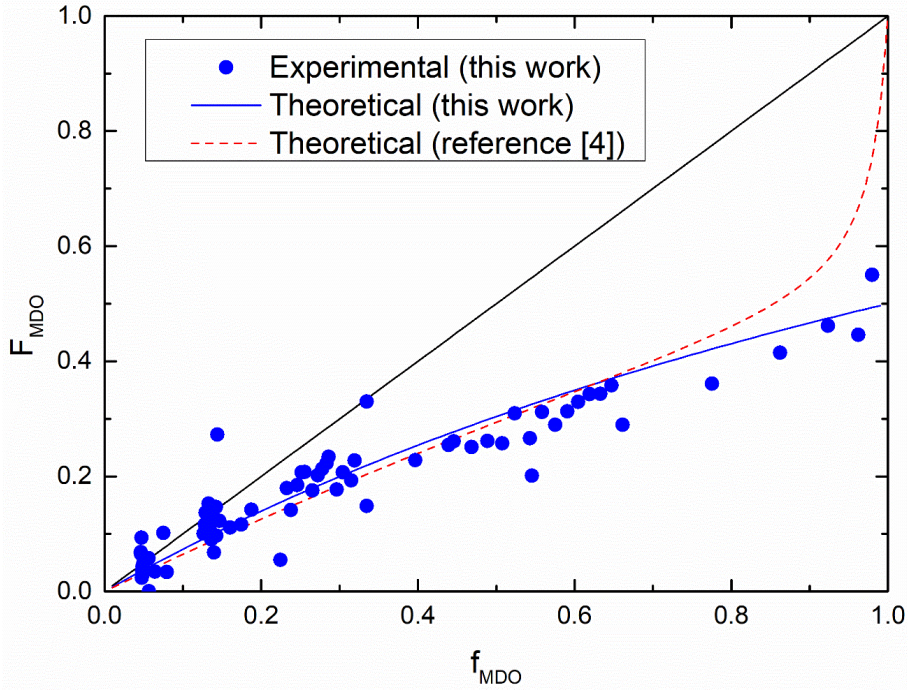

Figure IV.4. Mayo-Lewis plot for the MDO/2OA system. The theoretical instantaneous copolymer composition calculated from the reactivity ratios of this work (blue line), the instantaneous copolymer composition for the MDO/2EHA system using the reactivity ratios reported by Lena et al.[13] (red, dashed line), and the instantaneous copolymer composition determined from the evolution of the individual monomer conversions of MDO and 2OA (blue circles).

The Mayo-Lewis plot for the MDO/LMA system is depicted in IV.5.

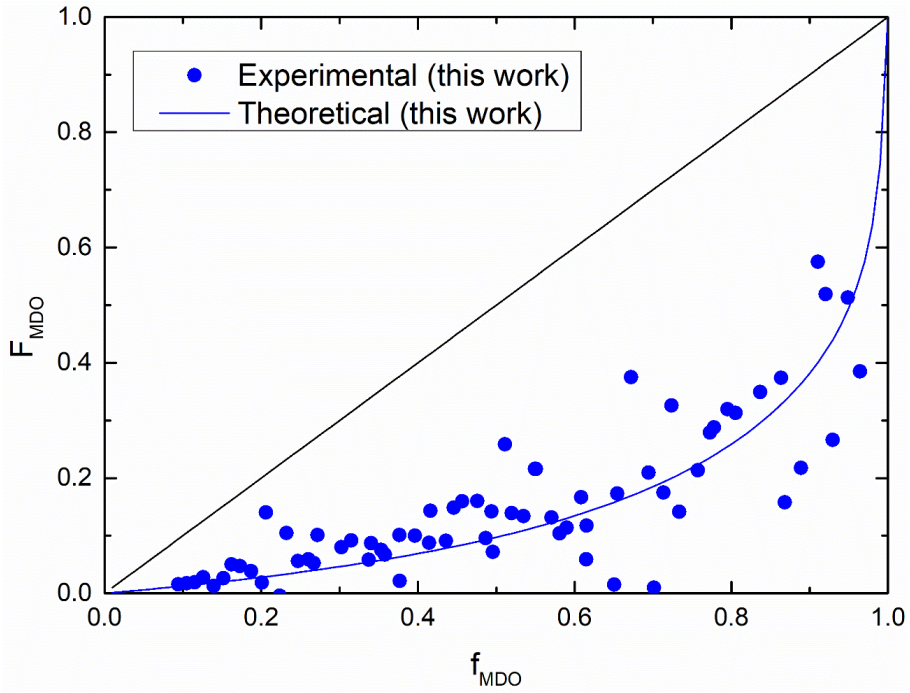

Figure IV.5. Mayo-Lewis plot for the MDO/LMA system. The instantaneous copolymer composition calculated with the reactivity ratios for MDO/LMA reported in this work (blue line) and instantaneous copolymer composition determined from the evolution of the fractional conversions of MDO and LMA (blue circles).

V. References

(1) Benedek, I. *Pressure-Sensitive Adhesives and Applications*, Second Edi.; Marcel Dekker: New York - Basel, 2004.

(2) Sun, S.; Li, M.; Liu, A. A Review on Mechanical Properties of Pressure Sensitive Adhesives. *Int. J. Adhes. Adhes.* **2013**, *41*, 98–106. https://doi.org/10.1016/j.ijadhadh.2012.10.011.

(3) Rudawska, A. *Surface Treatment in Bonding Technology*; Academic Press, 2019. https://doi.org/10.1016/B978-0-12-817010-6.00009-6.

(4) Lakrout, H.; Sergot, P.; Creton, C. Direct Observation of Cavitation and Fibrillation in a Probe Tack Experiment on Model Acrylic Pressure-Sensitive-Adhesives. *J. Adhes.* **1999**, *69* (3–4), 307–359. https://doi.org/10.1080/00218469908017233.

(5) Deplace, F.; Carelli, C.; Mariot, S.; Retsos, H.; Chateauminois, A.; Ouzineb, K.; Creton, C.; Carelli, C.; Mariot, S.; Retsos, H.; Chateauminois, A.; Ouzineb, K. Fine Tuning the Adhesive Properties of a Soft Nanostructured Adhesive with Rheological Measurements. *J. Adhes.* **2009**, *85*, 18–54. https://doi.org/10.1080/00218460902727381.

(6) Aguirreurreta, Z.; Dimmer, J.; Willerich, I.; Leiza, J. R.; De, J. C. International Journal of Adhesion & Adhesives Improving the Properties of Water-Borne Pressure Sensitive Adhesives by Using Non-Migratory Surfactants. *Int. J. Adhes. Adhes.* **2016**, *70*, 287–296. https://doi.org/10.1016/j.ijadhadh.2016.07.011.

(7) Siparsky, G. L.; Voorhees, K. J.; Miao, F. Hydrolysis of Polylactic Acid (PLA) and Polycaprolactone (PCL) in Aqueous Acetonitrile Solutions: Autocatalysis. *J. Environ. Polym. Degrad.* **1998**, *6* (1), 31–41.

(8) Korolev, G. V; Bubnova, M. L.; Makhonina, L. I. Free-Radical Copolymerization of Binary Mixtures of Vinyl Monomers of Various Compositions : Initiation Rate Constants 1. *Polym. Sci. Part A Polym. Chem.* **2007**, *49* (3), 242–248. https://doi.org/10.1134/S0965545X07030029.

(9) Dossi, M. Quantum Chemistry Study of Free-Radical Polymerization Kinetics, Politecnico de Milano, 2011.

(10) Reddy, S. K.; Cramer, N. B.; Bowman, C. N. Thiol - Vinyl Mechanisms . 1 . Termination and Propagation Kinetics in Thiol - Ene Photopolymerizations. *Macromolecules* **2006**, *39*, 3673–3680. https://doi.org/10.1021/ma060008e.

(11) Derboven, P.; Dagmar, R. D.; Stamenovic, M. M.; Espeel, P.; Marin, G. B.; Prez, F. E. Du. Kinetic Modeling of Radical Thiol−Ene Chemistry for Macromolecular Design: Importance of Side Reactions and Diffusional Limitations. *Macromolecules* **2013**, *46*, 1732–1742. https://doi.org/10.1021/ma302619k.

(12) Sun, L. F.; Zhuo, R. X.; Liu, Z. L. Synthesis and Enzymatic Degradation of 2-Methylene-1,3- Dioxepane and Methyl Acrylate Copolymers. *J. Polym. Sci., Part A Polym. Chem.* **2003**, *41* (18), 2898–2904. https://doi.org/https://doi.org/10.1002/pola.10868.

(13) Lena, J.; Jackson, A. W.; Chennamaneni, L. R.; Wong, C. T.; Lim, F.; Andriani, Y.; Thoniyot, P.; Herk, A. M. Van. Degradable Poly(Alkyl Acrylates) with Uniform Insertion of Ester Bonds, Comparing Batch and Semibatch Copolymerizations. *Macromolecules* **2020**, *53* (10), 3994–4011. https://doi.org/10.1021/acs.macromol.0c00207.

(14) Agarwal, S.; Kumar, R.; Kissel, T.; Reul, R. Synthesis of Degradable Materials Based on Caprolactone and Vinyl Acetate Units Using Radical Chemistry. *Polym. J.* **2009**, *41* (8), 650–660. https://doi.org/10.1295/polymj.PJ2009091.

(15) Undin, J.; Illanes, T.; Finne-wistrand, A.; Albertsson, A. Random Introduction of Degradable Linkages into Functional Vinyl Polymers by Radical Ring-Opening Polymerization , Tailored for Soft Tissue Engineering. *Polym. Chem.* **2012**, *3*, 1260–1266. https://doi.org/10.1039/c2py20034a.

(16) Hedir, G. G.; Bell, C. A.; Ieong, N. S.; Chapman, E.; Collins, I. R.; Reilly, R. K. O.; Dove, A. P. Functional Degradable Polymers by Xanthate-Mediated Polymerization. *Macromolecules* **2014**, *47*, 2847–2852. https://doi.org/10.1021/ma500428e.

(17) Lena, J.; Herk, A. M. Van. Toward Biodegradable Chain-Growth Polymers and Polymer Particles : Re-Evaluation of Reactivity Ratios in Copolymerization of Vinyl Monomers with Cyclic Ketene Acetal Using Nonlinear Regression with Proper Error Analysis. *Ind. Eng. Chem. Res.* **2019**, *58*, 20923–20931. https://doi.org/10.1021/acs.iecr.9b02375.

(18) Ding, D.; Pan, X.; Zhang, Z.; Li, N.; Zhu, J.; Zhu, X. A Degradable Copolymer of 2-Methylene-1,3-Dioxepane and Vinyl Acetate by Photo-Induced Cobalt-Mediated Radical

Polymerization. *Polym. Chem.* **2016**, *7*, 5258–5264. https://doi.org/10.1039/c6py01061j.

(19) Mayo, F. R.; Lewis, F. M. Copolymerization. I. A Basis for Comparing the Behavior of Monomers in Copolymerization; The Copolymerization of Styrene and Methyl Methacrylate. *J. Am. Chem Soc.* **1944**, *66* (9), 1594–1601. https://doi.org/https://doi.org/10.1021/ja01237a052.

Acronyms list

AA	Acrylic acid
AF4	Asymmetric flow field-flow fractionation
AIBN	Azobisisobutyronitrile
AMA	Allyl methacrylate
APS	Ammonium peroxodisulfate
BA	Butyl acrylate
BMDO	5,6-Benzyl-2-methylene-1,3-dioxepane
CHDF	Capillary hydrodynamic fractionation chromatography
cmc	Critical micelle concentration
CTA	Chain transfer agent
DA	Dodecyl acrylate
DAA	Diallyl adipate
DAP	Diallyl phthalate
DATP	Diallyl terephthalate
DBHQ	2,5-Di-*tert*-butylhydroquinone
DBU	1,8-Diazobicyclo[5.4.0]undec-7-ene
***t*-DDM**	*tert*-Dodecanethiol
DFT	Density functional theory
DLS	Dynamic Light Scattering
DMA	Dynamic mechanical analysis

DMSO	Dimethyl sulfoxide
DOT	Dibenzo[c,e]oxepane-5-thione
Dowfax 2A1	Dodecyl diphenyloxide disulfonate
Dp	Particle diameter
DSC	Dynamic scanning calorimetry
EDDT	2,2'-(Ethylenedioxy)diethanethiol
EDTA	Ethylenediaminetetraacetic acid
2EHA	2-Ethylhexyl acrylate
EP	Emulsion polymerization
$FeSO_4$	Iron(II)sulfate
FF6	2-Hydroxy-2-sulfinatoacetic acid disodium salt
GDMA	Glycol dimercaptoacetate
GPC	Gel Permeation Chromatography
4-HBA	4-Hydroxybutyl acetate
HEMA	2-Hydroxyethylmethacrylate
KPS	Potassium persulfate
LMA	Lauryl methacrylate
MA	Methyl acrylate
MALDI	Matrix assisted laser desorption ionization
MALS	Multi-angle light scattering
MDO	2-Methylene-1,3-dioxepane
MEP	Miniemulsion polymerization
MMA	Methyl Methacrylate

Mw	Weight average molar mass
$NaHCO_3$	Sodium hydrogencarbonate
NLLS	Non-linear least square
NMR	Nuclear Magnetic Resonance
Np	Number of particles
ñ	Average number of radicals per particle
2OA	n-Octadecyl acrylate
PCL	Poly(ε-caprolactone)
PE	Polyethylene
PEG	Polyethylene glycol
PETMP	Pentaerythritol tetra(3-mercaptopropionate)
PLA	Poly(lactic acid)
PMMA	Poly(methyl methacrylate)
PP	Polypropylene
PS	Polystyrene
PSA	Pressure-sensitive adhesive
RI	Refractive index
ROP	Ring opening polymerization
RROP	Radical ring opening polymerization
SAFT	Shear adhesion failure temperature
SEC	Size exclusion chromatography
SC	Solids Content
SDS	Sodium dodecyl sulfate

S	Styrene
T	Temperature
TBD	1,5,7-Triazobicyclo[4.4.0]dec-5-ene
TEM	Transmission electron microscopy
THF	Tetrahydrofuran
TMPDAE	Trimethylolpropane diallyl ether
TMPMP	Pentaerythritol tetrakis(3-mercaptopropionate)
TOF	Time of flight
UV	Ultraviolet light
UV-Vis	Ultraviolet-visible light
VAc	Vinyl acetate
Veova EH	Vinyl 2-ethylhexanoate
VOC	Volatile organic compounds
wbm	Weight based in monomer
wt	Total weight